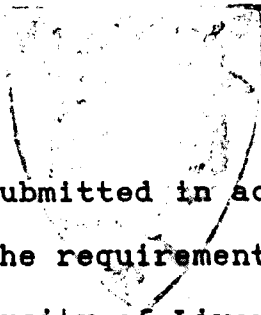A study of recent Secular Variation of the

Geomagnetic field as recorded by lavas from

Mount Vesuvius and the Canary Islands.

LIVERPOOL
UNIVERSITY

Thesis submitted in accordance

with the requirements of the

University of Liverpool

for the degree of

Doctor in Philosophy

by

Andrew Malcolm Tulloch

20/07/1992

PAGE NUMBERING AS

ORIGINAL

ABSTRACT

A study of recent Secular Variation of the
Geomagnetic field as recorded by lavas from
Mount Vesuvius and the Canary Islands.

by Andrew Malcolm Tulloch.

        Historically dated lava flows from Mount
Vesuvius (1697-1944) and the Canary Islands (1470-1971)
were sampled to facilitate the assessment of palaeofield
variation as recorded by those lavas. This assessment
was carried out in two phases. The first phase required
the measurement of field directions from the period and
was carried out using a parastatic magnetometer and A.F.
demagnetisation. The results obtained showed a high
level of correlation with those of direct observation
(Bloxham and Gubbins, 1985) and those of smaller scale
studies of the same area. The second phase involved the
measurement of palaeointensity variation. Results were
obtained for 207 Vesuvian and 173 Canary Island samples
using the Tanguy (1975) and Boyd (1983) methods applied
to the SQUID and spinner magnetometers. The Thellier
method proved to be unsuitable for these samples. It
became apparent that palaeointensity results, from
equivalent samples, differed between the magnetometers
whilst falling within expected limits for the period.
The effect of cooling rate was investigated and the
large variations in remanent magnetisations of similar
samples could account for the variation in
palaeointensity results. Magnetic mineralogy studies
showed individual samples to be isotropic whilst samples
varied greatly within and between flows. Samples were
predominantly multi-domain magnetites or
titanomagnetites
        Development of the SQUID magnetometer during
this study involved the redesign of the oven assembly
and cooling arrangements to facilitate rapid repair and
sample cooling.

This work is dedicated to Catherine, my wife, without whose love and sacrifice I would have given up many times.

Magnetic functions, their units, values and symbols.

Intensity of Magnetisation : symbol M

S.I. unit Am^{-1} c.g.s unit emu cc^{-1}

conversion $1 Am^{-1} = 10^{-3}$ emu cc^{-1}

Magnetic Moment : symbol m

S.I. unit Am^2 c.g.s unit emu

conversion $1 Am^2 = 10^3$ emu

Magnetic Field Strength or Intensity: symbol H

S.I. unit Am^{-1} c.g.s unit Oe Oersted

conversion $1 Am^{-1} = 4\pi{*}10^{-3}$ Oe

Magnetic Flux density or Induction : symbol B

S.I. unit T Tesla   c.g.s. unit G Gauss

conversion $1T = 10^4$ Gauss

Magnetic Susceptibility per unit volume - a
function of M / H, symbol X dimensionless

conversion $1(S.I.) = 4\pi$ (c.g.s)

Abbreviations.

A.F.   -ALTERNATING FIELD

$alpha^{95}$ -95% ANGLE OF CONFIDENCE

ARM   -ANHYSTERETIC REMANENT MAGNETISATION

CRM   -CHEMICAL REMANENT MAGNETISATION

D   -DEMAGNETISATION FACTOR

DRM   -DETRITAL REMANENT MAGNETISATION

Fa   -ANCIENT MAGNETIC FIELD INTENSITY

Fl   -LABORATORY MAGNETIC FIELD INTENSITY

IRM   -ISOTHERMAL REMANENT MAGNETISATION

k   -PRECISION PARAMETER

ki   -INTRINSIC SUSCEPTIBILITY

ko   -OBSERVED SUSCEPTIBILITY

LP.   -LA PALMA   TN. -TENERIFE

LZ.   -LANZEROTE   V.-MOUNT VESUVIUS

MD   -MULTI DOMAIN

Ms   -SATURATION MAGNETISATION

Mrs   -SATURATION ISOTHERMAL REMANENCE

(P)NRM -(PARTIAL)NATURAL REMANENT MAGNETISATION

(P)TRM -(PARTIAL)THERMOREMANENT MAGNETISATION

RRM   -ROTATIONAL REMANENT MAGNETISATION

SD   -SINGLE DOMAIN

SQUID -SUPERCONDUCTING QUANTUM INTERFERENCE DEVICE

Tb   -BLOCKING TEMPERATURE

Tc   -CURIE TEMPERATURE

VRM   -VISCOUS REMANENT MAGNETISATION

CONTENTS

Chapter 5: The Curie balance: its principles, operation and results.

Chapter 6: Vibrating Sample Magnetometer: principles, operation and results.

Chapter 7: The directional component of secular variation.

Chapter 11: Historic field intensity determination using the Tanguy technique.

Chapter 12: The effect of cooling rate on magnetisation.

Chapter 13: Secular Variation summary.

Appendices

Chapter 1.

Palaeomagnetic background and project organisation.

The Earth's magnetic field is a complex phenomenon. It has many features which vary both with time and space, including magnetic field reversals and secular (short term) variations. This thesis addresses itself to the secular variation of the magnetic field. In particular the magnetisation of samples from Mount Vesuvius and the Canary Islands are used to plot the variation of the geomagnetic field over the last 500 years at these sites. To put these studies in context, it is necessary to give both a brief description of the Earth's magnetic field and the aims of the project.

1.1 The Earth's magnetic field.

Early studies of the Earth's field centred around its behaviour in relation to the lodestone compass, mainly as an aid to navigation. The magnetic field and magnetism remained subject to myth until the late 1500's when studies began in earnest. One of the first investigations was carried out in England by William Gilbert (1600). His experiments were often of a qualitative nature, although he did measure the direction of the field in England and showed that it

changed with latitude, proposing that the Earth was like a spherical magnet. Gellibrand in 1634 demonstrated that the Earth's magnetic field changed direction with time. He also demonstrated that Gilbert's magnetic sphere model was inadequate. Various other models were proposed to explain the Earth's magnetic field during the early 1800's but they proved unsatisfactory. The first accurate quantitative definition of the Earth's magnetic field was put forward by Gauss in 1839. His spherical harmonic analysis model allowed him to calculate the theoretical field direction and intensity at any location on the Earth's surface.

In simple terms the Earth's magnetic field has both a dipole and non-dipole component which vary independently with time giving rise to the complicated changes found in the records of the Earth's field. At present the main dipole, contributing some 90% of the field, is inclined at 11.5° to the rotational axis and is drifting west at about 0.01° per year (Barraclough, 1974). Superimposed on this dipole is a non-dipole field which is also drifting westwards (Vestine, 1947), at a rate of approximately 0.18° per year (Bullard, 1950). Thus the current drift in net field is about $0.2^{\circ}W$ longitude per year. The secular variation in the field cannot be explained by the drifting non-dipole theory alone. Yukutake & Tachinaka (1969) suggested

two separate non-dipole elements, drifting and standing
to explain secular variation.

Declination, inclination and field strength
all show short term secular variation ranging from a
few years up to a 1000 years. On a longer time scale,
studies have shown that the Earth's magnetic field can
reverse its polarity and that on average it has spent
as much time in this reversed state as in its present
normal polarity. The last major field reversal, the
Matuyama-Brunhes reverse to normal transition, occurred
730,000 years ago. Short term reversals which last for
tens of thousands of years are known as events, those
which last only a few thousands of years are known as
excursions. Excursions may be considered as aborted
field reversals or they may represent strong non-dipole
variation. Excursions can be geographically localised
events, such as the Lake Mungo excursion (Barbetti &
McElhinny, 1972, 1976). The intensity of the Earth's
magnetic field also changes with time. Direct
observations since 1830 show a decrease of 7% (Merrill
& McElhinny, 1983).

The history of the secular variation of the
Earth's magnetic field has been the subject of much
scientific research, known as palaeomagnetism,
particularily since 1839. It has become possible to
measure changes in the Earth's magnetic field using a
variety of techniques and materials. In particular
large quantities of directional information have been

amassed since 1936. Data sets for magnetic field intensity are not as common or as reliable, due to the difficulty in determining ancient field intensity. The commonly used Thellier & Thellier (1959) intensity method is particularily vulnerable to thermal alteration during measurement. To counter this effect techniques have been developed which either do not use heat or restrict its use. This has produced apparently reliable results from material previously considered unsuitable (Shaw, 1974; Rolph & Shaw, 1985; Walton, 1977 and Tanguy, 1975).

Palaeomagnetic data is important for evaluating models of the Earth's magnetic field. For example, the Bloxham & Gubbins model (1985) transfers surface information to the core mantle boundary and hence the geodynamo.

1.2 Project and aims.

The initial aims of the project were to:-

1) Collect historically dated lava samples.

2) To use these to define the secular variation for the collection areas.

3) Develop the "SQUID2" magnetometer for field intensity measurements.

4) Evaluate the secular variation data against the geomagnetic field model of Bloxham & Gubbins (1985).

4

Two areas were chosen, Mount Vesuvius in Southern Italy and the Canary Islands off the coast of Western Africa, as both areas have historic records of volcanic activity from 1400 A.D onwards. An extensive study of the rock mineralogy for both field areas was also planned, using a variety of techniques, in order to enhance the interpretation of palaeomagnetic results. Magnetic mineralogy can be used to indicate those samples which are most likely to prove suitable for intensity measurement. The mineralogy and grain size also control the stability of the magnetic moment over both geological and experimental time scales. Five parameters were to be measured. These were high and low temperature susceptibility, low field anisotropy, magnetic hysteresis and Curie temperature. These should provide an adequate picture which, whilst not complete, should give a good indication of the magnetic composition of the samples.

Secular variation studies were then to be carried out using both a spinner magnetometer and a new superconducing magnetometer referred to as "SQUID2", the development of which was also to be a major part of the study. On completion of the laboratory work a comparison was to drawn with the Bloxham & Gubbins model.

1.3 Thesis organisation.

This thesis is divided into six main sections. The first two cover the fieldwork and magnetic properties investigated in the study. Remaining sections contain the procedures undertaken in the four main areas of study. In order the six sections are:-

A) Introduction and fieldwork.

B) Magnetism and mineral properties.

C) Rock magnetic investigations.

D) Secular variation of direction.

E) Secular variation of intensity.

F) Effect of cooling rate.

Each of the above six sections is further sub-divided into numbered sections.

Chapter 2.

Sampling techniques and site locations.

To study secular variation over the last five
hundred years samples were collected from recent
volcanic lava flows of known age. The two sampling
areas were Mount Vesuvius in Southern Italy and the
Canary Islands off the West coast of Africa. Both
areas have experienced considerable vulcanism and have
erupted irregularly over the last 500 years.

The slopes of Mount Vesuvius (the only active
volcano on the European mainland) are subjected to both
forestry and intensive agriculture resulting in a
heavily overgrown sampling area. One of the few
obvious lava flows is that of the last eruption in
1944. The Canary Islands sites are just the opposite.
The flows of appropriate age occur on three different
islands, but were more accessible than those of Mount
Vesuvius due to the lack of vegetation and less intense
population pressure. Both areas were very diverse and
are described separately following a brief resume of
the techniques used in sample collection.

2.1 Sample collection and orientation.

Sample collection depends to a great extent
on a good working knowledge of the field areas.

Fortunately at both sites local experts were willing to help (see acknowledgments in appendix). Once located, the flows were examined for signs of post-cooling movement or reheating which could affect their suitability for study. Suitable flows were sampled using a petrol drill to obtain 2.5cm diameter cores up

Figure 2.1 Drilling a core from the 1944 lava flow on Mount Vesuvius.

to 12.5cm long (Figure 2.1). This system worked well except at altitudes above 3000m on Mount Teide in the Canaries where carburettor difficulties were encountered.

It was not possible to orientate the cores directly (Figure 2.2) using a magnetic compass due to

the magnetic field distortion produced by the surrounding rock. Cores were thus orientated using a sun compass and marked by a brass wire scribe before removal from the rock face (Figure 2.3). Sun compass data sheets containing the bearing of the sun, time and global position were then used for computer calculation of the orientation of the scribe line on the sample.
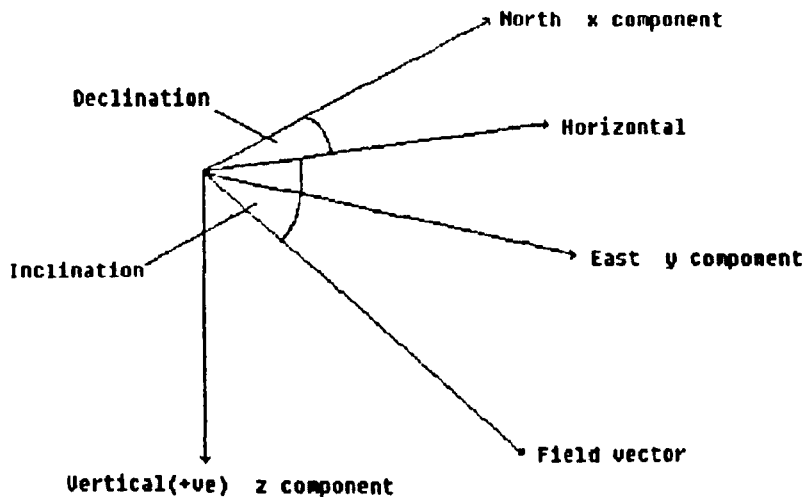
Figure 2.2 Sample orientation and vector components.

The minimum number of cores drilled per site was 10 while, at good exposures, up to 26 cores were drilled. Some sites were sampled for intensity purposes when directional information was not available due to shadow, or when post-cooling movement had taken place.

2.2 Field Errors.

A sample may have an error associated with it even before it reaches the laboratory and undergoes measurement. These errors arise during sample

orientation or from the drilling of sites which have
been the subject of post-cooling movement.

Figure 2.3   Sun compass ready for core orientation.

2.2.1 Orientation error.

When orientating a sample using a sun compass
the time, sample inclination and angular bearing of the
Sun with respect to the sample are recorded.   Each of

these is subject to error. The relative bearing of the
Sun to the sample was measured for a specific point in
time. The time taken at each measurement was correct
to within 2 minutes, so the error introduced due to
imprecise timing was insignificant; that is, less than
0.5°.

The inclination and position of the sun,
relative to the Y axis of the sample, were read from
the scales of the sun compass. These were graduated in
two degree steps allowing an accuracy of +/- 1 degree.
This must therefore be borne in mind when considering
the precision of results for each flow.

2.2.2 Post-cooling movement.

When a lava flow has cooled and locked in the
magnetic field any changes in its orientation will
produce a distorted set of magnetic results. Such
changes in orientation are not always apparent as
surface effects, erosion for example, often mask its
true history (Figure 2.4).
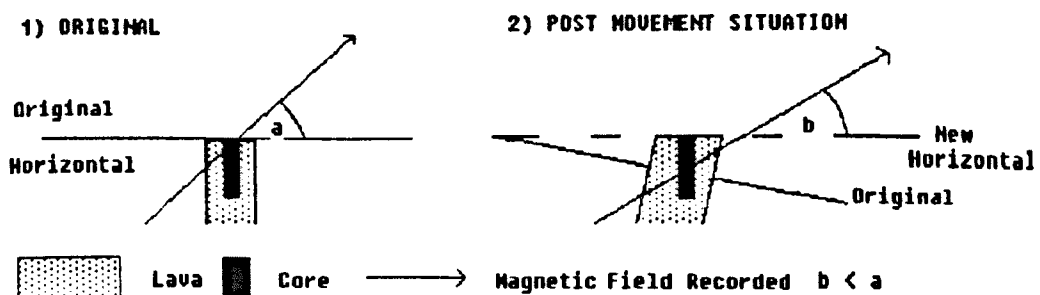
Figure 2.4 Post-cooling movement.

Such post cooling movement could result from the removal of the supporting media by erosion or the effects of blasting. Where it was possible to see cross-sections of the lava flows or view the surface over a long distance signs of such post-cooling movement were rarely visible and seem unlikely to be present. However, results from moved blocks within flows often have directional values which deviate considerably from the mean flow direction and can therefore be rejected.

2.3 Sample identification and preparation.

All samples were given descriptive code numbers. The codes were limited to 10 characters by the software but each code gave information on the geological age, the area and core number. For example QCNLP19406 corresponds to the Quaternary, Canary Islands, La Palma 1949 core 06.

On arrival at the laboratory, the 2.54cm diameter cores were sawn into cylinders of approximately 2.1cm in length and marked with the code number. Further preparation was required for SQUID samples where 0.9cm diameter cores were required of 0.8cm length. Rock magnetism experiments required only very small sample quantities for which the sawn ends from cores were used.

2.4 Canary Islands - sampling locations.

Seven inhabited and numerous uninhabited
islands make up the Canaries archipelago which extends
over 350 km from Lanzarote, 96 km from the Western
African coast, to nearly 448 km into the Atlantic Ocean
(Figure 2.5).
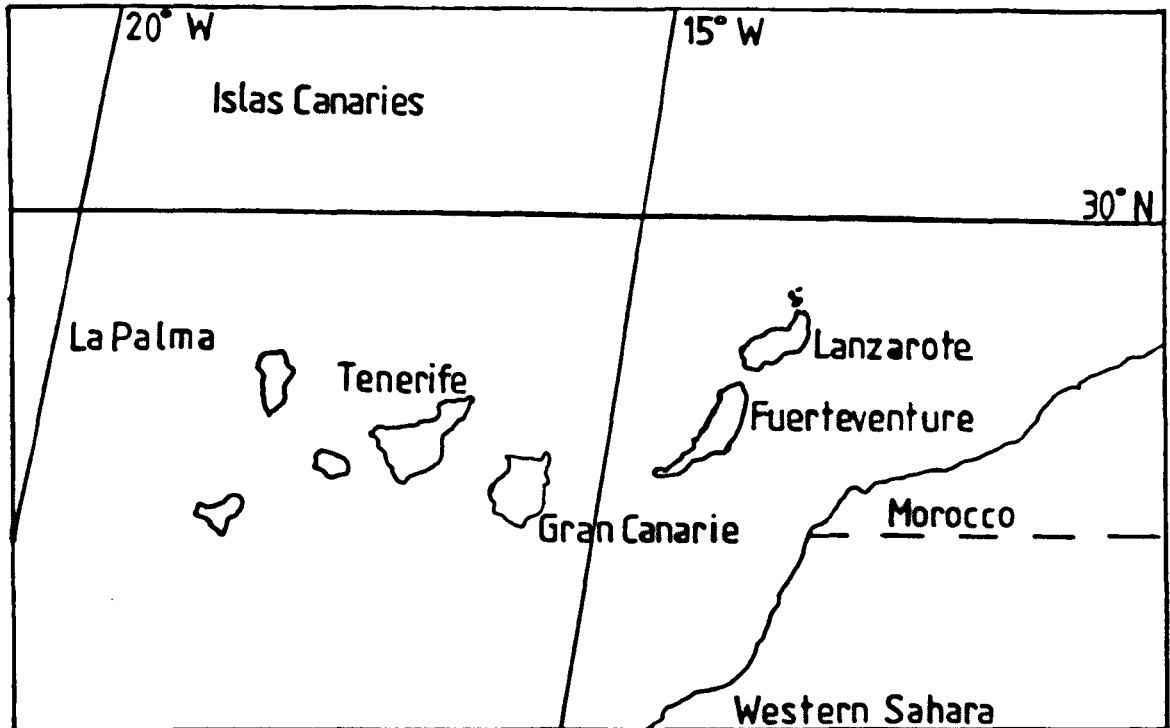
Figure 2.5 Location map of the Canary Islands.

The islands are volcanic and lie to the north east of
the modern main North Atlantic fracture zone. The
scale of volcanism can be seen when considering Mount
Teide, the main volcanic cone, on Tenerife. Mount
Teide stands 7118 m above the sea floor (Figure 2.6).

Samples were taken from three of the islands, Tenerife, La Palma and Lanzarote. A total of 19 flows, averaging about 2m thick were sampled with 15 different ages ranging from 1470 to 1971. The two oldest flows, sampled on Tenerife and La Palma, have both been dated at 1470. The date and position of these flows are based on records for the period and must be treated with caution.

Figure 2.6   Mt.Teide is 7118m above the seabed.

2.4.1 Tenerife. (28.1N, 16.3W)

Tenerife offers excellent opportunities for sample collection. The flows of interest are either very high in the mountains, and thus clear of vegetation, or at lower altitudes where they are

Figure 2.7 Tenerife sampling locations.
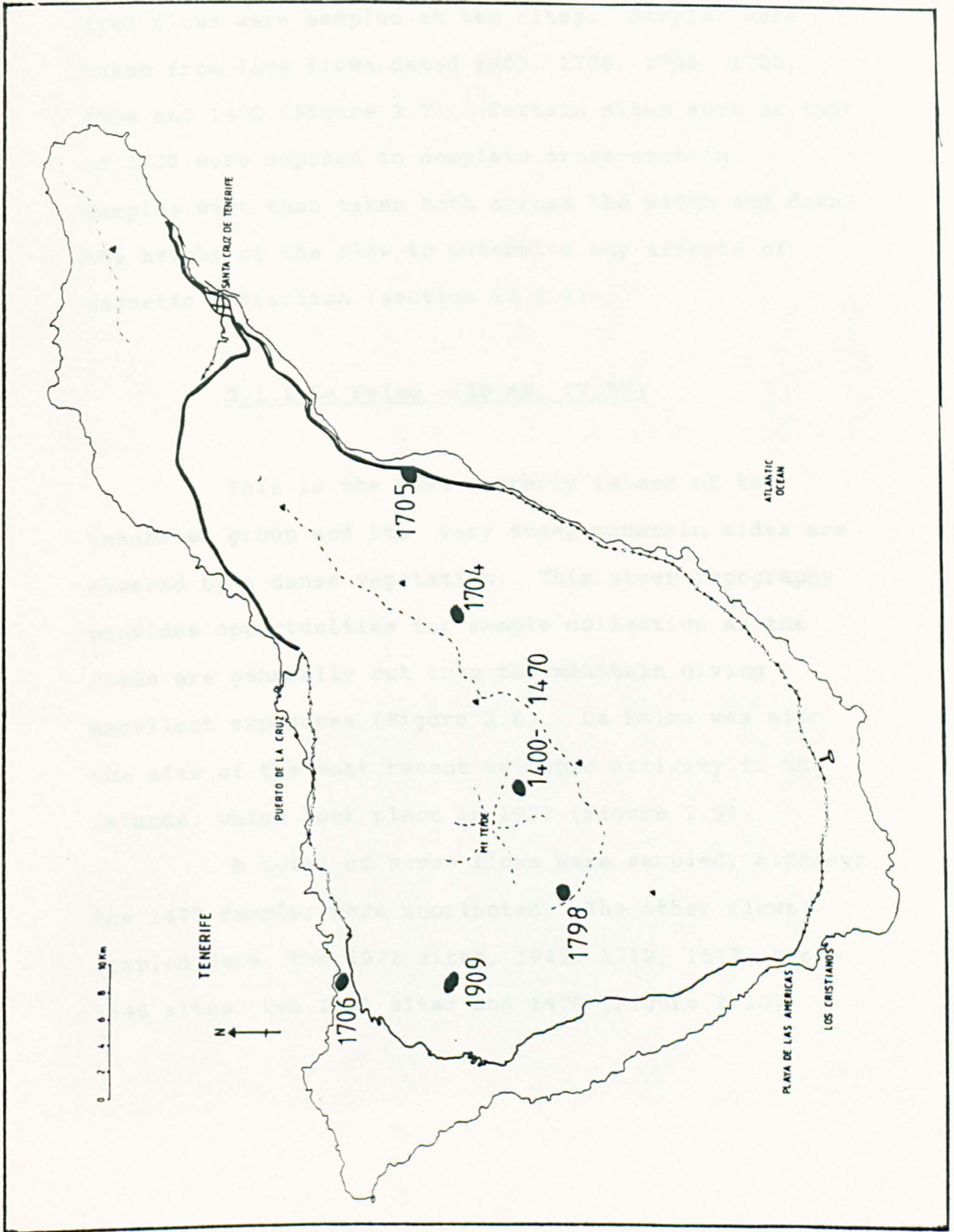
exposed in road cuttings. A total of six different aged flows were sampled at ten sites. Samples were taken from lava flows dated 1909, 1798, 1706, 1705, 1704 and 1470 (Figure 2.7). Certain sites such as that of 1705 were exposed in complete cross-section. Samples were then taken both across the width and down the height of the flow to determine any effects of magnetic refraction (section 13.2.2).

2.1.2 La Palma (28.4N, 17.5W)

This is the most westerly island of the inhabited group and its very steep mountain sides are covered by a dense vegetation. This steep topography provides opportunities for sample collection as the roads are generally cut into the mountain giving excellent exposures (Figure 2.8). La Palma was also the site of the most recent volcanic activity in the Islands, which took place in 1971 (Figure 2.9).

A total of seven flows were sampled, although the 1470 samples were unoriented. The other flows sampled were, two 1971 sites, 1949, 1712, 1677, two 1646 sites, two 1585 sites and 1470 (Figure 2.10).

Figure 2.8   The 1646 lava flow exposed in a long road
cutting on La Palma.

Figure 2.9   Cone of the 1971 La Palma eruption.

17

Figure 2.10 La Palma sampling locations.
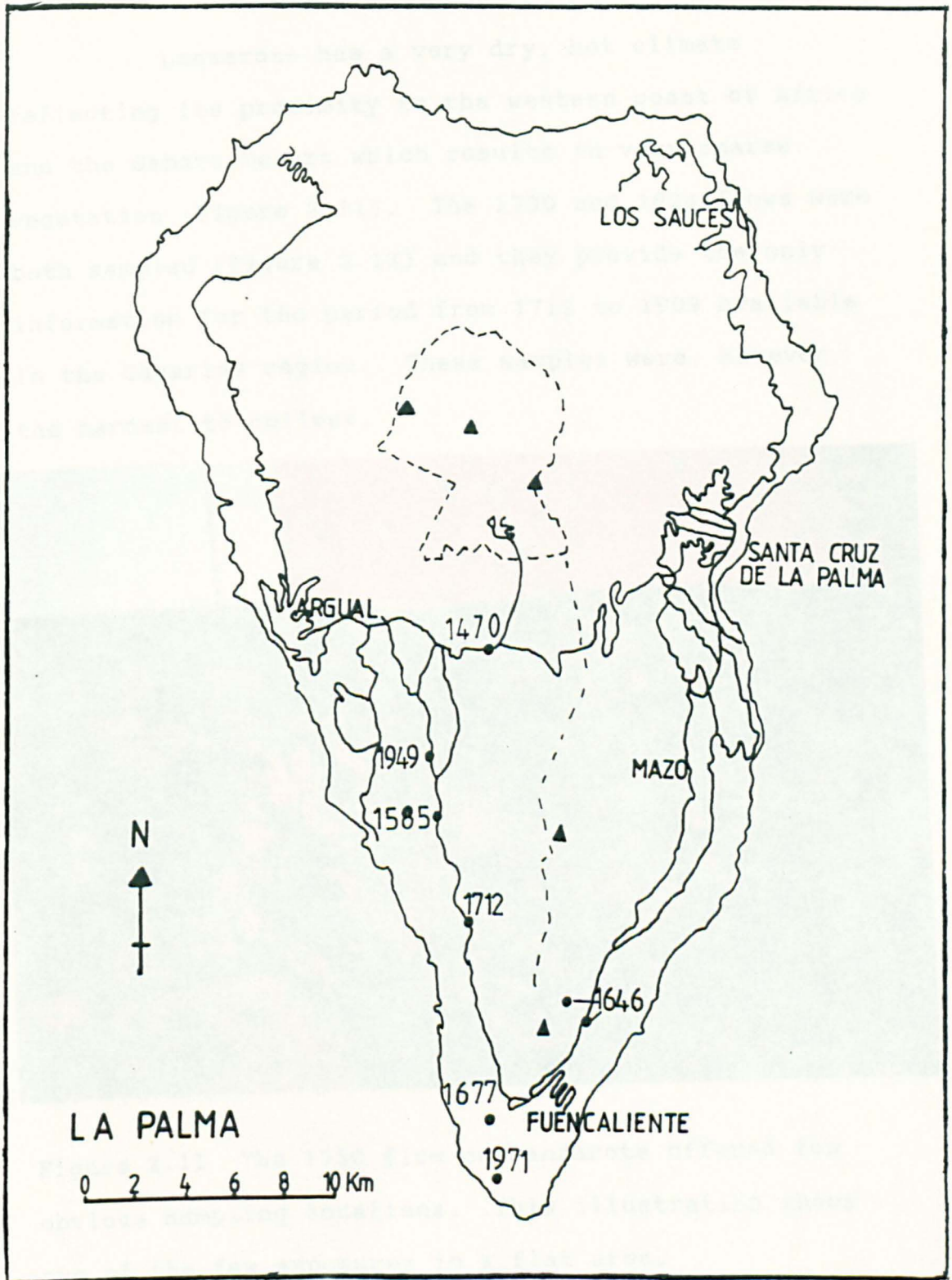
2.1.3 Lanzarote (29N, 13.3W)

Lanzarote has a very dry, hot climate reflecting its proximity to the western coast of Africa and the Sahara Desert which results in very sparse vegetation (Figure 2.11). The 1730 and 1824 flows were both sampled (Figure 2.12) and they provide the only information for the period from 1712 to 1909 available in the Canaries region. These samples were, however, the hardest to collect.

Figure 2.11 The 1730 flow on Lanzarote offered few obvious sampling locations. This illustration shows one of the few exposures in a flat area.

Figure 2.12 Lanzarote sampling locations.
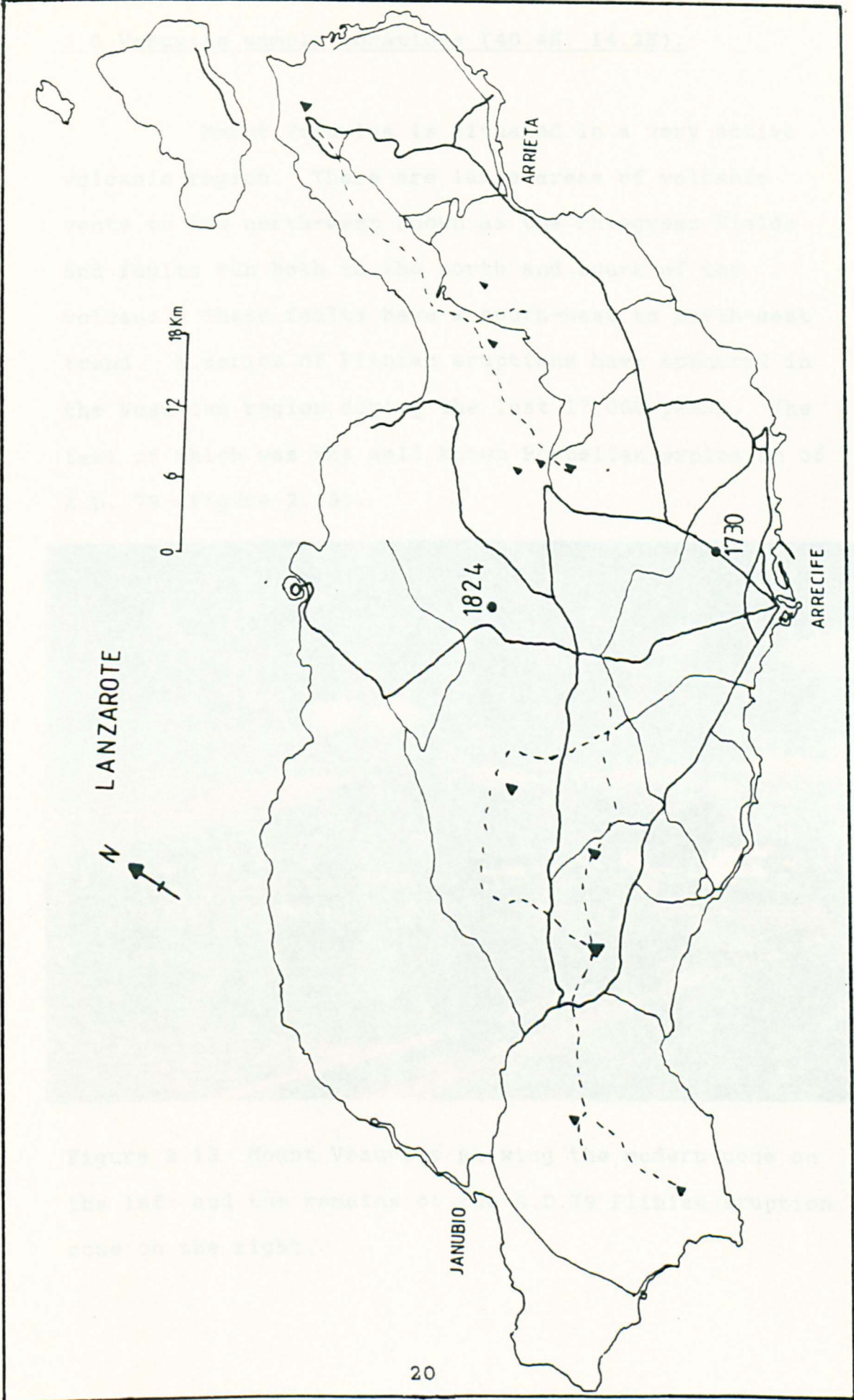
2.5 Vesuvian sample locations (40.4N, 14.2E).

Mount Vesuvius is situated in a very active volcanic region. There are large areas of volcanic vents to the north-west known as the Phlegrean Fields and faults run both to the north and south of the volcano. These faults have a south-west to north-east trend. A series of Plinian eruptions have occurred in the Vesuvian region during the last 17,000 years. The last of which was the well known Pompeiian explosion of A.D. 79 (Figure 2.13).

Figure 2.13 Mount Vesuvius showing the modern cone on the left and the remains of the A.D.79 Plinian eruption cone on the right.

The volcano, situated close to Naples (Figure
2.14), is under pressure to provide land for housing,
farming and, in its upper reaches, forestry. As a
result the lava flows are generally hidden by dense
vegetation or population and in-situ lava flows are
difficult to find with the exception of that from the
1944 eruption (Figures 2.15 & 2.16).
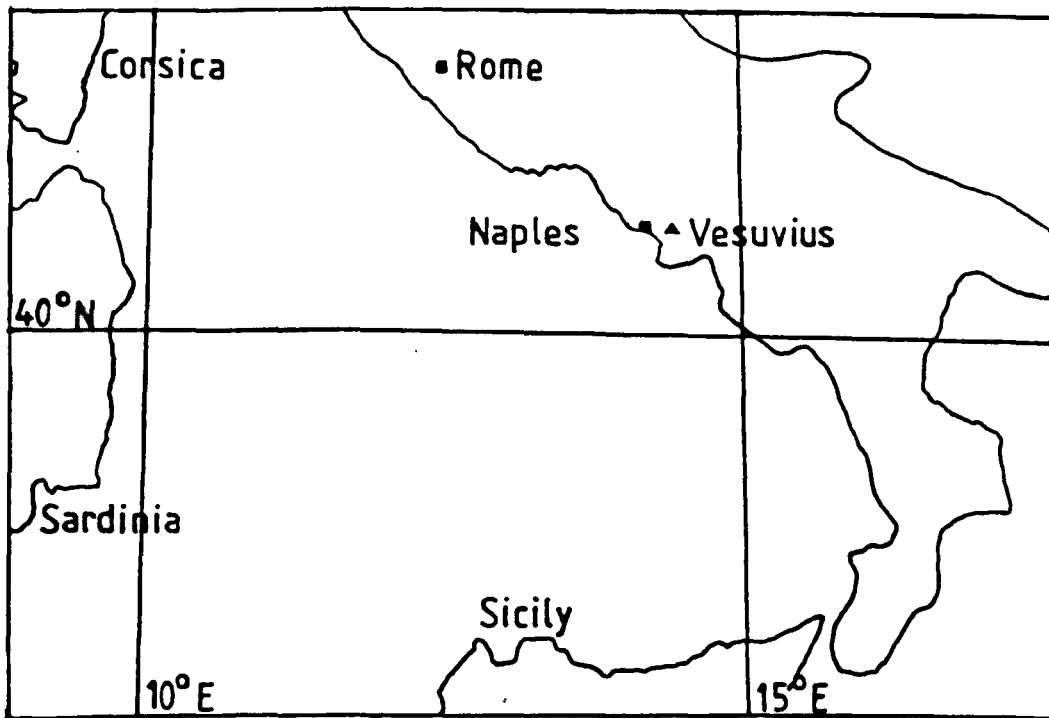
Figure 2.14 Location map for Mount Vesuvius.

The 79 A.D. eruption left large amounts of
airborne deposits but little lava. Accurate records
start with the explosive 1631 eruption. A total of
twenty lava flows, dated between 1697 and 1944, were
sampled from various locations around the mountain
(Figure 2.17).

Figures 2.15 & 2.16   The 1944 lava flow can be seen in the photographs heading towards Naples.
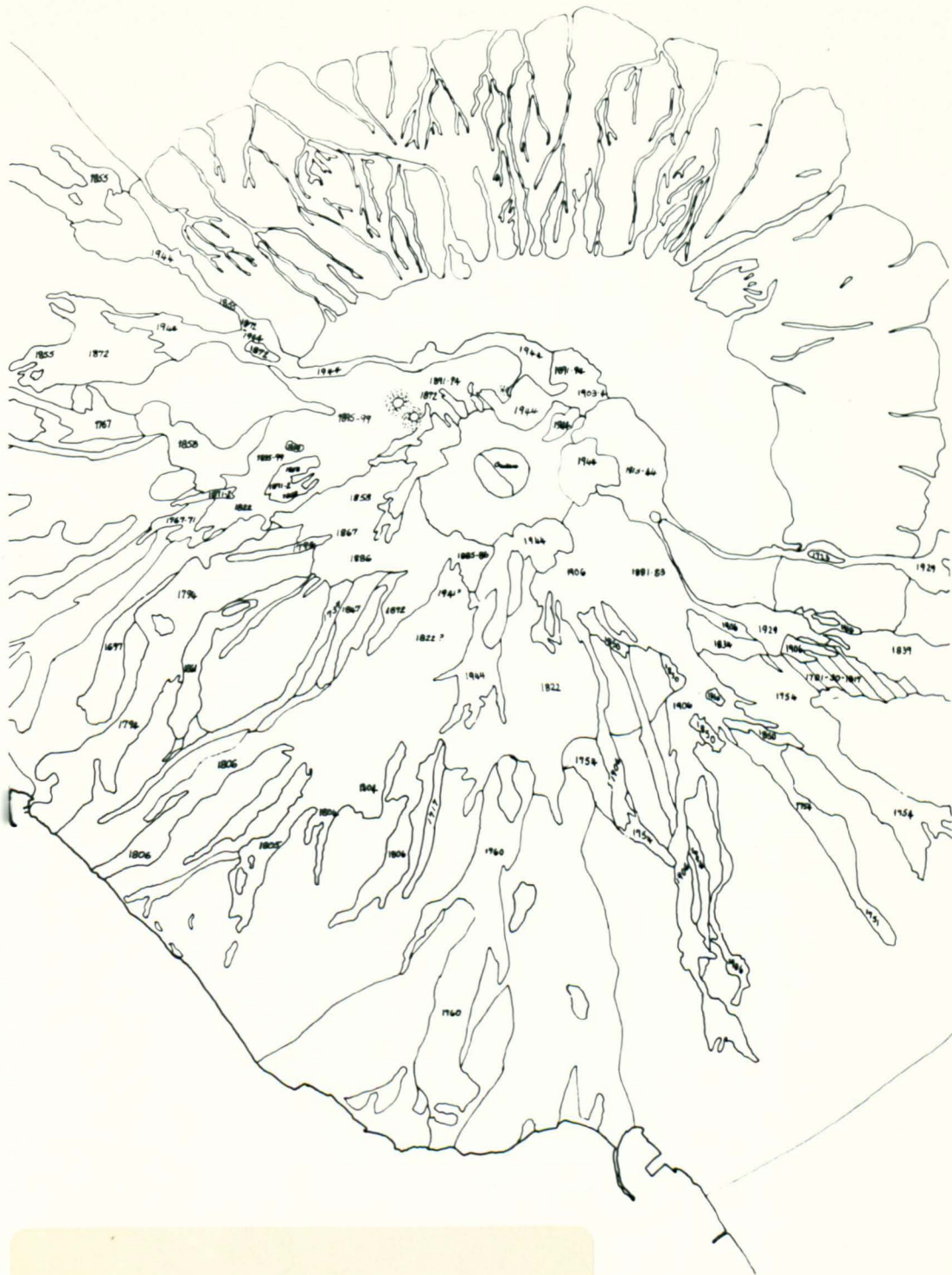
Figure 2.17 Mount Vesuvius sampling locations.

The thicknesses of the lava flows varied greatly but most exposures sampled were between 1 and 2m thick (Figure 2.18). The flows sampled were 1944, 1929, 1906, 1895, 1891, 1886, 1871, 1867, 1858, 1850, 1847, 1834, 1822, 1804, 1794, 1767, 1760, 1754, 1737 and 1697.

Figure 2.18 A quarry exposure showing the 1804-6 lava flow, between 1 and 2m thick, above two undated flows from earlier eruptions.

Magnetisation, magnetic properties and magnetic minerals.

This chapter discusses magnetism, magnetisation properties and the minerals which bear directly on this study. Explanations for the origin of the magnetic moment and domain structures within a magnetic mineral are included as they provide the basis for the macroscopic magnetic properties described.

The magnetisation of a rock depends on the way it became magnetised and the extent to which it is later demagnetised. This chapter contains explanations of both processes as well as details of the relevant magnetic minerals. A full explanation of the properties for the range of magnetic minerals can be found elsewhere (O'Reilly 1984).

3.1 Origin of Magnetic Moment.

All magnetic fields are created by the movement of electrons. The magnetic field of an atom results from two separate motions, the circular motion of the electron round the nucleus and the spin of the electron itself (Figure 3.1).

Schematic diagram showing
origins of para and
diamagnetism

electron spin
moment gives
rise to
paramagnetism

electron orbital
magnetic moment
important in diamagnetism
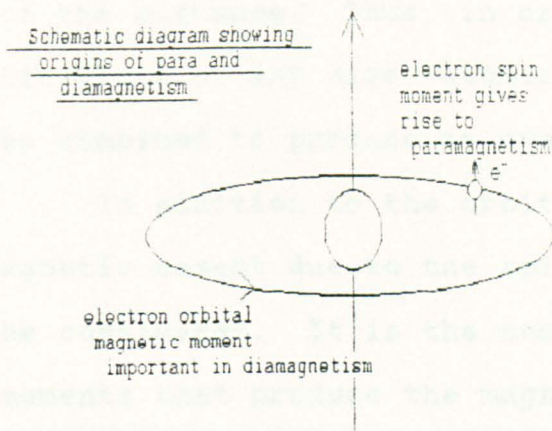
Figure 3.1 Simple model of the atom.

An electron moving at speed v round an orbit
radius r is equivalent to a current I moving round path
of length $2\pi r$, thus,

$$I = e v / 2 \pi r$$

where e = electronic charge. B, the magnetic field, can
be expressed as,

$$B = \mu I / 2 \pi r$$

and therefore

$$B = \mu e v / 4 \pi r^2,$$ where μ is the

permeability. However, $m_e v r$ has an integral value
of $h / 2 \pi$ where m_e is electron mass and h is Planck's
constant.

Substituting known values into this equation
the value for B is 6 Tesla, a very strong magnetic
field. This classical model of the atom shows that the
fields generated within the atom itself are much
greater than those emanating from outside.

A single atom's magnetic field, although
strong over a short distance, reduces as an inverse

cube of the distance. Thus, in order to produce a magnetic field of any size, atomic magnetic moments must be combined to produce an overall field.

In addition to the orbital magnetic moment the magnetic moment due to the spin of the electron must be considered. It is the combination of electron spin moments that produce the magnetic moments of importance in this study.

3.2 Magnetic Domains.

Spinning electrons arrange themselves within a crystal of a magnetic material and must fulfil the overall condition imposed on all systems; that of a tendency to the lowest possible energy level. The energy levels within a crystal depend in the main on crystalline anisotropy, exchange energy and magnetostatic energies due to an applied field. These must also be considered in conjunction with the energies required to separate the spin moments into units known as domains. As a single crystal, with all spins pointing in one direction, grows in size then its total energy level also grows. A point is reached where it is energetically more favourable to form regions containing antiparallel spins known as domains. The areas between regions of different spin are known as domain walls. The total energy after separation into domains is then lower than that before.

This process starts to occur at sizes greater than or equal to about 10^{-6}m in magnetite. Once it has started the condition for this subdivision to stop is given by:-

magnetisation energy = magnetisation + energy to form
before subdivision   energy after   a domain wall
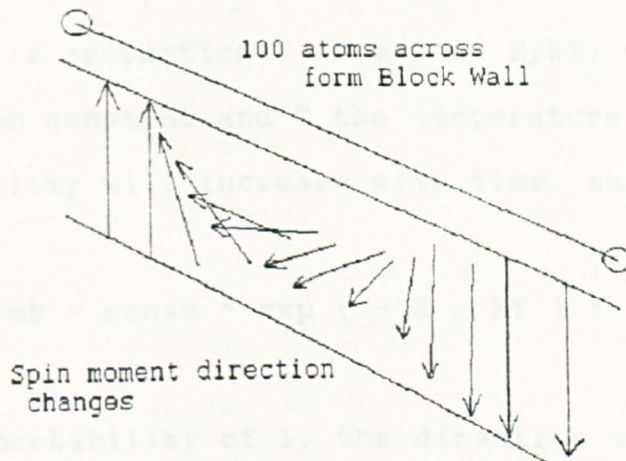
Figure 3.2 Domain (or Bloch) wall.

Domain walls are about 100 atoms thick and within them the direction of the atomic magnetic moment changes by 180 degrees (Figure 3.2). Domain walls are also known as Bloch Walls after Bloch (1930) who first described their function. Crystals in which more than one domain exist are known as multi-domain crystals. These spin arrangements are very temperature dependent. This temperature dependence is important since it determines the behaviour at the high experimental temperatures required to determine the secular

29

variation. The successful analysis of an assembly of single or monodomain grains was developed by Neel(1955). This theory dealt with the movement of a magnetisation between two directions.

The probability of a particle having the required energy, E, to change direction at a specific time, is governed by a Boltzmann distribution. Thus probability is proportional to exp (- E/kT) where k is the Boltzmann constant and T the temperature Kelvin. This probability will increase with time, such that:

$$prob = const * exp (- E / kT) * time.$$

Thus for a probability of 1, the direction will change, giving:

$$1 = const * exp (- E / kT) * time.$$

The time (t) likely to be required for one grain to change direction is known as its relaxation time which is given by:

$$1 / t = fo * exp (- E / kT).$$

Where fo is the frequency factor determining the response rate of the grains to the thermal vibration.

When considering a uniaxial system the energy
required is equal to the anisotropic constant K
multiplied by the grain volume v, therefore,

$$1 / t = fo * exp (- Kv / kT).$$

Thus the expression for the relaxation time
of a grain depends on the volume of the grain and the
temperature to which it is raised. There are therefore
two major functions which describe the grain. Firstly,
the blocking volume below which the magnetisation of a
grain, at a specific temperature, loses its
magnetisation. Secondly the blocking temperature above
which the grain remanence rapidly decays. The inverse
relationship of these functions can be seen on
examination of the above equation.

Single and multi-domain grains have very
different properties. For example, the saturation
remanence of multi-domain magnetite is a tenth of that
for single domain. On exposure to a magnetic field
their behaviour can also differ greatly depending upon
the exact nature of the field.

3.3 Macroscopic Magnetic Properties.

On an atomic level all materials react to
the presence of a magnetic field. The result of this
interaction will depend on which of the magnetic
moments, electron orbital or electron spin, is

dominant. In an atom with an even number of electrons the electrons are so arranged that the atom has zero net spin magnetic moment. This occurs because electrons are paired off with opposite spins in accordance with the Pauli Exclusion Principle. Thus in such an atom the orbital magnetic moment determines the magnetic field. In this case the application of a magnetic field alters the orbital angular velocity of the circulating electron. This induces a magnetic dipole moment which is in opposition to the field. The induced dipole has the effect of reducing the overall field within the material - an effect known as diamagnetism. The diamagnetic effect is present in all material subjected to a magnetic field. It is often hidden, however, because it is weak in comparison with the effect which results from net electron spin.

In some atomic and molecular structures the total electron spin angular momentum is not zero. Hence they have a net magnetic dipole moment in a particular direction. This is not normally observed, because the ordering influence of an applied magnetic field is required to line up the individual moments. Thermal agitation is usually sufficiently strong to stop any noticeable moment from being assembled. The effect is known as paramagnetism. Again it is a weak effect but stronger than that of diamagnetism. Paramagnetic and diamagnetic effects can both be present together.

None of the above effects are sufficiently strong or sufficiently long-lived to produce the magnetic storage capacity found in minerals such as magnetite. There must therefore be a stronger effect which has greater stability than those so far discussed.

Transition elements such as cobalt, manganese and iron have an arrangement of 3d electron orbits which allows the interaction of spin electrons. This interaction produces an ordered directional moment strong enough to withstand thermal agitation to very high temperatures. Thus they can store magnetic information over long periods of time. This interaction between spin electrons is known as an Exchange Interaction and the effect produced is known as ferromagnetism. Several variations exist producing varying degrees of ordered magnetisation in a magnetic field.

There are two special cases of ferromagnetism, ferrimagnetism and antiferromagnetism. It is into these groups that the magnetic minerals of interest fall. The perfect ordering of spins that exists in ferromagnets does not occur in ferrimagnetic behaviour. Here the spins are aligned in an antiparallel way, with one component larger in size than the other. This results in an overall magnetic moment in one direction which is stable up to high temperatures. In magnetite this spin ordering takes

place over longer distances than in iron. It is facilitated by an anion, usually oxygen and is known as superexchange. The temperature dependence of the exchange interaction gives rise to a point at which interaction breaks down, called the Curie point temperature.

Antiferromagnetic behaviour is the opposite of ferromagnetic behaviour. Instead of the spins being aligned in parallel they are antiparallel with a total magnetic moment for the electron spins of zero. It is only when this antiparallel alignment is imperfect that a net resultant magnetic moment exists. The temperature at which antiferromagnetism breaks down is known as the Neel temperature.

Thus a net magnetisation can be present due to three kinds magnetism, ferro, ferri and imperfect antiferromagnetism. Ferrimagnetic and imperfect antiferromagnetic behaviours are all present in the rocks in this study.

Superparamagnetism occurs when the magnetic grain size within a sample is very small, below its blocking volume (section 3.4.1) or the sample is above its blocking temperature. A material exhibiting superparamagnetism has no stability of remanence due to the continual realignment of the spin orientations by thermal vibration. It can, when exposed to a magnetic field, have a large magnetic moment, much stronger than that due to paramagnetic effects. The

grains are able to align with the field since thermal
vibration provides sufficient energy to overcome the
barrier between orientations. Consequentially the
susceptibility is greatly increased and the presence of
superparamagnetic material can therefore be
significant.

3.4 Remanent magnetisation.

The major relevant mechanisms by which rocks
in this study are rendered magnetic are outlined below.

3.4.1 Thermoremanent Magnetisation (TRM).

When a rock is cooled from above its Curie
temperature in a magnetic field it acquires a magnetic
moment as the individual grains cool through their
blocking temperatures. Grains do not all lock in their
magnetic moment at once. Multi-domain grains normally
do so first, within a few degrees of the Curie point,
the single domains follow as the rock cools further.
The intensity of magnetisation at a given temperature
is proportional to the applied field provided that
saturation does not occur. This provides a means of
determining the field value at the time of cooling.

The passage of time does not affect the
thermoremanent magnetisation of all grains since
relaxation times of single domain particles at $293^{\circ}K$

can be greater than that of geological time itself.
Partial reheating, due to an overlying lava flow, would
lift the rock's temperature above the ambient level but
still below that of the Curie temperature.
Consequentially when cooled a Partial Thermo Remanent
Magnetisation or PTRM can be formed.

3.4.2 Chemical Remanent Magnetisation (CRM).

A magnetic mineral produced either from an
altered magnetic mineral phase or a chemically produced
new mineral can acquire a magnetisation in the
direction of the ambient field. Such processes can
occur as a deposited material is subjected to the
increasing pressure of burial or as fluids move through
rock. These remanences can be stable in single domain
particles provided that the chemical reaction has
stopped.

3.4.3 Isothermal Remanent Magnetisation (IRM).

When a magnetic field is briefly applied to a
rock there may be a residual magnetisation the
magnitude of which depends on the strength of the field
which created it. This magnetisation is known as
Isothermal Magnetisation. Such IRM's can be caused by
lightning and can have strong moments. A large number

of such lightning struck samples were found in the
Vesuvian field area.

3.4.4 Viscous Remanent Magnetisation (VRM).

A viscous magnetic moment may be acquired
when a magnetic rock is left in an ambient field. An
increase in magnetisation in the field direction occurs
as grains on the boundary between superparamagnetic /
single domain have short relaxation time and therefore
continually remagnetise in the direction of an applied
field. The rate of acquisition of a viscous magnetic
moment is increased with increasing temperature. Very
few specimens in the study had any noticeable viscous
component. Those that did lost that component after
initial demagnetisation.

3.4.5 Anhysteretic and Rotational Remanent
Magnetisations.

Two remanences may be induced into a sample
during alternating field demagnetisation. Anhysteretic
moments are imparted when an alternating and constant
magnetic field are applied simultaneously to a sample
then a magnetic moment is imparted to the sample.
Consider the plane of the sample in which the steady
field acts. The sample is subjected to the constant
field plus or minus a component of the alternating

field. As a result the demagnetisation effect of the alternating field has a lesser effect in the direction of the steady field. The sample then has a residual magnetisation in the direction of the steady field after the alternating field has decreased to zero. This is called an Anhysteretic Remanent Magnetisation (ARM).

It is also possible to produce a Rotational Remanent Magnetisation (RRM) during the alternating field demagnetisation process. This is caused when the rotation of the sample is not in step with the applied alternating magnetic field. The sample is moved before the direction of the applied field is reversed. It is thus subjected to demagnetisation which is uneven in its application. This results in a net magnetic moment in a direction different to that originally present within the sample.

3.5 Demagnetisation techniques.

In order to analyse natural remanent magnetisations a variety of demagnetisation techniques can be employed. An outline of the two main procedures follows.

3.5.1 Alternating field demagnetisation.

Consider a rock sample containing both multi and single domain grains, with a range of coercive force values, and all initially magnetised in one direction but with random directions of easy magnetisation. Applying an alternating magnetic field of peak value F will drive those grains of coercive force less than F around a hysteresis loop. When this applied field is reduced slowly, grains with progressively lower coercive force align themselves along their easy axes. The randomisation of the magnetisation of these grains reduces the total magnetic moment. Thus by increasing the value of F the magnitude of the magnetic moment can be reduced in a stepwise fashion. Single domain grains generally have a higher coercive force than multi-domain grains. Consequentially they provide the more stable fraction of the moment, which becomes increasingly important at higher applied fields.

3.5.2 Thermal demagnetisation.

Thermal demagnetisation can be used to remove the whole or part of the magnetic moment of a sample. As a sample's temperature is increased the relaxation time of its grains is decreased so that, at a temperature T, a fraction of the grains will have

relaxation times of the same order as the time held at that temperature. Grains which have blocking temperatures at or below this temperature will probably resume a direction of magnetisation along their randomly orientated easy axes if they are cooling in zero field. Thus the magnetic moment of the sample is reduced. Increasing the maximum temperature after each measurement produces a series of magnetic moments of decreasing magnitude.

3.6 Magnetic minerals and their properties.

Iron oxide minerals are the carriers of magnetic moment relevant to this study. The level of titanium within them has an important role in the behaviour of these natural oxides. Four groups of minerals are described below; the first two contain the important magnetic minerals in igneous rocks and the third includes the weathered products of the former. The fourth group is that of the sulphides, which occur in both igneous and weathered rock.

3.6.1 Titanomagnetites

Titanomagnetites are solid solutions of Magnetite (Fe_3O_4) and Ulvospinel (Fe_2TiO_4). They have a face centred cubic structure of closely packed anions

(Figure 3.3). The end members of the titanomagnetite series are considered first.
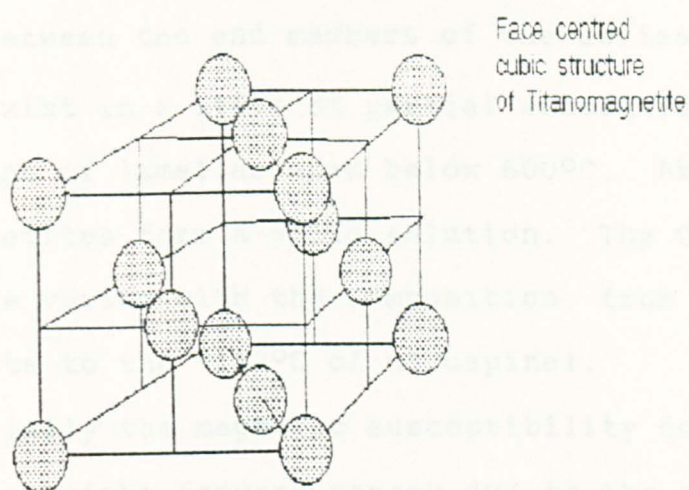
Face centred cubic structure of Titanomagnetite

Figure 3.3 Titanomagnetite.

Magnetite has a cubic inverse spinel structure and is ferrimagnetic by virtue of the arrangement of the Fe^{+2} and Fe^{+3} ions. Two of the three magnetic moments cancel leaving a resultant magnetic moment. The Curie temperature of magnetite is 580°C. At -150°C it undergoes a structural change from a cubic to an orthorhombic structure, called the Verwey Transition.

Ulvospinel, like magnetite, has an inverse spinel structure with one of the Fe^{3+} in the lattice framework being replaced by a Ti^{4+}. This titanium does not have a magnetic moment and so the magnetic moments of the iron cancel and only a weak ferrimagnetic effect is left. The Curie temperature is -153°C and thus it is a paramagnetic substance at room temperature.

41

Titanomagnetites have a formula which reflects their variable composition, $xFe_2TiO_4(1-x)Fe_3O_4$, between the end members of the series. They commonly exist in a state of partial exsolution as intergrowths of lamellae when below 600°C. Above 600°C titanomagnetites form a solid solution. The Curie temperature varies with the composition, from the 580°C of magnetite to the -153°C of ulvospinel. Consequentially the magnetic susceptibility does not vary in a straight forward manner due to the structure of the solid solution and fractions within it.

3.6.2 Titanohaematites

Ilmenohaematite compositions range between Haematite Fe_2O_3 and Ilmenite $FeTiO_3$.

Haematite is a major carrier of magnetic remanence in sediments, but it is not generally the main carrier of the initial magnetic moment in igneous rock. It is, however, found in igneous rocks as a result of alteration and in oxygen rich volcanics.

Haematite and titanohaematites have a hexagonal close packed, corundum type of structure (Figure 3.4). It has an antiferromagnetic magnetic moment, which is weak compared to that of the magnetites and is attributed to the imperfect cancellation of the spin magnetic moments due to a degree of spin canting.
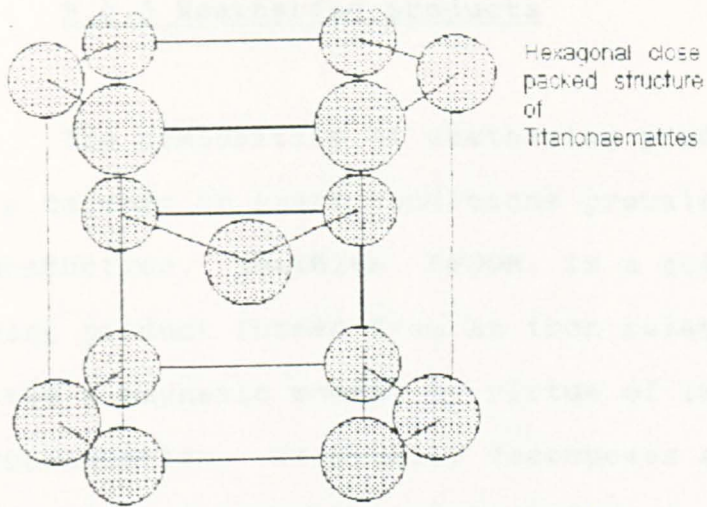
Figure 3.4 Titanohaematites.

The Curie point of haematite is 680°C and
haematite is very anisotropic in its susceptibility. A
low temperature change can sometimes be seen at -20°C,
called the Morin Transition, when the spin canting
disappears along with some of the recorded magnetic
information.

At the other end of the titanohaematite
series is ilmenite (FeTiO$_3$). Ilmenite exhibits
paramagnetism above 60°K and thus when pure does not
hold any useful information. Titanohaematitie
properties are a mixture of those of the two end
members of the series. Curie Temperatures range from
-213°C to 675°C depending on the composition.

3.6.3 Weathering products

The composition of weathering produced minerals depends on exact conditions prevalent during their production. Goethite, FeOOH, is a common weathering product formed from an iron related mineral. It carries a magnetic moment by virtue of imperfect antiferromagnetism. It usually decomposes at about $120^{\circ}C$ and has a theoretical Curie Point of about 250 - $300^{\circ}C$.

Maghaemite, Fe_2O_3, can be produced by weathering or lava oxidation and has the same composition as Haematite but the structure of magnetite. On reaching $300^{\circ}C$ it inverts to Haematite.

3.6.4 Sulphides

The only magnetic iron sulphide found in igneous rock is Pyrrhotite FeS_{1+x} where x has a value of between 0 and 1. It has a distinctive change in magnetic properties at $200^{\circ}C$ due to a structural reordering. This gives it a peak in magnetisation and susceptibility at $200^{\circ}C$. It has a Curie point of around $320^{\circ}C$, depending on composition.

Chapter 4.

Magnetic Susceptibility.

Accurate determination of the palaeomagnetic field ultimately depends on the rocks which record the magnetic field information. If they distort the ancient field then misleading results are obtained. Measurements of anisotropy of susceptibility show any preferential directions of magnetisation present in the sample allowing either a correction to be made or the samples to be discounted in any direction calculation.

This chapter covers the measurement of anisotropy of susceptibility; bulk, high and low temperature susceptibility. High and low temperature susceptibility measurements increase the information extractable from samples by exposing them to temperatures between -194 and $+700^{o}C$. Samples were then classified according to the group to which their resulting susceptibility curves belonged.

4.1 Anisotropy of magnetic susceptibility.

The lava samples were not magnetically homogeneous. Each had a magnetic fabric which could vary substantially according to the direction of an applied field; such rock is said to be anisotropic. In

an anisotropic rock an applied field will induce a component of magnetisation at 90° to the applied field.

The main factors affecting a sample's anisotropy are its shape, non uniform internal structure, net grain shape and the stress induced in the sample. Whilst the shape of samples is easily controlled, the magnetocrystalline structure, grain shape and strain anisotropy are not. A non uniform sample shape will have a non uniform magnetic field around it. Thus sample cores are sawn into lengths which produce the most uniform field. The optimum length to diameter ratio for a cylinder, according to Sharma (1966), is 0.9 and cores were sawn accordingly, (althougth many people take 0.87, Collinson 1983).

Anisotropic effects do, however, allow an insight into the rock fabric. By measuring the relative values of the susceptibility in different directions the internal rock fabric can be assessed and the extent of any flow structures becomes apparent.

4.1.2 Theory of susceptibility measurement.

Sample susceptibility, K, is measured along three mutually perpendicular axes. A sample with the same susceptibility in each of the three directions can be represented in terms of a sphere, no one direction having a greater susceptibility than any other. In most cases, however, samples have unequal

susceptibilities, K_{max}, $K_{intermediate}$ (K_{int}) and K_{min}. The susceptibility can then be represented in terms of an ellipsoid, where the susceptibility in each direction is represented by the magnitude of the semi-axis of the ellipsoid in that direction (Figure 4.1).
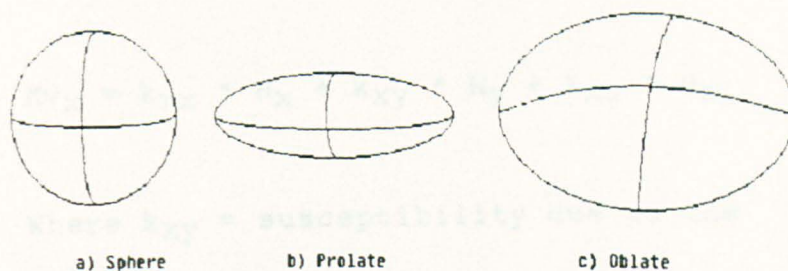

a) Sphere   b) Prolate   c) Oblate

Figure 4.1 Ellipsoids of susceptibility.

If K_{max} > K_{int} = K_{min} then the susceptibility ellipsoid is prolate, cigar-shape, its susceptibility is nearly linear. If K_{max} = K_{int} > K_{min} then the susceptibility ellipsoid is oblate, disc-shape and it has a planar shape or foliation (Tarling, 1983).

Results are usually presented in terms of the susceptibility ratios between the three normalized axes. The letters P, L and F refer to the ratios of one axis susceptibility to another where:

P = (K_{max} / K_{min}) : Degree of anisotropy.

L = (K_{max} / K_{int}) : Linearity; K_{max} > K_{int} = K_{min}.

F = (K_{int} / K_{min}) : Foliation; K_{max} = K_{int} > K_{min}.

47

4.1.3 Susceptibility measurement.

If a non isotropic sample is exposed to a
magnetic field H then the volume magnetisation, Mv, in
any one direction, say x, can be expressed as follows:-

$$Mv_x = k_{xx} * H_x + k_{xy} * H_y + k_{xz} * H_z.$$

Where k_{xy} = susceptibility due to the
contribution of field applied in the y direction
diverted along the x axis.
It can be shown that, by energy considerations,

$$k_{xy} = k_{yx} \qquad \text{(Collinson, 1983)}.$$

The relative values of susceptibility can
then be calculated from the measurement of the
magnetisation, Mv, about three mutually perpendicular
axis. This is done with a laboratory anisotropy meter
in which the sample is spun in a magnetic field of
approximately 0.7mT, generated by Helmholtz Coils, at a
frequency of 10kHz. A signal is generated by the
interaction of the field and sample which is detected
by an orthogonal pair of Helmholtz coils and Fourier
analysed.

The sample is turned about 3 mutually
perpendicular axes to produce the relative values of
susceptibility in each direction. Finally the values

of room temperature bulk susceptibility measurements
were included in the calculation of principle
susceptibilities. These bulk measurements were made
with a Bartington susceptibility meter at a frequency
of 1470Hz.

4.1.4 Results of susceptibility experiments.

The sample anisotropic susceptibilities were
measured for all the lava flows. The results can be
considered as two properties. The values of P give an
overall indication of the degree of anisotropy present
in the samples, while the relative sizes of L and F
determining whether lineation or foliation is dominant.

Table 4.1 Aniosotropy.

a) Canary Islands.

Year	Bulk Sus m-3	P	L	F
1470LP	57483	1.018	1.011	1.007
1470T	7487	1.090	1.025	1.064
1585S1	41157	1.013	1.008	1.005
1585S2	29767	1.020	1.012	1.008
1646S1	59699	1.028	1.018	1.010
1646S2	50098	1.011	1.009	1.003
1677	29514	1.013	1.021	1.028
1704	9922	1.016	1.005	1.011
1705	17904	1.002	1.002	1.000
1706	24532	1.034	1.024	1.010
1712	34228	1.014	1.004	1.010
1730	2801	1.004	1.003	1.001
1798	9799	1.026	1.013	1.013
1909	28668	1.041	1.019	1.022
1949	30868	1.004	1.002	1.002
1971S1	42782	1.044	1.009	1.035
1971S2	39992	1.041	1.012	1.029
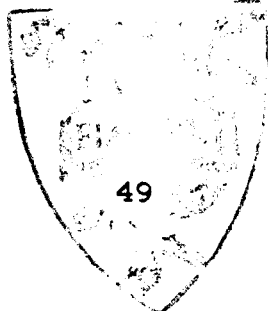
<u>b) Mount Vesuvius.</u>

Year	Bulk Sus m-3	P	L	F
V1697	9572	1.013	1.009	1.004
V1737	19086	1.008	1.003	1.005
V1754	15264	1.003	1.002	1.001
V1760	11316	1.006	1.003	1.002
V1767	15650	1.018	1.009	1.009
V1794	13181	1.004	1.001	1.003
V1804	31826	1.006	1.004	1.003
V1822	42847	1.005	1.004	1.001
V1834	5011	1.012	1.001	1.011
V1847	18737	1.007	1.002	1.005
V1850	21613	1.012	1.007	1.005
V1867	14351	1.004	1.001	1.003
V1871	34587	1.010	1.008	1.002
V1872	15415	1.004	1.002	1.001
V1886	37291	1.011	1.005	1.006
V1891	50218	1.011	1.004	1.007
V1895	37085	1.004	1.002	1.003
V1906	24218	1.005	1.003	1.002
V1929	10763	1.009	1.005	1.004
V1944	6524	1.006	1.005	1.001

As whole the samples show a very low degree of anisotropy (Figure 4.1), with the maximum difference in P being less than 5%.
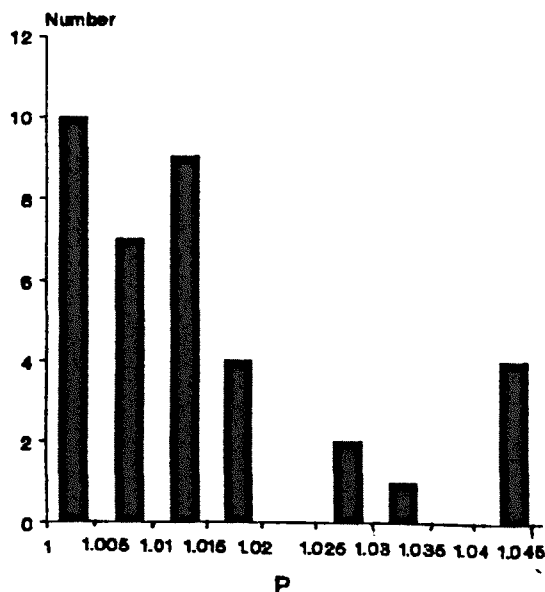

Figure 4.1   Histogram of the degree of susceptibility for all samples.

Neither the Canary Islands or Mount Vesuvius
samples proved to have a distinct lineation or
foliation although those from the Canary Islands did
show a slightly larger range of L and F values (Figure
4.2). These values, however, represent only small
changes in magnetic fabric as typical values range from
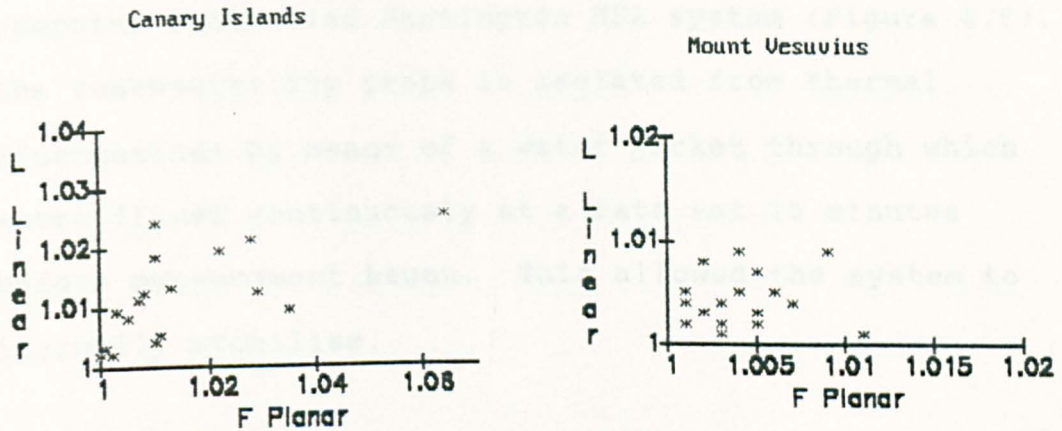1.01 to 1.20 in igneous rocks (Collinson 1983).

Canary Islands

Mount Vesuvius

Figure 4.2 Foliation / lineation.

4.2 Temperature dependance of magnetic susceptibility.

Susceptibility measurements above and below
room temperature present an opportunity to classify the
samples according to their behaviour. The
susceptibility of samples from each flow were measured
between room temperature (20°C) and either low(-194°C)
or high(700°C) temperature.

Variation of susceptibility with temperature
is more complex than for induced or saturation
magnetisation because the relaxation time of grains

varies according to crystal structure, grain volume and temperature.

4.2.1 High and low temperature susceptibility measurement.

The measurements were carried out on a computer controlled Bartington MS2 system (Figure 4.3). The susceptibility probe is isolated from thermal fluctuations by means of a water jacket through which water flowed continuously at a rate set 15 minutes before measurement began. This allowed the system to thermally stabilise.
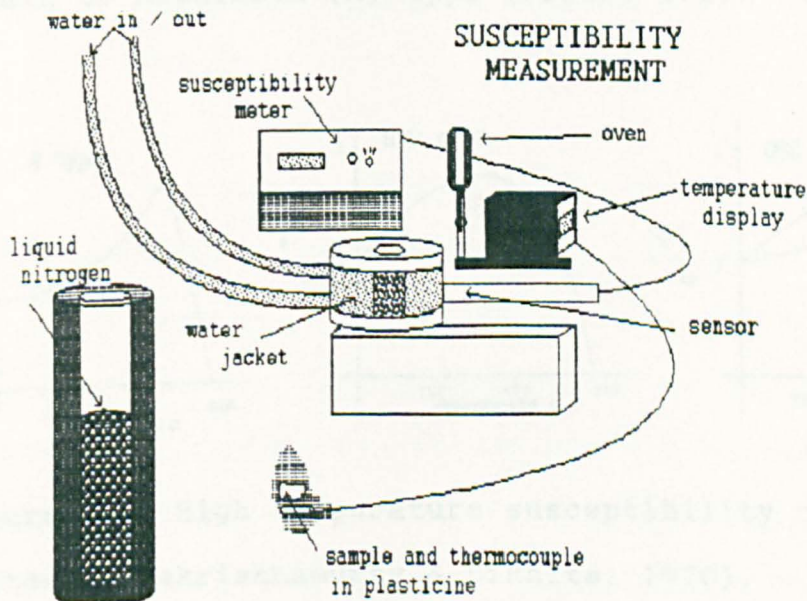

Figure 4.3   Susceptibility measurement.

Measurements could be made either as the samples were heated to 900°C in a small oven or as they

warmed to room temperature after they had been cooled
in liquid nitrogen (-194°C). The simple operation of
the susceptibility meter allowed a large number of
samples to be measured.

4.2.2 High temperature susceptibility result classification.

The results were interpreted using the work
of Radhakrishnamurty & Likhite (1970) which is based on
the separation of behaviour into three types.
The three basic categories described were single domain
(S/D) curves, quasi-single domain (QSD) and multi-
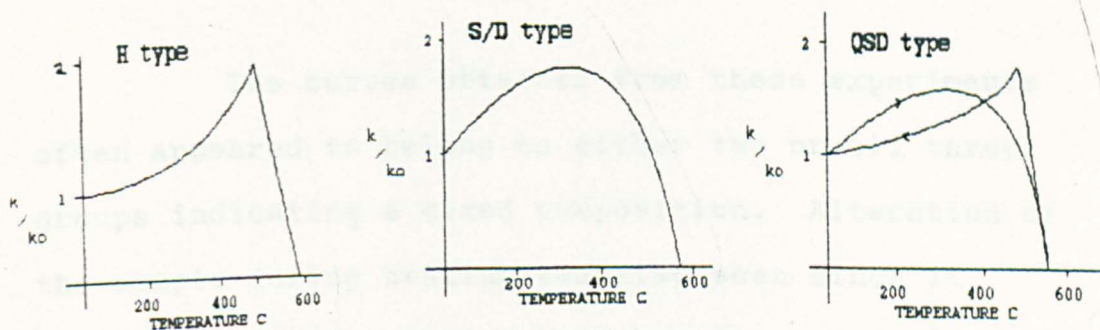domain or Hopkinson (H) type (Figure 4.4).

Figure 4.4 High temperature susceptibility curves.
(After Radhakrishnamurty & Likhite, 1970).

Single domain crystals produce a smooth peak
which is blocking temperature dependent. The
susceptibility ratio decreases far more slowly with
increased temperature than that for the Hopkinson type

multi-domain curves. Single domain crystals can
display different curves on heating due to their
dependence on crystal factors such as strain.
Radhakrishnamurty & Likhite (1970) describe one such
reaction in terms of a third group, quasi-single domain
behaviour. The heating curve appears like a single
domain but the cooling curve appears like that of a
multi-domain.

Hopkinson (1889) described an effect in iron
which involved the peaking of the susceptibility just
below the Curie temperature. This effect also occurs
in multi-domain magnetic mineral samples.

4.2.3 High temperature susceptibility
results.

The curves obtained from these experiments
often appeared to belong to either two or all three
groups indicating a mixed composition. Alteration of
the sample during heating was also seen since it
resulted in differently shaped heating and cooling
curves. A selection of the high temperature curves are
shown in Figure 4.5 and the results are listed in Table
4.2.

The V1944 sample illustrates the typical H
type multi-domain curve whilst the V1794 sample
approaches a pure single domain curve. In reality it

is a mixed curve illustrating the fall off associated

with the H type curve. Quasi-single domain (QSD)

Table 4.2 Low and high temperature susceptibility

results.

a) Canary Islands.

Year of flow	Lt Sus group	Ht Sus group
1971	1	MD
1949	3/1	MD
1909	1	MD/sd
1824	1	MD
1798	1	MD
1730	2/1	QSD
1712	1	MD
1706	3	MD
1705	3	MD
1704	1	MD
1677	1	MD
1646	1	MD
1585	1	MD
1470T	3	--
1470LP	3	QSD/MD

b) Mount Vesuvius.

Year of flow	Lt Sus group	Ht Sus group
1944	3/2	MD/sd
1929	1/3	MD/sd
1906	3	MD/sd
1895	3/1	MD
1891	1/3	MD/sd
1886	3	QSD/MD
1871	3/1	MD/sd
1867	3	SD
1858	1	MD
1850	3/1	QSD/MD
1847	3/1	MD
1834	2/1	MD
1822	1	MD/sd
1804	1	MD
1794	2	MD/sd
1767	1/3	MD
1760	1/3	MD
1754	3/2	MD/sd
1737	1/2	MD/sd
1697	1/3	MD

Figure 4.5 High temperature susceptibility curves

V1822   V1804   V1794
V1767   V1760   V1754
V1737   V1697   1971LP
1949LP   1909T   1824LZ
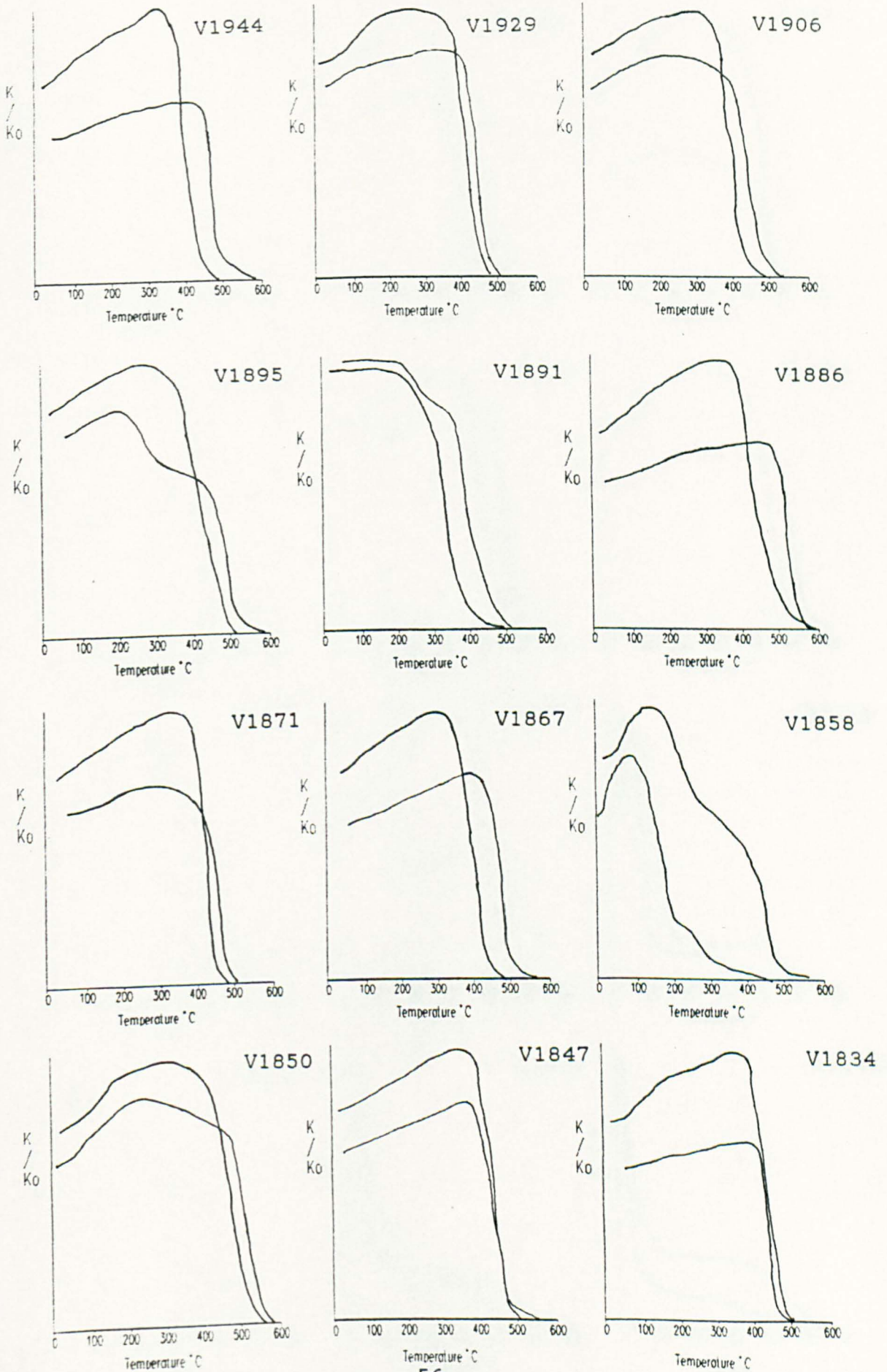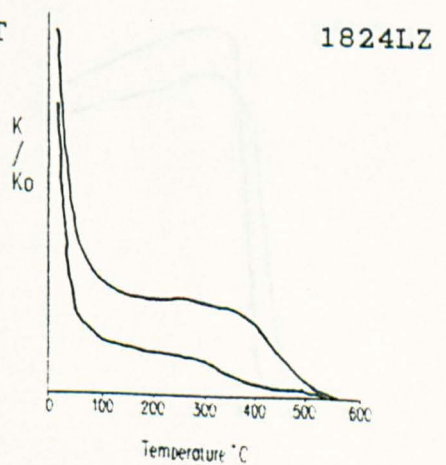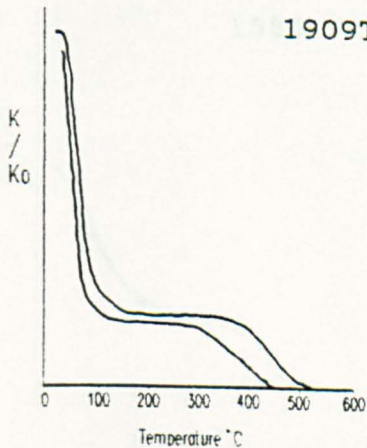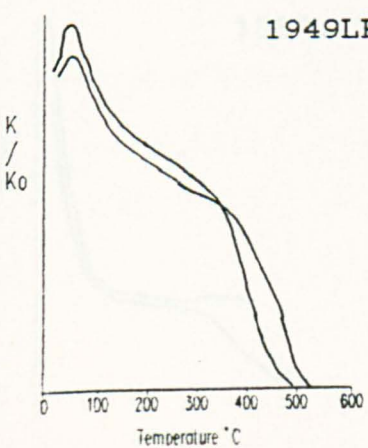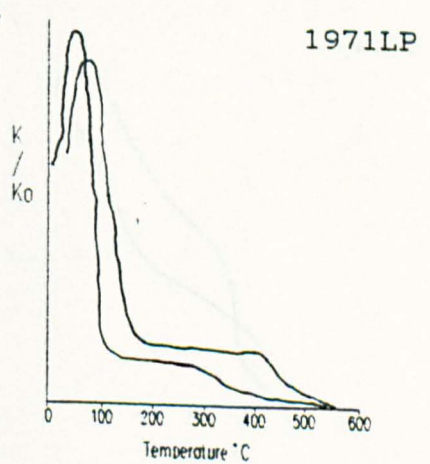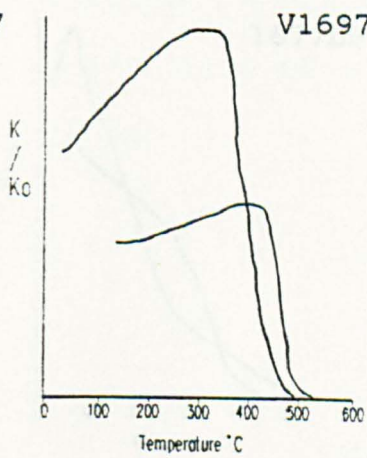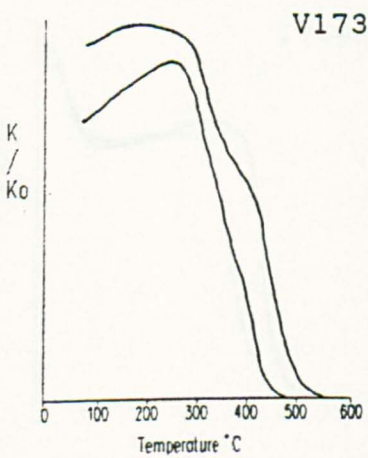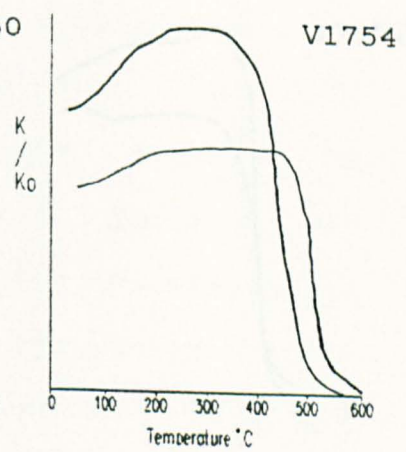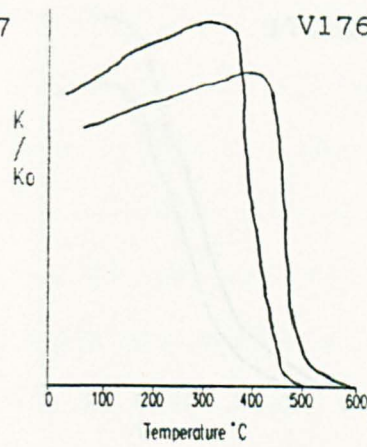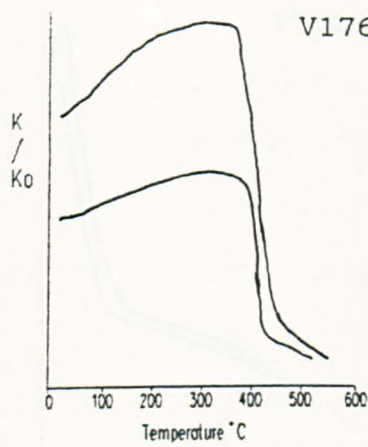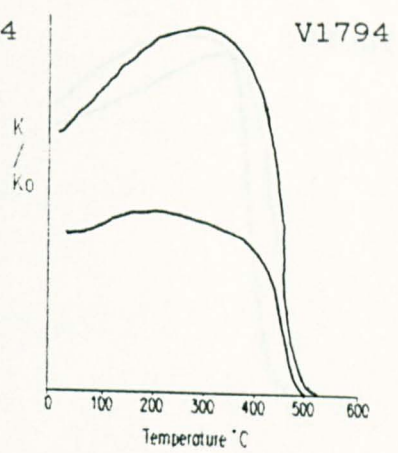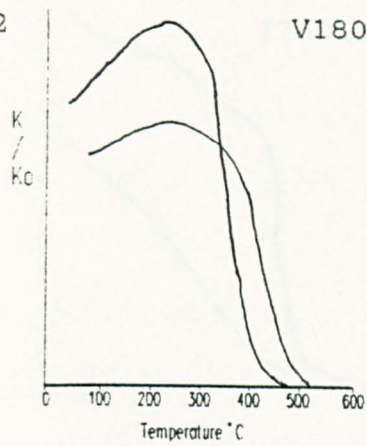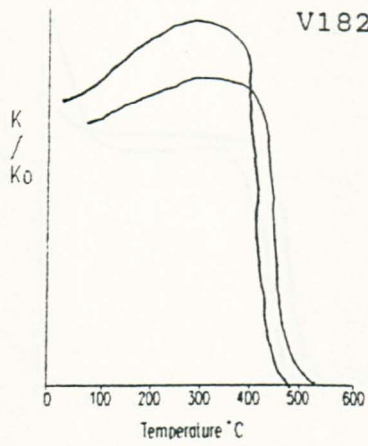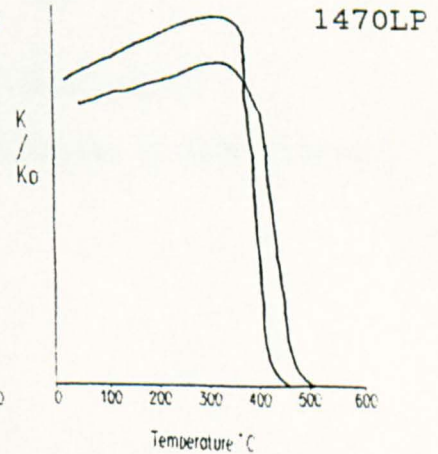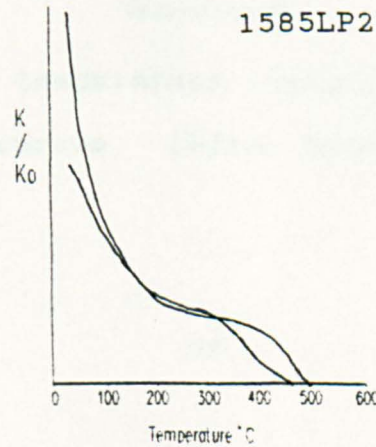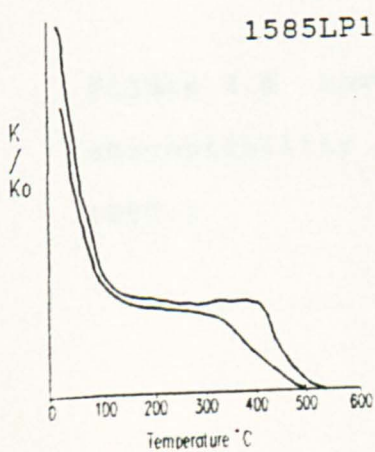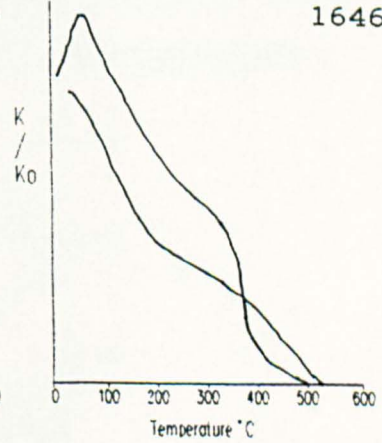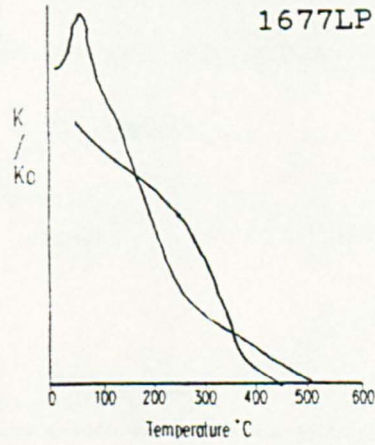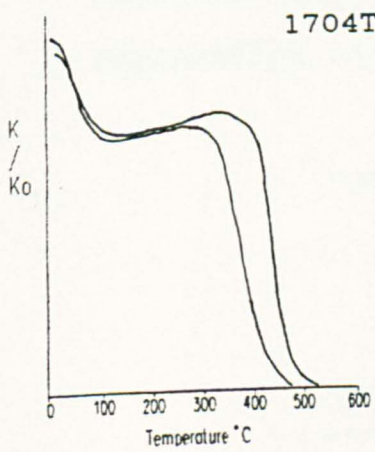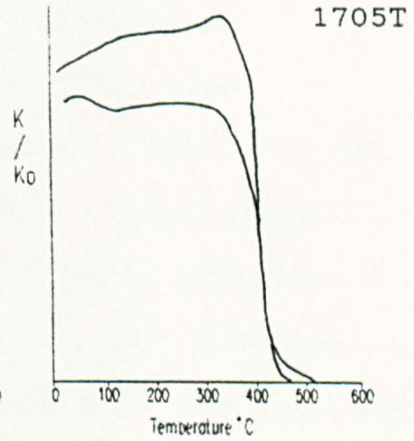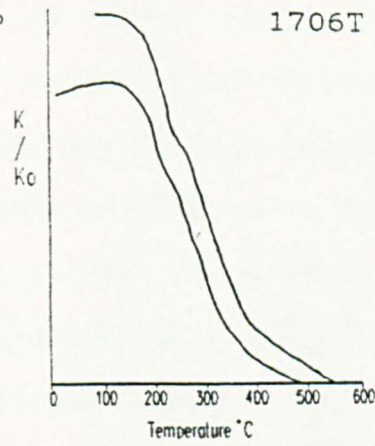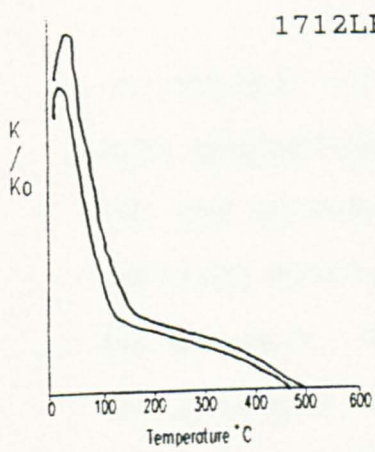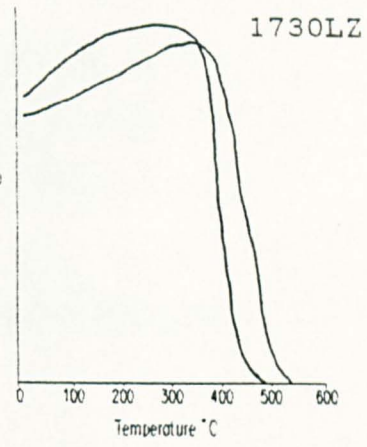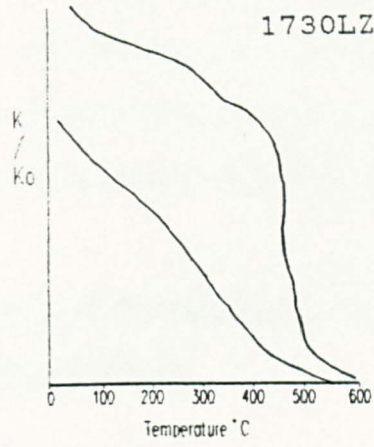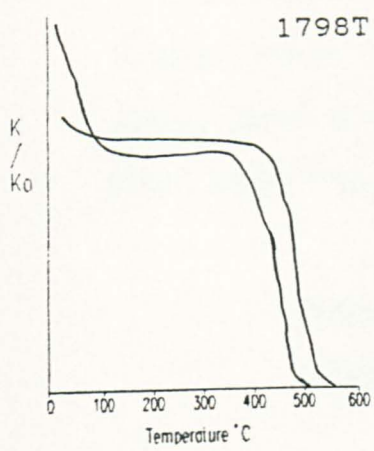
curves are shown by V1886 and 1730LZ. The 1705T sample
mirrors the Radhakrishnamurtys QSD + H type becoming an
H type curve with alteration superimposed on it.
Lower case characters indicate a small component of
that high temperature susceptibility group.

4.2.4 Low temperature susceptibility classification.

The interpretation of low temperature
susceptibility curves is still debatable. The
main protagonists are Radhakrishnamurty (1972, 77, 78,
79) and Senanayake & McElhinny (1981). Their ideas
conflict mainly on the explanation for the behaviour
for group 2. Radhakrishnamurty et. al. believe that
the presence of cation deficient magnetite explains the
behaviour whilst Senanayake & McElhinny believe the
explanation lies in the presence of titanomagnetite
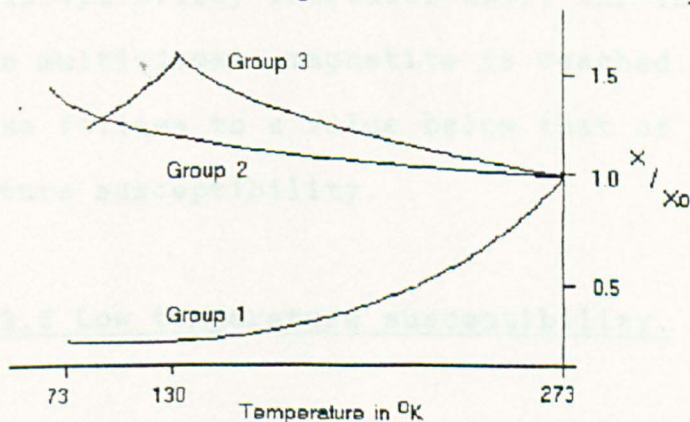
Figure 4.6 Low temperature classification of
susceptibility curves. (After Senanayake & McElhinney,
1980.)

59

containing exsolved ilmenite lamellae. The Senanayake
& McElhinny classification for low temperature
behaviour was used (Figure 4.6).

Group 1: these samples show a decrease in
susceptibility ratio down to around 0.1 to 0.5 with no
significant break in curve. This behaviour is
indicative of mainly multi-domain titanomagnetite rich
in titanium.

Group 2: McElhinny's theory states that
susceptibility increases to a value between 1.1 to 1.5
of that found at room temperature with no significant
break in curve. It is attributed to titanomagnetite
grains with exsolved ilmenite lamellae behaving as
single domains.

Group 3: When magnetite rich titanomagnetite
is present susceptibility increases until the isotropic
point of pure multi-domain magnetite is reached. A
rapid decrease follows to a value below that of initial
room temperature susceptibility.

4.2.5 Low temperature susceptibility.

Precise classification into one of the three
groups was not always possible. The mixed composition
of the samples produced combined curves. In addition
to mixed curves behaviours other than those described
above may be seen. Samples with different mineral

60

content to those included above will produce a different curve. Haematite or maghemite for example, give different curves altogether. Maghemite, of single domain structure, gives an almost flat line with very little change in susceptibility. Specimen sample results can be seen in Figure 4.7 and results are listed in Table 4.2.

Figure 4.7 Low temperature susceptibility curves.

63
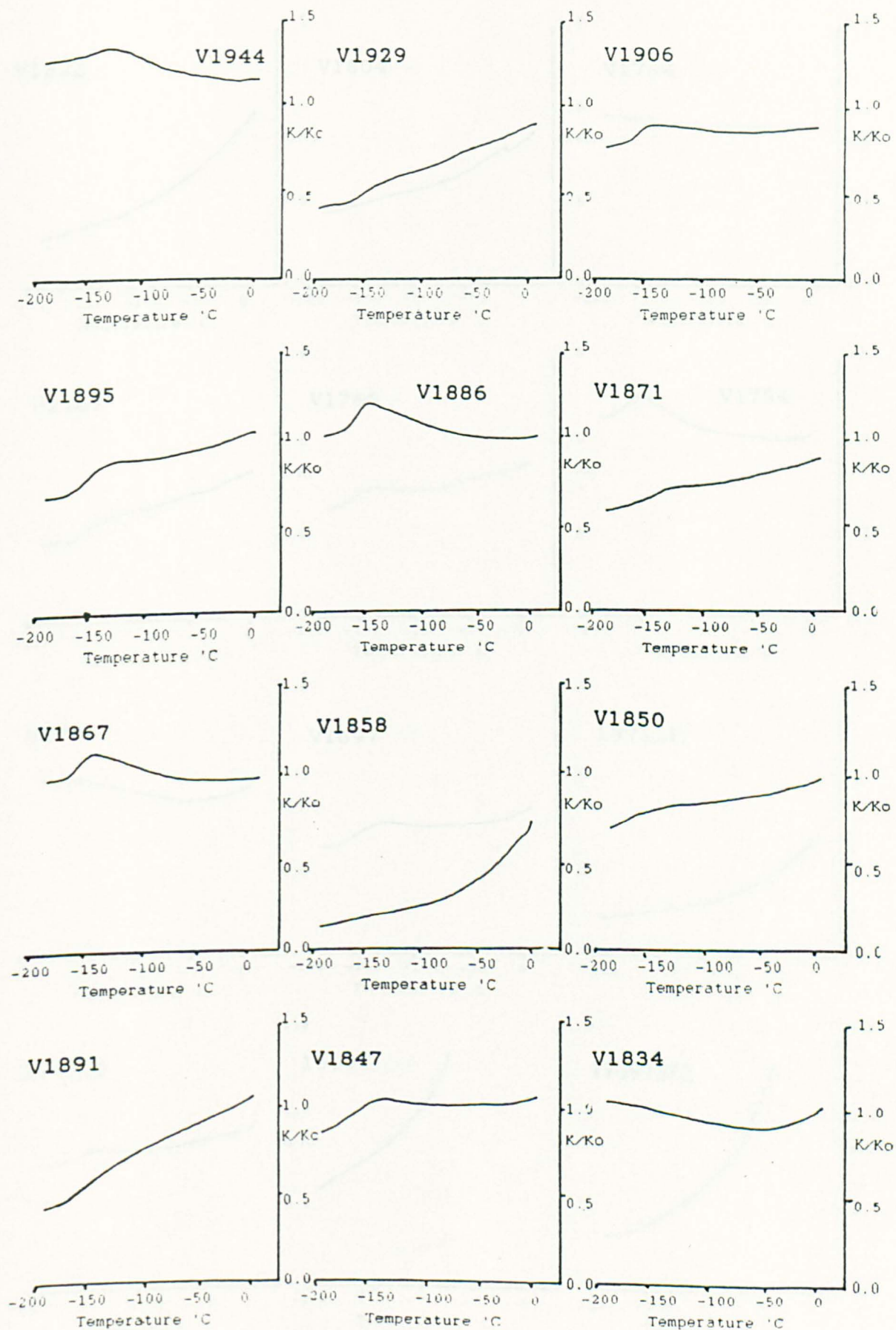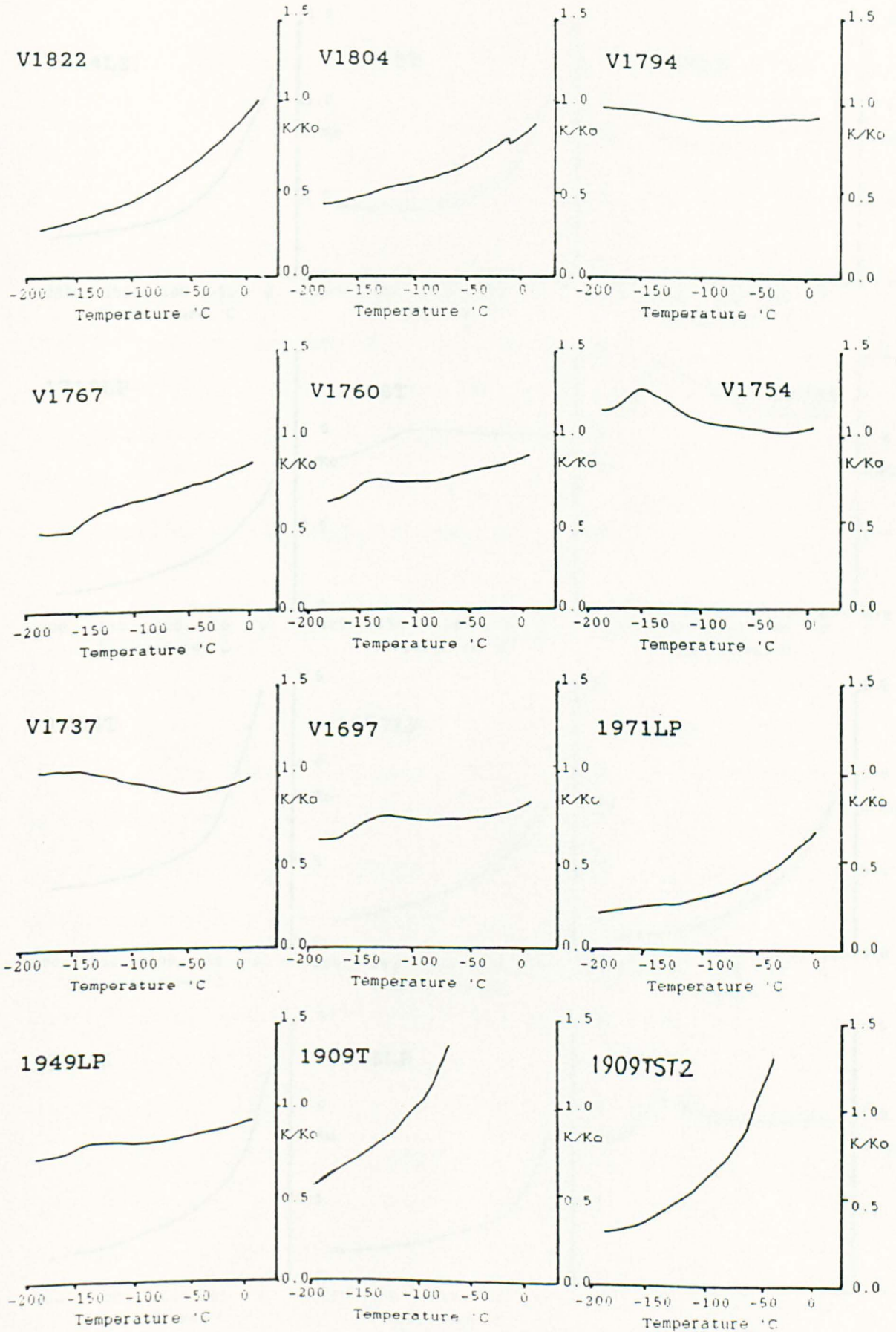
1824LZ
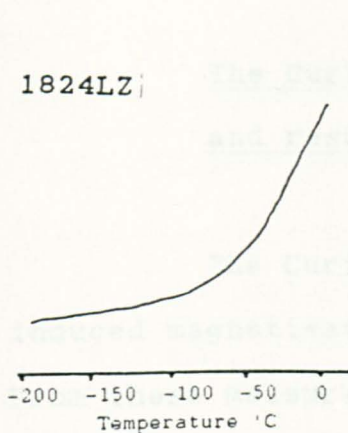
1798T
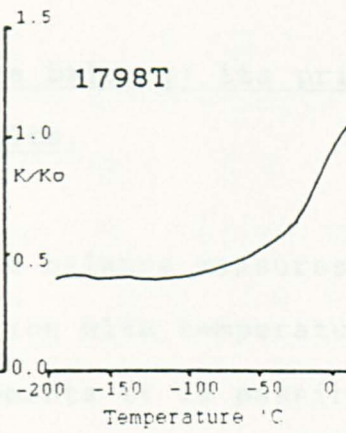
1730LZ
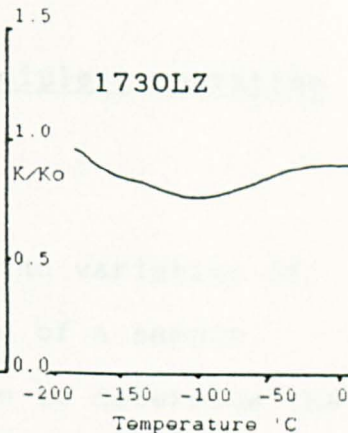
1712LP
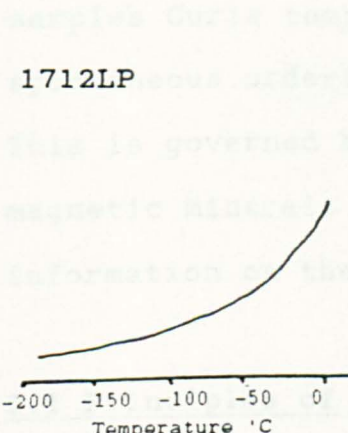
1706T
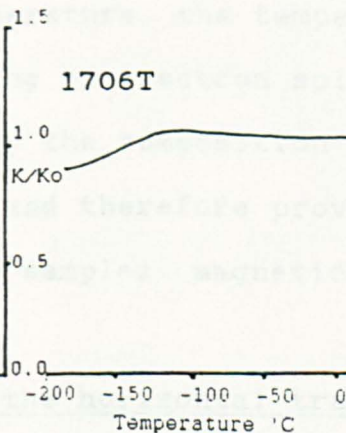
1705T
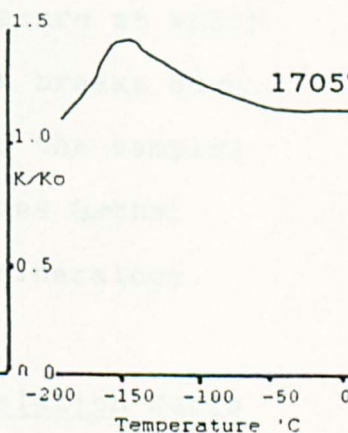
1704T
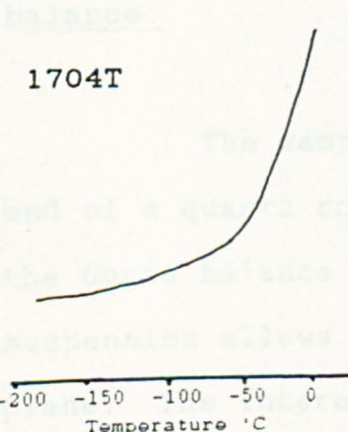
1677LP
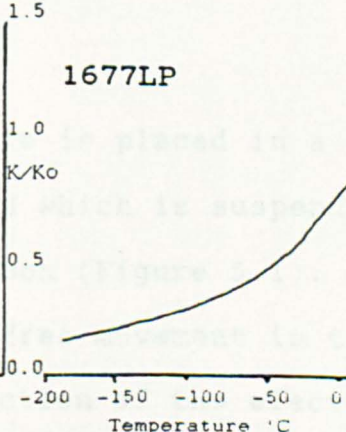
1646LP

1585LF

1585LP

147LP

K/Ko

1.5 1.0 0.5 0.0

Temperature 'C

-200 -150 -100 -50 0
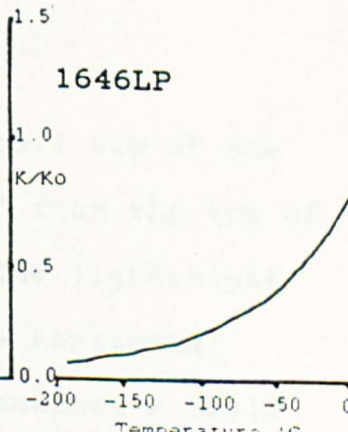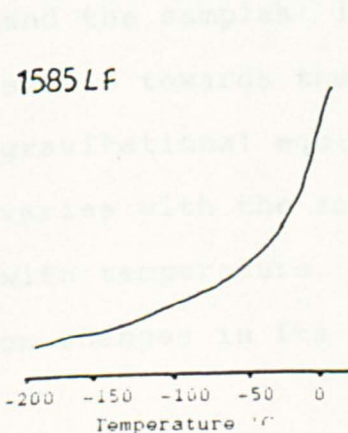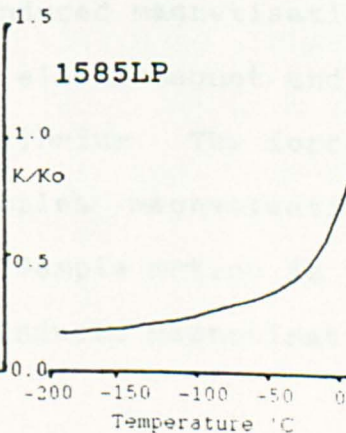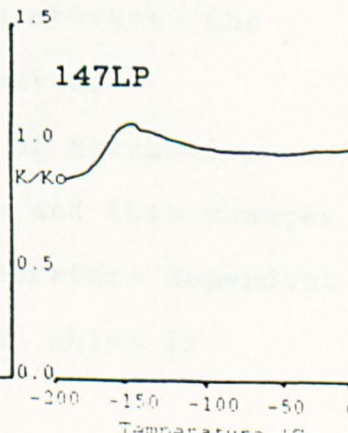
Chapter 5.

The Curie balance: its principles, operation and results.

The Curie balance measures the variation of induced magnetisation with temperature of a sample. From these measurements it is possible to determine the sample's Curie temperature, the temperature at which spontaneous ordering of electron spins breaks down. This is governed by the composition of the sample's magnetic minerals and therefore provides further information on the sample's magnetic mineralogy.

5.1 Principles of the horizontal translation Curie balance.

The sample is placed in a small cup at one end of a quartz rod which is suspended from the top of the Curie balance box (Figure 5.1). The lightweight suspension allows free movement in the horizontal plane. The interaction of the electromagnet's field and the sample's induced magnetisation attracts the sample towards the electromagnet and out of gravitational equilibrium. The force of attraction varies with the sample's magnetisation and this changes with temperature. Sample motion is therefore dependent on changes in its induced magnetisation which is

measured using a light dependent resistor (LDR) and vane arrangement, one of which is fixed to the other end of the quartz rod. When the rod moves the vane covers or uncovers the LDR producing a resistance which varies directly with sample position. A second vane sits in oil to dampen the oscillations.

SIDE VIEW OF CURIE BALANCE

PLAN VIEW OF CURIE BALANCE
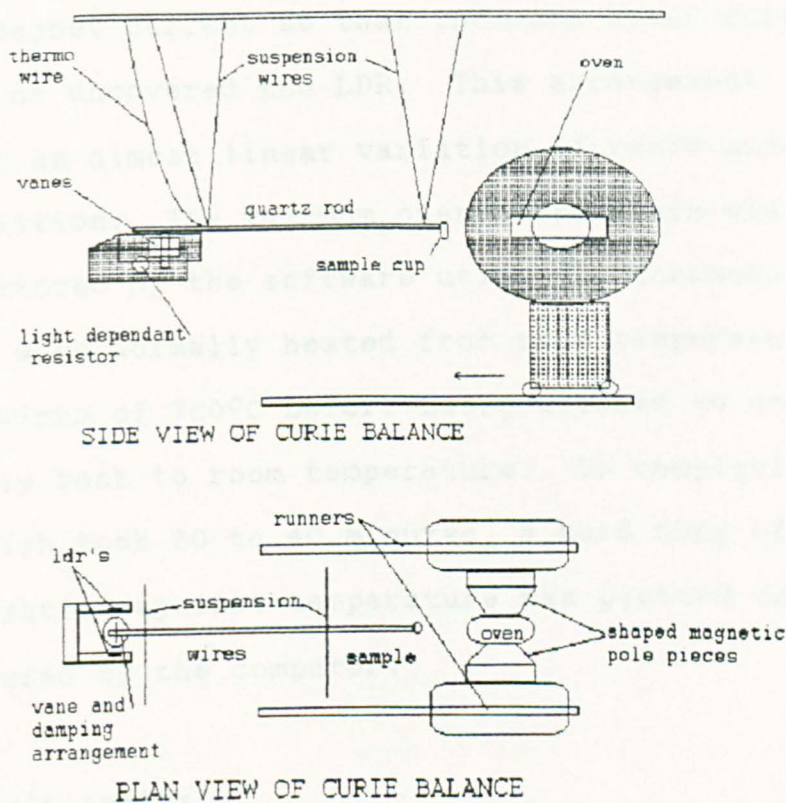
Figure 5.1   Side and plan views of the Curie balance.

The sample is heated in a non-inductively wound oven placed between the poles of the magnet and its temperature is measured by a thermocouple in the sample cup. The amplified output voltage of the thermocouple and the LDR/Wheatstone Bridge circuit's voltage were fed to an analog to digital converter and then to a computer for processing.

5.2 Operation of the Curie balance.

Half a gramme of sample fragments were loaded into the sample cup and the lightproof box surrounding the balance was closed. The LDR measurement bridge was then set for maximum sensitivity by adjusting the electromagnet current so that the vane never quite covered or uncovered the LDR. This arrangement produces an almost linear variation of resistance with vane position. The maximum oven temperature was set and monitored by the software using the thermocouple. Samples were normally heated from room temperature up to a maximum of 700°C before being allowed to cool naturally back to room temperature. On completion of a run, which took 30 to 40 minutes, a hard copy of magnetisation against temperature was plotted from the data stored by the computer.

5.3 Result analysis.

Curie temperature curves rarely show simple behaviour. For example, samples which contain more than one magnetic mineral type will produce curves which are a combination of the thermomagnetic behaviour of each type. Results were analysed initially to determine the Curie temperature of each magnetic mineral present and then in terms of curve shape.

5.3.1 Curie temperature analysis.

The number of magnetic components within a
sample can be determined from the shape of the curve
and from the recognition of their discrete Curie
temperatures. Figure 5.2 shows how Curie temperatures
are derived from the Curie curves, as suggested by
Gromme et al (1969).
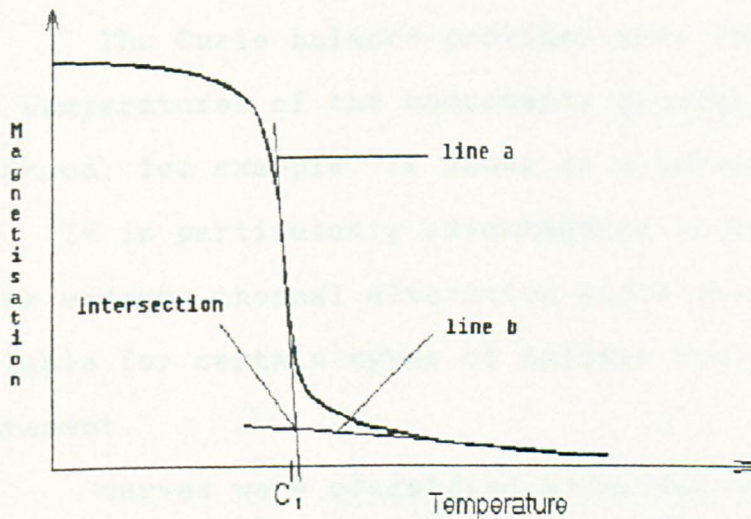
Figure 5.2 Curie curve analysis.

A tangent is drawn to the steepest part of
the Curie curve, line a. A second tangent is drawn
along from the shallow tail, line b. These lines cross
to give an intersection point. Point C, directly below
this intersection, gives the Curie temperature of the
mineral phase present. If more than one mineral phase
is present the process is repeated for each Curie
temperature.

The induced magnetisation at and above the
Curie point temperature may not fall to zero
immediately as samples may have a degree of exchange

interaction above the Curie temperature in addition to
a paramagnetic magnetisation. It is often hard to
separate this magnetisation from a small high
temperature component of magnetisation, for example,
due to haematite.

5.3.2 Curie curve classification.

The Curie balance provides more than the
Curie temperatures of the components present. Sample
alteration, for example, is shown as a non-reversible
curve. It is particularly advantageous to know which
samples undergo thermal alteration since they are
unsuitable for certain types of ancient field intensity
measurement.

Curves were classified according to the
system put forward by Mankinen et al. (1985) as revised
by Sherwood (1988). In this classification scheme
curves are split into 6 major types, numbered 1 to 6
with sub-types indicated by the letters a,b and c
(figure 5.3). The initial sample composition was
assumed to be titanium rich titanomagnetite (Haggerty,
1976).

Type 1 curves have a single magnetic phase
with a Curie temperature below 500°C and a reduced
magnetisation after heating. They result from titanium
rich titanomagnetite with no high temperature deuteric
oxidation.
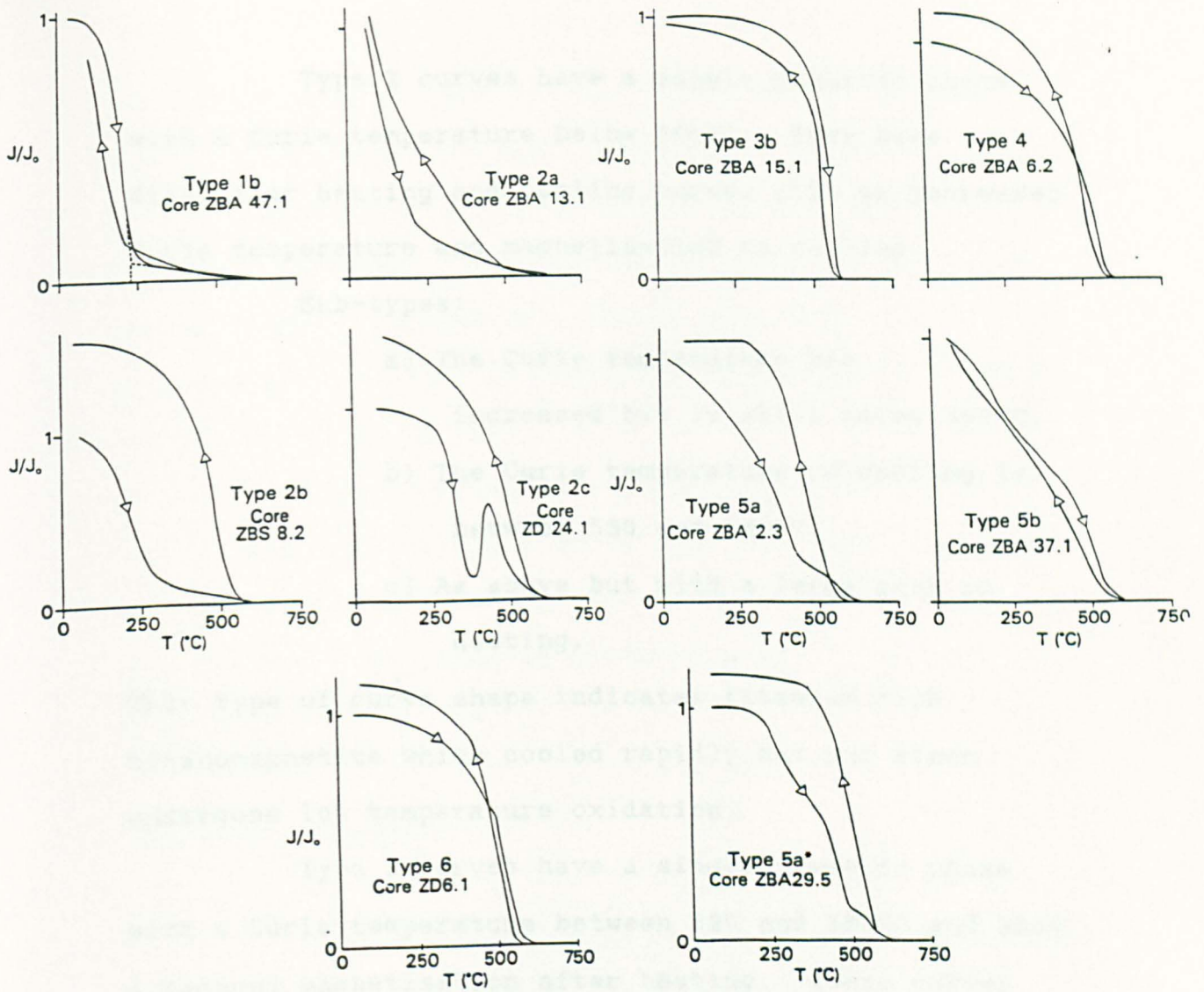
Figure 5.3 Curie curve classification from Sherwood (1988).

Type 1, Sub-types:
a) Very little curve shape change; <10% decrease in magnetisation on cooling.
b) Marked shape change; <10% decrease in magnetisation on cooling.
c) >10% decrease in magnetisation on cooling.

Type 2 curves have a single magnetic phase with a Curie temperature below 500°C. They have dissimilar heating and cooling curves with an increased Curie temperature and magnetisation on cooling.

Sub-types:

a) The Curie temperature has increased but is still below 500°C.

b) The Curie temperature on cooling is between 530 and 580°C.

c) As above but with a large peak on heating.

This type of curve shape indicates titanium rich titanomagnetite which cooled rapidly but has since undergone low temperature oxidation.

Type 3 curves have a single magnetic phase with a Curie temperature between 520 and 580°C and show a reduced magnetisation after heating. These curves are shown by titanium poor titanomagnetite with ilmenite lamellae. Sub-types are as described for type 1 curves.

Type 4 curves have a single magnetic phase with a Curie temperature between 520 and 580°C. The cooling curve crosses that for heating and shows a slight increase in magnetisation on cooling. Magnetic mineral phases are essentially similar to those of type 3.

Type 5 curves have two phases. The first has a Curie temperature in the range 200 to 400°C and the

second between 520 and 580°C. These curves are the
result of partial deuteric oxidation of titanium rich
titanomagnetite to titanium poor titanomagnetite with
ilmenite lamellae. Two sub-types exist; 5a, where the
low temperature phase is a cation deficient
titanomagnetite, and 5b where the low temperature phase
is preserved on heating.

Type 6 curves are shown by samples with two
Curie temperatures above 450°C with an inflection point
on heating but not on cooling. They are shown by
samples with two separate titanium poor titanomagnetite
populations.

5.4 Error analysis.

The Curie temperature values determined using
the above methods contain both instrument and
interpretation errors. In addition to these errors the
possibility of lava inhomogeneity must also be borne in
mind.

5.4.1 Instrumental errors.

The thermocouple is not an integral part of the
sample. Thus since the sample has a thermal capacity
its temperature will lag behind that recorded by the
thermocouple. This lag produces a Curie temperature
curve which does not reflect true sample temperature.

Sherwood (pers. comm.) gives the value of this error as normally less than +/- 10°C. It is possible to correct for this error by making the thermocouple part of the sample but this process would increase the length of sample preparation and wear on the thermocouple to unacceptable limits. No corrections were made to the results of this study for instrument error.

5.4.2 Interpretation error.

The interpretation method advocated earlier introduces error. The positioning of the lines a and b is an imprecise process hence any intersection and subsequent reading based on these lines is subject to an error which is related to the shape of each curve. The maximum error due to imprecise line placement is estimated to be of the order of +/- 20°C.

5.4.3 Lava inhomogeneity.

The Curie temperature of one sample may not be typical of the lava flow. So in 1986 a study was carried out in conjunction with V. Carey on two flows from Mount Vesuvius, V1929 and V1760. The 1929 samples had Curie temperatures of 540°C (1), 560°C (7), 570°C (2), 580°C (2) and 590°C (1). An average Curie temperature for this flow is 565 +/-12°C. The 1760 samples had Curie temperatures of 510°C, 520°C, 530°C,

540°C, 560°C (3) and 580°C, giving an average Curie temperature of 545 +/-22°C. With Curie temperatures varying by up to 70°C, the result of one, two or even three samples may not be an accurate representation of the lava flow. A case therefore exists for all samples to be subjected to Curie balance analysis. However, variation within the flow includes the error due to imprecise analysis, +/- 20°C, thus the inhomogeneity may be less significant than it first appears.

5.5 The change of induced moment with temperature.

Three studies were completed on the variation of magnetisation with temperature. Two were for the field areas of Mount Vesuvius and the Canary Islands and the third considered variation within two flows. Specimen results for each age lava are shown in Figure 5.5 and results are shown in Table 5.1.

No obvious variation with age exists for the results as shown in Figure 5.4. Only 5 out of 38 have a Curie temperature below 500°C and three show large high temperature components which may be due to either paramagnetic magnetisation or haematite.

Table 5.1 Results for two sub-samples from Vesuvius.

Year	Curie temperature °C		type
	A	B	
V1944	580	560	3c
V1929*	510	540	3c
V1906	550	550	3a
V1895	590	550	3a
V1891	500 H		3b
V1886	560	575	3b
V1871	575	560	3a
V1867	530	410 H	3a
V1858	340/600	300/600	5a
V1850	580	250 H	3a/2a
V1847	560	570	3c
V1834	530	570	3c
V1822	575	560	3a
V1804	500/300		5b
V1794	580	570	3b
V1767	480	530	3c
V1760*	560	560	3a
V1754	600	590	3a
V1737	550	530	3c
V1697	580	560	3a

* These results are in addition to separate studies carried out into Curie temperature variation through a flow, H indicates that the sample had a high temperature component (>580°C).
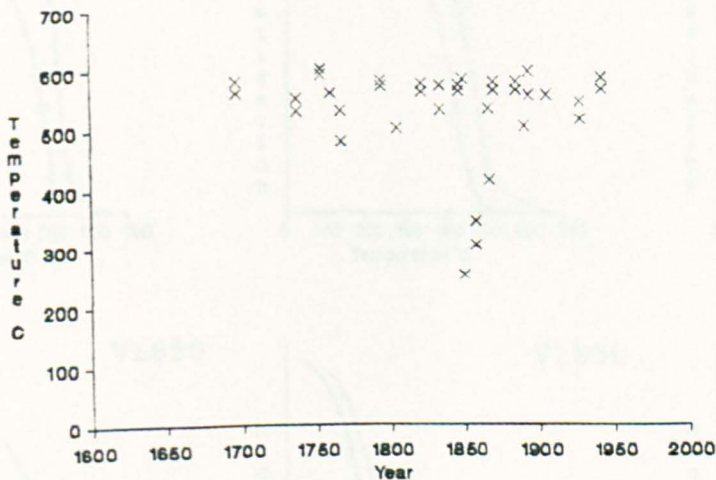
Figure 5.4   Curie temperature variation with year.

75

Figure 5.5 Curie balance curves for Mount Vesuvius samples.

V1834

V1822

V1804

V1794

V1767

V1760

V1754

V1737

V1697
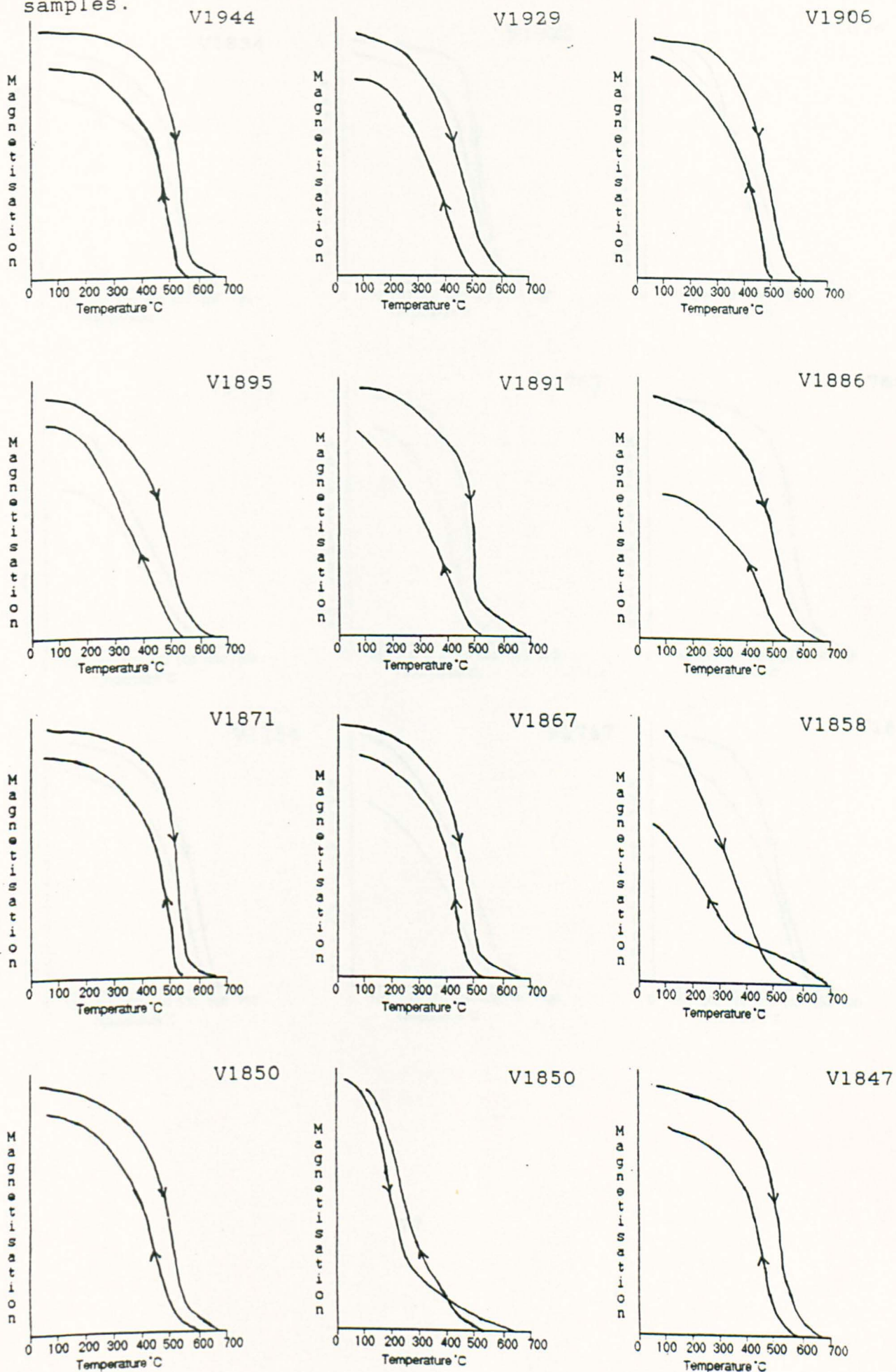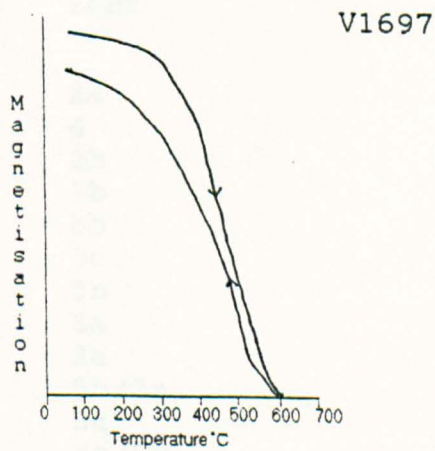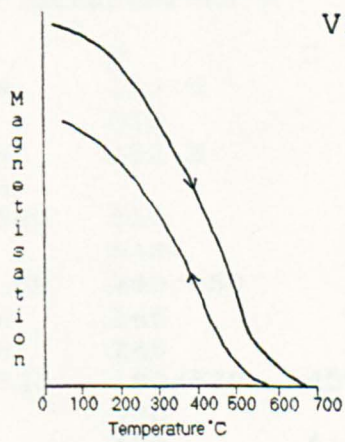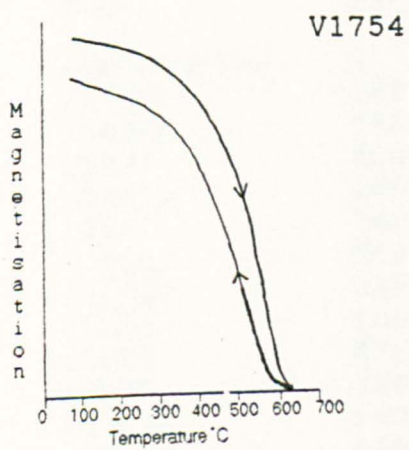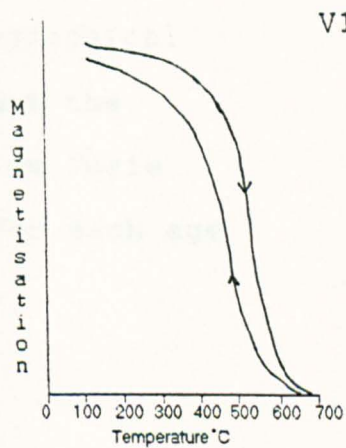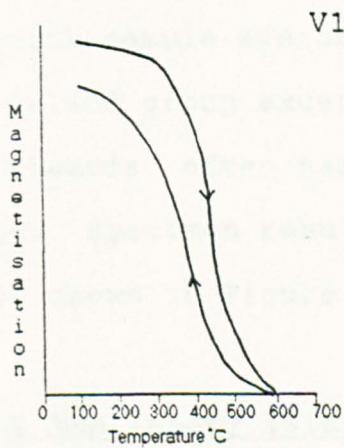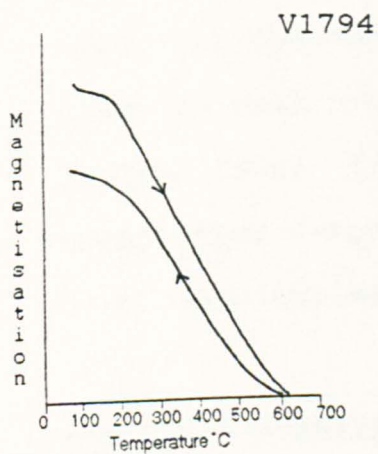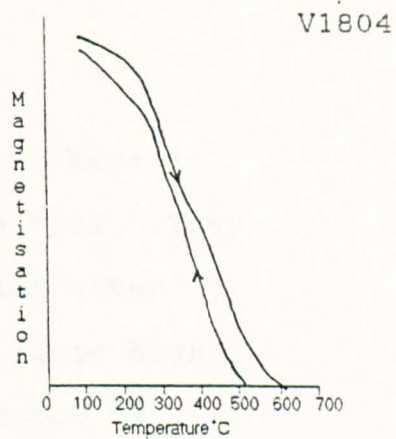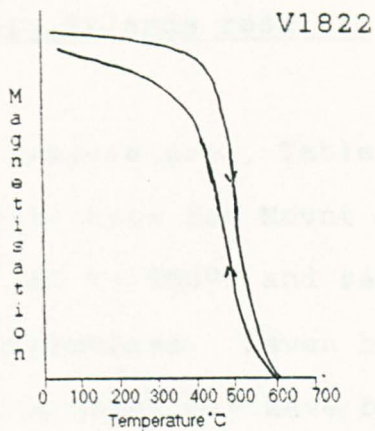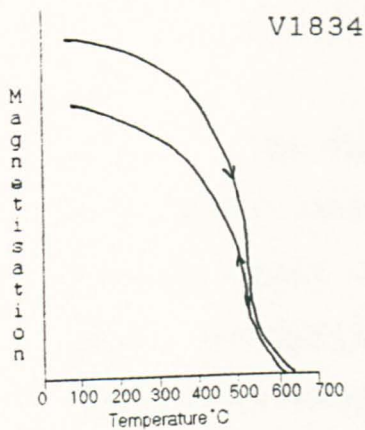
5.5.1 Canary Islands results.

The Curie temperatures, Table 5.2, have a much larger range than those for Mount Vesuvius. They covered values from 180 to 580°C and samples often showed two Curie temperatures. Seven had large high temperature components which may have been due to paramagnetic effects or haematite. No obvious variation was found with sample age or geographical location within the island group except that the younger lavas, 1704 onwards, often had a low Curie temperature component. Specimen results for each age lava flow sampled are shown in Figure 5.7.

Table 5.2 Results for the Canary Islands.

Year	Curie temperature°C			type
sub-samples	A	B	C	
1971LP	180 H	190 H		2a
1949LP	550	570		4
1909T	300 H	180 H		2b
1824LZ	160 H			1b
1798T	180/580	520		5b
1730LZ	560	540		3c
1712LP	230/540	240/550		5b
1706T	560 H	540		3a
1705T	550 H	540		3a
1704T	160/520	180/530	450	5b/2a
1677LP	560	570		3a
1646LP	560	530	510	3a/5b
1585LP	540	550		4
1470T	580	590		3a
1470LP	540	500		3a
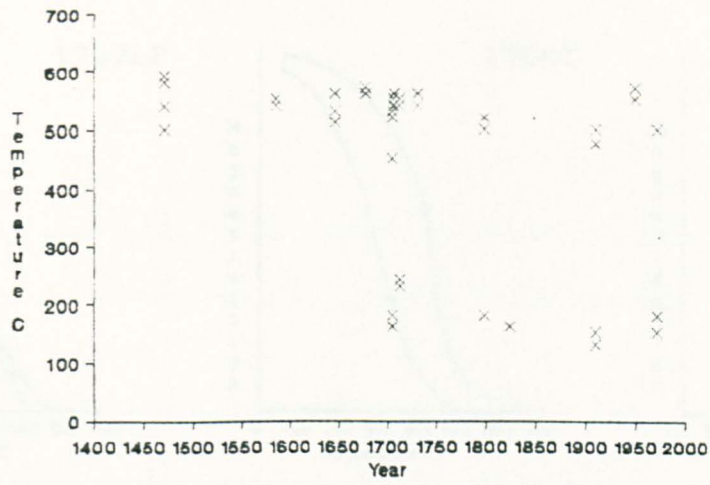
Figure 5.6   Curie temperature variation with year.

Figure 5.7   Curie balance curves for Canary Island samples.
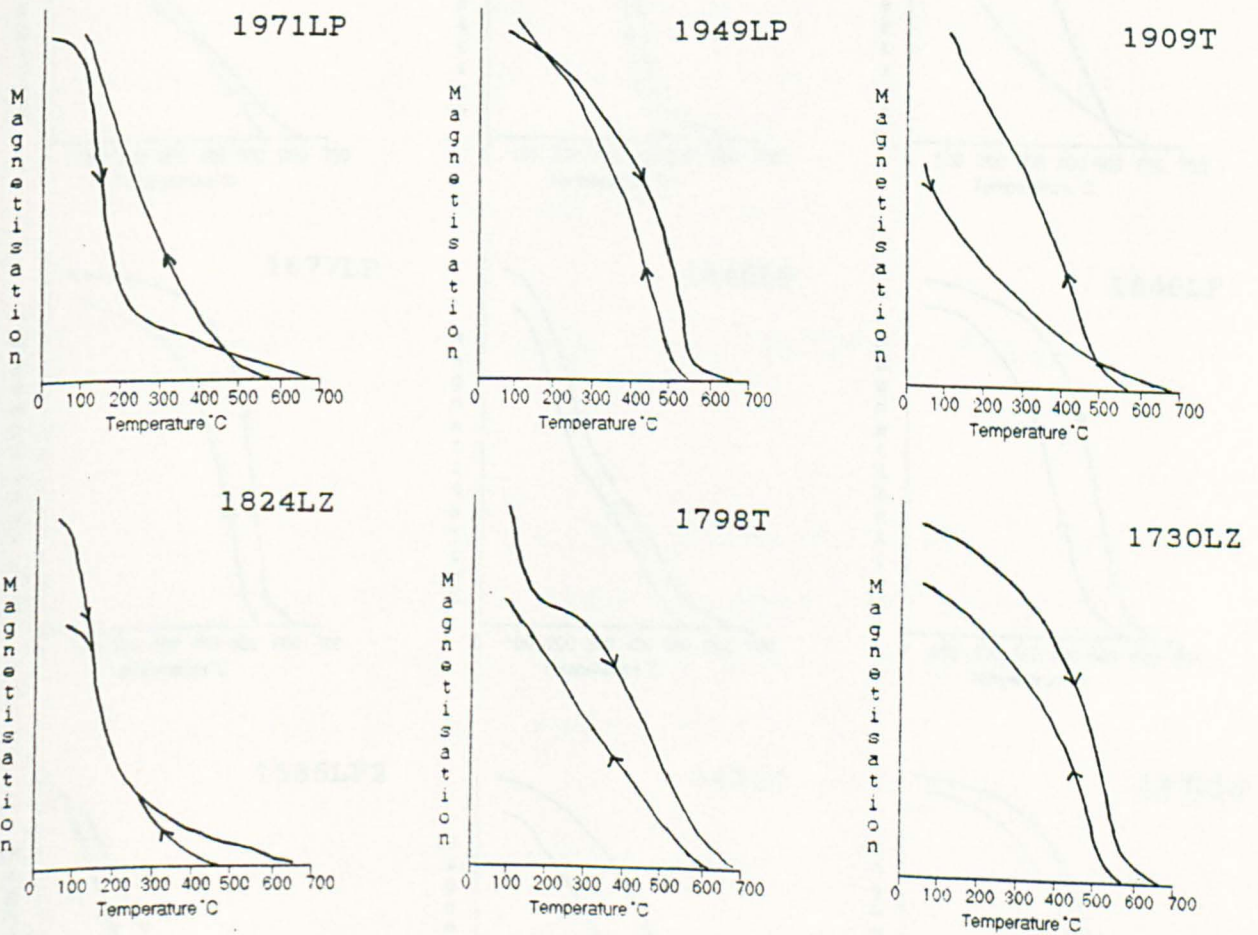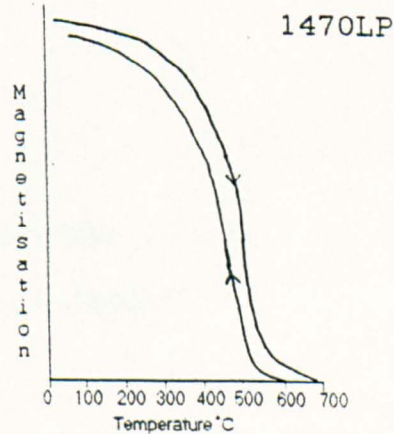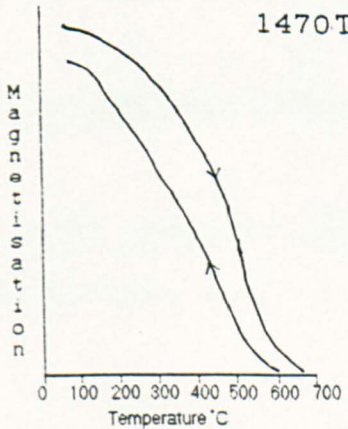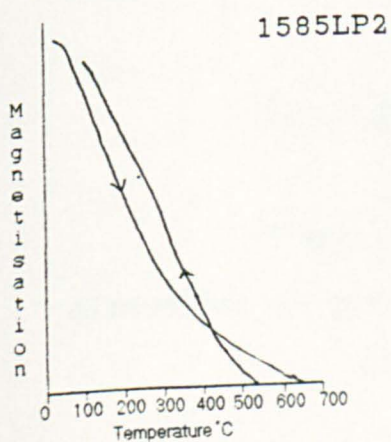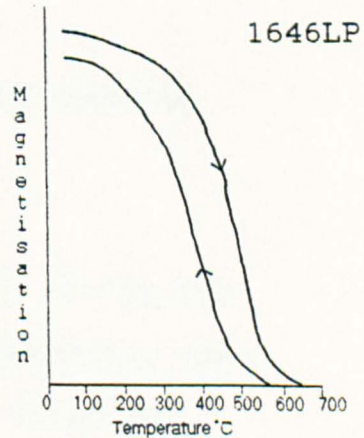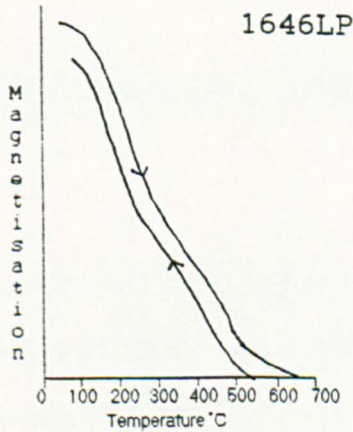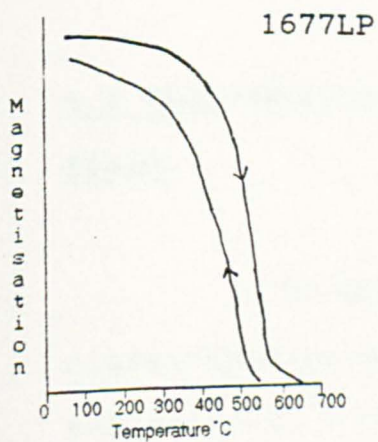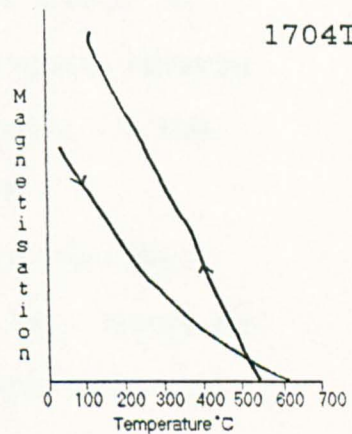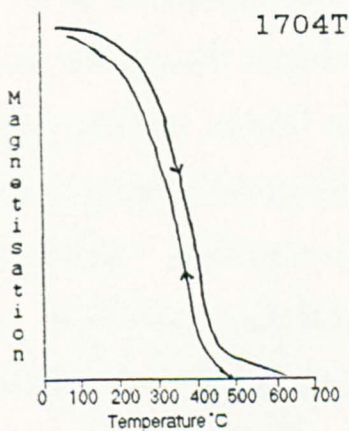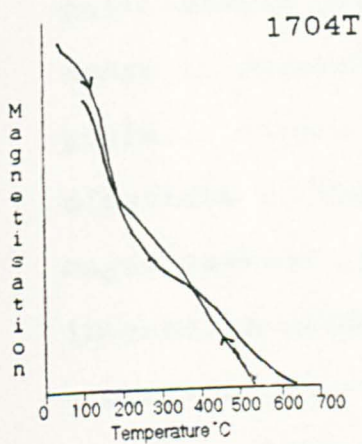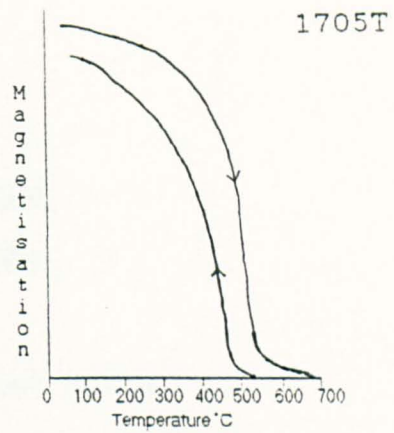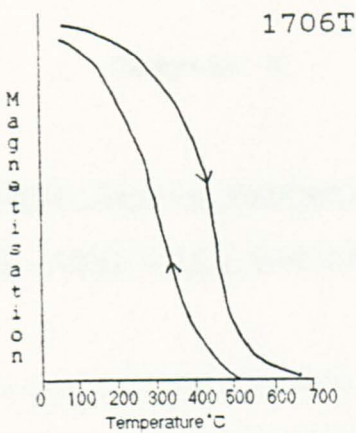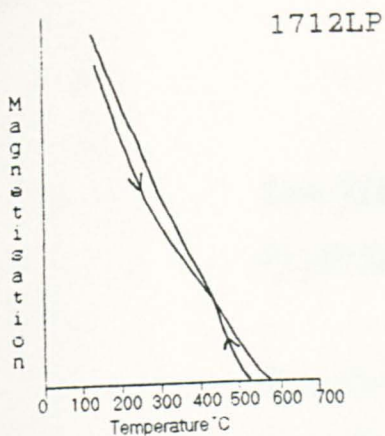
Chapter 6.

The Vibrating Sample Magnetometer:

Principles, operation and results.

The Vibrating Sample Magnetometer (VSM)
exploits the difference in behaviour of single and
multi-domain grains to a changing magnetic field in
order to determine the ratio of single to multi-domain
grains. Single domain grains react according to the
direction of the grain's easy direction of
magnetisation, multi-domain grains react by moving
internal boundaries. For most samples a lag, known as
hysteresis, occurs between the changing applied
magnetic field and the sample's magnetisation.

6.1 The reaction of material to a changing magnetic field.

The materials of this study fall within two
classification groups in terms of their behaviour when
subjected to a changing magnetic field. These are
single domain and multi-domain grains.

6.1.1 Single domains grains.

There are three possible orientations of the
direction of easy magnetisation of a single domain

grain with respect to an applied field - perpendicular, parallel and intermediate. Assuming that easy axes will have a random alignment within a sample, most grains will show intermediate behaviour (Figure 6.1).
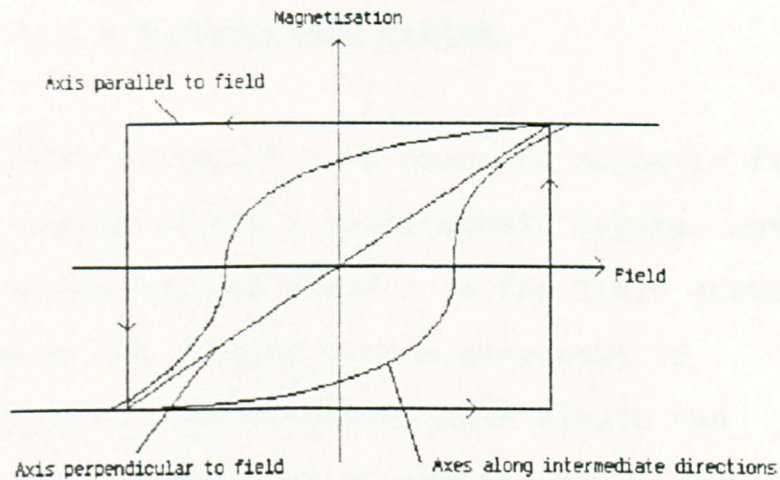
Figure 6.1 Single domain grains in a magnetic field. (After Thompson & Oldfield, 1986).

A single domain grain with a direction perpendicular to the field will magnetise in the field direction and follow it without a lag. The strength of the magnetisation is directly proportional to the applied field strength. When the field is removed the magnetisation returns to its original orientation. A sample with its direction parallel to the field, magnetised in the opposite direction, only shows a change in magnetisation when the applied field reaches a critical value when the direction in the domain "flips" by 180°. This reversal requires a relatively large field and produces a sudden change in magnetisation. Once reversed the electron spins do not

return to the original direction on removal of the field. Only when an opposite field reaches the critical value do the electron spins flip back to their original direction.

6.1.2 Multi-domain grains.

When subjected to a changing magnetic field the domain walls within a multi-domain crystal move in response to the applied field. As the field grows in one direction the domains with a component of magnetisation in that direction grow within the crystal. This reaction to an applied field is reversible in low fields as these produce a flexing or small movements within the domain region which, on removal of the field, returns to its previous state. As the field value is increased the movement becomes greater and irreversible changes occur (Figure 6.2). If the field strength is further increased, domains aligned in other directions are eventually turned parallel to the

Magnetisation

saturation

irreversible change

reversible change
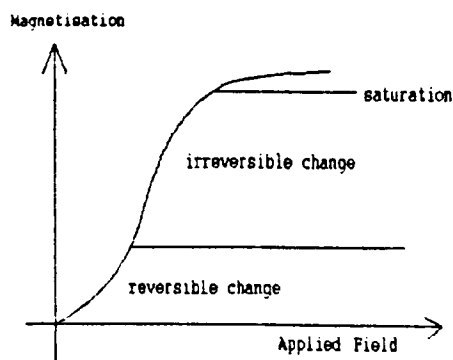
Applied Field

Figure 6.2 Reversible and irreversible changes in multi-domain material.

magnetisation
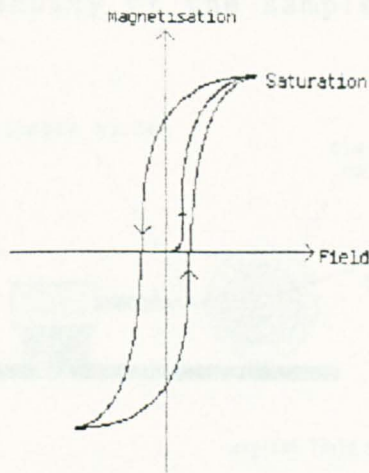
Saturation

Field

Figure 6.3 Hysteresis curve for multi-domain material.

field. This continues until a saturation point is
reached where magnetisation ceases to grow with the
applied field. This reaction to applied magnetic field
produces a hysteresis curve (Figure 6.3).

6.2 The Vibrating Sample Magnetometer (VSM).

The basic operation of the VSM involves
vibrating the sample whilst subjecting it to a large
steady magnetic field. This vibration is carried out
between two parallel pick-up coils which are positioned
either side of the sample within the steady applied
field. Current is not   generated in the pick-up
coils by the steady applied field, but a current is
generated by the moving magnetised sample. The
frequency of the current generated depends on the
frequency of sample movement, whilst the amplitude

depends on the intensity of the sample's induced
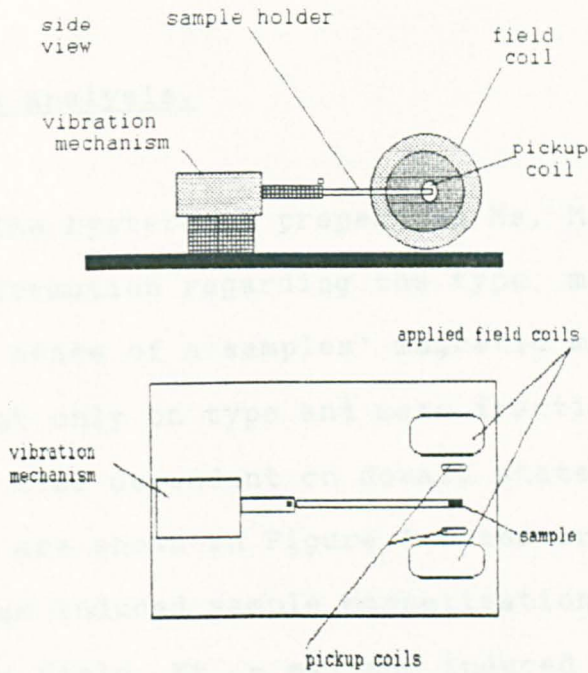
magnetisation.

Figure 6.4 Vibrating Sample Magnetometer, VSM.

Sample processing involves the stepwise

application of the steady field which is cycled between

+/- 1 Tesla. Plotting the induced magnetisation

against applied field produces a hysteresis curve for

the sample and from this curve the properties Ms

(saturation magnetisation), Mr (saturation remanence)

and Hc (coercivity) can be determined.

The equipment used was designed by Dr.

Molyneux of Newcastle University for measuring samples

with a mass of up to 0.5g and has a sensitivity of

$40\mu Am^2$. Samples are vibrated at 50Hz and the induced

magnetisation and applied field information is stored

on a computer disc. At the end of each run the

hysteresis curve is plotted on the screen and hard copy
provided via an attached printer.

6.3 Results analysis.

   The hysteresis properties Ms, Mr and Hc can
provide information regarding the type, mass fraction
and domain state of a samples' magnetic minerals. Ms
is dependent only on type and mass fraction while Mr
and Hc are also dependent on domain state. These
parameters are shown in Figure 6.5 and are defined as
Ms - maximum induced sample magnetisation measured in
the applied field, Mr - maximum induced remanence,
measured in zero field after sample has been given a
saturation magnetisation and Hc - the reverse field
required to remove saturation remanence or coercive
force.
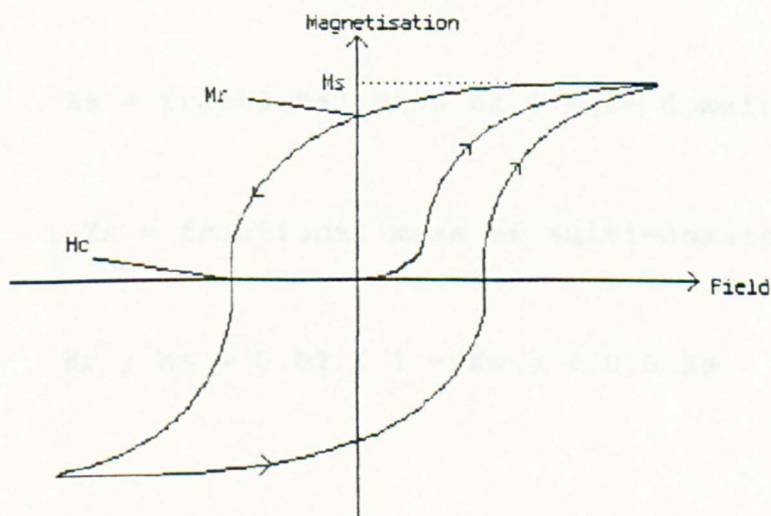
Figure 6.5 Features of hysteresis curve relevant to
the VSM calculations.

Curie curves indicate that the magnetic mineralogy of the lavas is primarily single phase titanomagnetite and this simplifies interpretation of the hysteresis data. While Ms is independent of domain state, Mr varies greatly from about $2Am^2/kg$ for multi-domain magnetite to about $45Am^2/kg$ for single domain magnetite, therefore Mr for a sample depends on both domain states and mass fraction of magnetic mineral. However, the ratio of Mr/Ms is independent of mass fraction and varies only according to the domain state of the magnetic mineralogy. Mr/Ms is approximately 0.5 for single domain magnetite and approximately 0.02 for multi-domain magnetite. Using these values obtained from our samples we can estimate the ratio of single domain to multi-domain grains as shown below (Sherwood, pers. comm.).

Xs = fractional mass of single domain

1-Xs = fractional mass of multi-domain

Mr / Ms = 0.02 (1 - Xs) + 0.5 Xs

thus

Mr / Ms = 0.02 + 0.48 Xs.

Once Xs is known from substituting in values

for Mr/Ms, it is a simple matter to determine 1 - Xs

and hence the fractional mass of multi-domain

magnetite.

6.4 Error analysis.

Errors arise from two possible sources -

instrumentation and processing. The use of a

simplified processing procedure, based on the

assumption of a single magnetic mineral phase, may have

introduced an error. The extent of this error will

vary for each sample and may be judged by reference to

the Curie curves (Chapter 5). In order to reduce error

due to the instrument drift a copper sulphate

calibration sample was used for standardisation before

each measurement session.

6.5 The ratio of single to multi-domain grains.

The majority of samples had a larger multi-

domain population. Only 13% of the samples showing a

ratio of single to multi-domain more than 0.5. The

Table 6.1 V.S.M results.

a) Canary Islands.

YEAR	MR /MS	Hc	SD/MD	MR /MS	Hc	SD/MD
	------Sample 1-------			------Sample 2----------		
1470L	0.091	7.44E3	0.164	0.038	1.38E3	0.389
1470T	0.095	7.16E3	0.176	0.110	6.43E3	0.230
1585S1	0.065	2.74E3	0.098	0.093	3.84E3	0.179
1585S2	0.113	6.71E3	0.230	0.110	4.86E3	0.230
1646S1	0.054	1.93E3	0.075	0.035	1.37E3	0.032
1646S2	0.087	3.45E3	0.164	0.067	2.61E3	0.110
1677	0.116	9.75E3	0.250	0.133	1.24E4	0.307
1704	0.090	4.15E3	0.160	0.078	3.51E3	0.137
1705	0.038	1.44E3	0.038	0.063	2.89E3	0.098
1706	0.044	2.05E3	0.052	0.046	1.97E3	0.057
1712	0.096	4.73E3	0.190	0.072	2.81E3	0.121
1730	0.342	2.77E4	2.030	0.331	2.47E4	1.840
1798	0.087	3.93E3	0.164	-	-	-
1824	0.149	6.66E3	0.350	0.070	2.79E3	0.116
1909S1	0.100	4.70E3	0.190	0.198	1.07E4	0.589
1909T	0.050	2.26E3	0.066	0.222	1.14E4	0.726
1909T2	0.300	3.00E3	1.398	0.125	5.43E3	0.280
1949	0.054	2.06E3	0.075	0.043	1.55E3	0.059
1971	0.063	2.59E3	0.160	0.067	2.48E3	0.108
1971S2	0.089	3.54E3	0.164	0.078	3.11E3	0.137

b) Mount Vesuvius.

V1697	0.088	3.97E3	0.164	0.067	2.90E3	0.108
V1737	0.186	9.69E3	0.520	0.188	9.24E3	0.538
V1754	0.118	1.28E4	0.250	0.098	9.34E3	0.194
V1760	0.194	1.43E4	0.560	0.058	3.31E3	0.085
V1767	0.146	1.06E4	0.350	0.124	1.05E4	0.276
V1794	0.162	8.36E3	0.400	0.148	7.48E3	0.363
V1804	0.103	5.26E3	0.200	0.154	1.19E4	0.387
V1822	0.124	1.14E3	0.260	0.087	8.06E3	0.162
V1834	0.151	8.40E3	0.360	0.083	6.02E3	0.151
V1847	0.132	1.36E4	0.290	0.128	1.28E4	0.290
V1850	0.165	1.17E4	0.420	0.141	8.47E3	0.337
V1858	0.058	2.49E3	0.080	0.211	1.22E4	0.660
V1867	0.123	1.23E4	0.260	0.144	1.51E4	0.348
V1871	0.143	1.02E4	0.344	0.094	8.59E3	0.182
V1872	0.130	9.78E3	0.287	0.136	9.71E3	0.318
V1886	0.240	2.24E4	0.818	0.148	1.37E4	0.363
V1891	0.090	7.60E3	0.169	0.116	7.60E3	0.250
V1895	0.048	2.04E3	0.060	0.050	2.42E3	0.066
V1906	0.124	1.19E4	0.260	0.109	9.28E3	0.227
V1929	0.135	1.34E4	0.300	0.078	4.40E3	0.137
V1944	0.155	1.41E4	0.380	-	-	-

number of samples in each category for a range of

single/multi-domain values and full results are shown

V1858   V1886
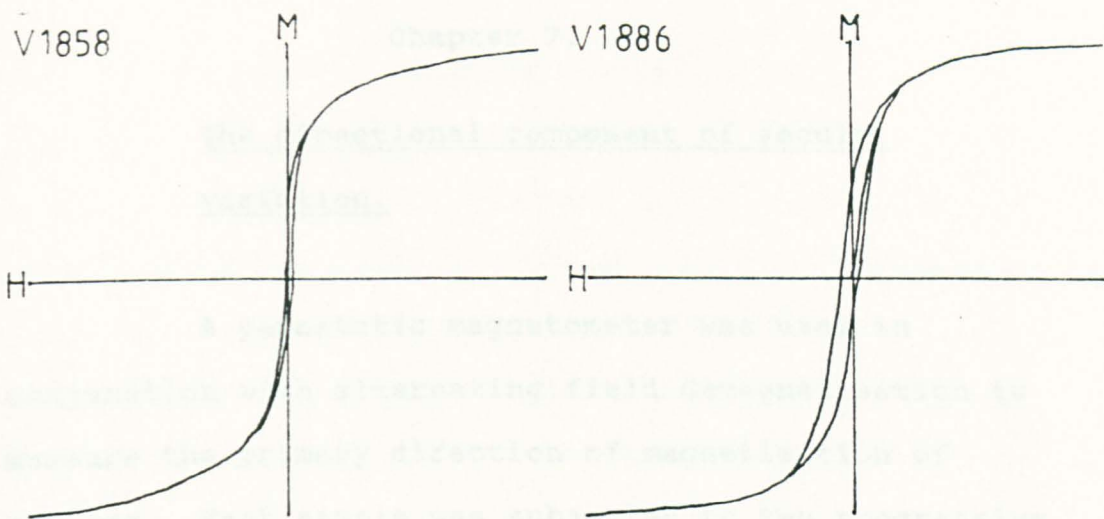
Figure 6.6 Typical V.S.M. hysteresis curves.

in Table 6.1 and Figure 6.7. The implications of this

on individual samples will be discussed in greater

detail later. However, it can be said that, on the

basis of these observations, multi-domain behaviour

should predominate in all but exceptional cases. Two

hysteresis curves are shown in Figure 6.6 to show

typical VSM outputs.
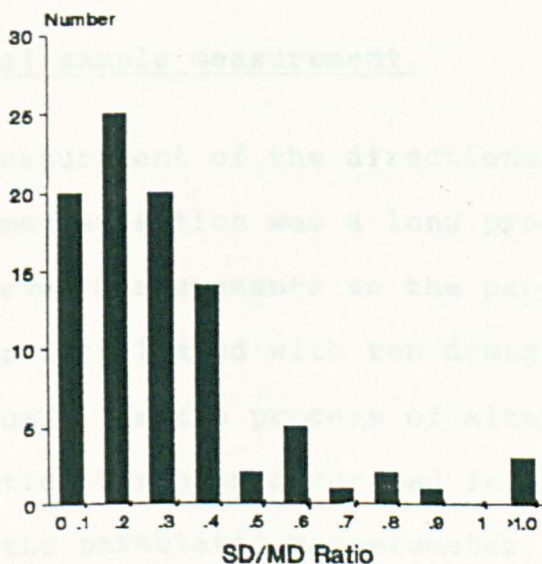
Figure 6.7 V.S.M. number per sd/md ratio.

The directional component of secular variation.

A parastatic magnetometer was used in conjunction with alternating field demagnetisation to measure the primary direction of magnetisation of samples. Each sample was subjected to ten progressive demagnetisation / measurement stages. These values were then analysed, using a principal component line-fit programme, from which the characteristic direction of magnetisation could be found. At least three samples per flow were then combined to provide a flow average, the error of which was determined using Fisher (1953) statistics. The flow averages were plotted against time to illustrate the secular variation of the direction of the geomagnetic field for each area.

7.1 Practical sample measurement.

Measurement of the directional component of the sample magnetisation was a long process since it involved eleven measurements on the parastatic magnetometer interleaved with ten demagnetisation steps from 5 to 50mT. As the process of alternating field demagnetisation has been described in Chapter 3 only details of the parastatic magnetometer, measurement process and error reduction will be discussed here.

7.1.1 The parastatic magnetometer.

A development of the older astatic design, the parastatic magnetometer is a viable measuring system under adverse conditions due to the arrangement of its magnets. It has three main sections: the suspended magnet assembly, the feedback loop and the air turbine (Figure 7.1).
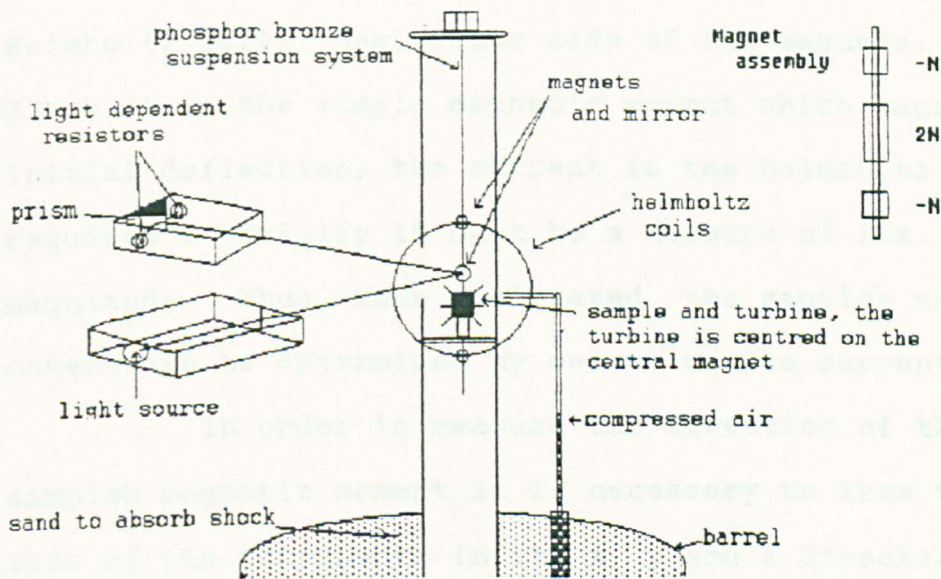
Figure 7.1 Parastatic magnetometer. (The centre magnet is twice as strong as the outer magnets and magnetised antiparallel to them thus forming a second order gradiometer.)

The components of the sample's magnetic moment are measured through their interaction with the central suspended magnet. The magnets are arranged to form a second order vertical gradiometer and only the horizontal component of the sample's magnetic field along the axis of rotation is measured. The magnet

assembly is hung from a phospher-bronze strip which
also carries a mirror. When a sample is brought up to
the centre magnet of the assembly it causes a rotation
of the magnets and hence the mirror which subsequently
deflects incident light onto a light dependent resistor
(ldr).

The resistance of the ldr is used to form the
basis of a feedback loop. The current flowing through
the loop corrects the magnet deflection by means of
Helmholtz coils, one either side of the magnets.
Since it is the sample magnetic moment which causes the
initial deflection, the current in the Helmholtz coils
required to nullify it must be a measure of its
magnitude. Thus, when calibrated, the sample's magnetic
moment can be determined by measuring the current.

In order to measure the direction of the
sample's magnetic moment it is necessary to know the
size of the components in the x, y and z directions. By
spinning the sample at speed only the component of
magnetisation along the axis of rotation is measured
and sample inhomogeneties are averaged out as the
response time of the magnet assembly is quite long
(several seconds). Samples are therefore rotated in a
turbine during each measurement. The turbine is driven
by compressed air rather than an electric motor to
reduce magnetic noise close to the magnet assembly.

The measured values of current, sample mass,
orientation information and calibration values are

processed on a B.B.C. micro computer which calculates the direction and intensity of magnetisation, saving the results on disc for further processing (section 7.2).

7.1.2 Measurement process.

The samples used were 2.5cm cylinders which were weighed and then fixed into a perspex cube with the sample's scribe line (section 2.1) along the orientation line on the cube. This cube was also marked with the X,Y and Z components which facilitates the measurement of the sample's three component directions in a specific order.

Measurement involves two processes, the actual measurement on the magnetometer and the demagnetisation prior to the next measurement. Parastatic measurements involved the sample cube being brought to the magnet assembly, spun whilst a reading was taken and then turned. All six faces of the cube were presented to the magnetometer so that the magnetic moments in the X, Y, Z, -X, -Y and -Z directions were measured. By reversing the components the zero position of the magnetometer becomes redundant and the accuracy with which the component is measured is increased. The demagnetisations were carried out using an alternating field demagnetiser manually set and controlled (Figure 7.2). The samples, still in the

cubes, were placed in a two axis reversing tumbler. On completion of each demagnetisation step samples were measured on the magnetometer.

helmholtz coils

tumbler and
sample

a.f. demagnetisation coil
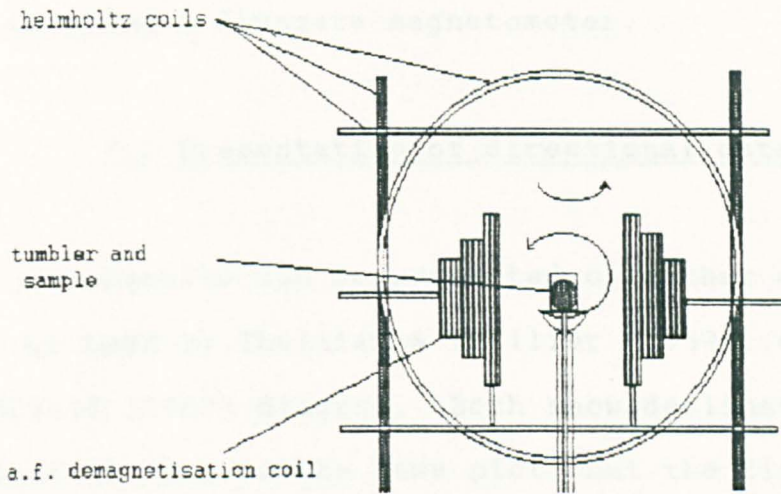
Figure 7.2 A.F. Demagnetiser. (The A.F. demagnetisation coils slide together once the sample has been inserted.)

7.1.3 Error reduction during measurement.

To ensure consistent measurement, the magnetometer was calibrated before each session. This was done by passing a known current through a small wire coil to produce a known field. The coil is placed in the normal sample position and the feedback current required to nullify its effect can then be calibrated.

A spurious remanent magnetisation may be induced in the sample during the demagnetisation stage if the external field is not nullified in the demagnetisation region (section 3.4.6). The currents

in three pairs of mutually perpendicular Helmholtz coils were adjusted at the beginning of each measurement session to reduce the ambient field to 50nT or less using a fluxgate magnetometer.

7.2 Presentation of directional data.

Results can be presented on either a stereo plot, as used by Thellier & Thellier (1959), or on a Zijderfeld (1967) diagram. Both show declination and inclination data on the same plot, but the Zijderfeld diagram and the earlier Wilson (1961) plot also include intensity information.

7.2.1 Zijderfeld diagrams.

The X, Y and Z components of a sample's magnetic moment can be plotted on a Zijderfeld diagram (section 2.1). The X and Y components are plotted on the ordinate and abscissa which represent the N/S and E/W directions respectively, this combination shows the declination directly. The inclination of the sample is not shown directly, the vertical component, Z, of the samples moment is plotted against the Y component of the declination plot by relabeling the ordinate with Up/Down to represent the Z direction (Figure 7.3).

96

7.2.2 Line-fit to Zijderfeld diagram.

Raw data points plotted on a Zijderfeld plot were examined using a line-fit programme. The programme used a three dimensional principal component analysis fit as suggested by Kirschvink (1980) for the X, Y and Z components. Although the data can be plotted in two dimensions it represents a magnetisation measurement made up of three directional components and any line-fit to such a function must reflect this. Sherwood (1986) describes it as "equivalent to a least squares line-fit in 3D". It is the nature of least square fits that the greater the number of algebraic terms in the polynomial, describing the line, the better the fit to the data. Successive additional terms have increasingly smaller effects.

7.2.3 Error treatment.

Before hard copies were printed each plot was subjected to a visual inspection during which viscous remanences and inconsistent or "bad" points were eliminated from the plot. Viscous remanences were normally removed during the early stages of demagnetisation. Their removal reduced the sample plot error calculated by the programme which redrew the plot after each edit. Bad points were normally the result of operator error, they were easily identified (the

demagnetisation curves produced in this study were almost perfect straight lines) and removed. Once analysed the plots were printed by means of a screen dump routine together with the values for declination, inclination and errors (Fisher, 1953).

7.3 Fisher statistics.

Once individual sample results had been evaluated from Zijderfeld plots they were analysed as a body. In order to place a degree of magnitude on the scatter of sample directions Fisher (1953) statistics are used. These statistics treat the distribution of the sample directional vectors as if they were points on a sphere. There are certain basic definitions involved;

ϕ = angle subtended between a specific direction and the mean direction.

k = function of the spread of points called the precision parameter.

This varies from k = infinity where all directions are superimposed to k = 0 when results are completely uniformly distributed.

The value of the precision parameter k involves the definition of two other variables:

N - the number of directions and

R - the resultant of the vectorial addition of the directions involved.

R is given by:

$$R^2 = \left(\sum_{i=1}^{N} x_i\right)^2 + \left(\sum_{i=1}^{N} y_i\right)^2 + \left(\sum_{i=1}^{N} z_i\right)^2$$

thus k can be estimated by:

$$k = \frac{N - 1}{N - R} \quad \text{for } k \geq 3$$

The probability of finding a direction within an angle ϕ of the mean direction when the precision parameter equals k is P. Probability P is given by:

$$P = \frac{k\,(\exp(k * \cos\phi))}{(4 * \pi * \sinh k)}$$

Generally P = 0.05 is the accepted value so that of a zone of confidence round the mean of 95 % or alpha95 can be estimated by:

$$\text{alpha}_{95} = 140\,(k * N)^{\frac{1}{2}} \cdot \text{ provided k and N}$$

are adequately defined.

These two functions were used throughout the directional work and gave a good definition of accuracy, which improves as N increases.

7.4 Canary Island directional secular variation.

Directional results were obtained for seventeen of the eighteen flows sampled and specimen Zijderfeld diagrams are shown in Figure 7.3. Flow average declination and inclination were taken from up to 7 but never less than 4 cores.

7.4.1 Canary Islands results.

Table 7.1 Canary Island direction results.

Year	Decln	Inc	alpha95	K	No samples
1971LP	349.1	43.1	3.7	421	4
1971LP	351.2	38.6	3.7	258	7
1949LP	350.1	41.0	3.4	488	5
1909TN	340.8	40.1	4.1	256	6
1824LZ	338.7	54.5	4.5	213	6
1798TN	350.5	53.8	3.4	388	6
1730LZ	343.1	64.4	2.5	1270	4
1712LP	354.5	56.5	1.3	2657	6
1706TN	357.9	59.2	2.5	674	6
1705TN	355.6	55.1	3.2	424	6
1704TN	359.6	63.1	2.7	752	5
1677LP	358.3	55.4	4.6	211	6
1646LP	002.4	54.4	3.4	304	7
1646LP	003.7	55.1	3.4	490	5
1585LP	002.1	48.7	2.6	622	6
1585LP	009.1	52.3	4.0	351	5
1470TN	009.2	17.3	3.6	273	7

7.4.2) Discussion of flow results.

Alpha95 values range between a minimum of 1.3 degrees up to a maximum 4.6 degrees, the average error is 3.4 degrees. This suggests that the results are valid for paleomagnetic work and this view is supported by the confidence value K which remains high for all flows.

7.4.3 Secular variation curves.

Flow results were used to plot the secular variation of declination and inclination with respect to time. Curves were drawn to fit these data points using a least squares fit of order five which produced a relatively close fit to the data set.

Figure 7.3 Specimen Zijderfeld plots for the Canary
Islands. A + indicates the horizontal component, a x
represents a vertical component.

Sample 1971 LP

Dec   352.31
Incl   36.86
Alpha95   1.11

Sample 1949 LP

Dec   349.32
Incl   37.74
Alpha95   1.44
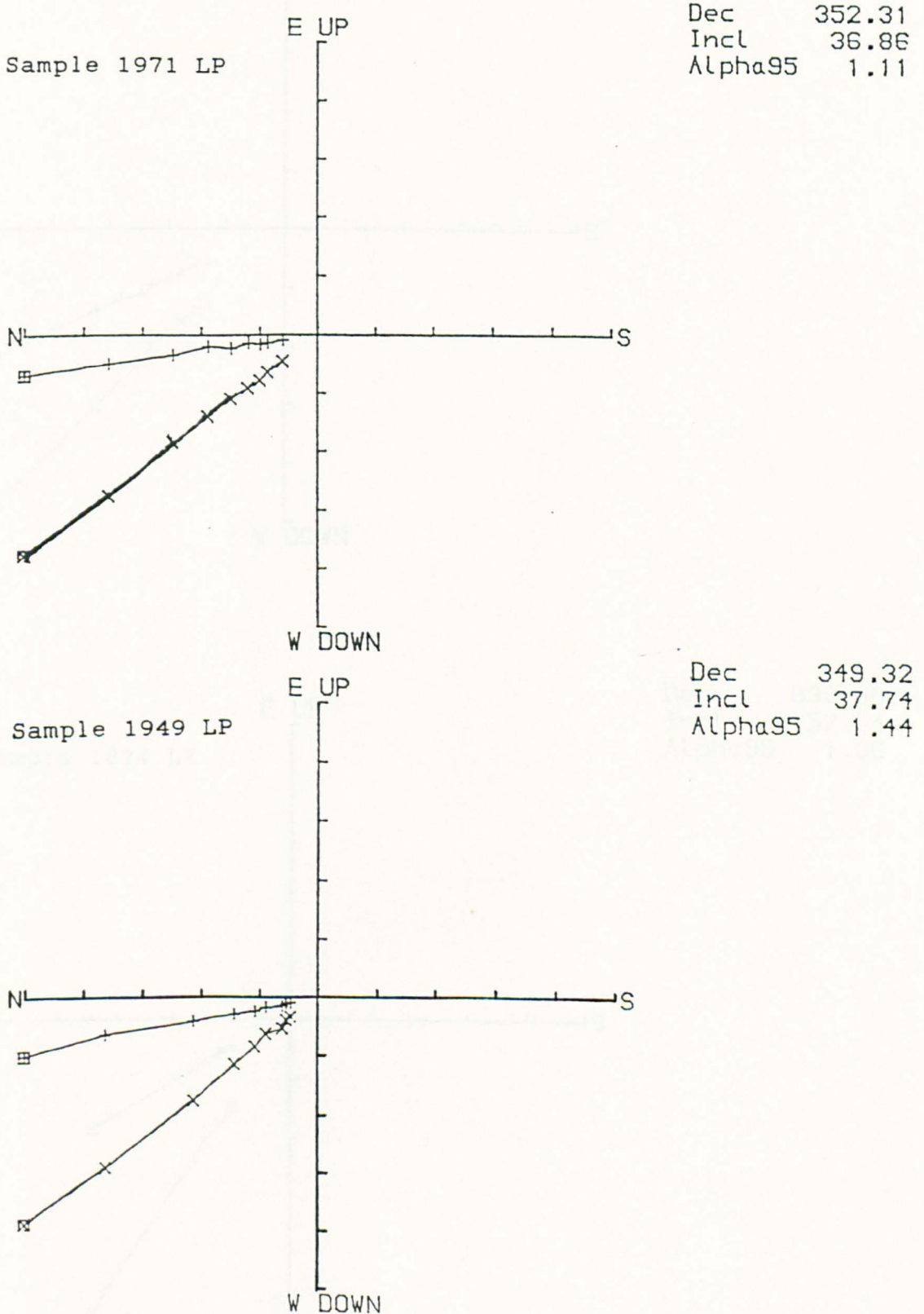
Sample 1909 T
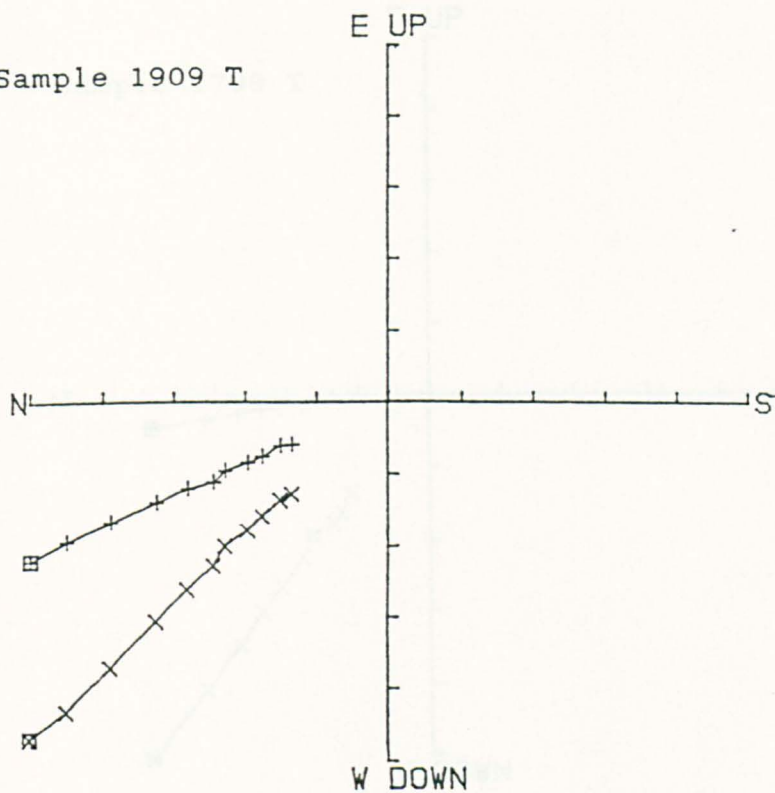
Dec 336.45
Incl 41.64
Alpha95 1.46

Sample 1824 LZ
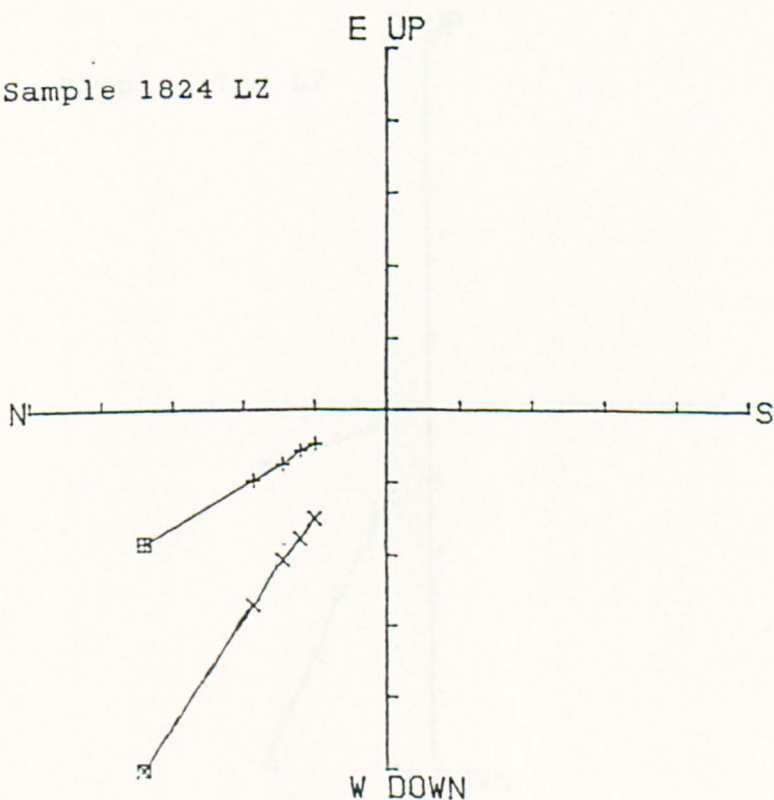
Dec 330.36
Incl 52.04
Alpha95 1.06

Sample 1798 T
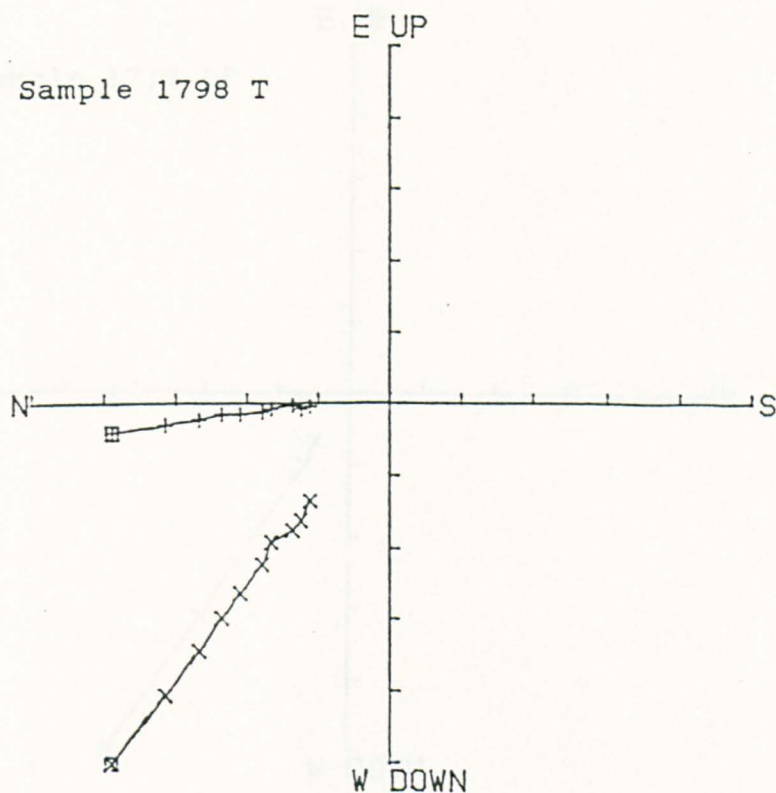
Dec   352.50
Incl   52.64
Alpha95   1.81

E UP

N'   S

W DOWN

Sample 1730 LZ
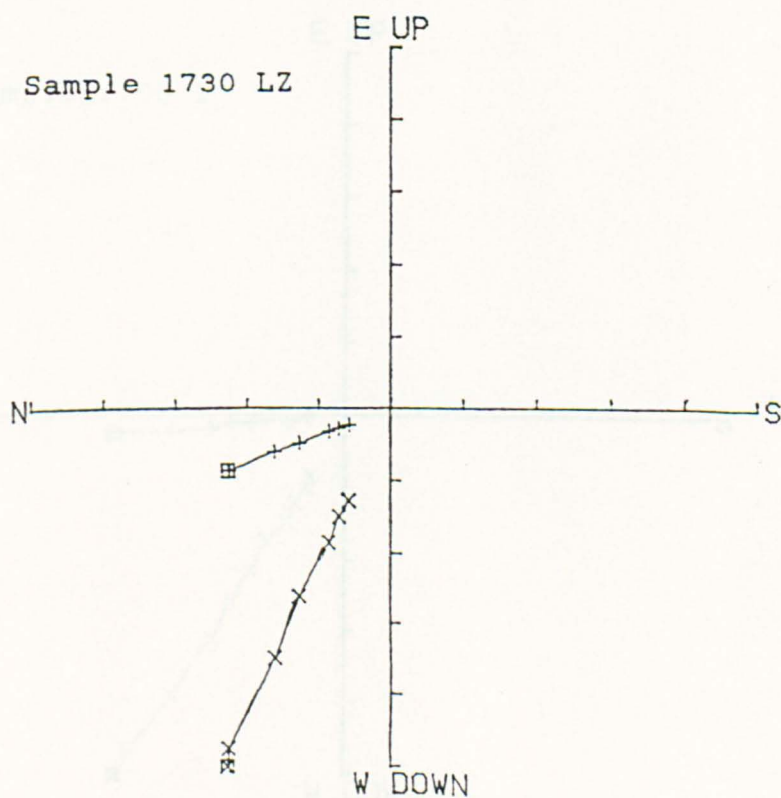
Dec   339.52
Incl   63.81
Alpha95   1.29

E UP

N'   S

W DOWN

Sample 1712 LP

E UP

N

S

W DOWN
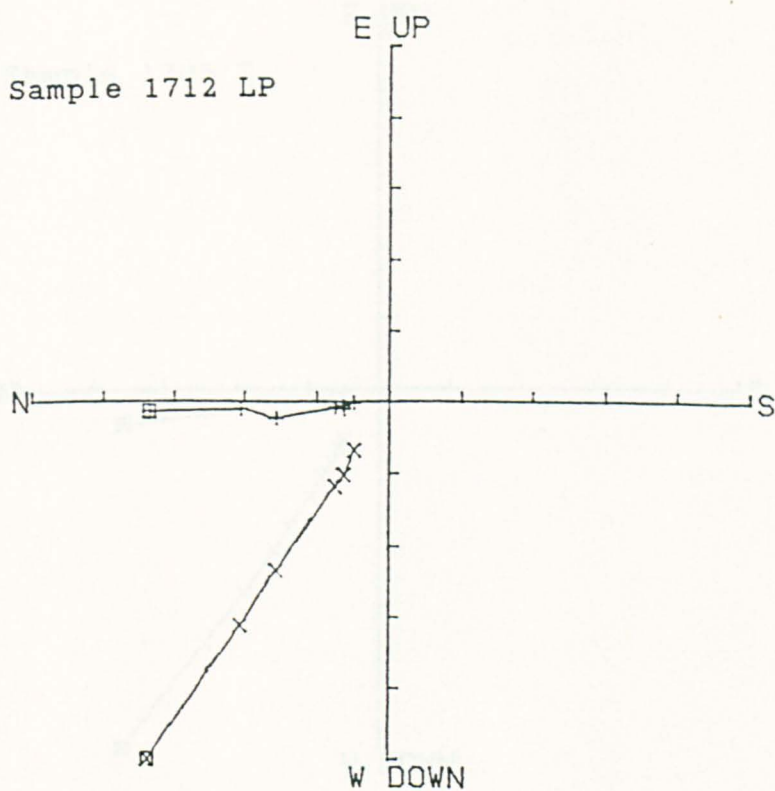
Dec   358.13
Incl   56.02
Alpha95   1.99

Sample 1706 T

E UP

N

S

W DOWN
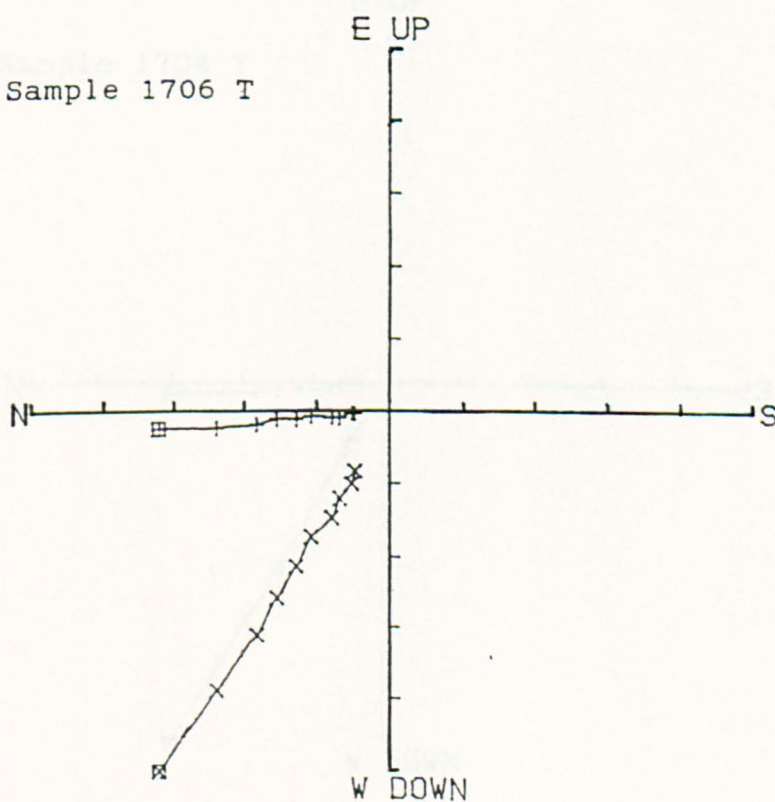
Dec   355.42
Incl   56.87
Alpha95   1.69

104
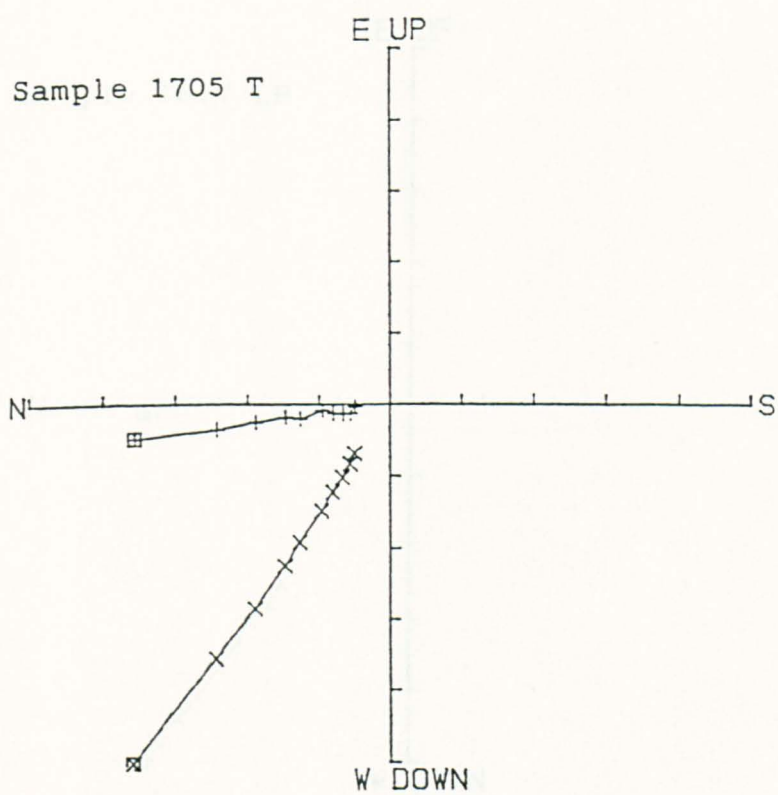
Sample 1705 T

Dec   352.61
Incl   54.32
Alpha95   1.88

E UP

N ⌐   ⌐ S

W DOWN

Sample 1704 T
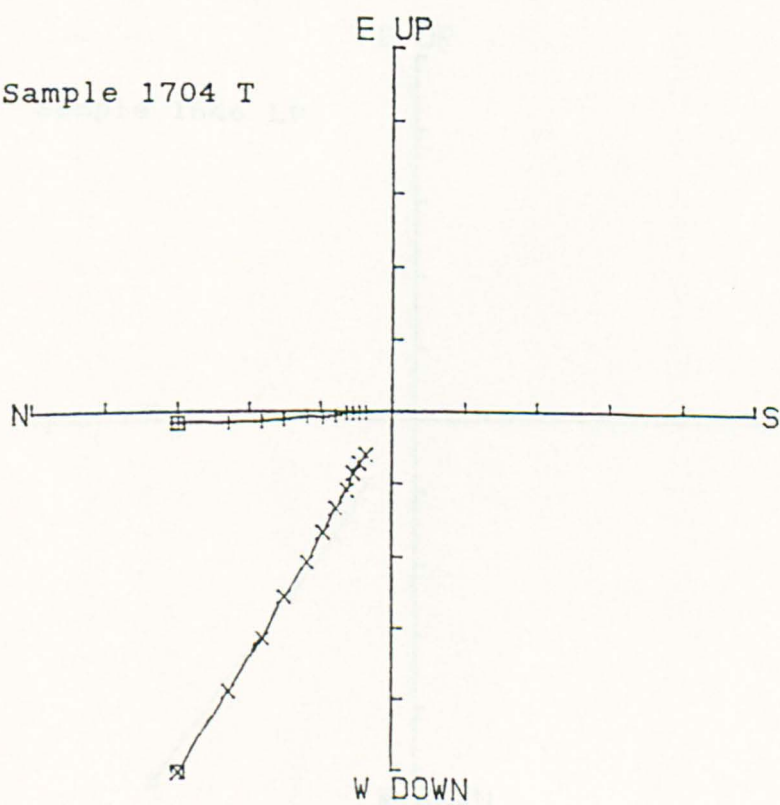
Dec   356.60
Incl   59.42
Alpha95   0.99

E UP

N ⌐   ⌐ S

W DOWN

Sample 1677 LP
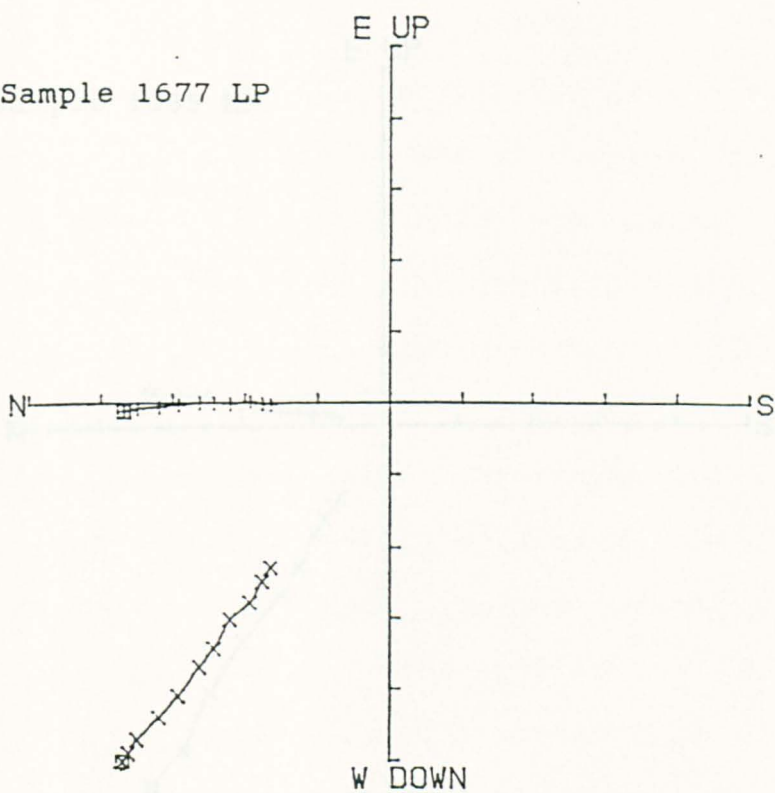
Dec   357.27
Incl   52.83
Alpha95   2.00

E UP

N

S

W DOWN

Sample 1646 LP
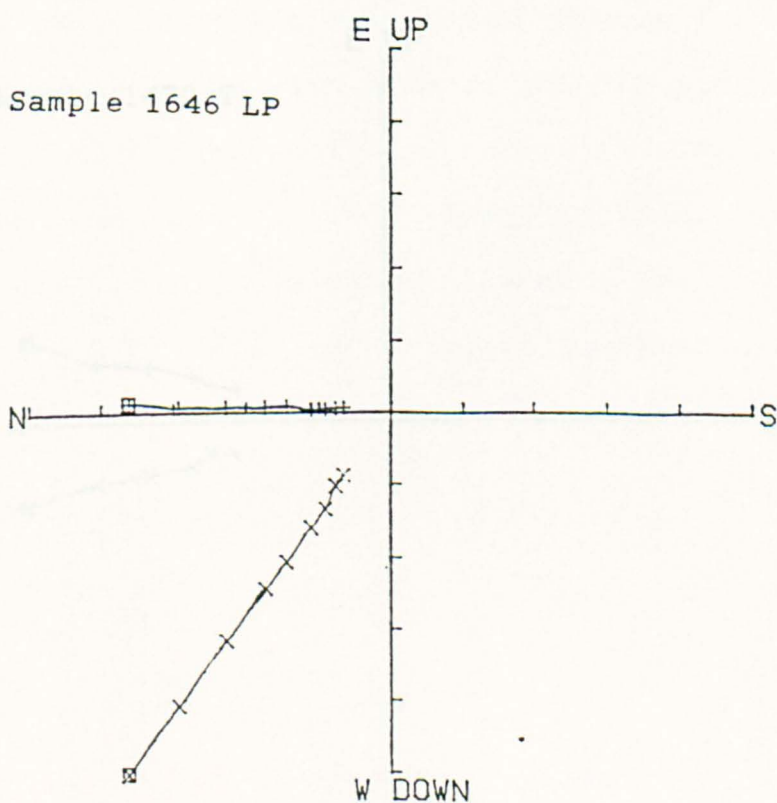
Dec   1.23
Incl   54.12
Alpha95   1.03

E UP

N

S

W DOWN

Sample 1585 LP
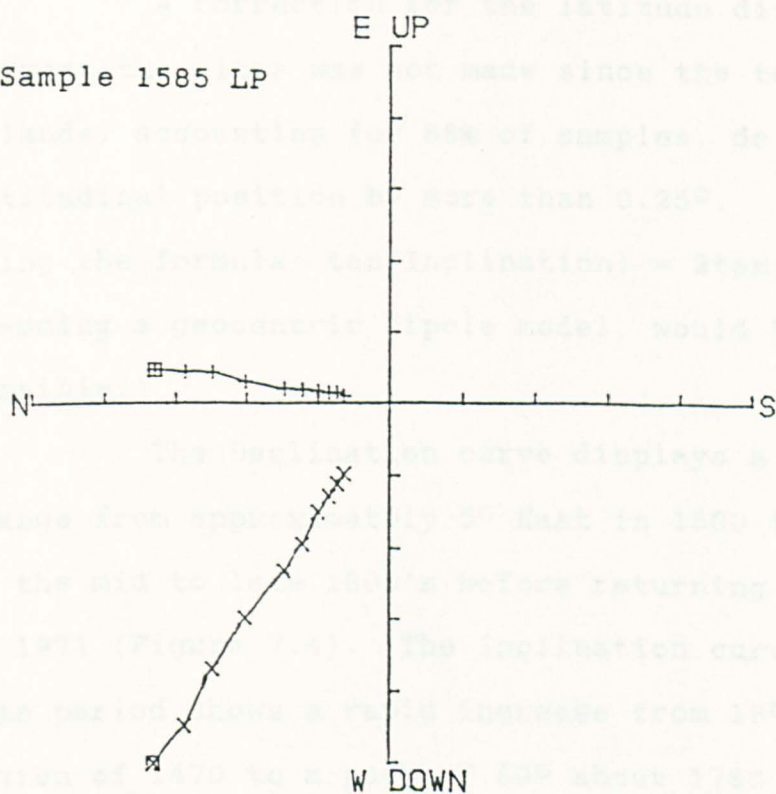
Dec   8.23
Incl   56.40
Alpha95 1.52

E UP

N ———————————— S

W DOWN

Sample 1470 T
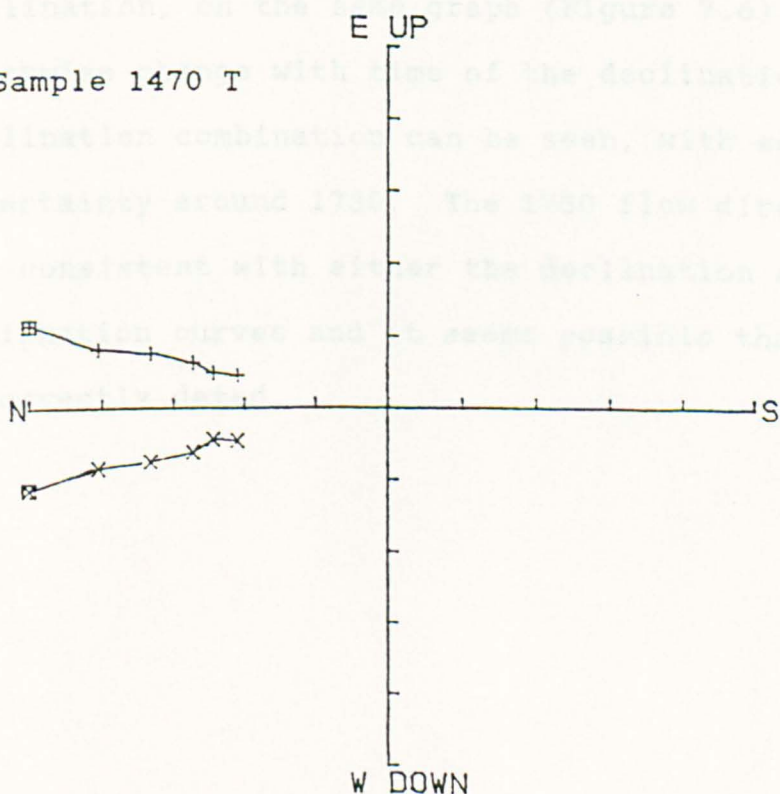
Dec   13.06
Incl   12.69
Alpha95 3.25

E UP

N ———————————— S

W DOWN

A correction for the latitude differences between the sites was not made since the two main islands, accounting for 88% of samples, do not vary in latitudinal position by more than 0.25°. (A correction using the formula: tan(Inclination) = 2tan(Latitude), assuming a geocentric dipole model, would have been possible.)

The Declination curve displays a relative change from approximately 5° East in 1500 to 18° West in the mid to late 1800's before returning to 7° West in 1971 (Figure 7.4). The Inclination curve over the same period shows a rapid increase from 18° in the region of 1470 to a peak of 60° about 1780 and then falls to its present value of 43° (Figure 7.5). Results were also plotted using declination and inclination, on the same graph (Figure 7.6). The clockwise change with time of the declination and inclination combination can be seen, with some uncertainty around 1730. The 1730 flow direction is not consistent with either the declination or inclination curves and it seems possible that it is incorrectly dated.

Figure 7.4 Variation of declination with time for the Canary Island samples.
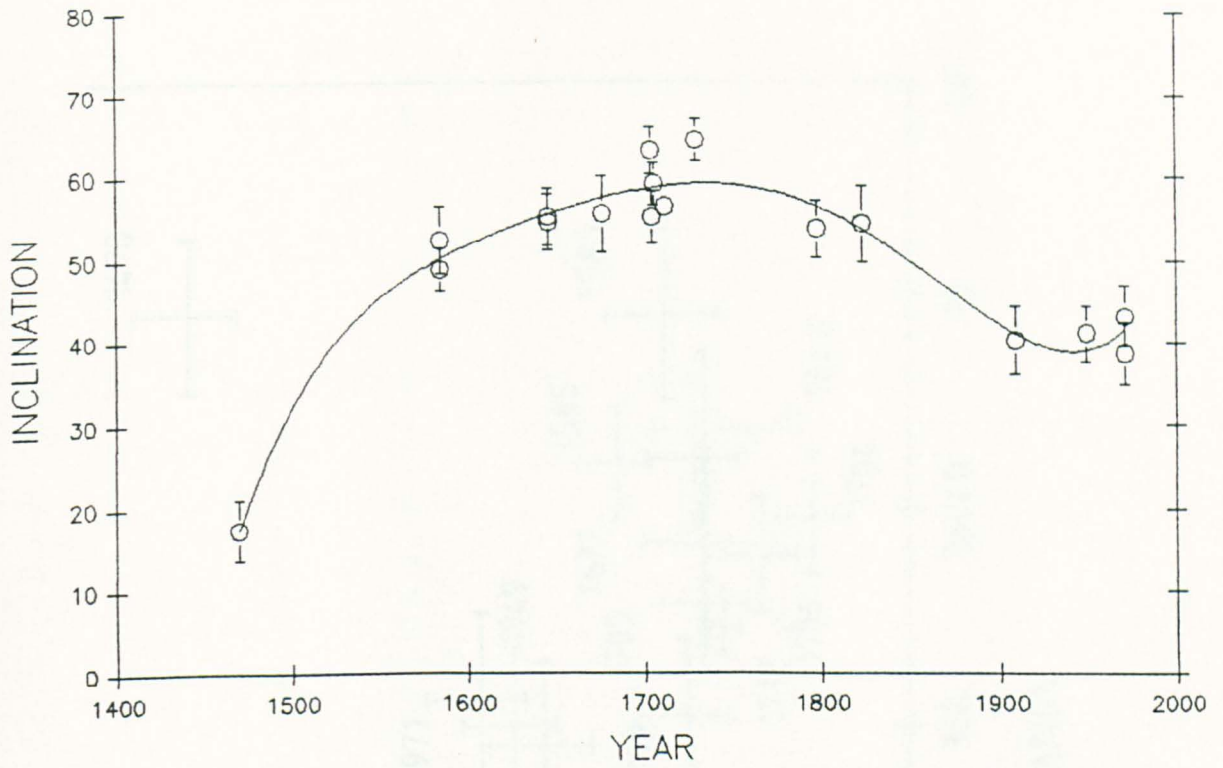
Figure 7.5 Variation of inclination with time for the Canary Island samples.
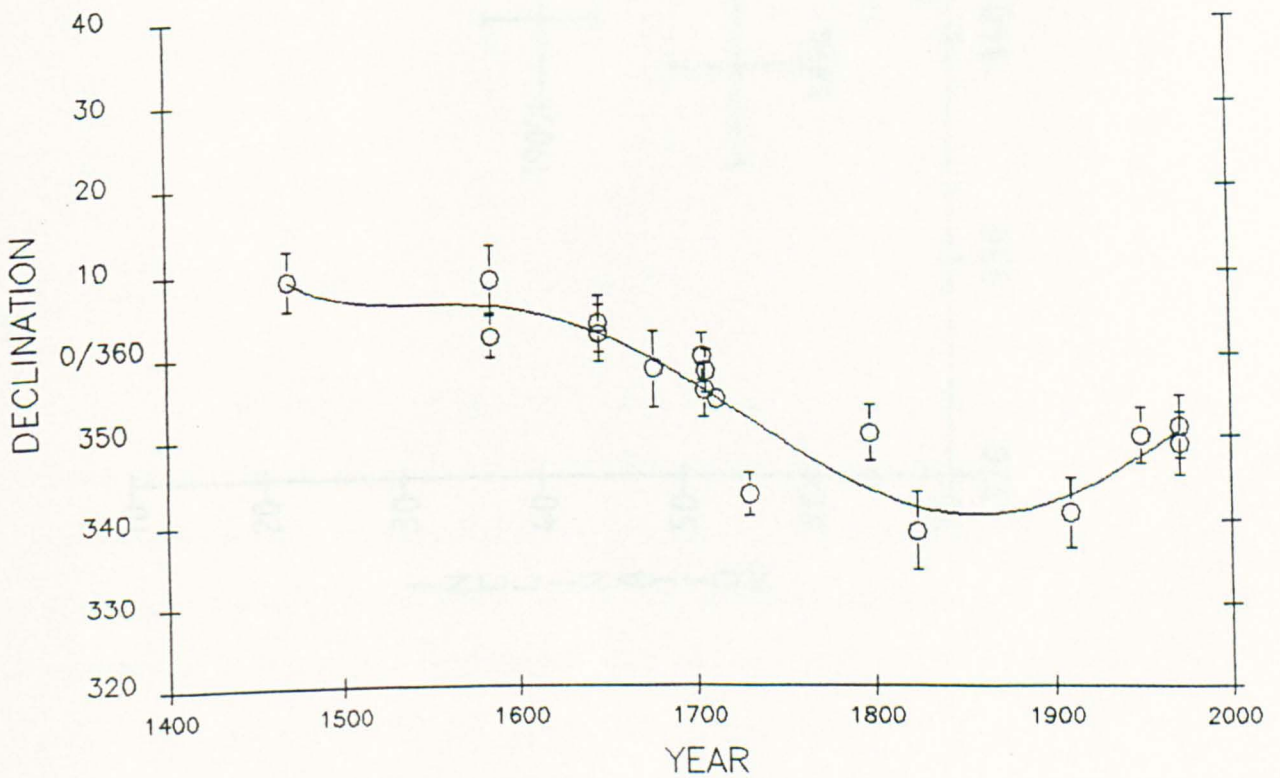
Figure 7.6 Variation of declination and inclination for the Canary Islands.
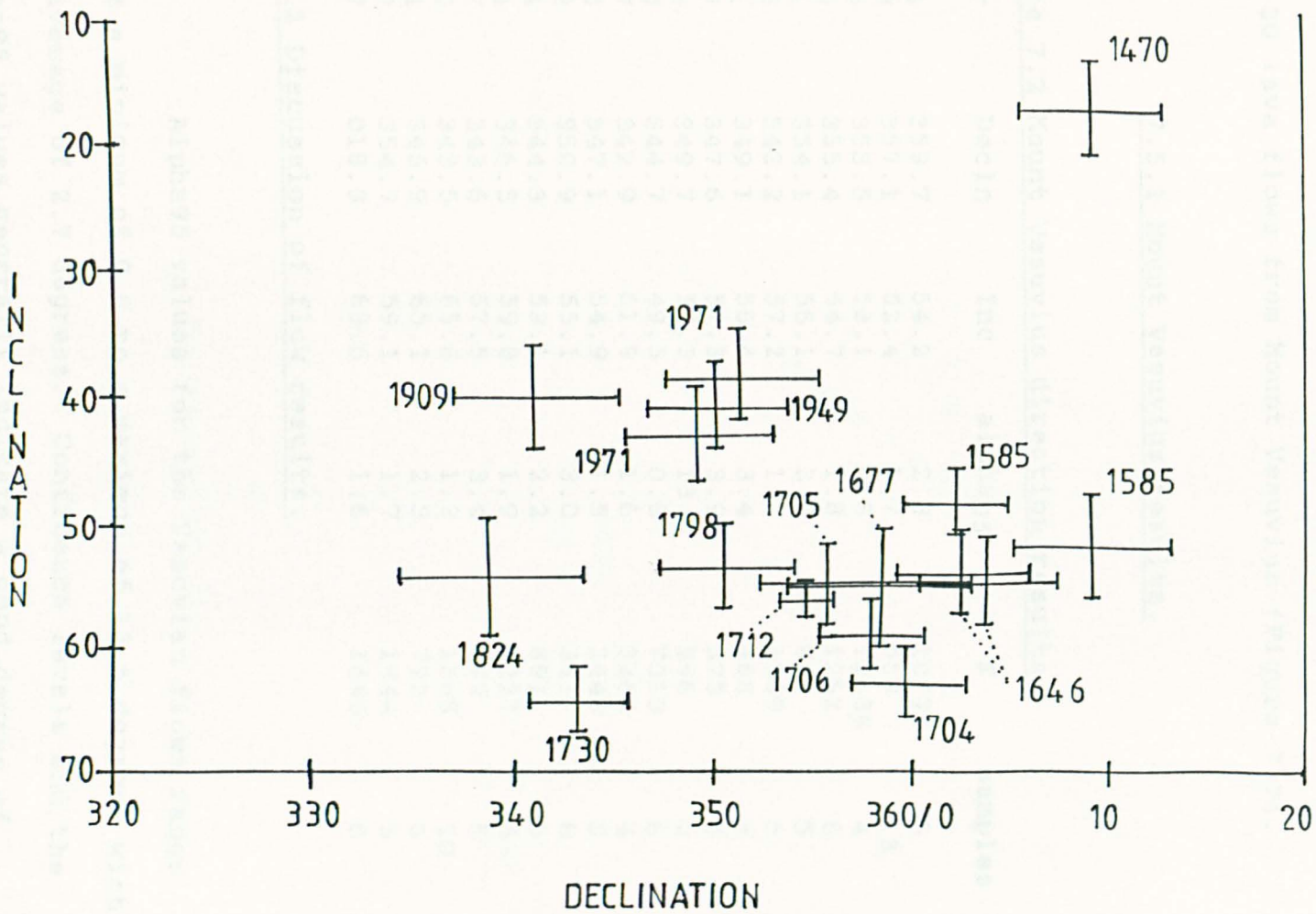
7.5 Mount Vesuvius directional secular variation.

The declination and inclination were measured for 20 lava flows from Mount Vesuvius (Figure 7.7).

7.5.1 Mount Vesuvius results.

Table 7.2 Mount Vesuvius direction results.

Year	Decln	Inc	alpha95	K	samples
1944	359.7	54.2	2.3	1077	5
1929	357.1	52.4	1.7	559	13
1906	353.5	53.1	0.8	12638	4
1895	355.4	54.7	1.8	1252	6
1891	354.1	56.1	2.5	921	5
1886	343.2	57.2	1.7	1839	5
1871	349.1	56.4	3.4	488	5
1867	347.6	57.3	3.9	375	5
1858	349.7	54.3	13.5	346	2
1850	344.7	49.5	0.8	7013	6
1847	342.9	61.9	1.6	3262	4
1834	347.1	54.9	1.5	2449	5
1822	350.9	55.1	3.0	341	8
1804	344.3	53.1	2.2	891	6
1794	346.5	59.8	1.9	1227	6
1767	343.6	57.5	3.4	499	5
1760	343.5	65.6	1.3	1365	10
1754	345.9	65.1	2.3	792	6
1737	354.7	59.1	1.7	1944	5
1697	018.3	63.6	1.6	1646	6

7.5.2 Discussion of flow results.

Alpha95 values for the Vesuvian flows range from a minimum of 0.8 to a maximum of 13.5 degrees with an average of 2.7 degrees. Confidence levels and the alpha95 values generally indicate a good degree of accuracy. There is, however, one exception, the 1858 flow has an alpha 95 value of 13.5 degrees, a value which is approximately four times larger than any other

Figure 7.7 Specimen Zijderfeld plots for the Mount
Vesuvius. A + indicates the horizontal component, a x
represents a vertical component.

Sample V1944

Dec	357.65
Incl	50.98
Alpha95	1.12

Sample V1929

Dec	352.66
Incl	52.77
Alpha95	0.69

Sample V1906

E UP
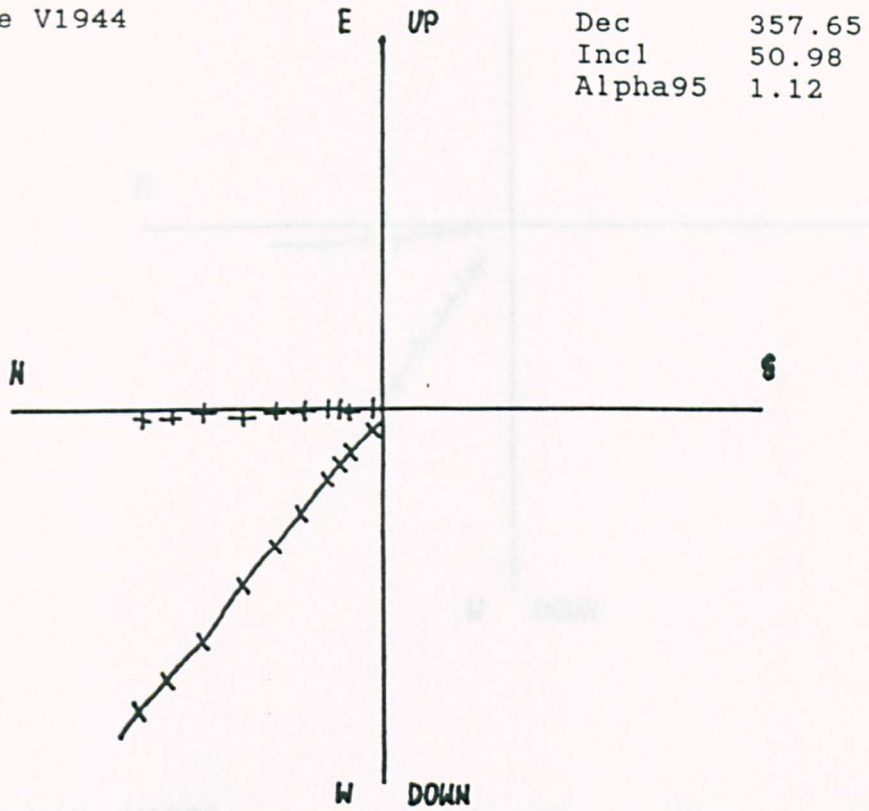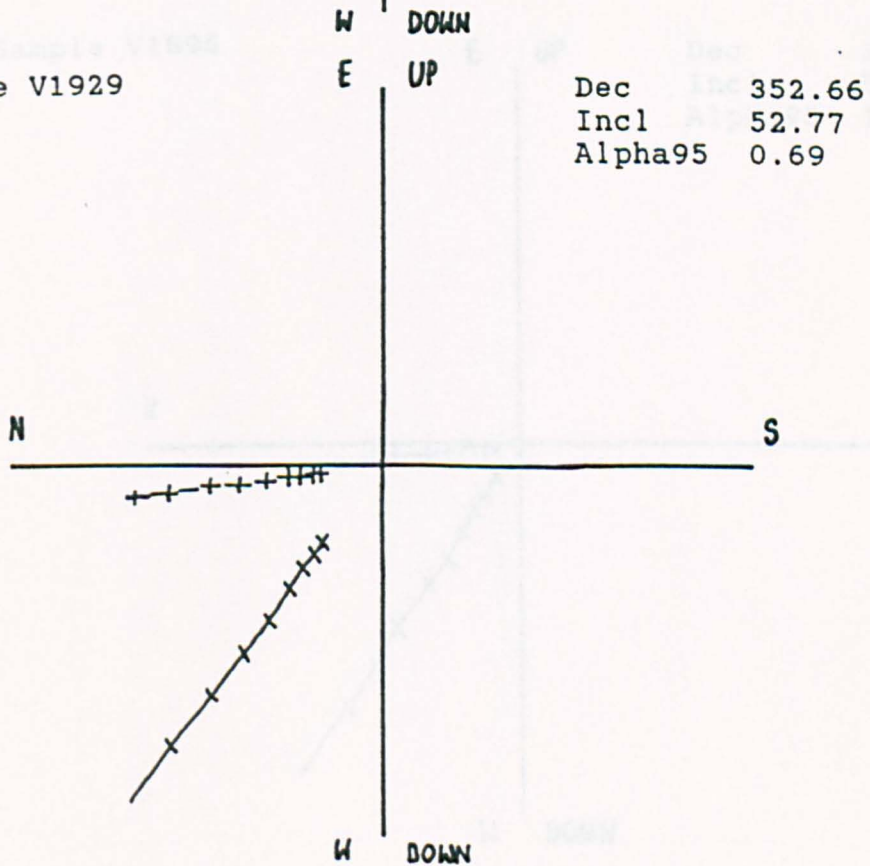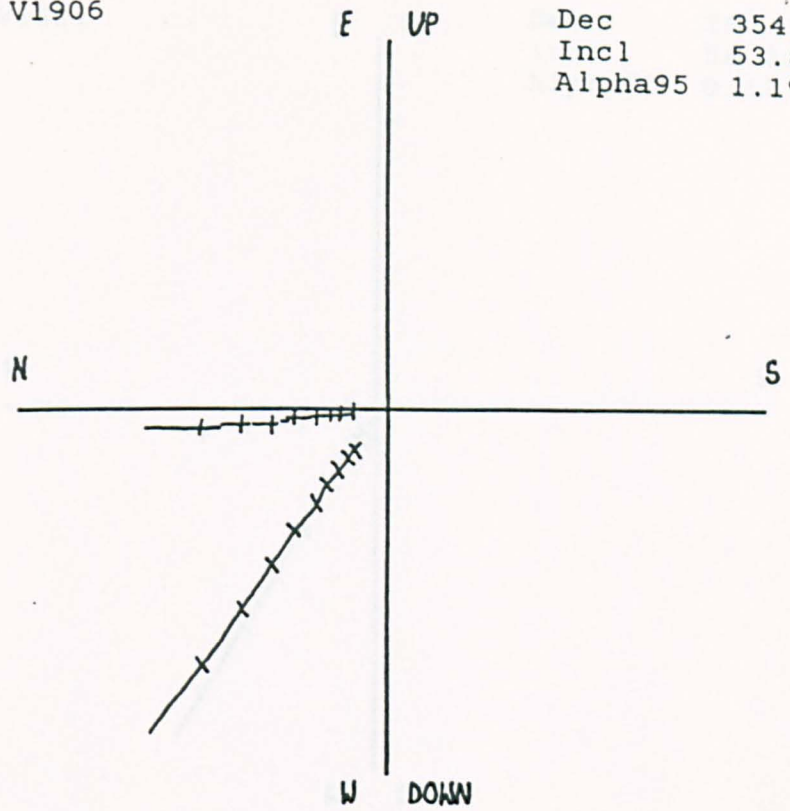
Dec   354.35
Incl   53.84
Alpha95   1.19

N   S

W   DOWN

Sample V1895

E UP
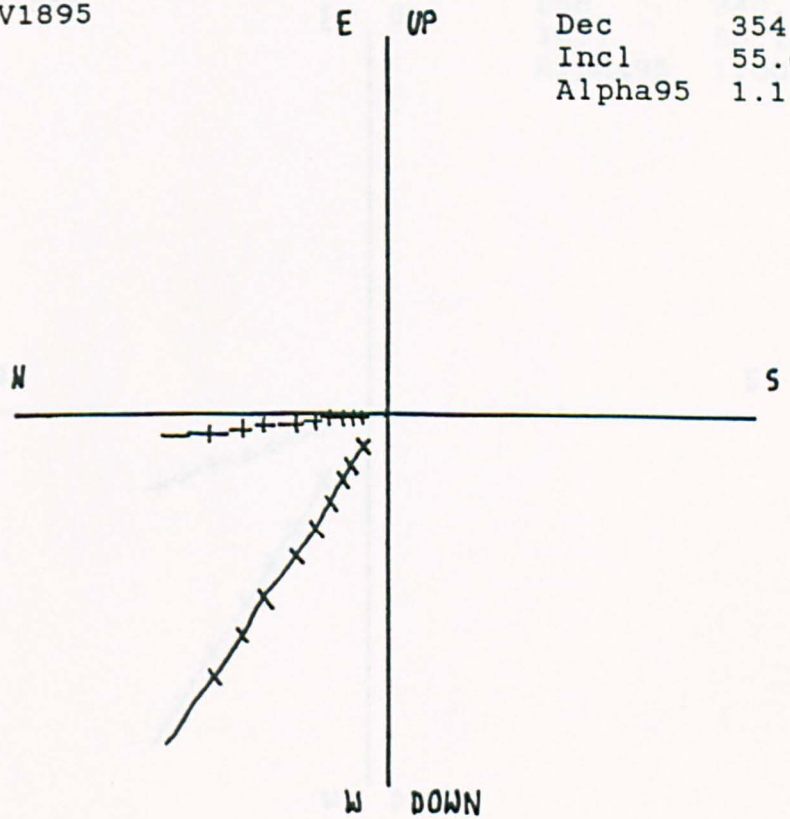
Dec   354.24
Incl   55.68
Alpha95   1.15

N   S

W   DOWN

Sample V1891

E   UP

Dec   352.34
Incl   58.86
Alpha95 0.67

W

S

W   DOWN
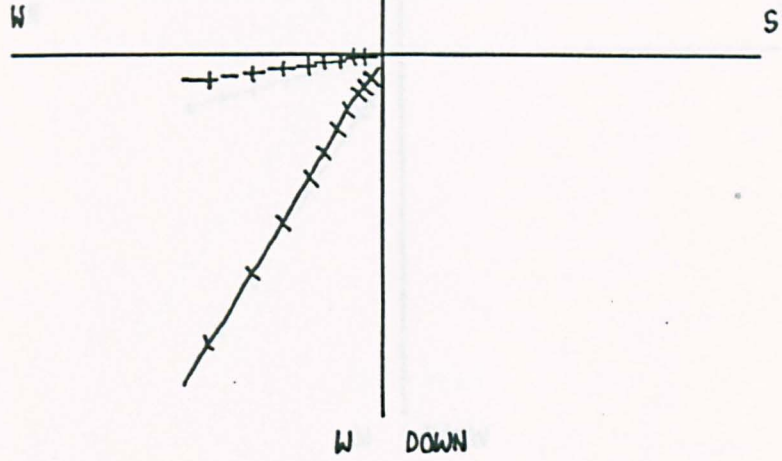
Sample V1886

E   UP

Dec   340.87
Incl   56.13
Alpha95 1.00

N

S

W   DOWN
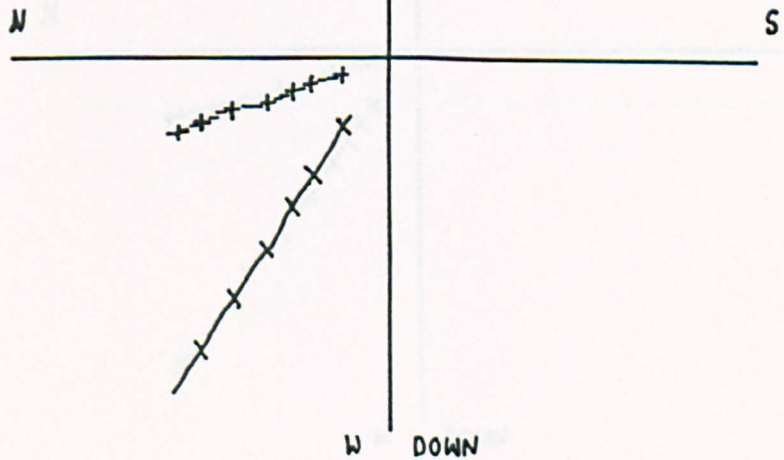
Sample V1871

E   UP

Dec   344.33
Incl   56.15
Alpha95   0.62

N

S

W   DOWN
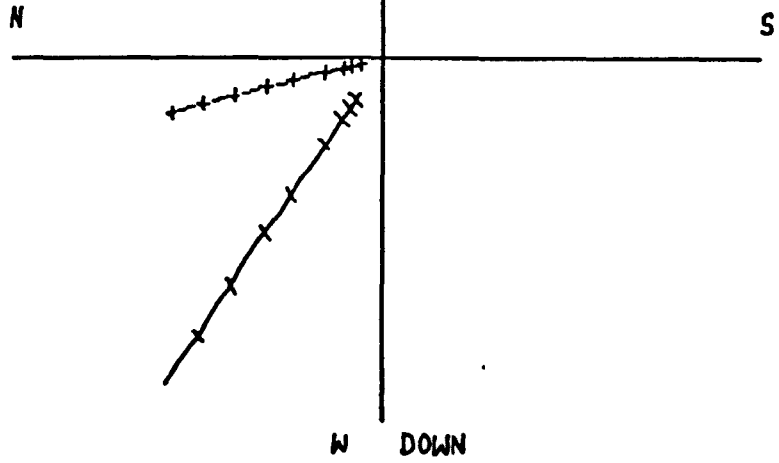
Sample V1867

E   UP

Dec   344.90
Incl   51.89
Alpha95   0.59

N

S

W   DOWN
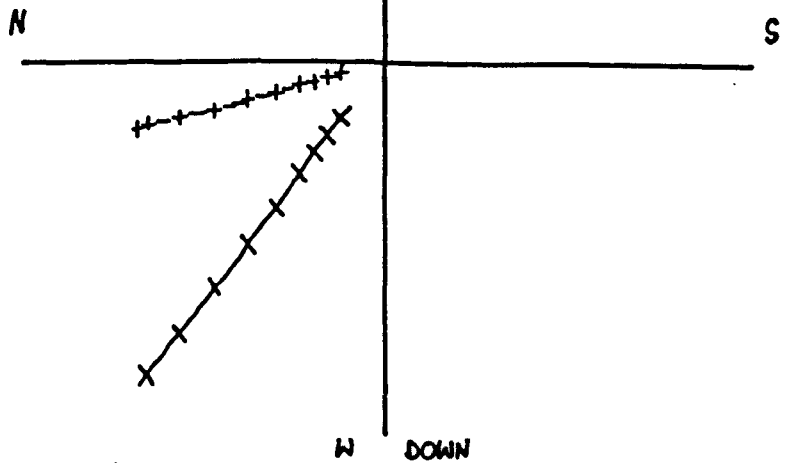
Sample V1858

E UP

Dec	346.42
Incl	51.99
Alpha95	0.76

N   S

W   DOWN
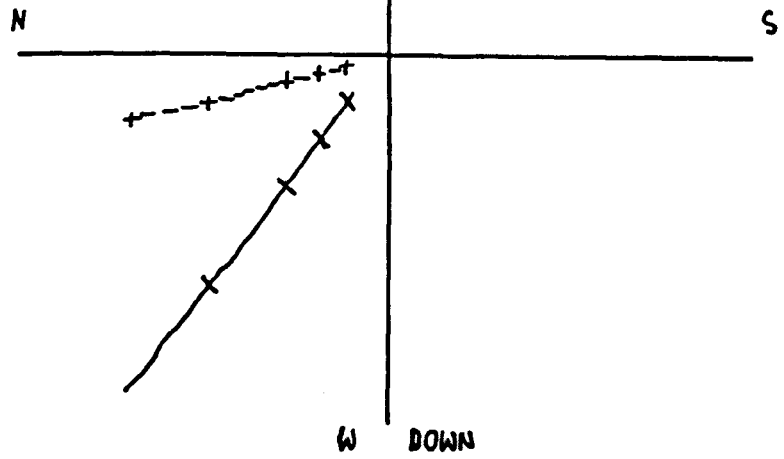
Sample V1850

E UP

Dec	344.58
Incl	49.24
Alpha95	0.83

N   S

W   DOWN
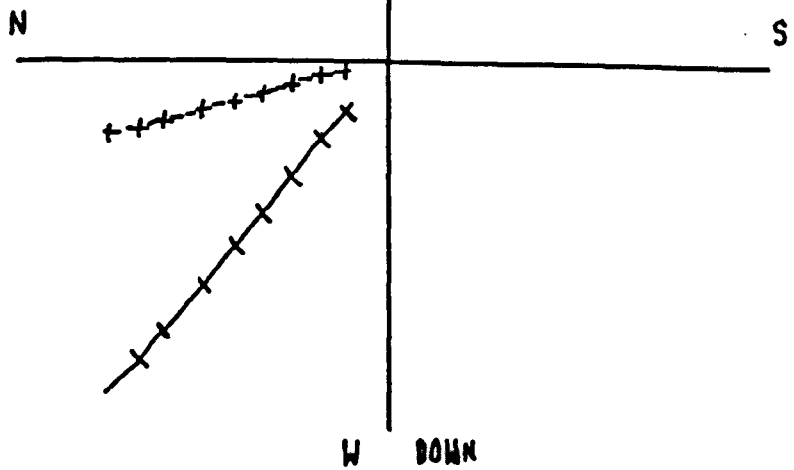
Sample V1847

E UP

Dec 344.72
Incl 61.59
Alpha95 0.48

N

S

X

W DOWN
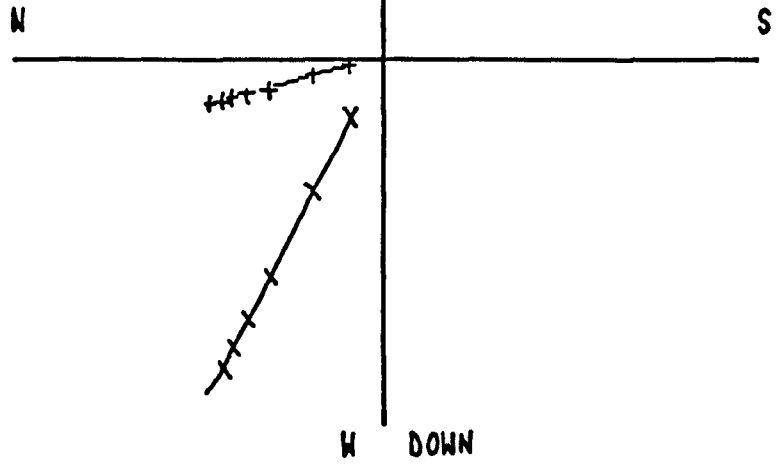
Sample V1834

E UP

Dec 344.38
Incl 54.56
Alpha95 1.11

N

S

W DOWN
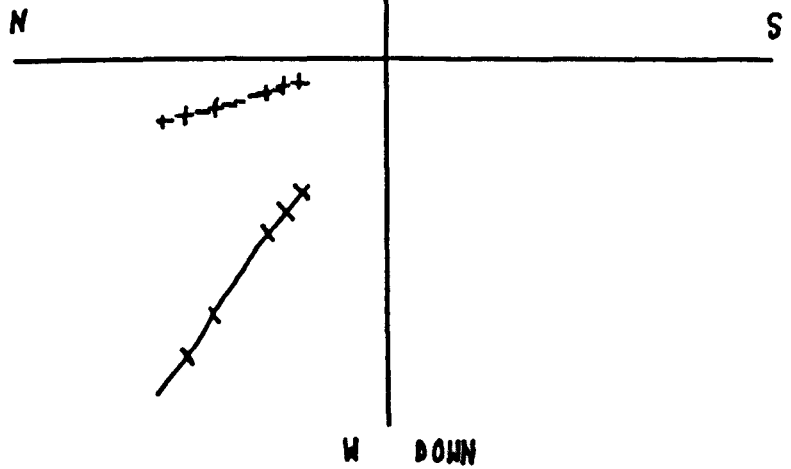
Sample V1822

E UP

Dec 346.42
Incl 54.89
Alpha95 1.06

N

S

N DOWN
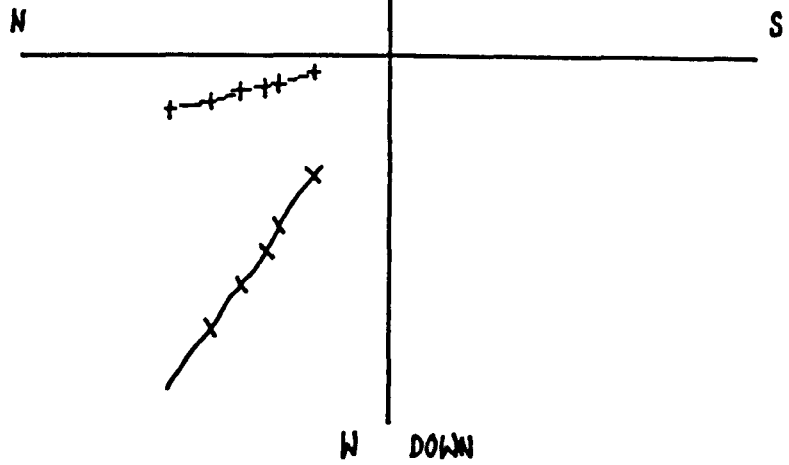
Sample V1804

E UP

Dec 343.46
Incl 50.89
Alpha95 1.57

N

S

N DOWN
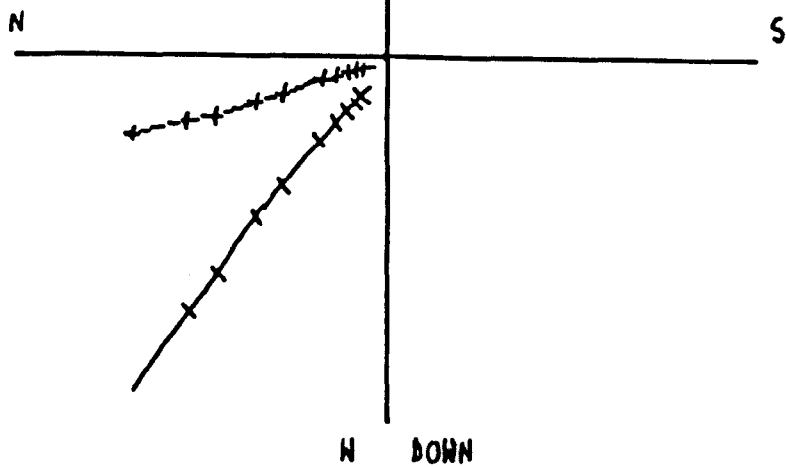
Sample V1794

E UP

Dec   351.16
Incl   60.36
Alpha95   0.67

N   S

W   DOWN
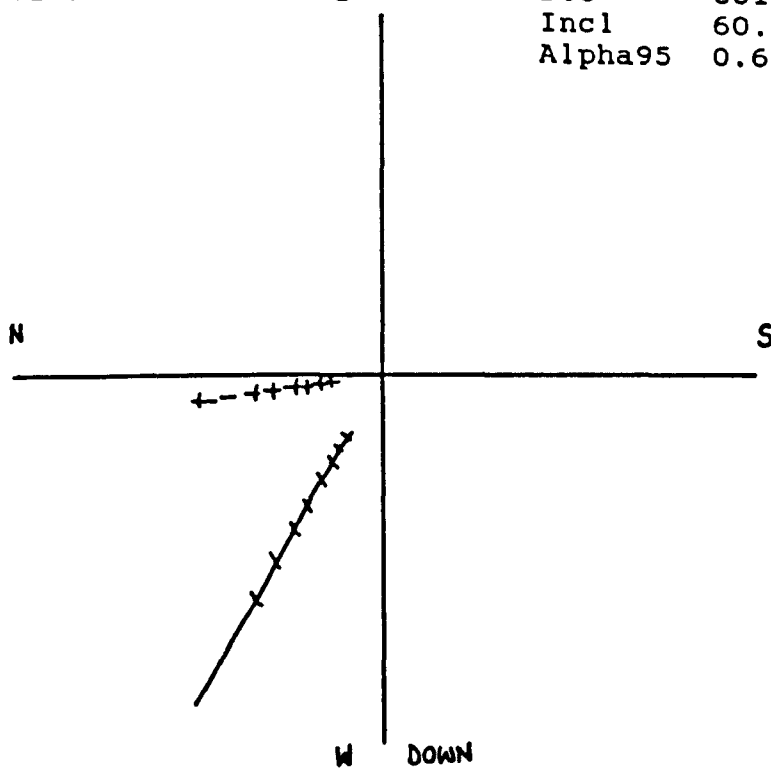
Sample V1767

E UP

Dec   346.78
Incl   56.17
Alpha95   0.95

N   S

W   DOWN

119
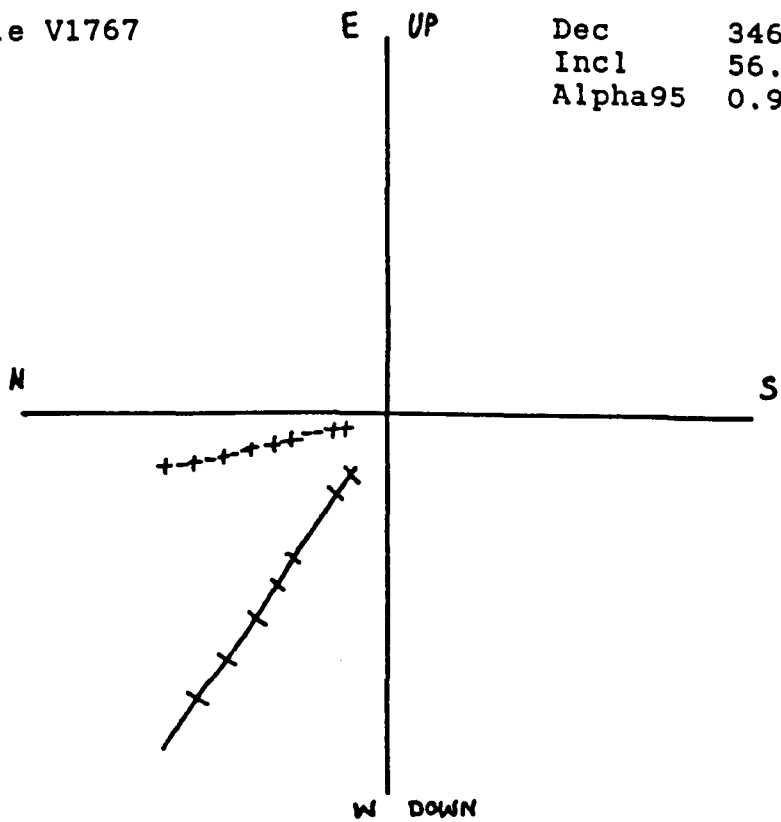
Sample V1760

E UP

Dec 344.63
Incl 64.75
Alpha95 1.12

N

S

W DOWN
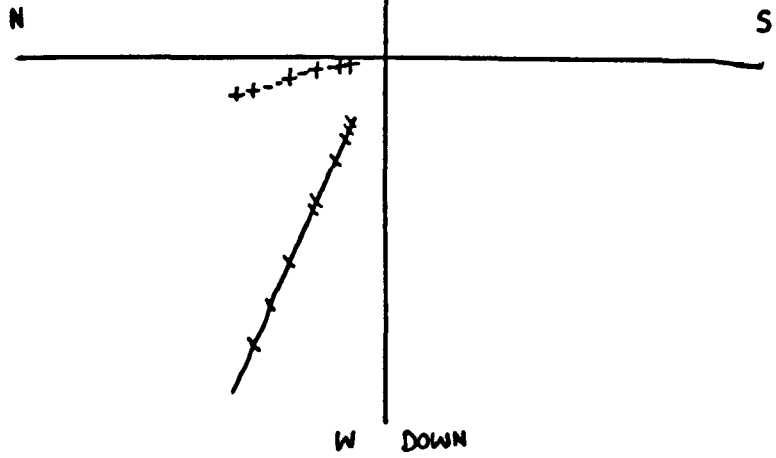
Sample V1754

E UP

Dec 357.25
Incl 60.32
Alpha95 0.60

N

S

W DOWN
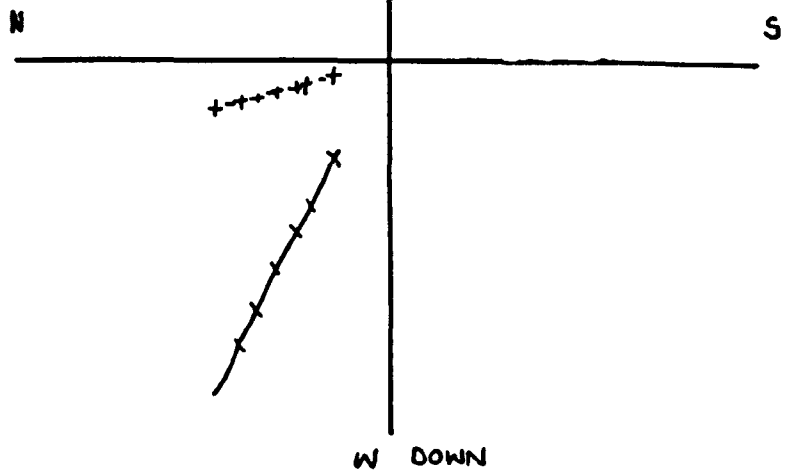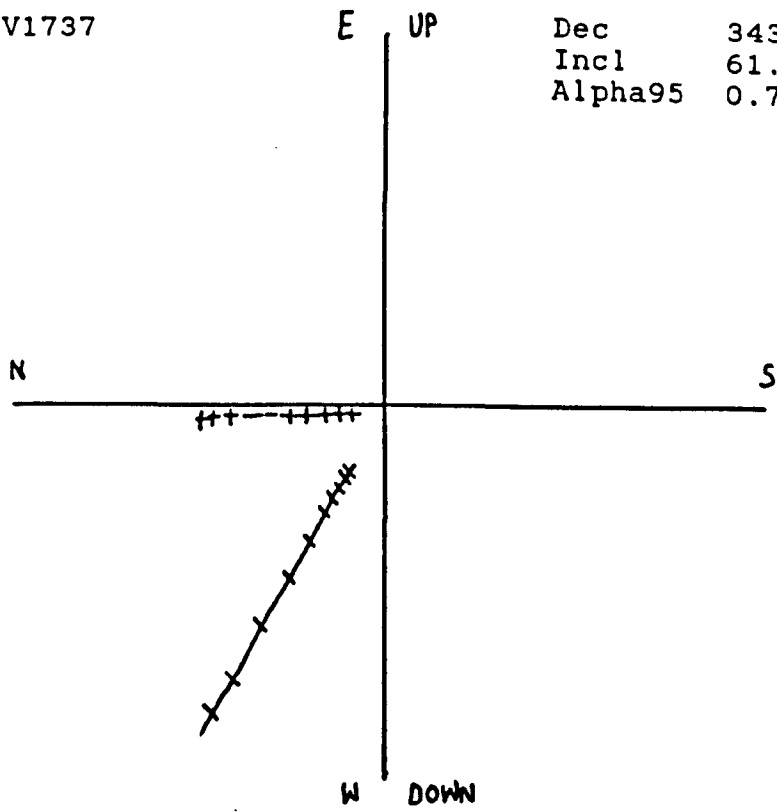
Sample V1737

Dec	343.31
Incl	61.83
Alpha95	0.78

Sample V1697
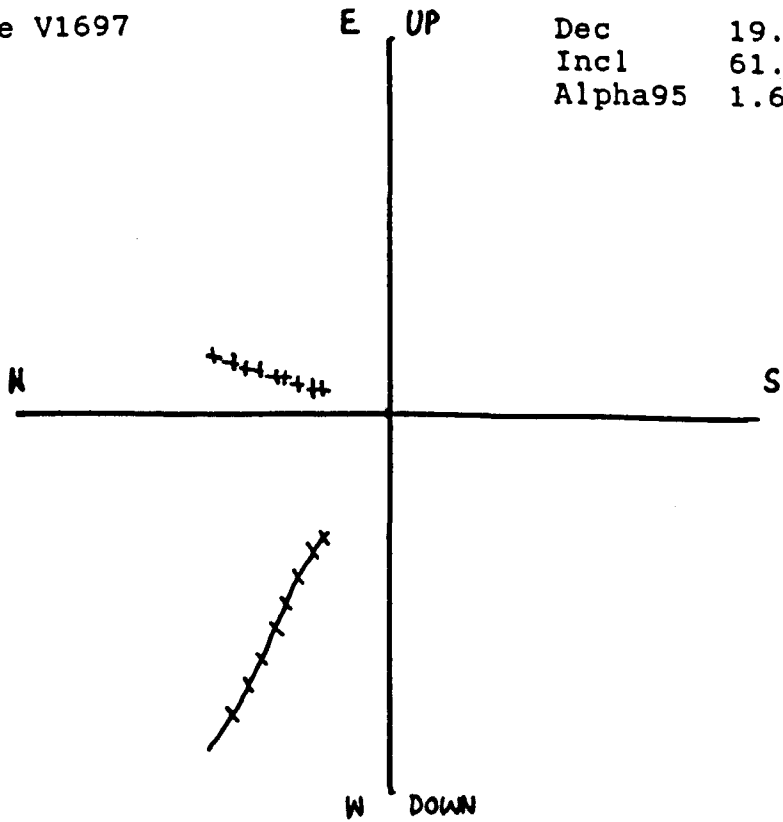
Dec	19.04
Incl	61.42
Alpha95	1.66

lava flow. The site can be singled out as being prone
to major alteration from work done on rock magnetism,
(Chapter 13) so its value must be viewed with some
caution.

7.5.3 Secular variation curves.

The results found for Vesuvius are plotted in
the same manner as those for the Canary Islands using a
least squares fit of order five. The declination curve
shows a rapid change from 18° east in 1697 to around
18° west in 1790 before swinging very steadily east to
almost zero in 1944 (Figure 7.8). The Inclination
curve shows an overall decrease in inclination from 63°
to 54° over the time period from 1697 to 1944 (Figure
7.9). A declination against inclination graph was also
plotted (Figure 7.10).

7.6 Comparisons and Conclusions.

The swing to the west of the declination is
one feature which stands out when the two sets of data
are compared. It has its maximum around 1865 for the
Canary Islands and 1785 for Mount Vesuvius, a
difference of 80 years. There is an angular difference
between the two sites of 30° of longitude and 12° of
latitude. Setting aside the latitudinal difference for
a moment, there is a drift rate for the feature of

0.37° per year to the west. The similarity of this value and that suggested by Yukatake (1979) of 0.3° per year for the drifting part of the Earth's field is encouraging.

Figures 7.8 & 7.9 Variation of declination and
inclination with time for the Mount Vesuvius samples.
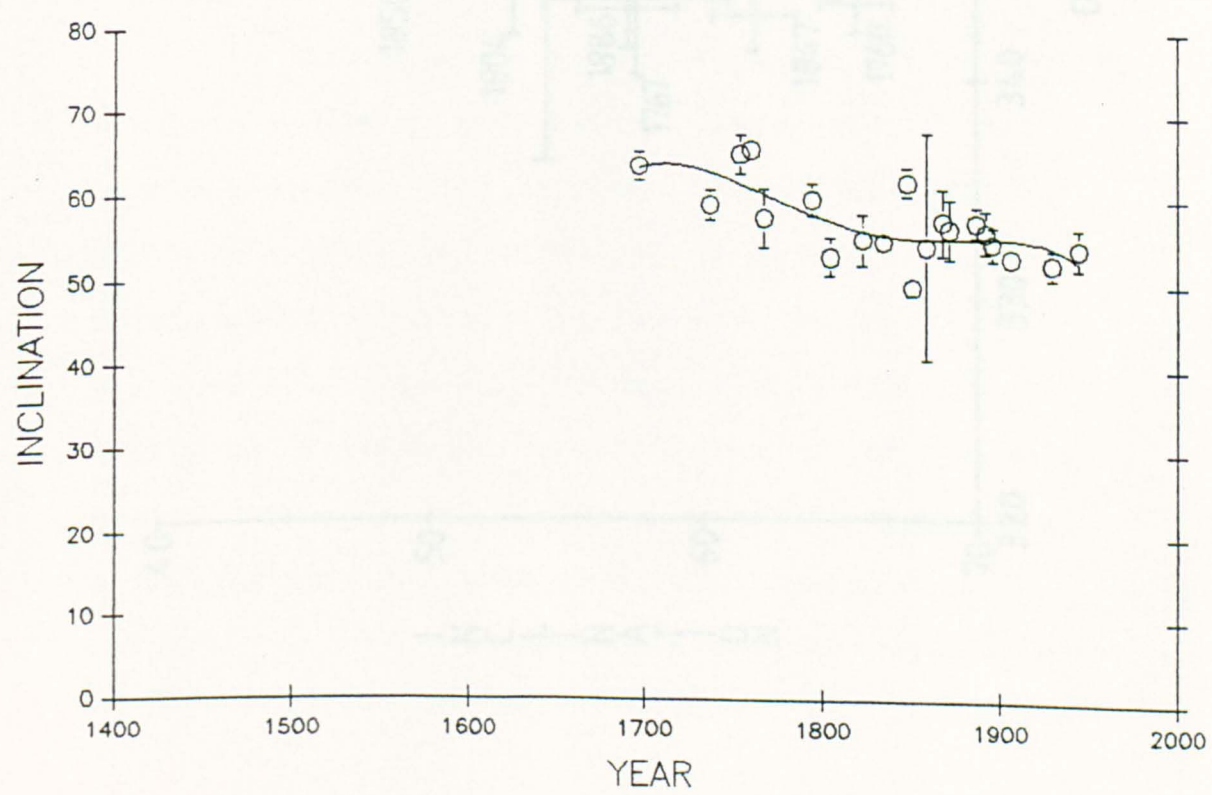
Figure 7.10 Variation of declination and inclination for Mount Vesuvius.
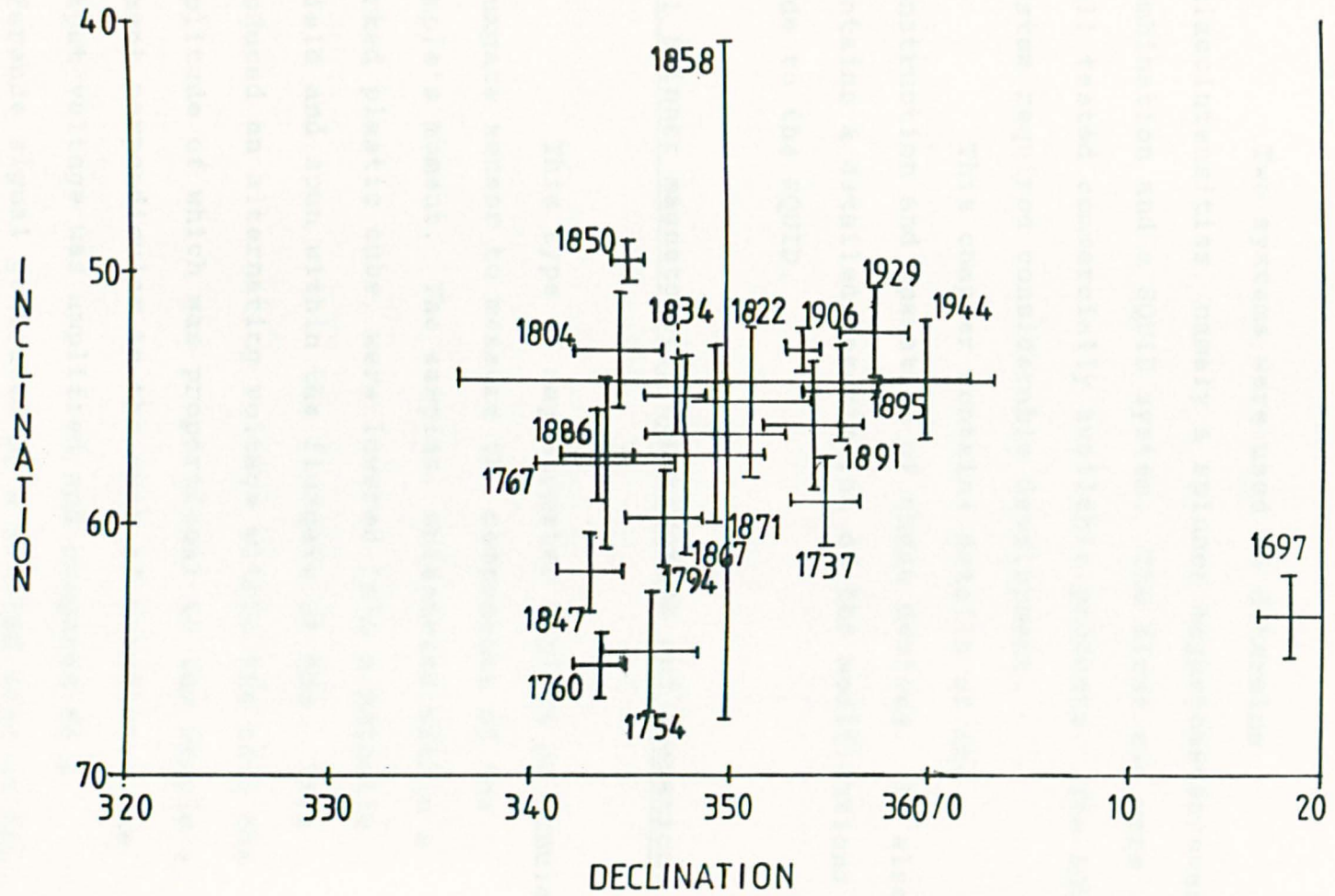
Chapter 8.

Instrumentation used to determine palaeointensity.

Two systems were used to determine palaeointensities, namely a spinner magnetometer/oven combination and a SQUID system. The first two were well tested commercially available products. The SQUID system required considerable development.

This chapter contains details of the construction and operation of these devices. It also contains a detailed description of the modifications made to the SQUID.

8.1 Spinner magnetometer construction and operation.

This type of magnetometer employs an annular fluxgate sensor to measure the components of the sample's moment. The samples, orientated within a marked plastic cube, were lowered into a magnetic shield and spun within the fluxgate at 6Hz. This produced an alternating voltage within the coil the amplitude of which was proportional to the sample's moment perpendicular to the axis of rotation. The output voltage was amplified and compared to a reference signal generated by a slotted disc at the base of the rotating shaft (Figure 8.1). The slots

were optically sensed and the reference signal compared
with the phase of the sample output signal to determine
the direction of the magnetic moment.
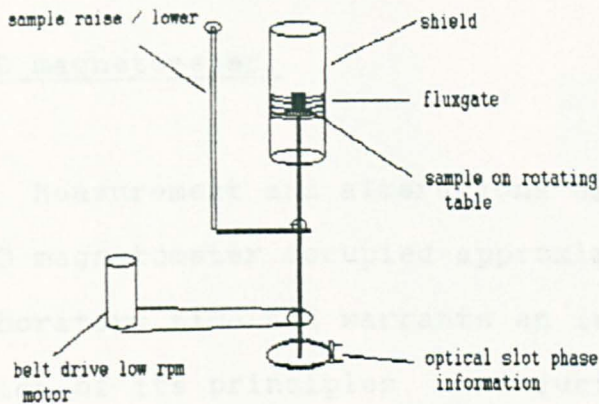
Figure 8.1 Spinner Magnetometer.

The number of spins were software switchable
between a total spin time of 6 or 24 seconds after
which the samples were raised to allow a change of
orientation. Two measurements were made along each of
the three orthogonal directions and the results were
analyzed by an on-line computer. Calibration was
checked at the start of each session using a specimen
of known magnetisation and at 3 hour intervals during
longer sessions. The magnetometer was capable of a
sensitivity of approximately 0.1mA/m when using the 24
second spin time.

8.2 Thermal demagnetisor.

The spinner magnetometer was used in
conjunction with a thermal demagnetiser. This is a

large temperature controllable oven which excluded
magnetic fields by the use of mu-metal shielding. It
could hold up to 18 2.54cm cores or 50 0.9cm cores.

8.3 SQUID magnetometer.

Measurement and alterations carried out on
the SQUID magnetometer occupied approximately half the
total laboratory time and warrants an in-depth
explanation of its principles, construction and
problems.

SQUID is an acronym for Superconducting
Quantum Interference Device. The photograph of the
SQUID magnetometer system, Figure 8.2, shows both the
Mu-metal shielding and the ramp which samples travel up
to reach their measuring position.

8.3.1 Superconductivity

Certain materials become superconducting, ie
have no electrical resistance, at very low
temperatures, as discovered in 1911 by Kamerlingh
Onnes. In 1933 Meissner discovered that a
superconductor expels all magnetic flux from within
itself and becomes a perfectly diamagnetic material.
Thus when a superconducting material is formed into a
ring and its temperature lowered at the point where it

becomes superconducting, the material becomes

diamagnetic and in the presence of a magnetic field
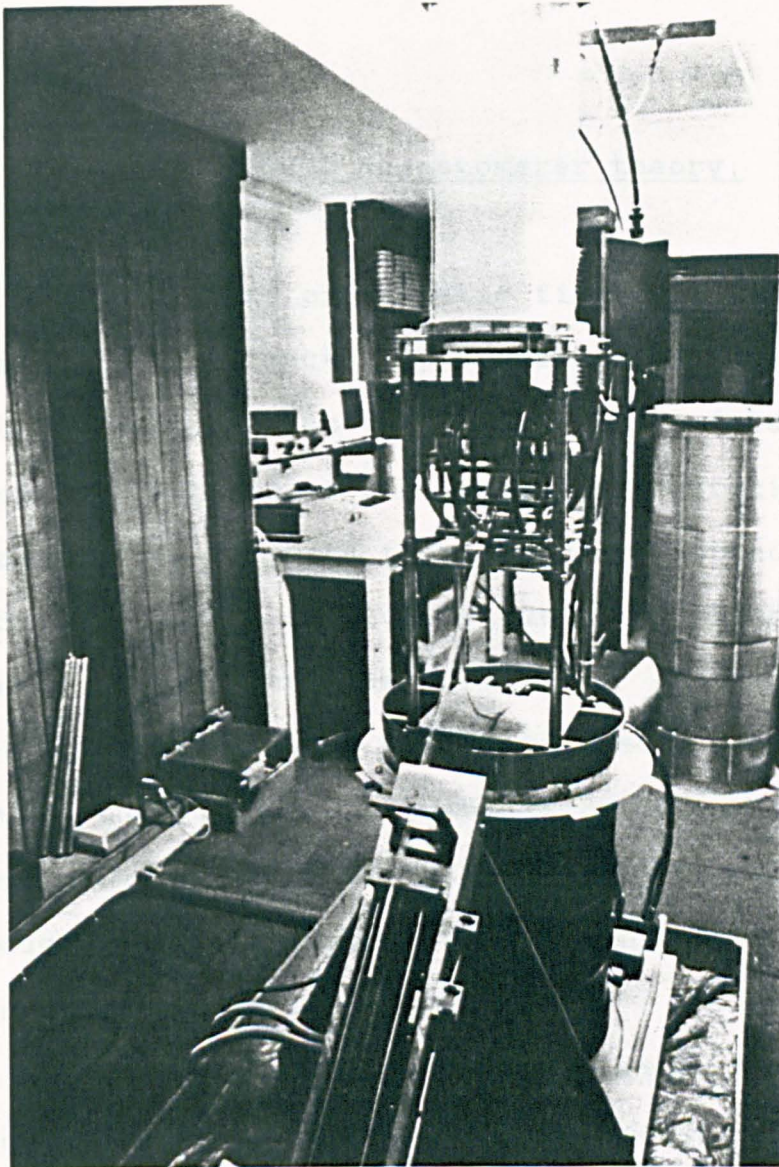
Figure 8.2   SQUID magnetometer without shields.

a current is created on the inner and outer surfaces of

the material. On removal of the field the external

circulating current disappears leaving only the current

on the inner surface and this gives rise to a "trapped"

magnetic field. (This phenomenon presents problems if

a SQUID is not cooled in zero field). The magnetic

flux within the ring in such a situation has some
multiple value of the Flux Quantum, that is, a multiple
of 2.07×10^{-15} Wb.

8.3.2 SQUID Magnetometer theory.

The size of magnetic field applied to a
superconductor affects the superconducting state and it
is this feature which the SQUID uses to detect magnetic
moments. If the size of the applied magnetic field is
increased the currents flowing on the surfaces of the
conductor reach a critical value after which the
superconducting state is destroyed. At this point the
resistive conductivity normally present returns and
reduces the current until the material again becomes
superconducting. It is this change between the
conducting states that is detected by the SQUID
magnetometer electronics.

The actual SQUID used enhances this effect
through two weak links in the superconducting ring.
Weak links are points in the superconducting ring where
the cross sectional area is reduced (Figure 8.3).
Since the critical current depends on cross sectional
area, the maximum current set-up in the superconductor,
before that state is destroyed, will also be reduced by
a weak link. Weak links increase the sensitivity of
the device since they reduce the value of magnetic flux

Diagram showing the
currents flowing in
a superconducting ring
in a magnetic field.

Currents flowing in
opposite directions
around the inside and
outside of the
material
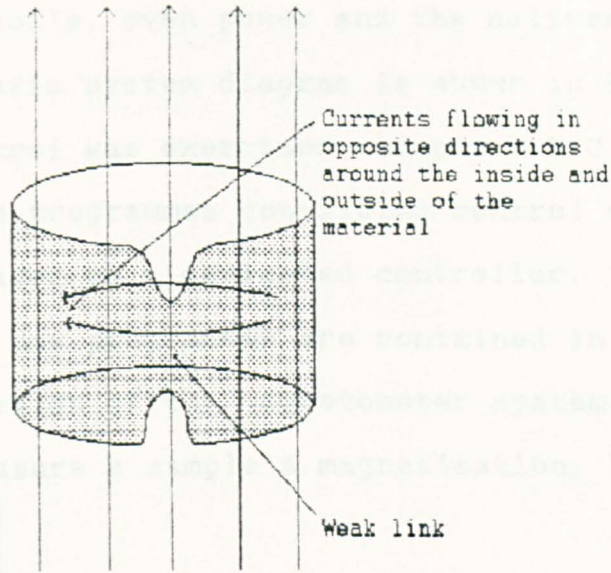
Weak link

Figure 8.3 Weak link in superconductor.

at which the superconducting state is destroyed.
Theoretically it is possible to detect a single Flux
Quanta but noise levels prevent this in practice.

The SQUID magnetometer used in this study was
a biomedical device supplied by the SHE Corporation.
The second order gradiometer arrangement of the sensor
coils reduces the interference caused by time varying
sources.

8.3.3 SQUID system description.

The system was built by Share (1987). Its
most useful facet was its ability to measure a sample's
magnetic moment while held at temperatures up to 700°C,
reducing the problems associated with repeated heating
and cooling cycles. System features included automated
mechanical sample positioning, the electronic control

of applied field coils, oven power and the delivery of
cooling air. A basic system diagram is shown in Figure
8.4. Overall control was exercised using a B.B.C.
computer which ran programmes containing control codes
which were downloaded to a dedicated controller. (The
commands used and new programmes are contained in the
appendix). The design of the magnetometer system made
it possible to measure a sample's magnetisation, heat
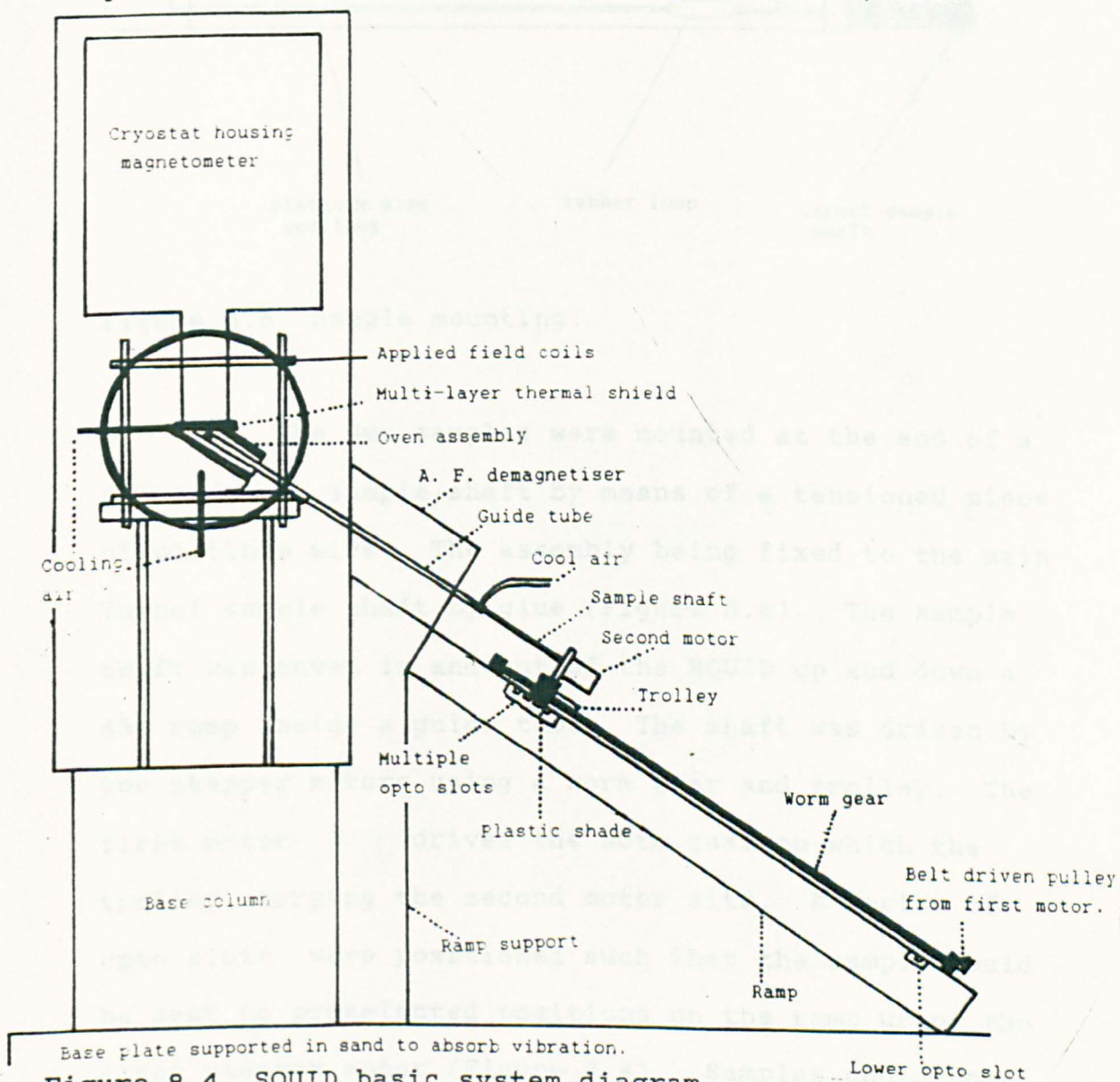
Figure 8.4   SQUID basic system diagram.

it and apply magnetic fields without removing it from
the oven.   Arranged in three mutually perpendicular
pairs oriented North/South, East/West and Vertical, the
field coils were calibrated using a fluxgate
magnetometer (Figure 8.5).

Sample mounting on shaft
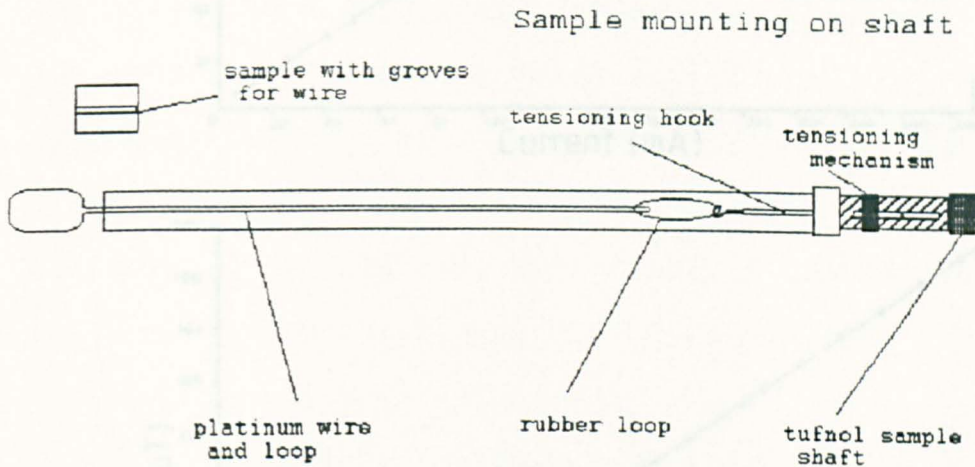
Figure 8.6   Sample mounting.

The 9mm samples were mounted at the end of a
short quartz sample shaft by means of a tensioned piece
of platinum wire.   The assembly being fixed to the main
Tufnol sample shaft by glue (Figure 8.6).   The sample
shaft was moved in and out of the SQUID up and down a
45° ramp inside a guide tube.   The shaft was driven by
two stepper motors using a worm gear and trolley.   The
first motor   drives the worm gear on which the
trolley carrying the second motor sits.   A series of
opto slots were positioned such that the sample could
be sent to preselected positions on the ramp using the
first stepper motor (Figure 8.4).   Samples could then
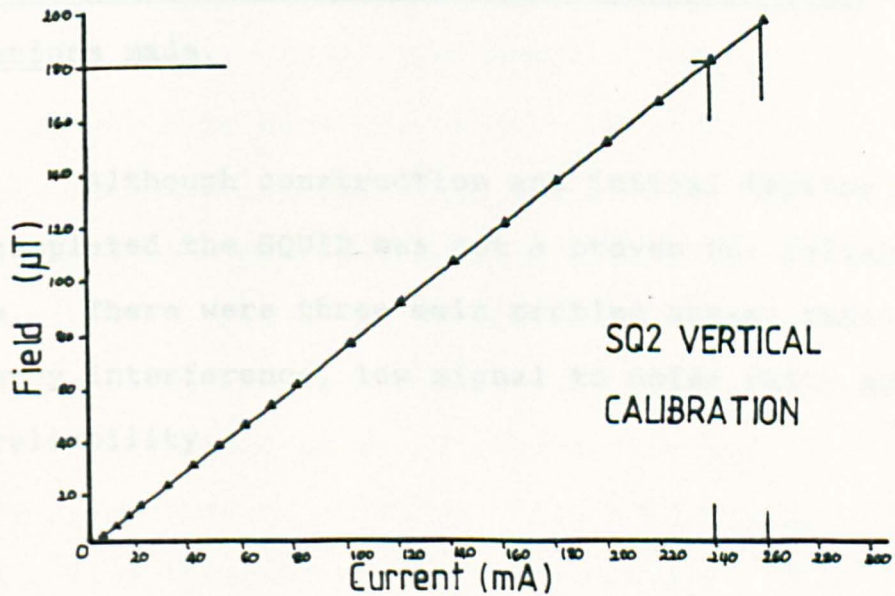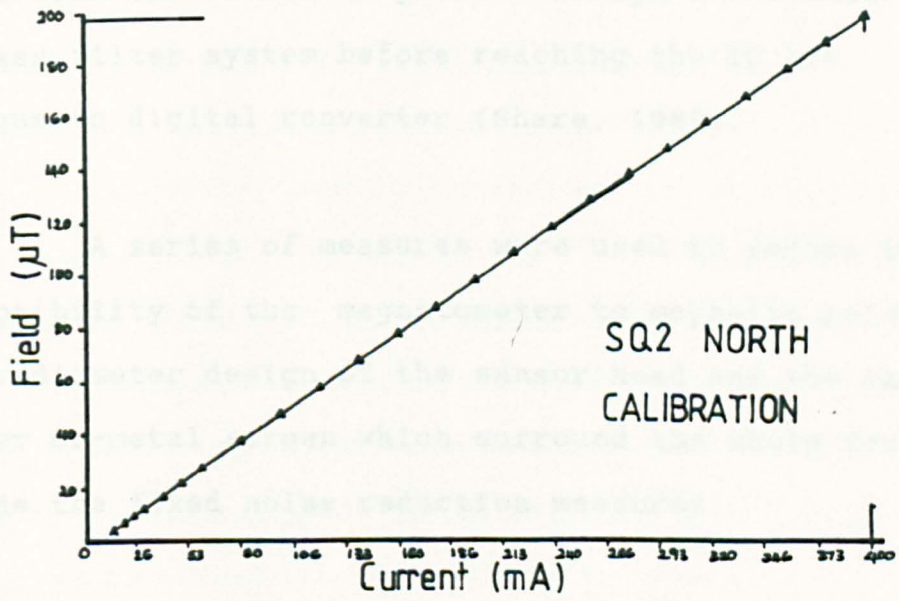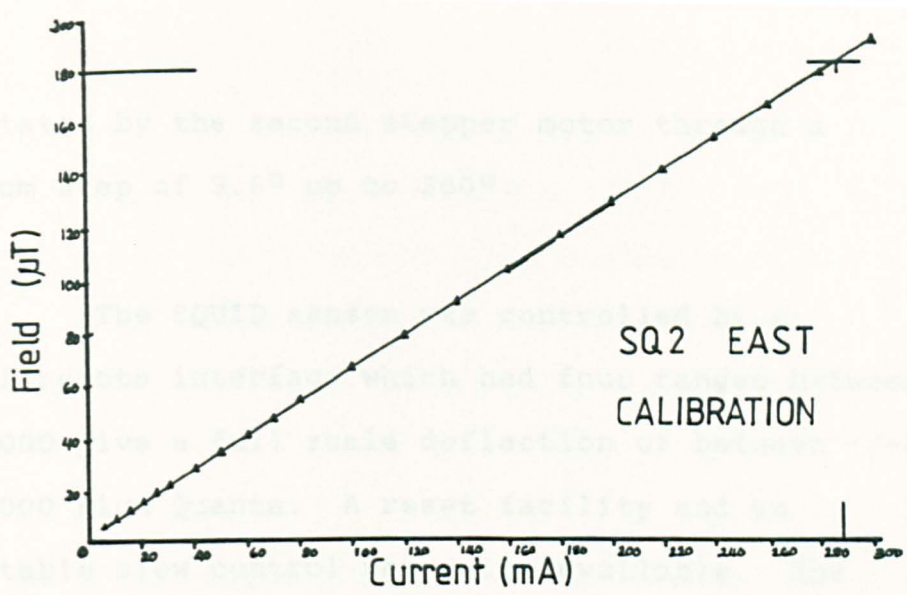
Figure 8.5   Applied field coil calibration.

be rotated by the second stepper motor through a minimum step of 3.6° up to 360°.

The SQUID sensor was controlled by a manual/remote interface which had four ranges between 1 and 1000 give a full scale deflection of between +/-2 and 2000 Flux Quanta. A reset facility and an adjustable slew control were also available. The signal from the sensor is passed through a switchable low pass filter system before reaching the 16 bit analogue to digital converter (Share, 1989).

A series of measures were used to reduce the susceptibility of the magnetometer to magnetic noise. The gradiometer design of the sensor head and the large 3 layer mu-metal screen which surround the whole device provide the fixed noise reduction measures.

8.4 Problems with SQUID Magnetometer operation and alterations made.

Although construction and initial testing had been completed the SQUID was not a proven nor reliable device.   There were three main problem areas: radio frequency interference, low signal to noise ratio and oven reliability.

(i) The low electrical signal to noise ratio, normally 20%, meant that the SQUID output was of insufficient strength to provide reliable measurement. This fault was eventually rectified by movement of the sensor head and produced a signal to noise ratio of 50%.

(ii) The SQUID, the leads running from it and the control interface could not be shielded completely from the effects of radio frequency interference. The strength and proximity, 500 metres, of the local police transmitter served to defeat all attempts to exclude its influence. The unpredictable duration and irregular transmission times also made it impossible to run the SQUID to a timetable. Several measures were attempted to circumvent the problem including working nights, using multiple readings and running as many samples as possible on short runs.

Multiple measurements proved to be of little value. However by using large sample numbers sufficient results were available to have results for three or more samples for every flow. The samples were run on three hour programmes with up to 6 being run each day.

(iii) The original oven design had three inherent problems, of which only two were completely solved during the period of experimentation. The first

was that of a physical weakness in the oven structure,
the second was providing a sufficiently rapid cooling
rate and the third was producing an oven capable of
providing heat over extremely long periods.

When the SQUID required internal alteration
the mu-metal shields had to be removed. This
necessitated the withdrawal of the sample guide tube
from the centre of the oven through the A.F.
Demagnetiser coils and out of the shields. This proved
very difficult since to ensure a good fit all
measurements allowed minimal clearance and as a
consequence the oven often snapped (Figure 8.7). The
problem was magnified due to the oven's inbuilt
weakness which resulted from the high temperature welds
used to secure the capillary tubes that carry the
platinum heating elements. The capillary tubes were
welded onto the glass at both ends causing weak spots
in two circles round the oven.

During the early stages of experimental work
a large number of ovens were broken and, since
replacement took two weeks, a considerable delay was
introduced. A new oven was designed (Figure 8.8) which
could be constructed in about 30 minutes. The design
involved cutting groves into a glass cylinder of a
larger diameter than the original oven and running the
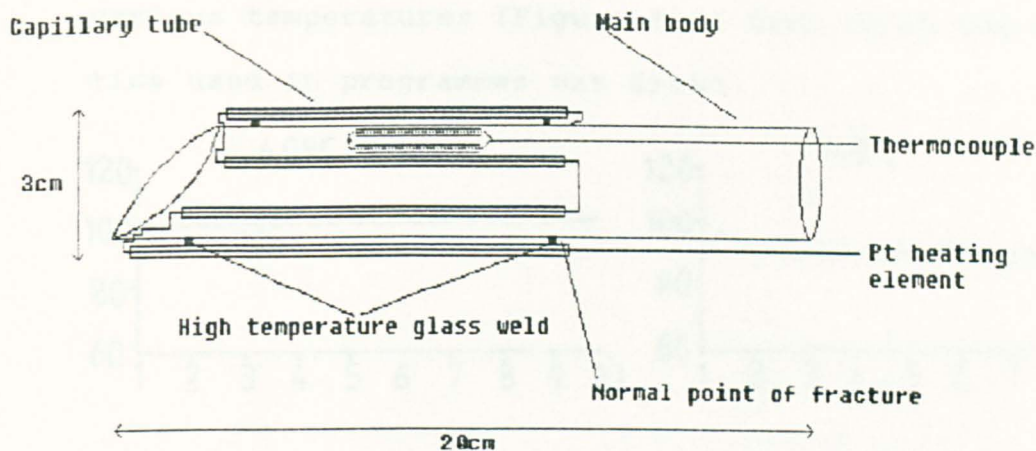
Figure 8.7 Original oven design.

element wires between it and the original layer of
glass. The wires were held in place by a ceramic
packing material, rather than running through capillary
tubes. It was then possible to remove, make and
reinstall an oven in a single morning, cutting both the
cost of repair and the associated delay.
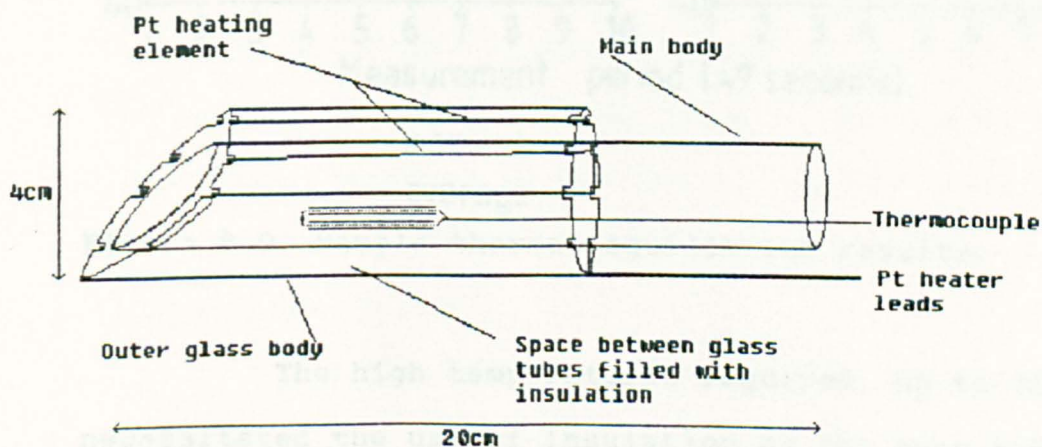
Figure 8.8 New oven design.

After the design change a series of experiments
were carried out to assess the length of time the
sample took to reach thermal equilibrium. The magnetic
moment of ten samples were monitored with time at

138

various temperatures (Figure 8.9) from which the hold
time used in programmes was drawn.
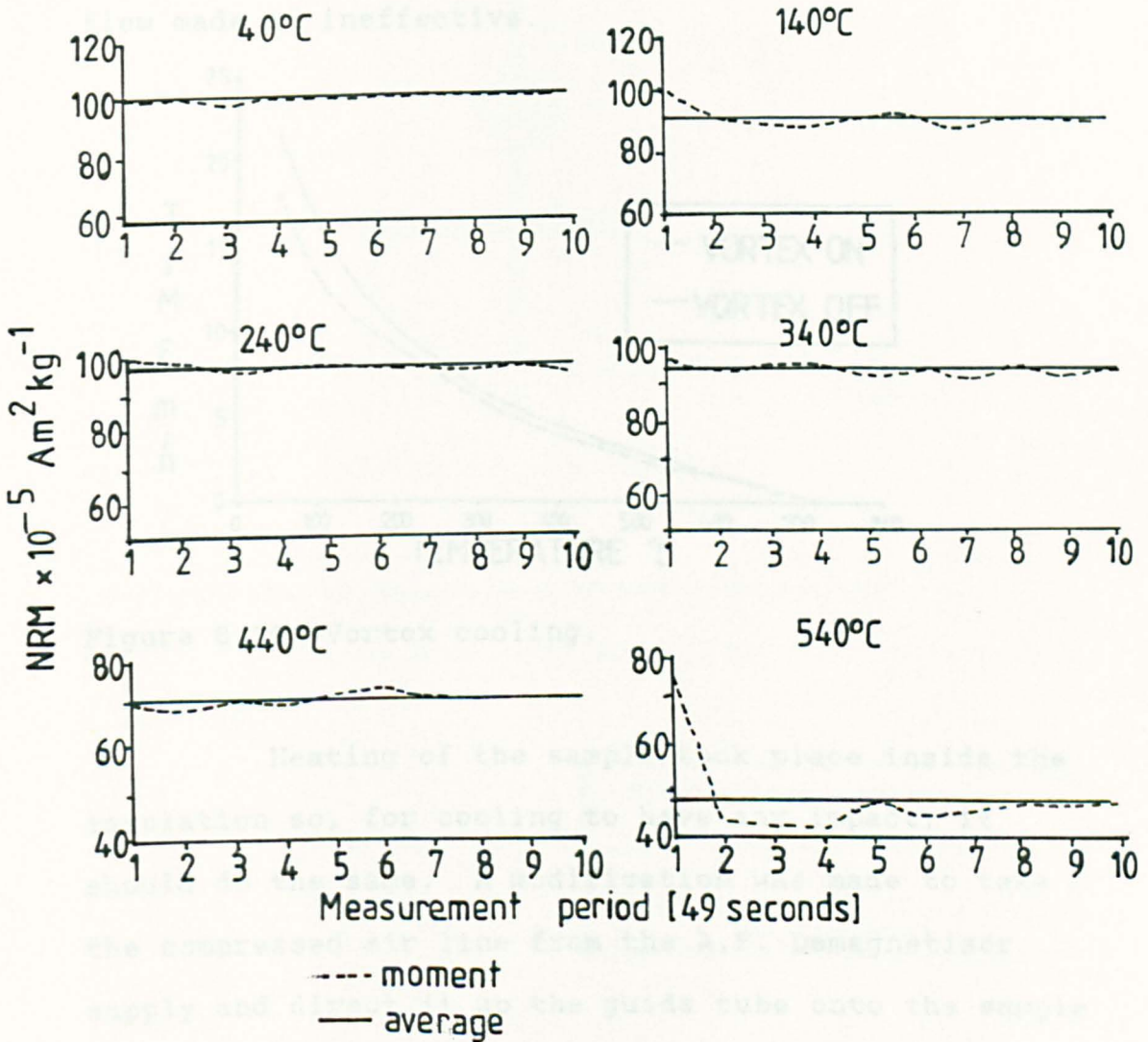
Figure 8.9 Sample thermal equilibrium results.

The high temperatures required, up to 700°C,
necessitated the use of insulation on the oven but this
increased the cooling time and reduced the number of
samples which could be processed in a day. A number of
methods were tried to increase the cooling rate. A
vortex cooler, which reduces the air temperature coming
from the compressed air line, was tried first. This

produced a marginal improvement in cooling (Figure
8.10), by producing colder air but the reduction in air
flow made it ineffective.
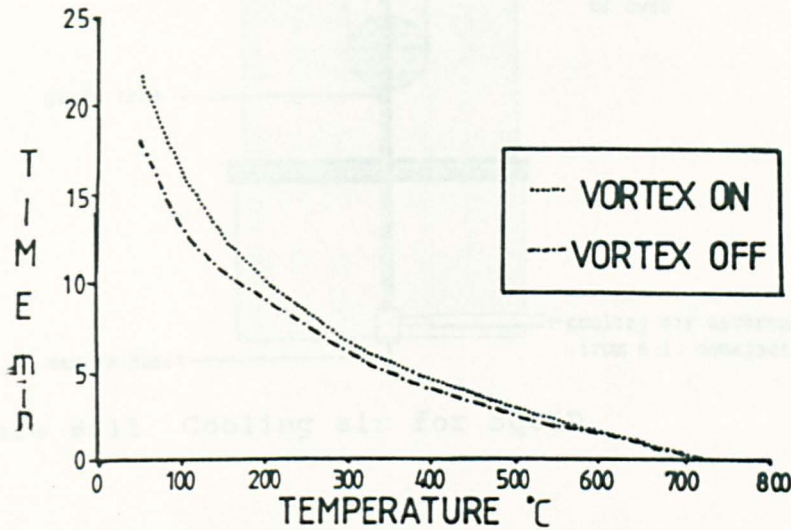
Figure 8.10   Vortex cooling.

Heating of the sample took place inside the
insulation so, for cooling to have any impact, it
should do the same. A modification was made to take
the compressed air line from the A.F. Demagnetisor
supply and direct it up the guide tube onto the sample
(Figure 8.11). The effectiveness of this measure can
be seen (Figure 8.12).

For the laboratory study of the cooling rate
effect on sample magnetisation, the oven was required
to keep the samples at an elevated temperature for
periods up to 16 hours. Very few experiments were
completed, as the platinum element normally burnt out
because the oven power supply used a system of full
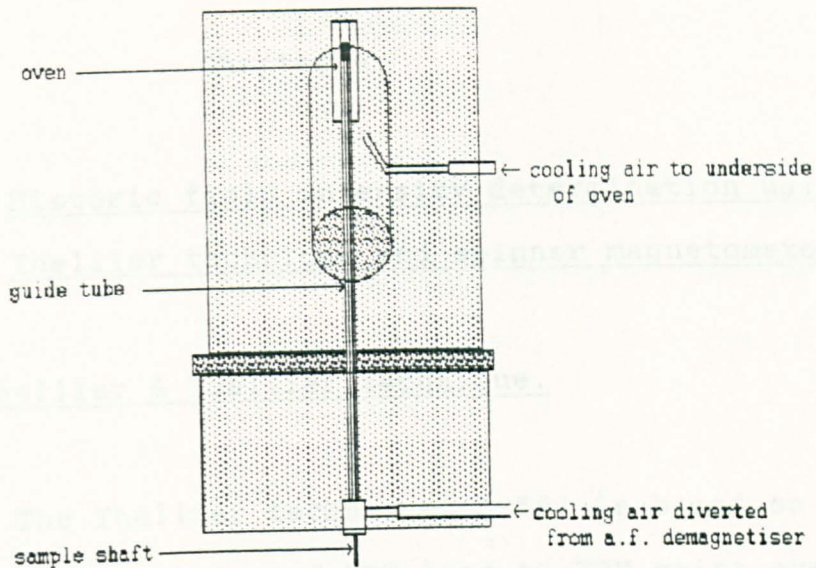
Figure 8.11 Cooling air for SQUID.

power bursts to maintain a steady temperature.
Insufficient time precluded any alteration to the oven
power supply.
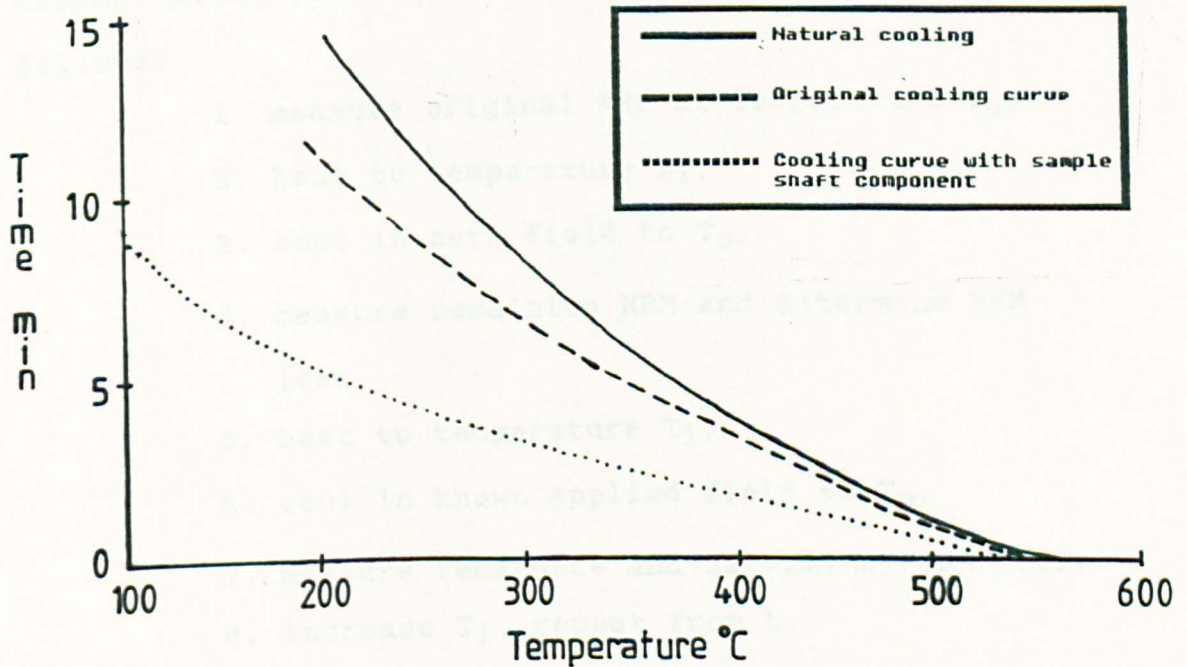
Figure 8.13 Oven cooling curve.

141

Chapter 9.

Historic field intensity determination using
Thellier technique and spinner magnetometer.

9.1 The Thellier & Thellier technique.

The Thellier technique (1959) is based on
comparisons of a series of NRM loss to TRM gains over
specific temperature intervals. Whilst simple in
principle, the technique has been the subject of many
modifications (Boyd, 1986; Hoffmann et al., 1989) since
samples processed in this way are very susceptible to
thermal alteration. The measurement routine is as
follows:

1. measure original NRM at temperature T_0,

2. heat to temperature T_1,

3. cool in zero field to T_0,

4. measure remaining NRM and determine NRM
   loss,

5. heat to temperature T_1,

6. cool in known applied field to T_0,

7. measure remanence and determine PTRM gain,

8. increase T_1, repeat from b.

Using the above stages for a series of
temperature steps the NRM loss can be plotted against
TRM gain. The magnitude of a TRM is proportional to
the strength of the applied field for fields <100 T,

142

(Nagata, 1943) in which it is created. Thus the ratio
of the NRM to a TRM created in the sample over the same
boundary conditions is equivalent to the ratio of the
ancient to laboratory field strengths. As the value of
the laboratory field used to create the TRM is known
the ancient field strength used to create the NRM can
be calculated.

9.2 Experimental procedure.

Samples were measured on a spinner
magnetometer and heated in a programmable oven. A
solenoid wound around the oven and connected to a
constant current source was used to provide a magnetic
field of 50μT. A series of measurements were carried
out after treatment within the temperature range 150
and 300°C. A low temperature range was chosen to
minimise alteration in the initial measurement stages
with the intention of extending the range if the
samples proved suitable.

9.3 Result analysis.

Anistropy of susceptibility measurements for
the samples showed such low levels of anistropy that
the NRM (which has components of magnetisation in the
X, Y, and Z direction) could be compared to a TRM which
was imparted only in the Z direction. Thus the NRM

lost (in X, Y, and Z) is compared to the PTRM gained (in Z only).

An example of the initial results table for sample 1867 02 is shown in Table 9.1. It can be seen that there is a regular increase in TRM, (values underlined,) as NRM decreases, with the exception of the readings taken at 200°C.

Table 9.1) Specimen results for the 1867 02 sample.

Temp	Total Moment	Dec	Inc	Gain/Loss	Z Axis
0	175	146	-42		-71
150	167	152	-31	-5	-66
150	165	149	-30	+7	-73
175	151	147	-38	-8	-63
175	152	155	-33	+10	-73
200	156	151	-26	-5	-66
200	144	157	-32	+19	-85
225	151	148	-37	-9	-62
225	137	159	-27	+20	-82
250	136	150	-33	-15	-56
250	144	140	-33	+21	-77
300	127	151	-29	-19	-52
300	144	140	-25	+21	-83
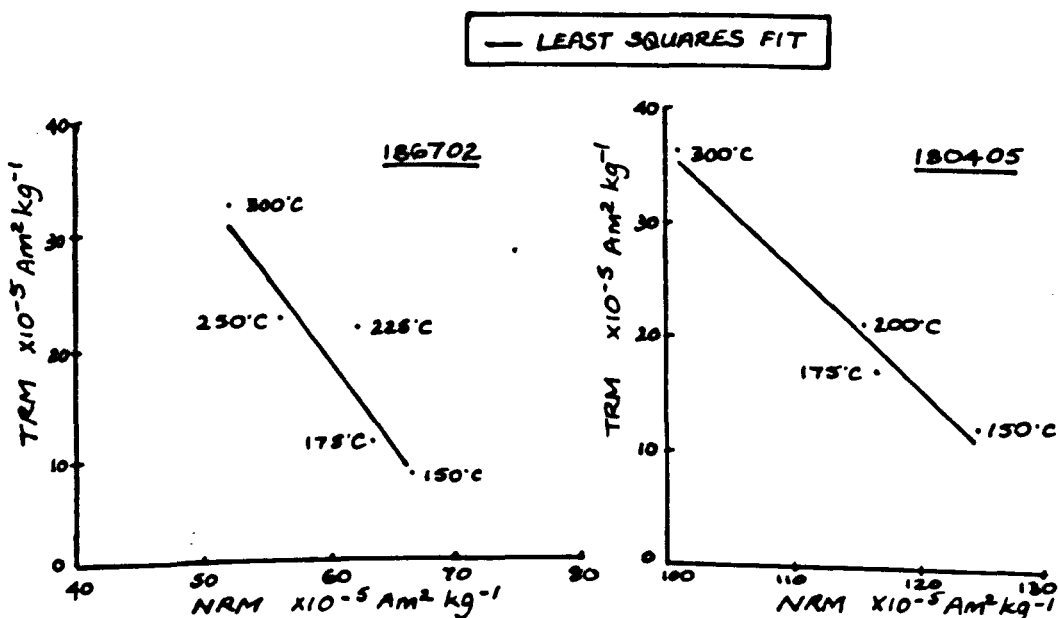
Figure 9.1 TRM/NRM graphs for the Thellier technique.

144

These results were converted into graphs of TRM gain against NRM loss so that a least squares fit could be applied and a gradient for TRM/NRM found. Two examples of such graphs can be seen in Figure 9.1. Provided no sample alteration has taken place and the laboratory field, Fl, is <100μT, the ancient field strength, Fa, can be calculated from:

$$Fl / Fa = TRM \text{ gain} / NRM \text{ loss}$$

9.4 Overall results

Very few samples from the data set showed results like those above; values for the historic field were obtained from only 11 out of 56 samples, a success rate of 19% (Table 9.2).

Table 9.2 Thellier & Thellier technique results.

1886-01	71μT	1872-05	83μT	1872-04	32μT
1871-14	30μT	1867-02	32μT	1850-07	80μT
1822-12	30μT	1822-04	30μT	1804-05	49μT
1804-09	42μT	1760-01	89μT.		

9.5 Conclusion.

The lack of success in defining the palaeofield strength appears to be due to sample alteration during the ten minutes during which the samples were held at temperature in the oven. It was decided not to test the samples from the Canary Islands using this technique because samples were limited and the success rate of the technique very low.

Historic field intensity determinations using
Boyd technique and SQUID magnetometer.

10.1 The Boyd technique.

In order to minimise thermal alteration, Boyd
(1986) used a method which measures the sample's
magnetic moment whilst hot. The technique was thus
ideally suited to the new SQUID magnetometer and
removes the requirement to cool the sample to room
temperature before measuring its moment, then reheating
for the next stage of demagnetisation. In this method,
samples were heated to an initial temperature, T_0,
200°C, held at that temperature for time t1, to ensure
thermal equilibrium, before the moment, M1, was
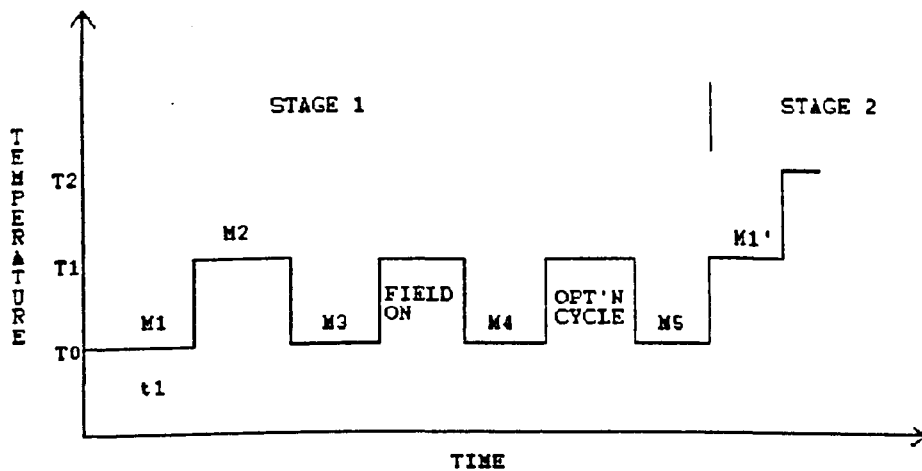
Figure 10.1 Boyd measurement routine.

measured. They were then heated to the first stage temperature, T_1, held for t1 minutes and the moment, M2, measured. The temperature was then reduced to T_o, moment M3 measured before reheating to T_1 and cooling in a known magnetic field to obtain final magnetic moment measurement M4. At this point an optional third heating to T_1 and cooling in zero field could be included to check for alteration, (Figure 10.1), but this was discontinued since it promoted further alteration. Alteration was monitored by comparing the moment M2 with the initial moment M1' of the next stage. (Full programme details can be found in the appendix listed as BOYD222).

10.2 Experimental procedure.

The greatest potential problem was that of sample alteration although its effects were reduced by decreasing the hold time at elevated temperatures. When thermal equilibrium was required the minimum 3 minute delay was used (section 8.4.3). In addition the removal of the optional alteration measurement stage also reduced alteration since it reduced the number of heating cycles required.

10.3 Results Analysis.

An typical example of the raw results are given below for the 1906-05 sample (Table 10.1) for different processing stages.

Table 10.1 Sample 1906-05, Stage 1. $M \times 10^{-8} Am^2kg^{-1}$

TEMP°C	M1	M2	M3	M4	%ALTR'N
200	119045	114130	117802	122096	
232	117746	107180	110514	116446	+3.1
263	106615	100852	104751	109892	-0.5
297	99609	94072	96784	101530	-1.2
355	93564	83394	86275	91078	-0.5
382	81812	74806	78026	82998	-1.9

The processing stage of this work is more complex than the simple NRM loss/PTRM gain involved in the Thellier method since it involves the normalisation of all the measurements to that of the first temperature step. It is best illustrated by example (Tables 10.2 & 10.3). Conversion factors J1 and J2 are successively calculated from the columns as shown in brackets. The values of NRM and TRM can be found by using the conversion factors (Table 10.3). The letters in brackets refer to the rows and columns in stage 2.

The second of the two alteration checks, equivalent to Thellier's linearity check, also becomes available during the processing of the stage 3 results.

Table 10.2 Sample 1906-05, Stage 2.   M $\times 10^{-8}Am^2kg^{-1}$

	M1	M3	M4	J1	J2
A	119045	117802	122096	1 (M3A/M1B)	1 (J1A*1)
B	117746	110514	116446	1.03(M3B/M1C)	1.03(J1B*J2A)
C	106615	104751	109892	1.05	1.08
D	99609	96784	101530	1.03	1.12
E	93564	86275	91078	1.05	1.17
F	81812	78026	82998		

Table 10.3 Sample 1906-05, Stage 3.

NRM		PTRM	$\times 10^{-8}Am^2kg^{-1}$
119045 (M1A)		1	0
117802 (M3A)		2	(M4A - M3A)= 4289
110514 (M3B)* 1 (J3A)=		3	4289 + ((M4B - M3B)*J3A)=
104751 * 1.03=107893		4	15516
96784 * 1.08=104526		5	20641
86275 * 1.12=96628		6	26020
78026 * 1.17=91290		7	31837

It involves the calculation of the ratio of NRM loss to PTRM gain for each temperature stage. In the case of the above results it fluctuates between 0.83 to 0.70, and does not show any of the extreme alteration that was a feature of the Thellier technique.

The values of NRM against PTRM were plotted (Figures 10.1 & 10.2) with a least squares line fit.

The gradient of the line was found and the historic field calculated using: Fa = Fl x slope. Results were statistically combined to obtain a mean for each site.
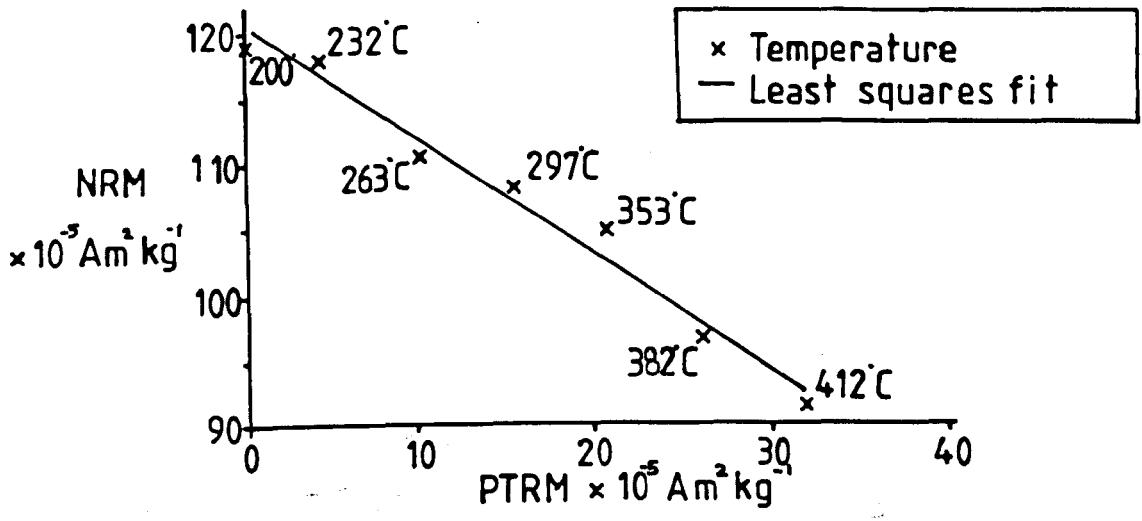
Figure 10.1 1906 05 NRM/PTRM graph.
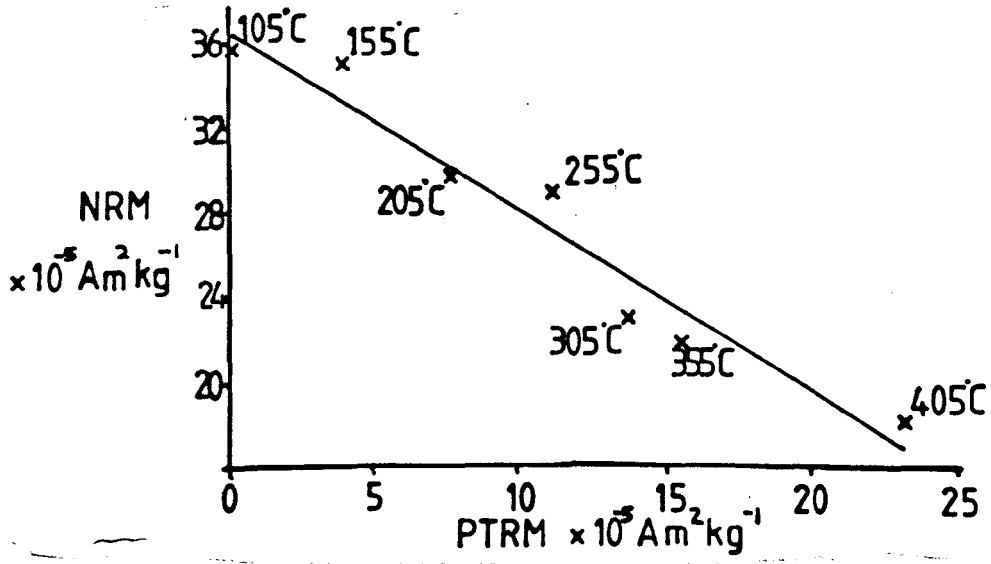
Figure 10.2 1824 11 NRM/PTRM graph.

10.4 Overall results.

The results are given in Tables 10.4. The gaps in the table indicate the unsuitability of

Table 10.4 Boyd technique results.

Year	Fa	+/-	Fa	+/-	Fa	+/-	Fa	+/-	Average Fa	+/-
a) Canaries										
1470	36.0	4.0	25.5	1.0	51.0	2.0	47.5	2.0	40.9	9.16
	44.5	4.5	----	---	----	---	----	---		
1585	40.0	4.0	57.0	4.0	60.5	1.0	70.0	15.	54.1	11.1
	43.0	3.0	----	---	----	---	----	---		
1646	51.5	6.0	32.5	3.5	41.0	5.0	40.0	2.5	41.2	6.76
1677	25.0	5.0	86.0	6.0	33.5	1.0	33.0	1.5	44.3	24.2
1704	22.0	4.0	47.0	4.5	37.5	1.0	----	---	35.5	10.3
1705	32.5	2.0	65.0	3.0	41.0	1.0	----	---	46.1	13.7
1706	28.5	3.0	30.0	2.5	----	---	----	---	29.3	0.75
1712	47.0	2.5	65.0	5.5	43.5	1.5	39.5	4.0	46.8	9.55
	39.0	2.5	----	---	----	---	----	---		
1730	58.0	6.0	72.5	7.0	67.0	5.0	----	---	65.8	5.97
1798	41.5	7.0	51.0	3.0	49.0	8.0	47.5	5.0	47.3	3.55
1824	42.5	5.0	45.5	5.0	26.0	3.0	42.5	5.0	39.1	7.67
1909	49.0	1.5	40.0	3.0	36.0	3.0	43.5	1.0	43.5	5.08
	49.0	1.0	----	---	----	---	----	---		
1949	30.0	1.5	65.0	3.0	----	---	----	---	47.5	17.5
1971	37.5	35	63.0	2.5	48.5	10	46.0	5.0	47.0	11.6
	51.5	1.5	41.0	5.0	26.0	3.0	62.5	2.5		
b) Vesuvius.										
1697	61.5	20	43.0	4.5	40.5	4.5	36.0	5.5	42.9	8.00
	41.0	4.5	42.0	1.5	36.0	3.0	----	---		
1737	65.0	12	43.0	1.5	----	---	----	---	54.0	11.0
1754	48.5	1.5	----	---	----	---	----	---	48.5	1.50
1760	45.0	1.0	46.0	1.0	53.5	5.0	63.0	20	51.9	7.21
1767	40.5	2.0	27.5	1.5	30.5	2.0	41.1	2.5	36.9	5.17
	40.5	1.5	38.0	2.0	40.5	2.0	----	---		
1794	70.0	5.0	39.0	1.5	29.5	3.0	31.7	2.5	42.6	16.2
1804	37.5	1.5	23.0	1.0	26.7	3.0	29.5	3.0	29.1	5.33
1822	49.0	1.5	42.5	5.0	40.5	3.0	42.3	1.5	42.6	3.42
	39.0	4.0	----	---	----	---	----	---		
1834	32.0	5.0	32.0	5.5	46.5	7.0	37.0	6.5	37.7	5.55
	41.0	4.5	----	---	----	---	----	---		
1847	38.5	3.0	25.0	5.0	31.0	1.5	28.3	1.5	32.0	5.21
	37.5	4.0	----	---	----	---	----	---		
1850	44.5	5.0	42.0	3.0	44.5	9.0	----	---	43.6	1.17
1858	60.0	2.0	----	---	----	---	----	---	60.0	20.0
1867	76.5	4.0	51.0	1.5	48.5	0.5	33.8	2.0	51.9	13.7
	50.0	2.5	----	---	----	---	----	---		
1871	40.3	3.0	37.0	4.0	53.0	5.0	39.0	2.0	42.3	6.27
1872	30.0	5.0	23.8	6.0	36.0	2.0	----	---	29.9	4.96
1886	46.5	1.5	32.2	3.0	45.0	12	----	---	41.2	6.41
1891	47.0	1.0	36.5	5.0	----	---	----	---	41.8	5.25
1895	29.5	2.0	47.9	2.5	48.5	5.0	54.0	16	45.7	8.43
	41.0	4.5	53.5	1.5	----	---	----	---		
1906	46.5	1.5	53.0	5.3	55.0	6.0	37.5	7.0	45.0	6.72
	39.5	5.0	39.0	4.0	38.9	3.5	51.0	2.0		
1929	48.5	2.5	43.0	5.5	39.0	4.0	46.5	6.0	41.6	6.20
	31.0	1.5	----	---	----	---	----	---		
1944	51.5	1.5	53.0	8.0	35.0	2.0	51.0	1.0	47.6	7.32

samples or unsuccessful runs due to SQUID noise. The combined results were then plotted on an intensity time graph with least squares line-fits. It can be seen (Figures 10.3 & 10.4) that the results, despite alteration and noise problems, form reasonable secular variation curves.

10.5 Conclusions.

The Boyd technique, with its short hold times and reduced thermal cycling, proved to be a more suitable technique than the Thellier method. Alteration was expected and measures were taken to reduce it but the experiments were badly affected by extended external radio interference which interfered with approximately one third of the measurements. Despite this, comprehensive results were obtained by running large sample numbers.

Figure 10.3 Boyd technique intensity variation for Mount Vesuvius.
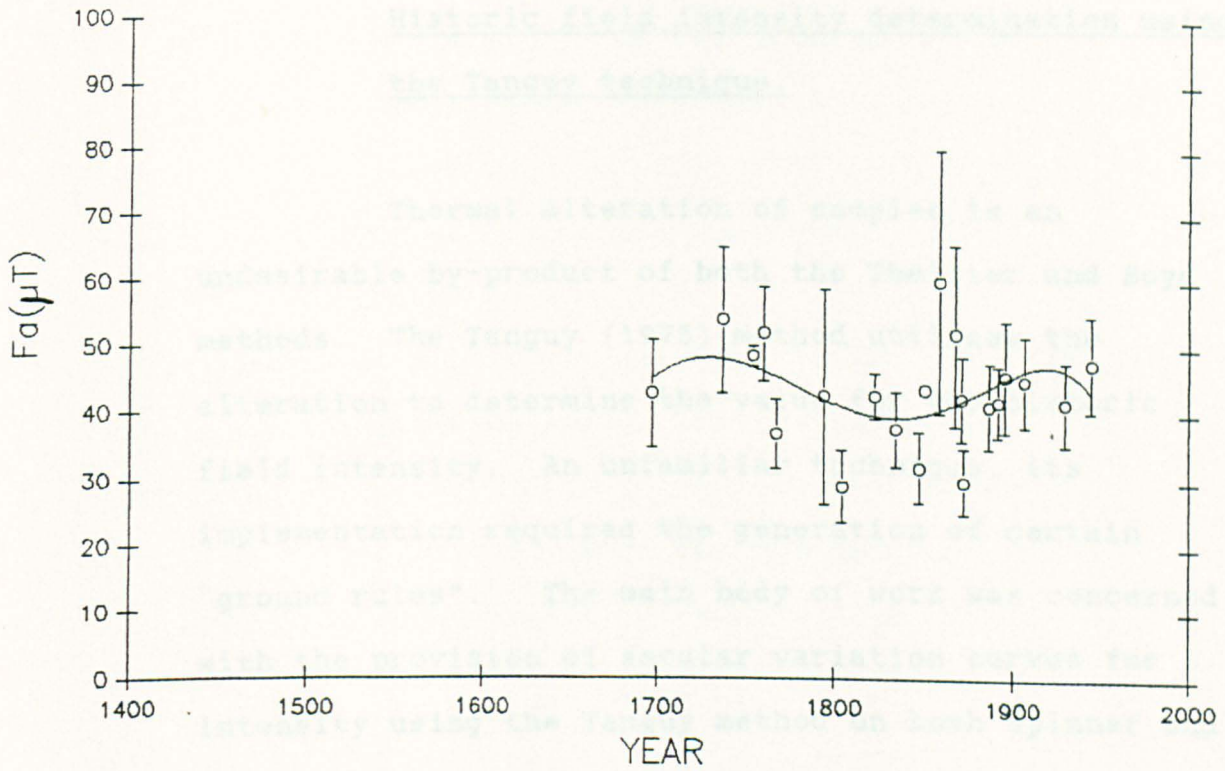
Figure 10.4 Boyd technique intensity variation for the Canary Islands.
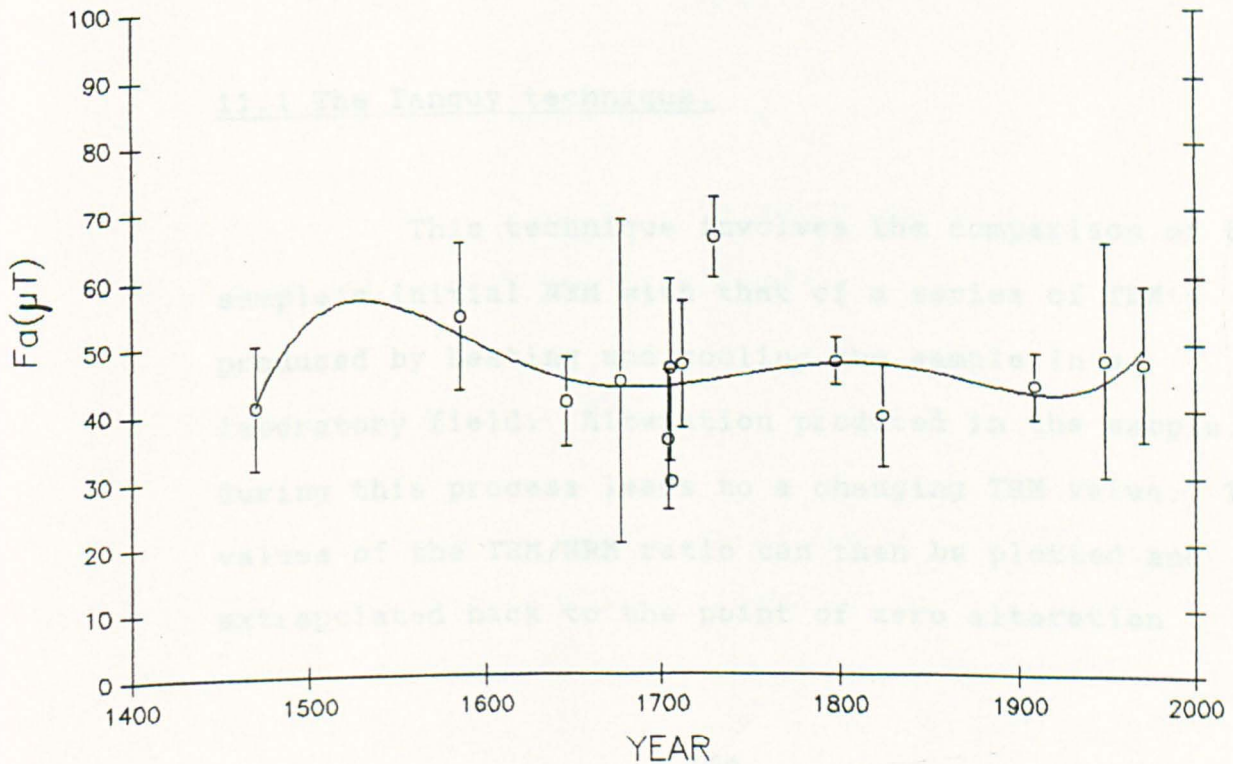
Historic field intensity determination using the Tanguy technique.

Thermal alteration of samples is an undesirable by-product of both the Thellier and Boyd methods. The Tanguy (1975) method utilises the alteration to determine the value for the historic field intensity. An unfamiliar technique, its implementation required the generation of certain "ground rules". The main body of work was concerned with the provision of secular variation curves for intensity using the Tanguy method on both Spinner and SQUID Magnetometers. It also provided an opportunity to compare of the performance obtained from the two magnetometers (Chapter 12).

11.1 The Tanguy technique.

This technique involves the comparison of the sample's initial NRM with that of a series of TRM's produced by heating and cooling the sample in a laboratory field. Alteration produced in the sample, during this process leads to a changing TRM value. The values of the TRM/NRM ratio can then be plotted and extrapolated back to the point of zero alteration

giving a value for the unaltered TRM/NRM. The
experimental procedure was as follows:

1. the original NRM was measured at 20°C
2. sample heated to 700°C, held for t minutes
3. sample was cooled to 20°C in a known field
4. TRM of sample was measured
5. return to 2.

This loop, 2 to 5, was repeated five times, as five TRM
values were considered sufficient to produce an
extrapolated curve. The results were then obtained
using Fa = F1*(NRM/TRM) where the NRM/TRM value is
obtained from extrapolation (Figure 11.1).
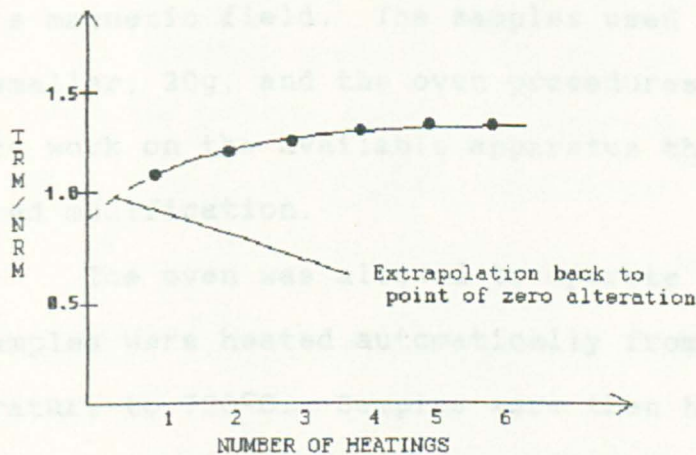
Figure 11.1 Extrapolation of Tanguy results to
determine the unaltered TRM/NRM ratio.

11.2 Experimental procedure.

Two aspects of the practical application of
Tanguy's technique were studied separately. They were
the time, t, which samples should be left at maximum
temperature (stage 2 above), and the removal of viscous

or isothermal remanence from the initial NRM measurement. The spinner magnetometer/oven combination was chosen for these investigations because of the flexibility allowed.

11.2.1 The ideal duration of maximum temperature.

Tanguy describes the use of samples weighing between 50 and 70g, which were introduced into an oven, preheated to 700°C. Having reached 700°C themselves, the samples were removed and allowed to cool in the Earth's magnetic field. The samples used in this study were smaller, 20g, and the oven procedures different. Thus to work on the available apparatus the technique required modification.

The oven was allowed to operate normally. The samples were heated automatically from room temperature to 700°C. Samples were then held at 700°C for T minutes and cooled in an applied field of 50μT before being measured once at room temperature. (Tanguy found negligible change between measurements pre and post storage for 24 hours).

Normal oven proceedure required holding cores at the maximum temperature for 15 minutes but times of 2 and 10 minutes were judged to be more appropriate, preventing cores from reaching thermal equilibrium, as specified by Tanguy, as well as preventing excessive

alteration. A sequentially increasing hold time of 2^n minutes, where n was the number of heatings, was also tried. In order to provide direct comparison five samples from the 1949 La Palma flow were each cut into three specimens, one for each hold time.

Results.

Samples were processed using the different hold times and the results plotted (Figure 11.2). The TRM/NRM ratios for the different samples are given in Table 11.1. The results show that the shortest hold time, that of 2 minutes, gave a value for Fa closest to the measured value for the Canary Islands in 1949 (Soler.V, pers. com.), Fa = 43μT, equivalent to a TRM/NRM of 1.16.

Table 11.1 TRM/NRM ratio's for different hold times.

Time	Sample number.									
min	15	+/-	14	+/-	04	+/-	11	+/-	03	+/-
10	1.48	0.08	1.39	0.40	1.36	0.44	1.69	0.02	1.39	0.40
	Average = 1.46 +/- 0.12									
2	1.14	0.03	0.95	0.00	1.26	0.00	1.21	0.03	1.31	0.48
	Average = 1.17 +/- 0.12									
Seq	1.29	0.53	2.58	0.17	0.90	0.11	1.97	0.21	2.84	4.14
	Average = 1.92 +/- 0.73									
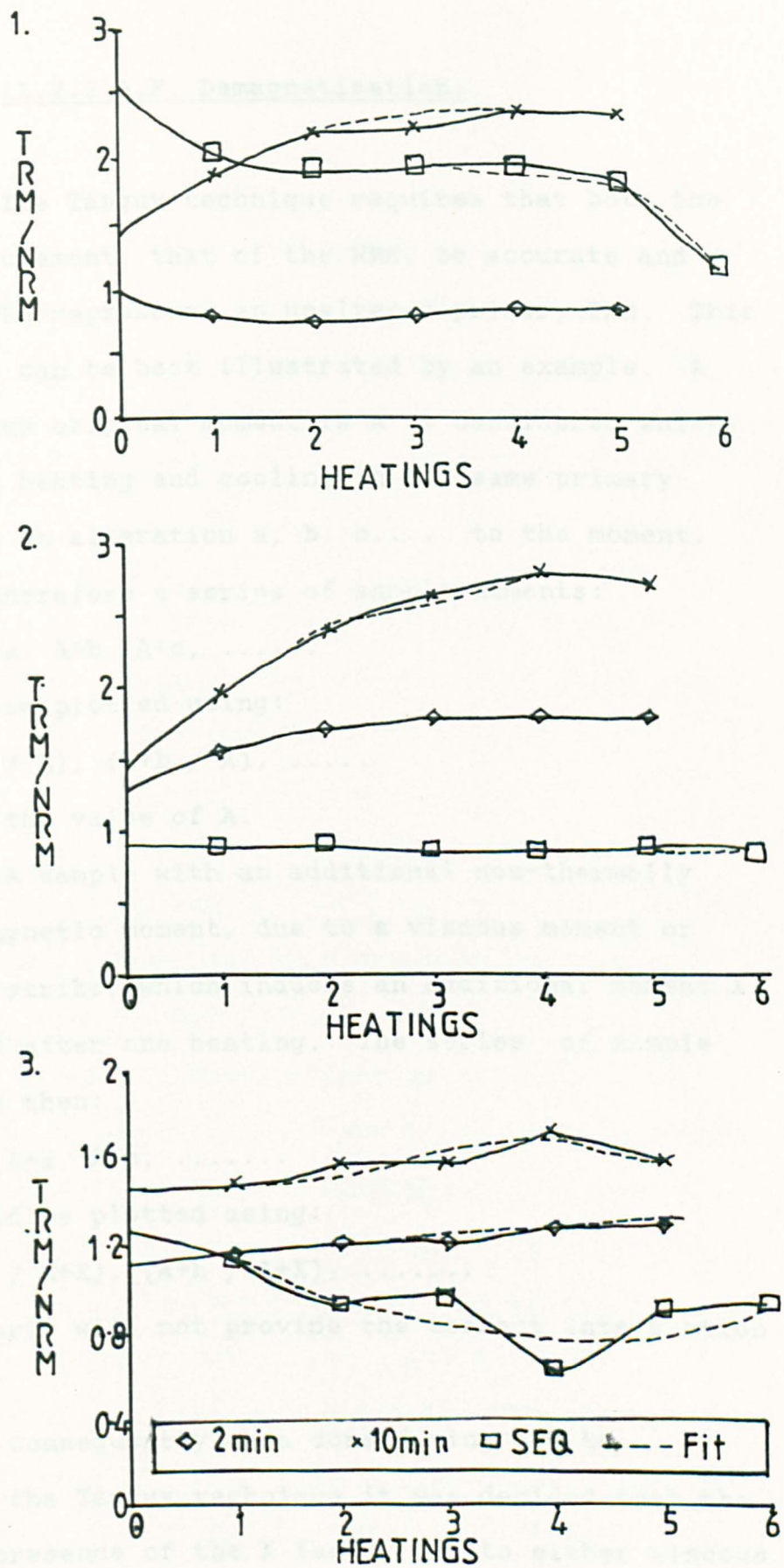
fig 11.2) Variation of TRM/NRM ratio with hold time.

◇ 2min   × 10min   □ SEQ   ▲--- Fit

11.2.2 A.F. Demagnetisation.

The Tanguy technique requires that both the first measurement, that of the NRM, be accurate and that the NRM represents an unaltered primary TRM. This dependence can be best illustrated by an example. A sample whose original moment is A is considered which, after each heating and cooling in the same primary field, has an alteration a, b, c.... to the moment. There is therefore a series of sample moments:

A, A+a, A+b, A+c, ...

which can be plotted using:

(A+a / A), (A+b / A), ...

to obtain the value of A.

A sample with an additional non-thermally induced magnetic moment, due to a viscous moment or lightning strike, which induces an additional moment X, is removed after one heating. The series of sample moments is then:

A+X, A+a, A+b, ...

which would be plotted using:

(A+a / A+X), (A+b / A+X), ...

which clearly will not provide the correct intersection point.

Consequently when considering how to implement the Tanguy technique it was decided that the possible presence of the X factor due to either viscous
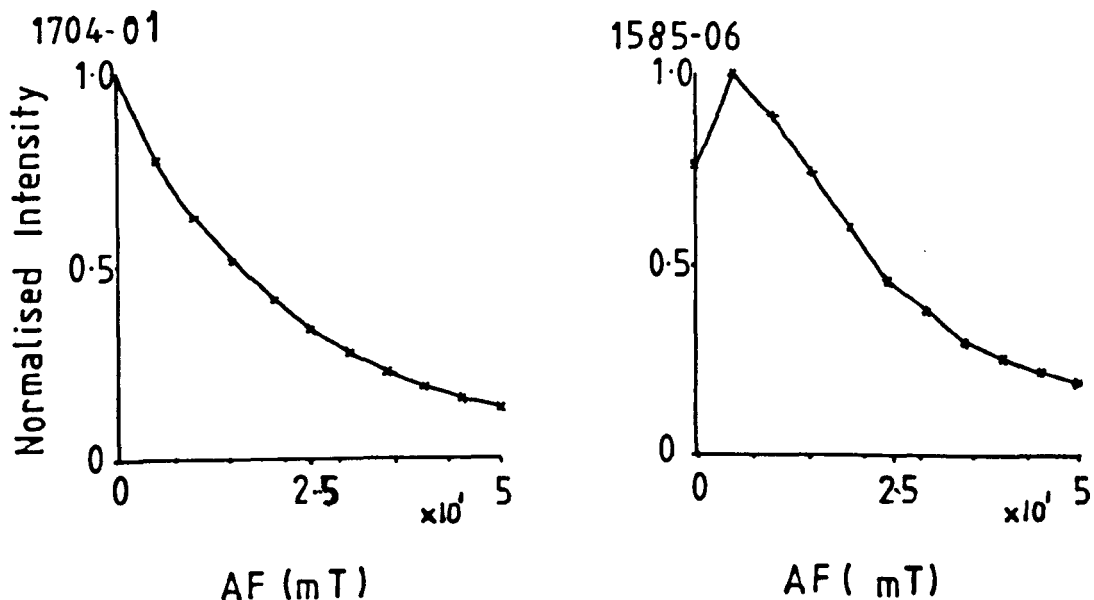
Figure 11.3 The 1704-01 demagnetisation curve is typical for this study, the 1585-06 curve shows the removal of a viscous moment.

or IRM source could not be ignored. During directional studies only a few samples had been found to have such an additional moment and this had been removed by A. F. demagnetisation to 5mT (Figure 11.3). Cleaning the samples using A. F. demagnetisation was therefore considered the best option since it did not interfere with the process of thermal alteration. It can, however, induce an error of its own - the magnitude of which depends on the proportion of the sample's moment removed by the demagnetisation. Let A' and a' represent the fraction of the initial NRM and the alteration removed by cleaning respectively. The NRM measured will the be A - A' and the TRM's after cleaning:

$$A - A' + a - a', \quad A - A' + b - b' \ldots \ldots$$

A − A'+ a − a',   A − A' + b − b'......

This would give:

(A − A' + a − a') / (A − A'), ...

as the series to be extrapolated back to the point of
zero alteration.   This can be simplified to:

1 + (a − a') / (A − A'), ...

Provided A' and a' are either small or that the same
percentage of sample moment is removed from both A and
a by cleaning, the series returns to that of the ideal
sequence:

1 + a / A,   1 + b / B, ...

If not, an error larger than that introduced by X may
result.

Practical implementation.

Twenty two different samples from eight flows
were subjected to the following measurement regime:

1. measure NRM,

2. A. F. demagnetise to 5mT,

3. measure NRM again,

4. heat to 700°C and cool in magnetic field,

5. measure TRM_1,

6. A. F. demagnetise to 5mT,

7. measure $TRMc_1$, repeat from 4.

This produced cleaned and uncleaned results in parallel
from the same sample.   The results were processed in
the normal way to give an extrapolated value for the
NRM/TRM ratio for zero alteration (Table 11.2).

Discussion.

It is apparent that no definitive increase or decrease in moment occurs when samples are cleaned (Figure 11.4), nor did the results indicate that A.F. cleaning increased the accuracy of the results as the standard deviation of both sets of data were 0.28. The removal of the A' and a' fractions of the moment inducing a spread of results of the same size as that produced by IRM or viscous moment.

Table 11.2 Comparison of cleaned and uncleaned Tanguy results.

Sample number	Uncleaned	Cleaned
1	1.00	0.82
2	1.47	1.31
3	1.12	1.42
4	0.85	0.73
5	0.87	0.75
6	1.93	1.69
7	0.90	0.90
8	·0.99	1.05
9	1.19	1.17
10	0.95	0.87
11	0.95	0.87
12	1.21	1.12
13	0.84	1.15
14	1.12	1.05
15	1.36	1.34
16	1.19	1.31
17	1.18	0.58
18	1.01	0.89
19	1.27	1.16
20	0.88	0.70
21	1.04	0.95
22	1.66	1.50
Average	1.13+/-0.28	1.06+/-0.28

This experimental series lacks the results which were found later in this study showing massive

ancient field strengths caused by the superimposition

of the "X" factor for which A.F. cleaning may have

produced more accurate results. It would have been

beneficial to extend this work to the larger data set.
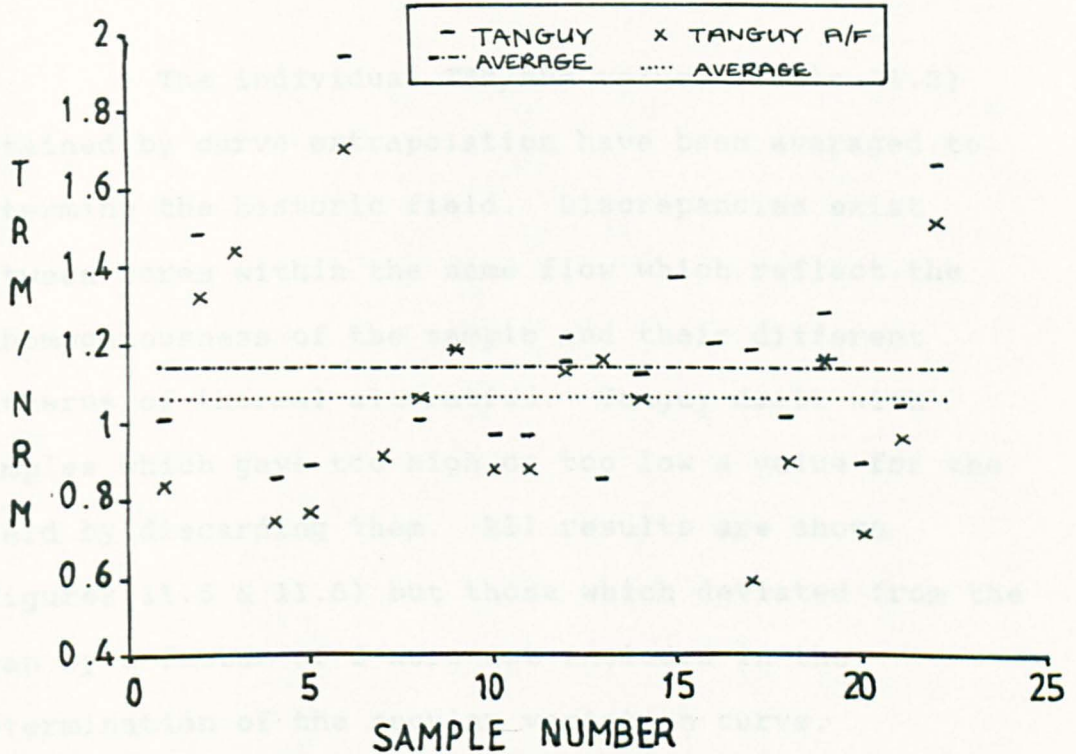
Figure 11.4 Comparison of A. F. cleaned and uncleaned
Tanguy results.

On older rocks with greater changes occurring to alter

the original NRM, the value of A.F. cleaning may make

the extra time involved in processing worthwhile.

11.3 The Tanguy technique and spinner magnetometer.

The technique used to determine the historic

field intensity has been described in Section 11.1.

Samples were kept at the maximum temperature for 2 minutes and a TRM created in them five times.

11.3.1 Results.

The individual TRM/NRM values (Table 11.3) obtained by curve extrapolation have been averaged to determine the historic field. Discrepancies exist between cores within the same flow which reflect the inhomogenousness of the sample and their different patterns of thermal alteration. Tanguy dealt with samples which gave too high or too low a value for the field by discarding them. All results are shown (Figures 11.5 & 11.6) but those which deviated from the mean by a factor of 2 were not included in the determination of the secular variation curve. Consequently results such as that for 1798 were considered marginal and are given in Table 11.3 but are not included in the least squares fit for the Canary Islands results.

It can be seen that the overall values show good agreement with those expected for the period of around 40 - 50μT (Gubbins, 1989). Comparison with results of other workers are given in chapter 13.

Table 11.3 Tanguy technique results from the spinner.

Year	TRM NRM	+/-	TRM NRM	+/-	TRM NRM	+/-	Fa (µT)	+/-
a) Canaries.								
1971/1	1.36	0.07	1.68	0.08	1.22	0.17	37.87	6.500
	1.61	0.15	1.03	0.06	----	----	-----	-----
1971/2	0.98	0.09	1.33	0.10	----	----	43.29	7.800
1949	0.86	0.14	0.79	0.03	1.18	0.23	46.90	12.60
	1.34	0.14	1.21	0.03	----	----	-----	-----
1909	1.35	0.21	0.95	0.02	1.21	0.24	42.73	7.050
1824	1.15	0.14	0.79	0.03	0.96	0.01	51.72	9.280
1798	0.78	0.02	0.61	0.28	0.64	0.42	75.87	9.170
	0.60	0.51	----	----	----	----	-----	-----
1730	1.40	0.13	1.33	0.01	----	----	36.63	1.000
1712	0.85	0.62	1.29	0.17	1.09	0.07	37.00	11.50
	1.42	0.34	1.78	0.13	----	----	-----	-----
1706	1.19	0.62	1.05	0.24	1.19	0.27	43.73	2.680
1705	1.67	0.17	0.78	0.07	1.78	0.27	35.21	22.27
	2.11	0.23	0.76	0.06	----	----	-----	-----
1704	1.68	0.52	1.15	0.30	0.93	0.25	41.19	12.40
	1.09	0.13	----	----	----	----	-----	-----
1677	1.41	0.08	1.25	0.10	1.40	0.06	39.40	4.100
	1.15	0.04	1.13	0.04	----	----	-----	-----
1646	1.16	0.18	1.91	0.08	1.42	0.18	33.40	7.050
	1.65	0.02	1.34	0.03	----	----	-----	-----
1585/1	1.15	0.27	1.29	0.27	1.70	0.14	40.50	11.60
	1.86	0.22	1.16	0.30	----	----	-----	-----
1585/2	1.42	0.04	1.35	0.10	1.34	0.09	36.33	0.900
	1.39	0.07	----	----	----	----	-----	-----
1470TN	0.62	0.15	0.68	0.16	0.66	0.05	77.6	3.270
	0.65	0.04	0.61	0.05	----	----	-----	-----
1470LP	0.99	0.16	1.67	0.17	0.87	0.04	40.00	15.67
	1.69	0.14	1.04	0.27	----	----	-----	-----
b) Vesuvius.								
1944	1.31	0.01	1.23	0.04	1.41	0.06	37.97	2.250
1929	1.10	0.02	1.04	0.04	1.43	0.01	42.00	7.000
1906	1.29	0.08	1.37	0.05	1.26	0.06	38.00	1.430
1895	1.28	0.25	1.08	0.08	1.10	0.10	43.25	3.500
1891	1.15	0.02	1.16	0.06	----	----	43.29	0.000
1886	1.72	0.44	1.39	0.27	1.20	0.21	34.80	6.120
1871	1.39	0.04	1.24	0.02	1.25	0.01	38.65	2.170
1867	1.70	0.14	1.16	0.14	0.96	0.21	39.30	12.70
1858	0.97	0.14	2.02	0.04	----	----	31.50	20.00
1850	1.16	0.13	1.32	0.14	1.15	0.01	41.32	2.840
1847	1.05	0.03	1.15	0.03	1.07	0.06	45.87	1.900
1834	0.91	0.06	1.09	0.15	0.96	0.07	50.64	4.270
1822	1.14	0.22	1.00	0.03	1.27	0.02	43.82	4.630
1804	1.19	0.05	0.95	0.02	----	----	46.72	5.900
1794	0.88	0.02	1.34	0.05	1.04	0.02	46.05	9.800
1767	1.36	0.04	1.17	0.06	1.35	0.03	38.70	2.750
1760	0.95	0.08	1.54	0.02	1.21	0.04	50.00	9.100
1754	0.85	0.06	0.89	0.01	1.69	0.02	43.74	22.65
1737	1.00	0.00	1.47	0.02	----	----	40.40	10.00
1697	0.91	0.06	1.41	0.14	1.00	0.03	45.47	9.400
	1.12	0.03	----	----	----	----	-----	-----

Figure 11.5 Variation of intensity for the Canaries
found using the Tanguy technique on the spinner.
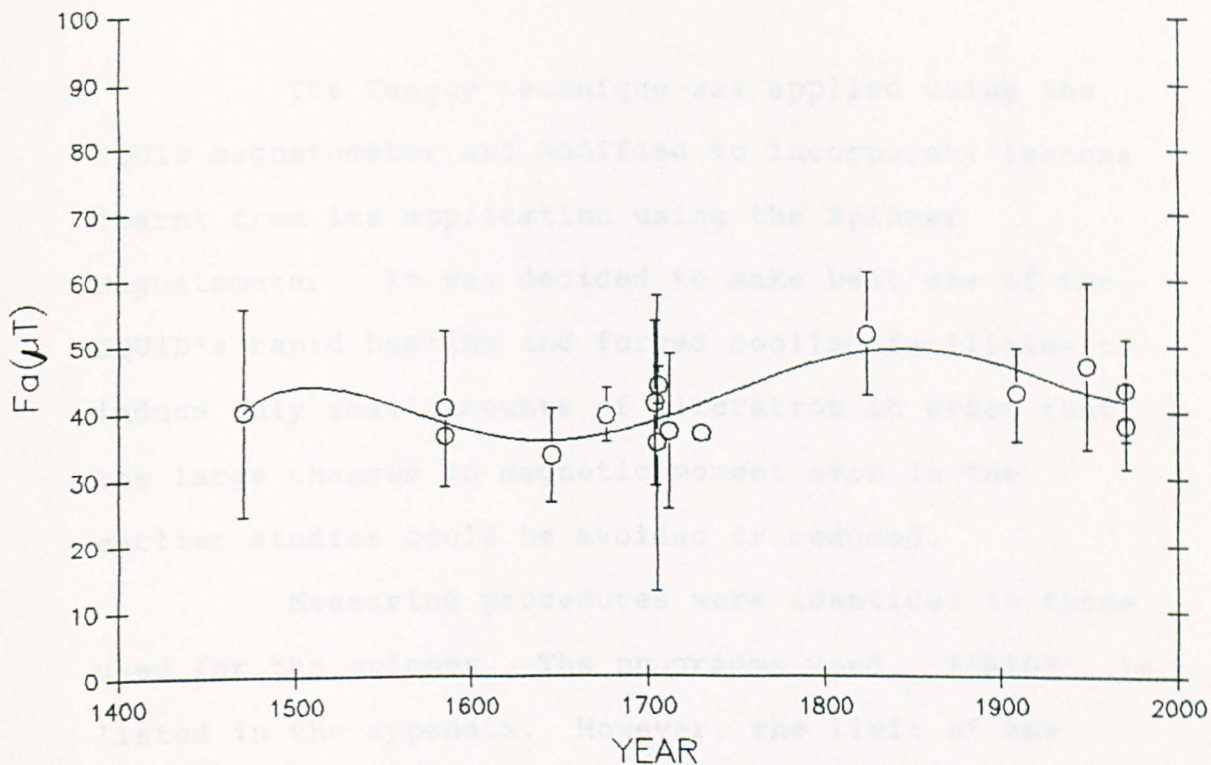
Figure 11.6 Variation of intensity for Vesuvius found
using the Tanguy technique on the spinner.
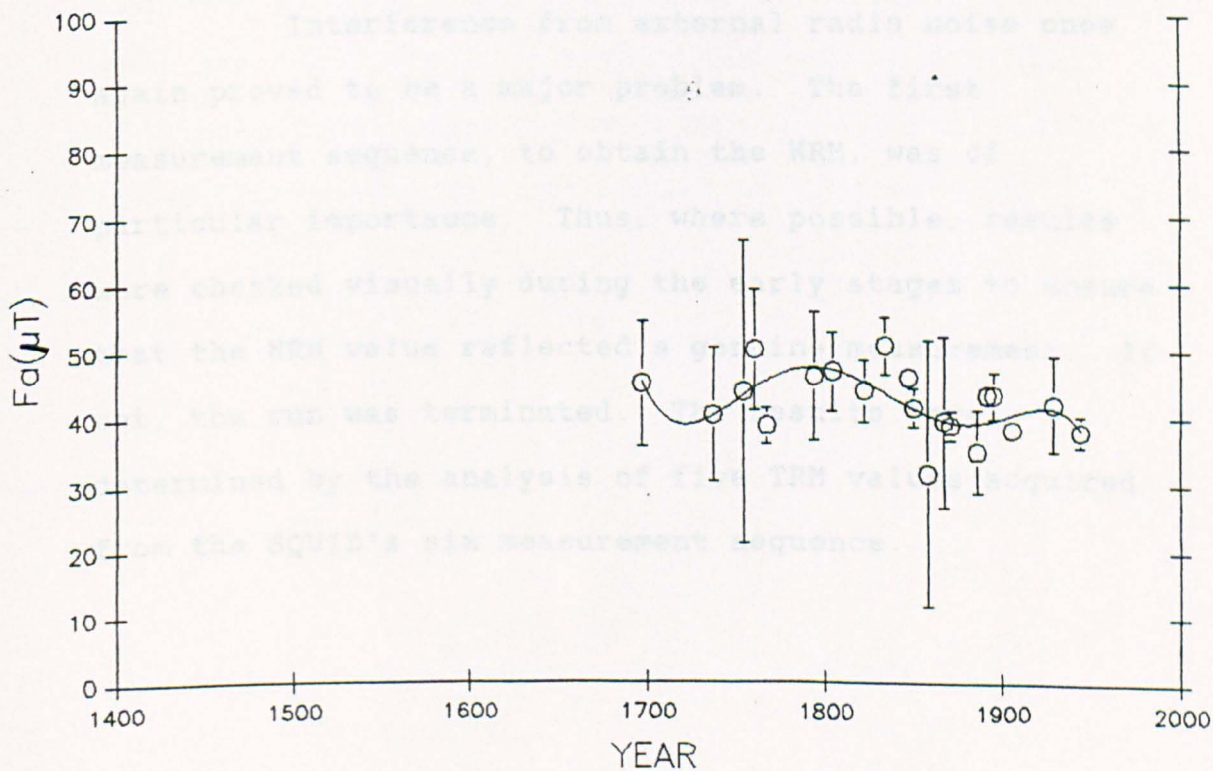
11.4 The Tanguy technique and SQUID magnetometer.

The Tanguy technique was applied using the SQUID magnetometer and modified to incorporate lessons learnt from its application using the Spinner Magnetometer. It was decided to make best use of the SQUID's rapid heating and forced cooling facilities to induce only small amounts of alteration in order that the large changes in magnetic moment seen in the earlier studies could be avoided or reduced.

Measuring procedures were identical to those used for the spinner. The programme used, "TAN103", is listed in the appendix. However, the limit of one sample per run meant that it took three hours per sample on the SQUID as opposed to fifteen samples in eight hours on the spinner.

Interference from external radio noise once again proved to be a major problem. The first measurement sequence, to obtain the NRM, was of particular importance. Thus, where possible, results were checked visually during the early stages to ensure that the NRM value reflected a genuine measurement. If not, the run was terminated. The results were determined by the analysis of five TRM values acquired from the SQUID's six measurement sequence.

11.4.1 Results.

The results (Table 11.4) were used to draw the secular variation curves with least squares line-fits (Figures 11.6 & 11.7). They show a good level of agreement with the expected values for the period 1400 to 2000 A.D. (40 - 50μT).

11.4.2 Conclusions.

Tanguy's technique gave results for samples that the Thellier and to a lesser extent the Boyd methods had previously found unsuitable. With further development, sample NRM cleaning for example, the technique will become a valuable additional device for the extraction of palaeointensity data. Cleaning the NRM will be of greater benefit on older samples since they are more likely to have a CRM, VRM or IRM which will make them unusable for a pure Tanguy run. Spinner and SQUID results are contrasted in Chapter 13.

Table 11.4 Tanguy technique results from the SQUID.

Year	TRM/NRM	+/-	TRM/NRM	+/-	TRM/NRM	+/-	Fa (μT)	+/-

a) Canaries.

Year	TRM/NRM	+/-	TRM/NRM	+/-	TRM/NRM	+/-	Fa (μT)	+/-
1971	1.05	0.01	1.87	0.03	1.64	0.00	32.90	7.350
1971/2	2.03	0.07	1.13	0.15	1.43	0.00	32.60	7.500
1949	0.79	0.12	----	----	----	----	63.30	10.00
1909/1	0.77	0.04	1.15	0.03	----	----	52.00	10.00
1909/2	1.08	0.01	0.70	0.02	0.89	0.01	56.10	9.500
1824	2.07	0.10	1.71	0.14	1.90	0.19	26.50	2.000
1798	0.80	0.00	0.91	0.00	0.62	0.01	64.90	9.500
1730	1.00	0.00	----	----	----	----	50.00	1.000
1712	2.10	0.06	0.82	0.00	1.16	0.02	36.80	14.50
1706	1.94	0.13	0.81	0.17	1.00	0.00	40.00	16.00
1705	1.06	0.29	0.91	0.02	1.61	0.26	41.60	10.00
1704	2.14	0.17	1.21	0.15	----	----	29.70	8.200
1677	1.48	0.02	1.17	0.00	1.53	0.04	36.20	4.000
1646/1	1.06	0.35	1.25	0.04	0.97	0.03	45.50	5.000
1646/2	0.89	0.33	----	----	----	----	56.00	20.70
1585/1	1.23	0.08	0.96	0.02	1.13	0.01	45.50	5.000
1585/2	1.26	0.15	1.15	0.01	----	----	41.60	2.000
1470TN	0.95	0.01	----	----	----	----	52.60	1.000
1470LP	1.32	0.30	1.84	0.01	1.34	0.01	33.30	6.000

b) Vesuvius.

Year	TRM/NRM	+/-	TRM/NRM	+/-	TRM/NRM	+/-	Fa (μT)	+/-
1944	0.93	0.02	0.86	0.01	1.04	0.05	53.20	4.00
1929	1.18	0.03	1.07	0.10	0.90	0.07	47.60	5.00
1906	0.88	0.04	1.02	0.13	0.91	0.00	53.70	4.00
1895	0.89	0.04	0.98	0.03	0.96	0.17	53.10	3.00
1891	1.11	0.43	1.49	0.05	0.77	0.02	44.60	13.0
1886	0.63	0.01	1.67	0.05	0.92	0.04	46.70	18.0
1871/1	1.13	0.05	1.46	0.24	1.25	0.01	39.00	4.00
1871/2	0.93	0.07	0.94	0.02	0.94	0.13	53.20	1.00
1867	1.20	0.08	1.03	0.04	0.83	0.04	49.00	8.00
1858	1.15	0.07	1.32	0.09	----	----	40.40	4.00
1850	1.25	0.01	1.07	0.03	1.17	1.31	43.00	4.00
1847	0.70	0.35	0.89	0.01	0.78	0.01	63.00	7.00
1834	1.02	0.09	0.85	0.03	1.01	0.05	52.00	5.00
1822	1.02	0.15	1.44	0.07	1.12	0.05	42.00	5.00
1804	0.90	0.11	1.17	0.08	1.29	0.10	44.60	5.00
1767	1.06	0.06	0.88	0.01	1.01	0.07	51.00	5.00
1760	1.07	0.25	1.63	0.30	0.80	0.04	43.10	12.5
1754	1.11	0.09	0.91	0.06	0.86	0.02	52.00	6.00
1737	0.95	0.22	2.69	0.87	1.00	0.02	51.30	2.00
1697	0.87	0.04	1.01	0.01	0.87	0.06	54.30	4.00

Figure 11.7 Variation of intensity for the Canaries found using the Tanguy technique on the SQUID.
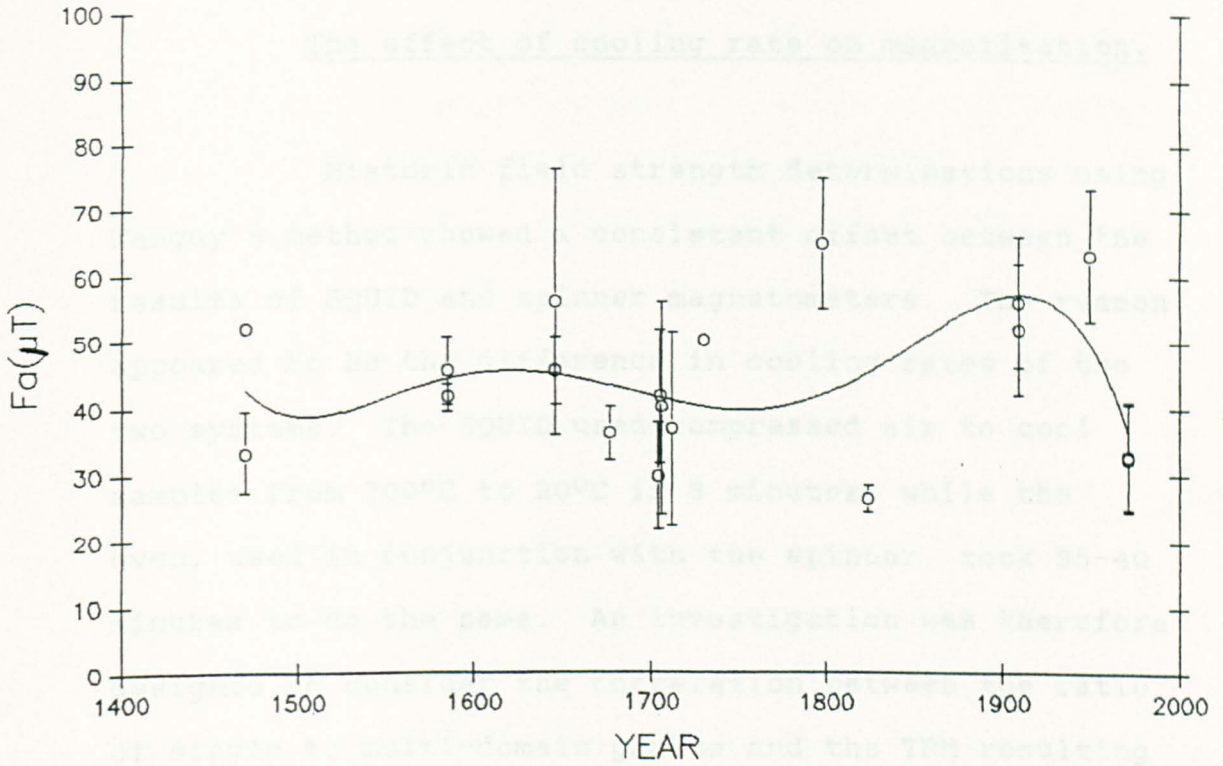
Figure 11.8 Variation of intensity for Vesuvius found using the Tanguy technique on the SQUID.
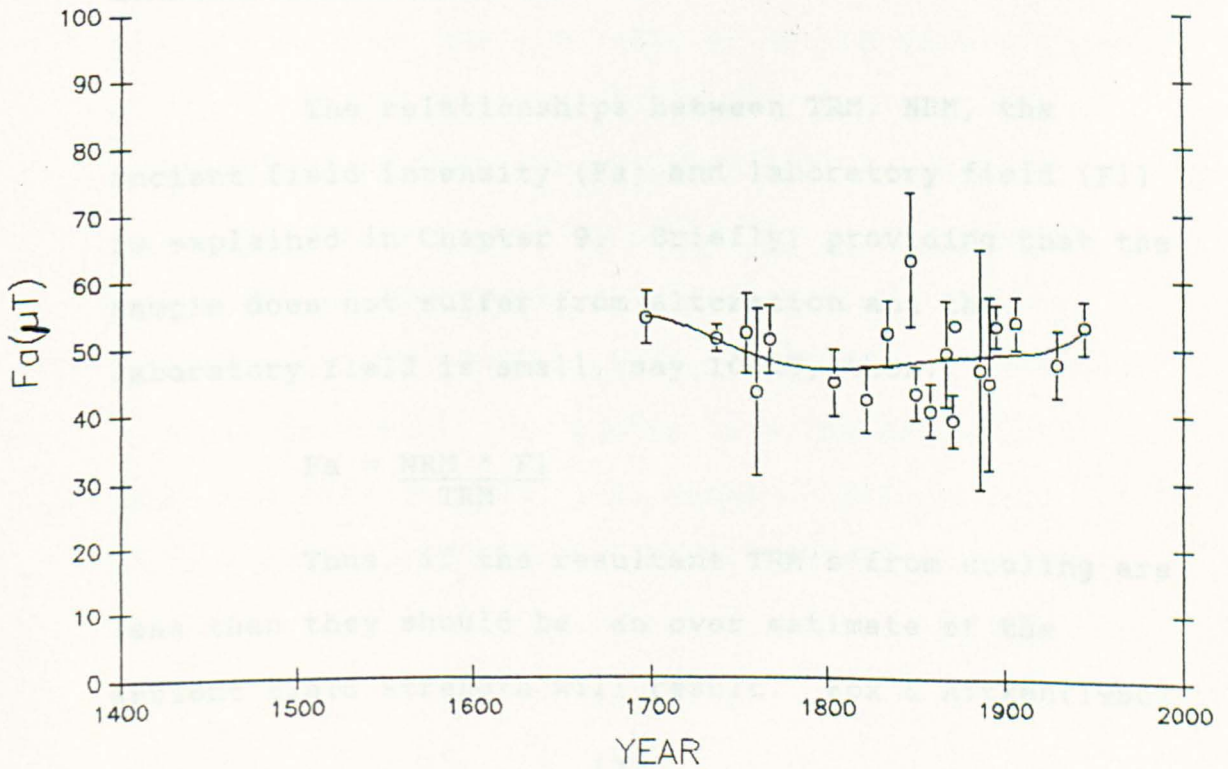
The effect of cooling rate on magnetisation.

Historic field strength determinations using Tanguy's method showed a consistent offset between the results of SQUID and spinner magnetometers. The reason appeared to be the difference in cooling rates of the two systems. The SQUID used compressed air to cool samples from 700°C to 20°C in 8 minutes, while the oven, used in conjunction with the spinner, took 35-40 minutes to do the same. An investigation was therefore designed to consider the correlation between the ratio of single to multi-domain grains and the TRM resulting from fast and slow cooling rates.

12.1 Theoretical background.

The relationships between TRM, NRM, the ancient field intensity (Fa) and laboratory field (Fl) is explained in Chapter 9. Briefly, providing that the sample does not suffer from alteration and the laboratory field is small, say 100mT, then:

$$Fa = \frac{NRM * Fl}{TRM} \quad .$$

Thus, if the resultant TRM's from cooling are less than they should be, an over estimate of the ancient field strength will result. Fox & Aitken(1980)

found an increase in pottery magnetisation of 10-20%
when cooled over 7 hours rather than the normal 30
minutes. Work by Dodson & McClelland-Brown (1980) on
cooling rate and magnetic blocking temperatures found a
magnetisation "increase of a few percent for each order
of magnitude decrease in cooling rate" for single
domain magnetite and haematite.

The blocking temperature (Tb) is the most
important factor in determining the samples
magnetisation when cooling. O'Reilly (1984) states
that "The effect of a decreased cooling rate or an
increased field is to lower Tb". Thus a difference in
cooling rate between systems will produce offset
results. A single domain material cooled slowly
acquires a larger magnetic moment due to a greater
fractional alignment of the magnetic moments within the
sample. Changes in the magnetisation of single domain
grains have a relatively large effect on sample moments
since their magnetisation is large. Cooling multi-
domain material more slowly provides a greater
opportunity for thermal agitation to promote the
population of the lowest energy state and thus the
external magnetic field, and hence TRM's are reduced.
In-depth references are available which explain the
numerical interdependence of magnetic moment and
cooling rate (eg. Williams, 1986; Halgedahl et al.,
1980).

172

12.2 Technique of investigation.

The SQUID magnetometer's ability to run independently of an operator over long periods made it the ideal instrument for cooling rate effect determinations. To this end it was programmed for the following order of operation:

1. moment measured at 100°C,

2. sample heated to 650°C,

3. 50mT field applied,

4. sample rapidly cooled to 100°C,

5. moment measured (alteration check),

6. sample heated to 650°C,

7. 50mT field applied,

8. sample cooled at rate R1 to 100°C,

9. moment measured,

10. repeated with logarithmically increasing cooling rate R1.

A series of values for the sample's magnetic moment for successively longer cooling periods were obtained from the procedure outlined above. SQUID magnetometer programming allowed for cooling periods of between 30 minutes and 16 hours. An initial cooling rate was calculated from a value supplied by the operator, the optimum value to be determined after the initial trial period. (Further details of programming can be found in the appendix "FOX223").

173

The effects of alteration during these experiments were measured by means of a rapid cool cycle inserted between each long cool cycle. This rapid cooling cycle provided a control value against which the true moment change could be determined. Alteration, which affects the value of the samples moment after a long cooling, will have a similar affect on the following rapid cool cycle. This format does not exclude errors due to alteration but provides a method of normalisation without over complication.

Thus the results were processed as follows:

M1 = moment after slow cool 1 for time T1

m1 = moment after ensuing 8 minute rapid cool

$$P1 = \frac{(M1 - m1)*100}{m1} = \text{percentage change in magnetic moment}$$

12.3 Experimental procedure.

The SQUID magnetometer had the ideal control system for the experimental work necessary but not the required reliability. It proved to be impossible to complete a full sample run without oven failure and as a result considerable time was spent redesigning the SQUID oven (Chapter 8). Consequently only a small number of results were obtained.

174

12.4 Results of cooling rate experiments.

The results are given in Table 12.1. The incomplete appearance reflects the developmental nature of the work and the reliability problems.

Table 12.1 Percentage change in magnetic moment.

Cooling time in minutes.

Year	32	62	86	107	122	213	243	484	740	966
1470	-11	*	*	-9	*	*	*	*	*	*
1585	*	18	*	*	*	*	7	12	10	*
1585	*	5	*	*	*	*	8	5	*	*
1585	16	-14	*	*	*	*	*	*	*	*
1697	*	-33	*	*	*	-34	*	*	-13	*
1704	10	12	*	*	4	*	21	*	*	*
1754	*	11	*	*	14	*	3	2	*	*
1760	-20	13	*	*	-13	*	*	*	*	*
1822	*	14	*	*	*	*	8	*	*	8
1886	36	*	9	*	*	*	*	*	*	*
1891	11	*	*	*	*	*	*	*	*	*
TEST	*	-6	*	*	*	-1	*	*	*	*

The results show a mixed reaction to an increased cooling period reflecting the conflicting effects of increasing the cooling time on single and multi-domain grains. In 3 of the 12 samples a stable decrease in moment resulted from slower cooling (up to 34% less for 1697) over the moment acquired during rapid cooling (Figure 12.1). Two cases showed mixed behaviour in which the change in magnetic moment varied from increase to decrease over the course of the experiment. The remaining 7 samples show a moment increase with increased cooling time. A curve showing

Figure 12.1 Effect of increased cooling time on samples from 1760, 1697 and 1585.
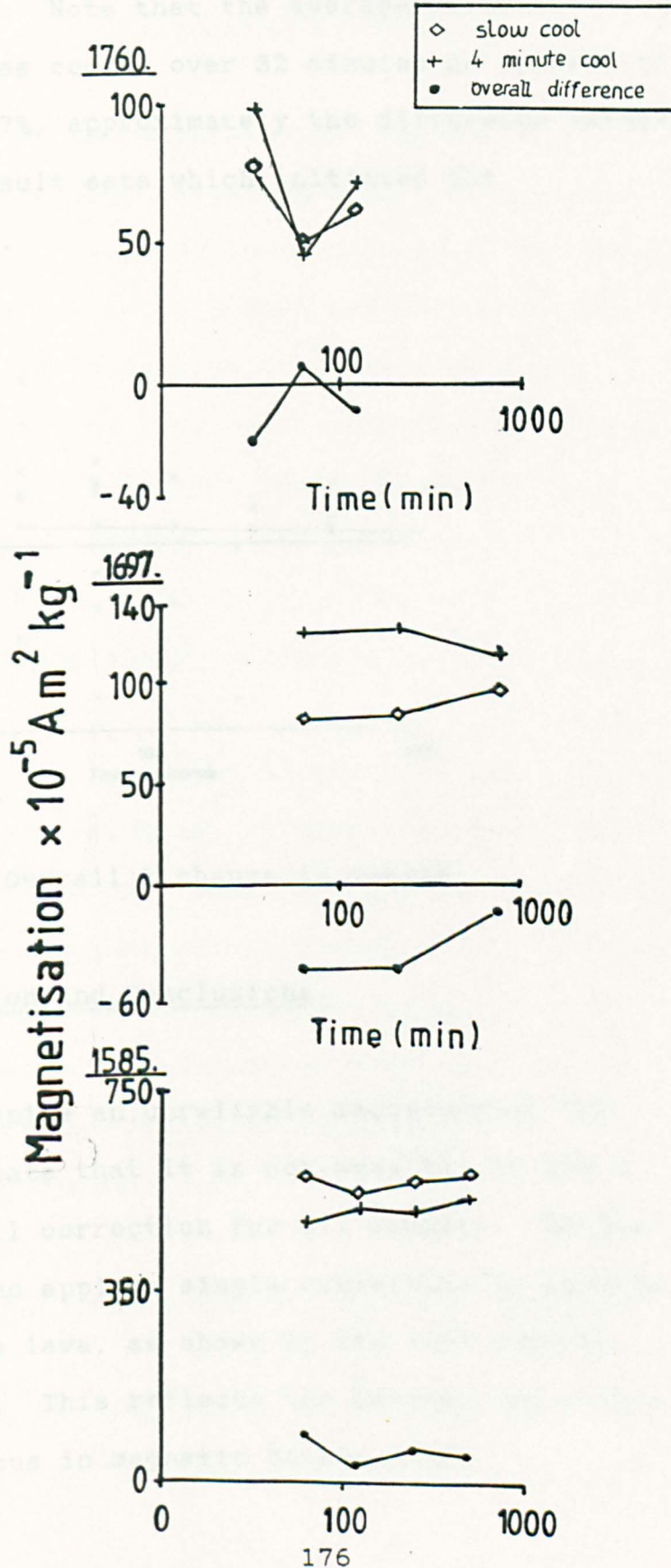
all the results has a logarithmic regression fit
(Figure 12.2). Note that the average difference found
between samples cooled over 32 minutes as opposed to 8
minutes was +7%, approximately the difference between
two Tanguy result sets which initiated the
investigation.
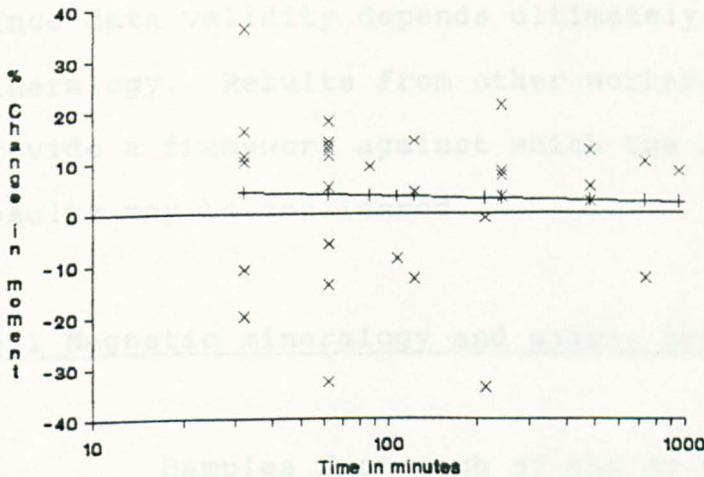
Figure 12.2 Overall % change in moment.

12.5 Discussion and Conclusions.

Despite an unreliable magnetometer the
results indicate that it is not possible to use a
single overall correction for all samples. Neither is
it possible to apply a single correction to samples
from the same lava, as shown by the 1585 samples
(Chapter 14). This reflects the between and within
flow variations in magnetic domain state.

Secular variation summary

One of the main project aims was the aquisition of secular variation data for the sampled areas. This chapter contains a summary of the data acquired and a review of sample magnetic mineralogy since data validity depends ultimately on that mineralogy. Results from other workers are included to provide a framework against which the accuracy of results may be considered.

13.1 Magnetic mineralogy and sample pre-selection.

Samples from each of the 35 dated lava flows were subjected to a series of magnetic mineralogy tests (Chapters 4, 5 and 6). Each test provided information on a particular aspect of the sample. When compiled (Table 13.1) the variety of sample types present becomes apparent and provides an overview which may be used for the pre-selection of both materials and analytical techniques.

13.1.1 Canary Islands magnetic mineralogy.

Samples from the Canary Islands show a very mixed set of magnetic mineral characteristics and

Table 13.1 Overall rock magnetism results.

a) Canary Islands.

Year of flow	SD/MD ratio	----- Curie ----- temp	class	altn	Lt Sus group	Ht Sus group
1971	0.14	185	2	a	1	MD
1949	0.07	560	4		3/1	MD
1909	0.33	300	2	b	1	MD/sd
1824	0.23	160	1	b	1	MD
1798	0.16	180/520	5	b	1	MD
1730	1.94	550	3	c	2/1	QSD
1712	0.07	235/545	5	b	1	MD
1706	0.05	550	3	a	3	MD
1705	0.07	545	3	a	3	MD
1704	0.15	200/525	2a / 5a		1	MD
1677	0.28	565	3	a	1	MD
1646	0.10	530	3a / 5b		1	MD
1585	0.18	545	4		1	MD
1470T	0.20	585	3	a	3	--
1470LP	0.28	520	3	a	3	QSD/MD

b) Mount Vesuvius.

Year of flow	SD/MD ratio	----- Curie ----- temp	class	altn	Lt Sus group	Ht Sus group
1944	0.38	570	3	c	3/2	MD/sd
1929	0.21	525	3	c	1/3	MD/sd
1906	0.24	550	3	a	3	MD/sd
1895	0.06	570	3	a	3/1	MD
1891	0.21	500	3	b	1/3	MD/sd
1886	0.59	570	3	b	3	QSD/MD
1871	0.26	570	3	a	3/1	MD/sd
1867	0.30	470	3	a	3	SD
1858	0.37	320/600	5	a	1	MD
1850	0.38	580 250	3a / 2a		3/1	QSD/MD
1847	0.29	565	3	c	3/1	MD
1834	0.25	550	3	c	2/1	MD
1822	0.21	570	3	a	1	MD/sd
1804	0.29	300/500	5	b	1	MD
1794	0.38	575	3	b	2	MD/sd
1767	0.81	505	3	c	1/3	MD
1760	0.32	560	3	a	1/3	MD
1754	0.22	595	3	a	3/2	MD/sd
1737	0.53	540	3	c	1/2	MD/sd
1697	0.14	570	3	a	1/3	MD

little can be said about the group in general other

than it is inhomogeneous. However two properties were

common to the majority of samples, firstly the very low

levels of anisotropy and secondly the low single domain

to multi-domain populations. Anisotropy of susceptibility was less than 3% for all but the 1971, 1909 and 1706 flows which had values of up to 5% and the 1470T flow with up to 9%. The single to multi-domain ratio, for all samples except 1730LZ, had a value of 0.16 +/- 0.09. Only the 1730LZ flow had a high single to multi-domain ratio, 1.94, indicating a large single domain component, confirmed by its high temperature susceptibility curve which was of the quasi-single domain type.

No single type of Curie curve dominates the results, 6 of the 15 samples have low or intermediate Curie temperatures, that is below 500°C. Low temperature susceptibility curves do not show any particular trend but curve types 1 and 3 dominate.

13.1.2 Mount Vesuvius magnetic mineralogy.

The Vesuvian samples showed a more regular sample magnetic mineralogy than those of the Canary Islands. None of the samples tested had anisotropy of susceptibility which was greater than 2%. On average samples had a much higher single domain population than those of the Canary Islands, as the average SD/MD ratio was 0.32 +/- 0.16. Curie curves, normally type 3, show samples to be principally single phase with Curie temperatures in the range of 500 to 580°C. The only exceptions were the 1858, 1850 and

1804 flows. Low and high temperature susceptibility results reflect the relatively higher proportion of single domain crystals in the samples.

13.1.3) Sample selection, based on low temperature susceptibility.

A possible sample pre-selection, based on low temperature susceptibility, was proposed by Senanayake & McElhinny (1982). Groups 2 and 3 were considered suitable for elevated temperature measurement since they are stable to 500°C whereas group 1 samples are subject to oxidation after 300°C. It might be expected therefore that a direct link would be visible between the low temperature susceptibility group and the degree of alteration seen in the results from the Curie balance; this is not the case. This may indicate that the proposal is incorrect but it is more likely that the samples subjected to Curie balance analysis were not maintained at elevated temperatures sufficiently long to experience noticeable oxidation. It was not therefore possible to confirm, or deny, the link between low temperature susceptibility and thermal alteration. Samples were run without any preselection but the low temperature susceptibility groups were borne in mind when considering the reliability of final intensity results obtained after thermal demagnetisation.

13.2 Secular variation of direction.

Data sets for the secular variation of both areas were obtained using a parastatic magnetometer (Table 13.2) and these were used to plot secular variation curves (Figures 13.1 and 13.2).

Table 13.2 Directional results.
a) Canary Islands

Year	Decln	Inc	alpha95	K	No samples
1971LP	349.2	43.2	3.7	421	4
1971LP	351.3	38.6	3.8	258	7
1949LP	350.1	41.0	3.4	488	5
1909TN	340.9	40.2	4.2	256	6
1824LZ	338.7	54.5	4.6	213	6
1798TN	350.5	53.8	3.4	388	6
1730LZ	343.1	64.5	2.5	1270	4
1712LP	354.6	56.5	1.3	2657	6
1706TN	357.9	59.2	2.6	674	6
1705TN	355.6	55.2	3.3	424	6
1704TN	359.7	63.2	2.8	752	5
1677LP	358.3	55.5	4.6	211	6
1646LP	002.5	54.5	3.4	304	7
1646LP	003.7	55.1	3.5	490	5
1585LP	002.2	48.8	2.6	622	6
1585LP	009.1	52.4	4.1	351	5
1470TN	009.2	17.4	3.7	273	7

b) Mount Vesuvius.

Year	Decln	Inc	alpha95	K	samples
1944	359.7	54.3	2.3	1077	5
1929	357.2	52.4	1.8	559	13
1906	353.6	53.1	0.8	12638	4
1895	355.5	54.8	1.9	1252	6
1891	354.1	56.1	2.5	921	5
1886	343.3	57.3	1.8	1839	5
1871	349.2	56.4	3.5	488	5
1867	347.7	57.3	4.0	375	5
1858	349.8	54.3	13.5	346	2
1850	344.8	49.6	0.8	7013	6
1847	342.9	61.9	1.6	3262	4
1834	347.2	54.9	1.5	2449	5
1822	351.0	55.1	3.0	341	8
1804	344.3	53.1	2.2	891	6
1794	346.6	59.8	1.9	1227	6
1767	343.7	57.6	3.4	499	5
1760	343.5	65.7	1.3	1365	10
1754	346.0	65.1	2.4	792	6
1737	354.8	59.1	1.7	1944	5
1697	018.4	63.7	1.7	1646	6
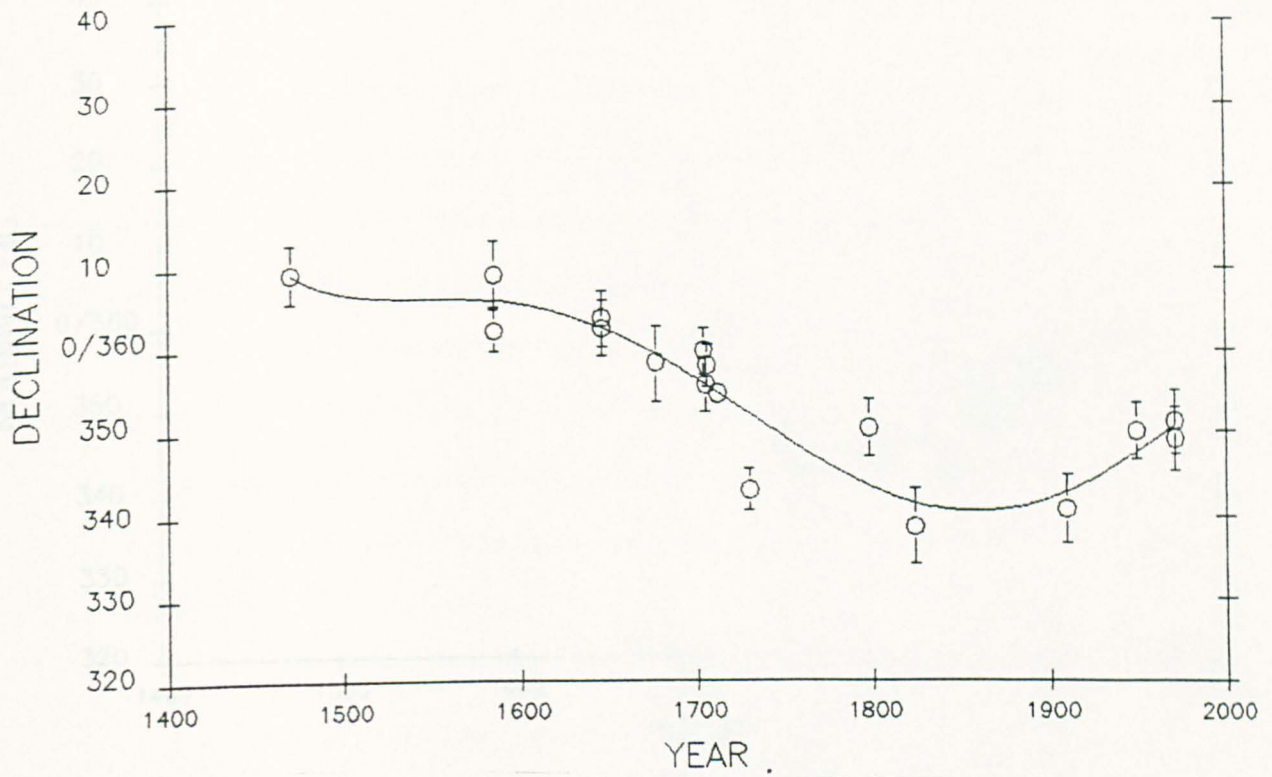
Figure 13.1 Variation of declination
and inclination with time for the Canary Islands.
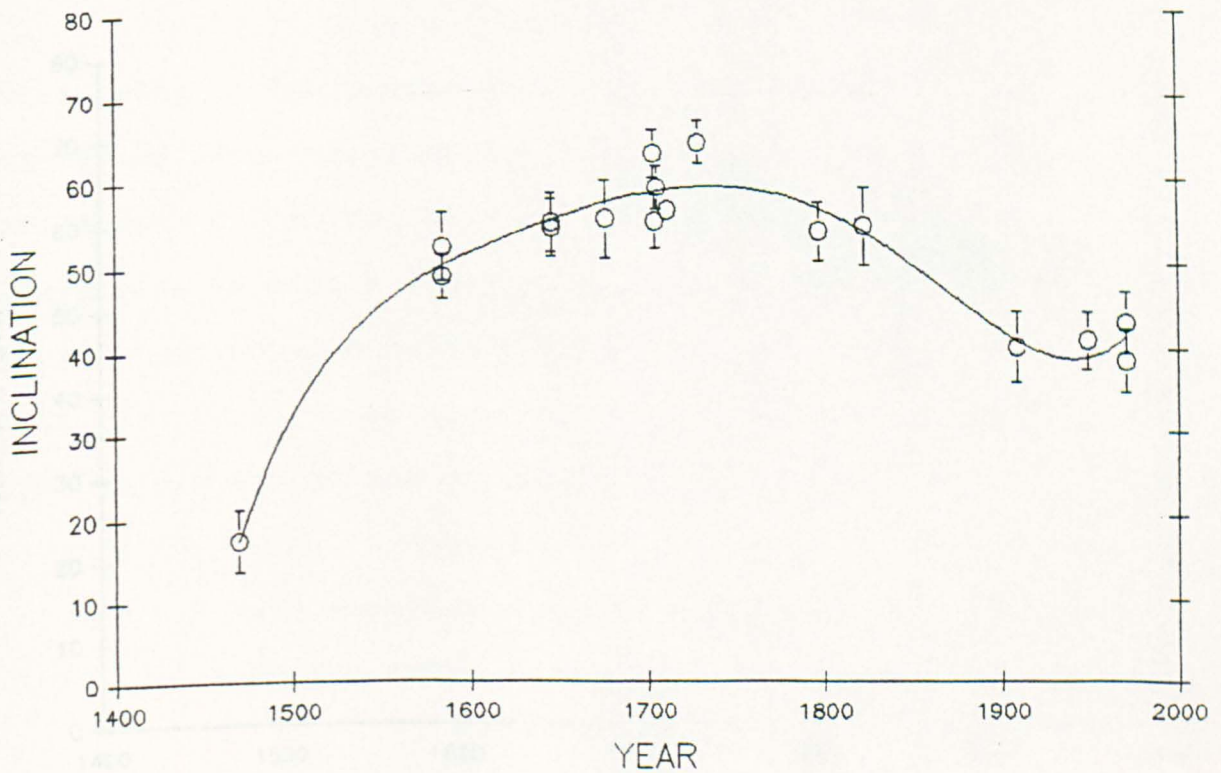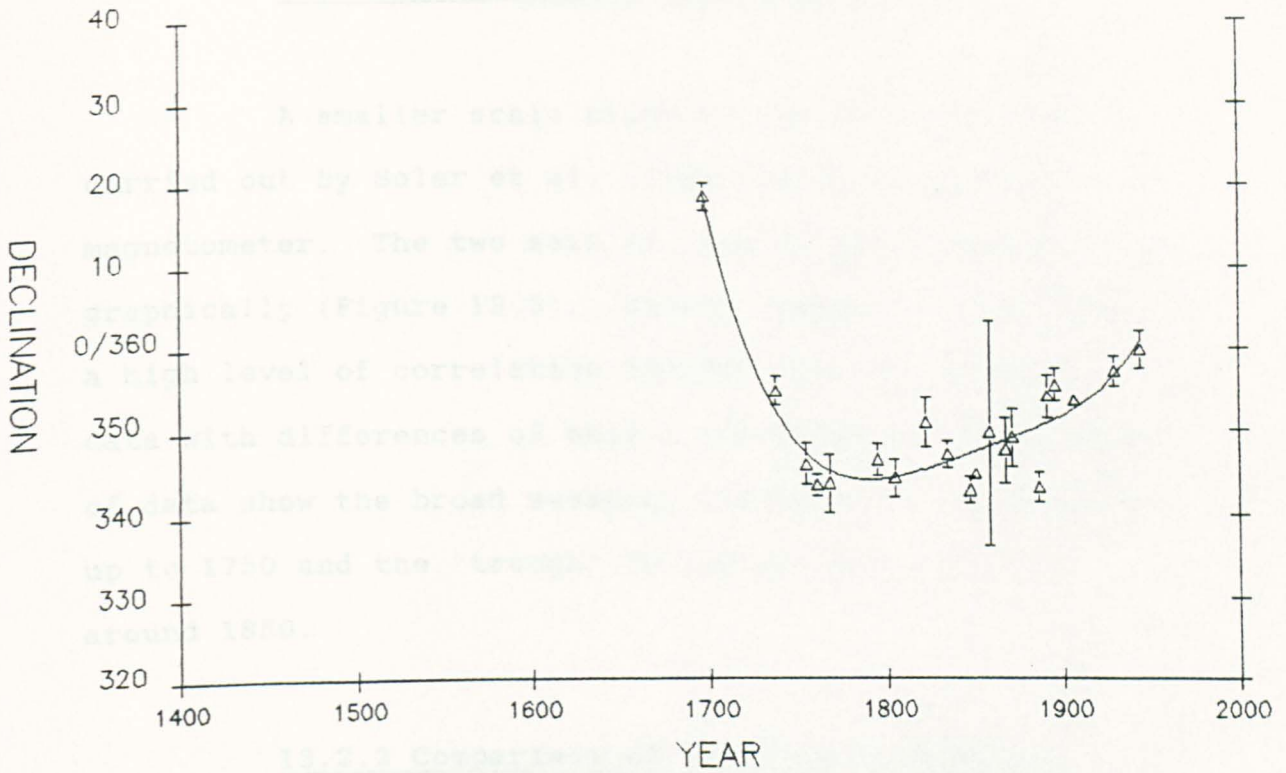
Figure 13.2 Variation of declination and
inclination with time for Mount Vesuvius.
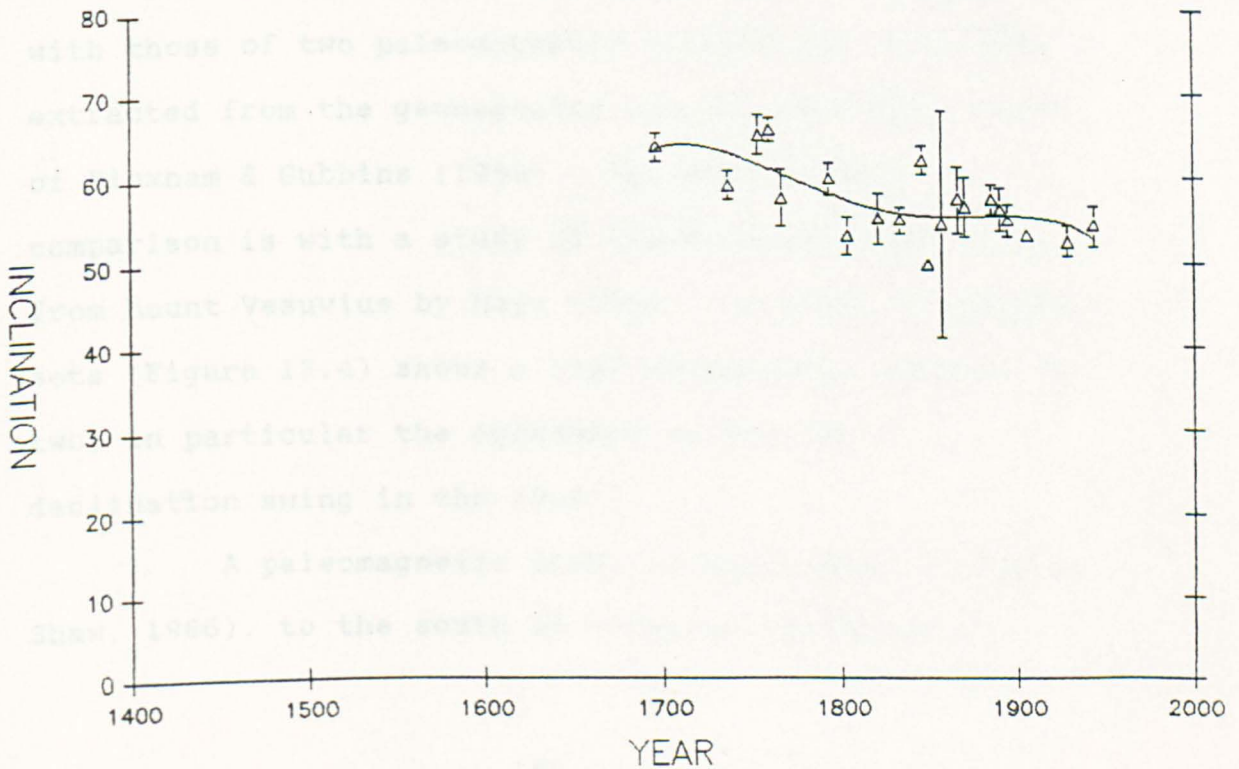
13.2.1 Comparison of Canary Island directional secular variation results.

A smaller scale study of the same area was carried out by Soler et al. (1984) using a spinner magnetometer. The two sets of results are compared graphically (Figure 13.3). Visual inspection indicates a high level of correlation between the two sets of data with differences of only a few degrees. Both sets of data show the broad sweeping increase in inclination up to 1750 and the "trough" in the declination plot around 1850.

13.2.2 Comparison of Vesuvian directional secular variation results.

The results of this study can be compared with those of two paleomagnetic studies and with data extracted from the geomagnetic secular variation model of Bloxham & Gubbins (1985). The most direct comparison is with a study of eleven dated lava flows from Mount Vesuvius by Hoye (1981). A plot of the data sets (Figure 13.4) shows a high concurrence between the two, in particular the agreement on the large declination swing in the 1700's.

A paleomagnetic study of Mount Etna (Rolph & Shaw, 1986), to the south of Vesuvius, provides a
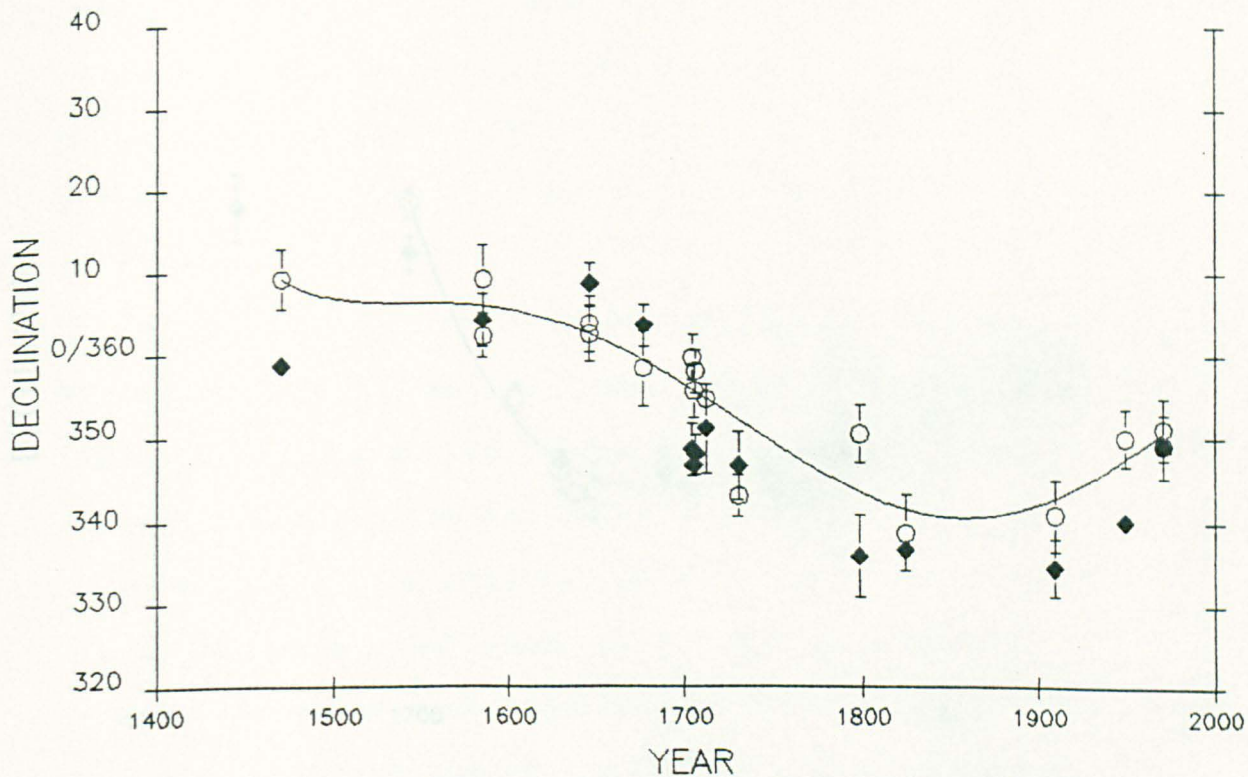
Figure 13.3 Canary Island results comparison with
those of Soler et al (1984). (Results from this study
are shown as circles those of Soler et al as diamonds.)
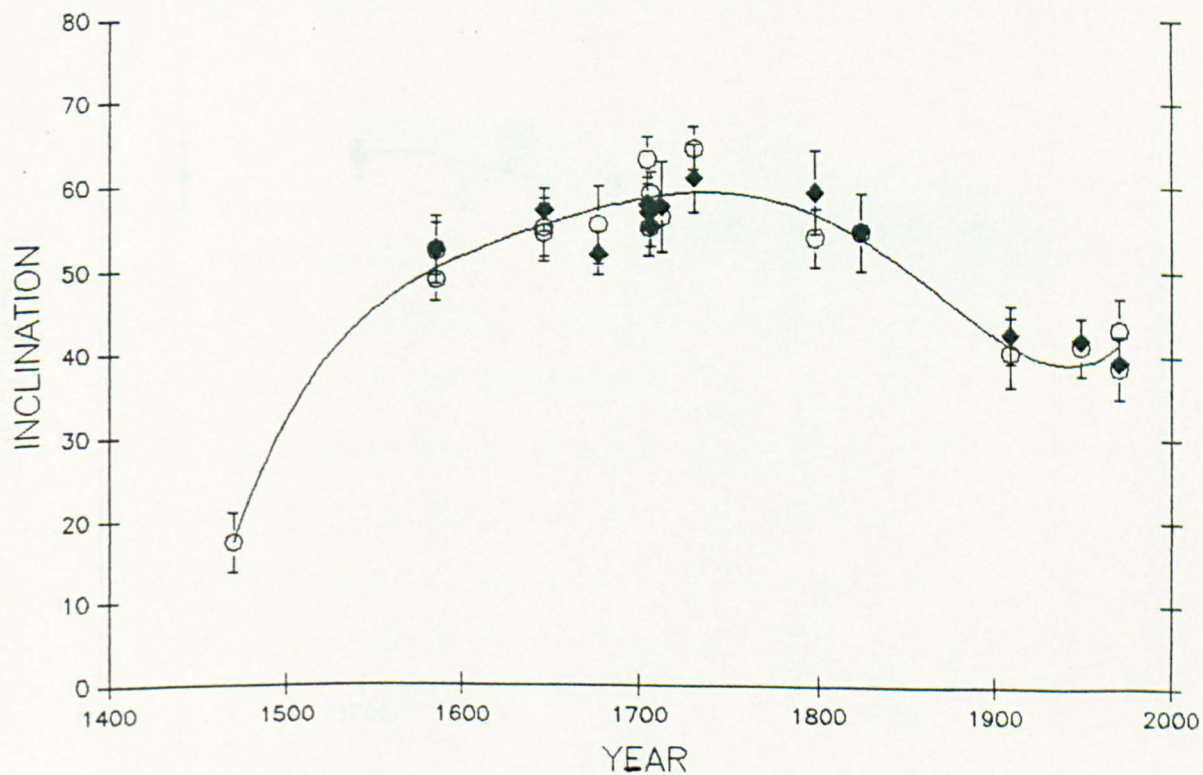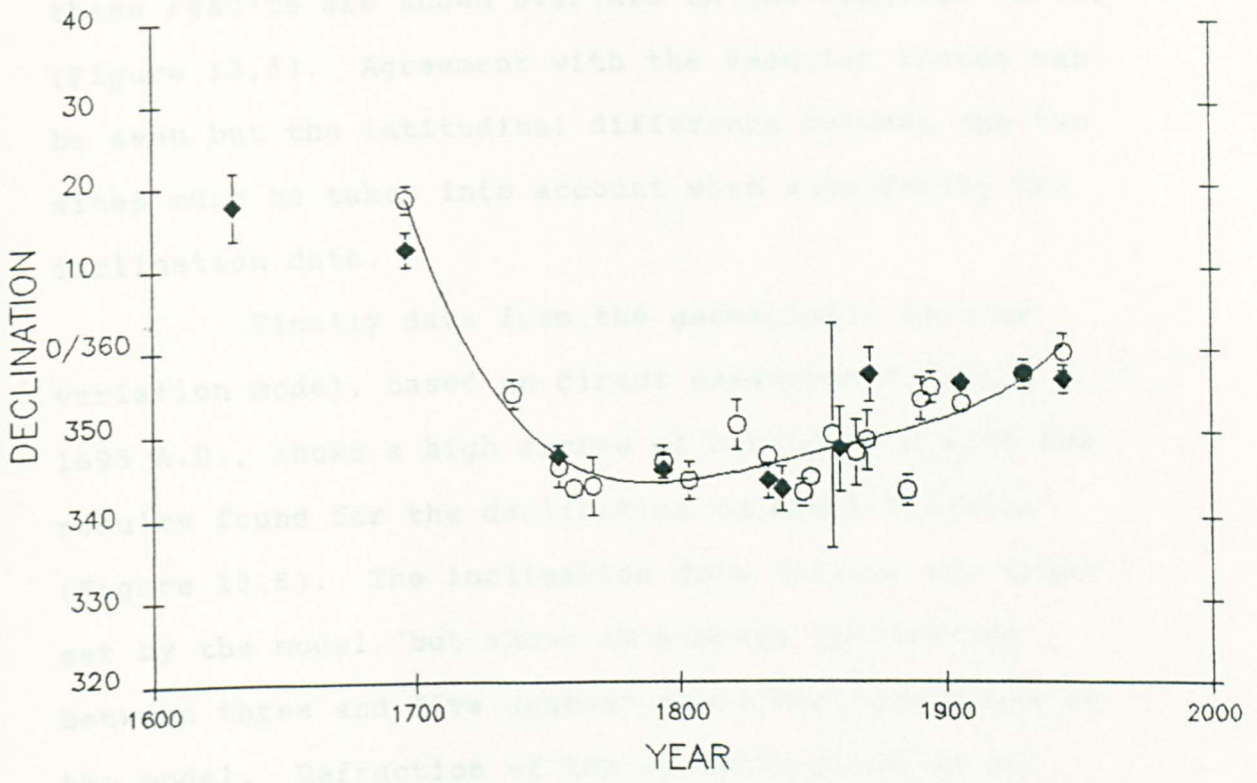
Figure 13.4   Vesuvian results comparison with those of
Hoye (1981).   (Results from this study are shown as
circles those of Hoye as diamonds.)
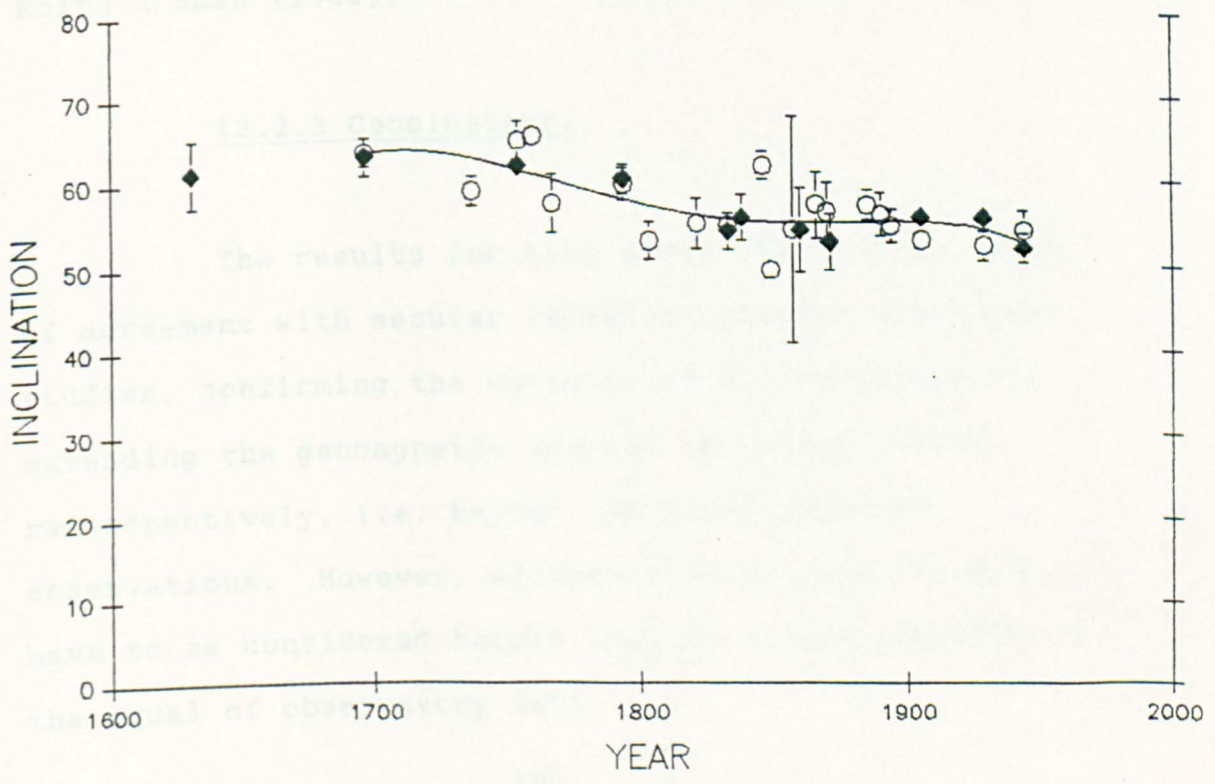
second, though less direct, comparison. Once again these results are shown overlaid on the Vesuvian curves (Figure 13.5). Agreement with the Vesuvian trends can be seen but the latitudinal difference between the two sites must be taken into account when considering the inclination data.

Finally data from the geomagnetic secular variation model, based on direct measurements since 1695 A.D., shows a high degree of correlation with the results found for the declination on Mount Vesuvius (Figure 13.6). The inclination data follows the trend set by the model, but shows an average inclination between three and five degrees shallower than those of the model. Refraction of the magnetic field as it enters the lava could explain this shallowness. A similar effect has been found by other workers, notably Rolph & Shaw (1986).

13.2.3 Conclusions.

The results for both areas show a high level of agreement with secular variation results from other studies, confirming the validity of the technique for extending the geomagnetic secular variation record retrospectively, i.e. beyond the first recorded observations. However, effects such as refraction will have to be considered before results can be regarded as the equal of observatory data.
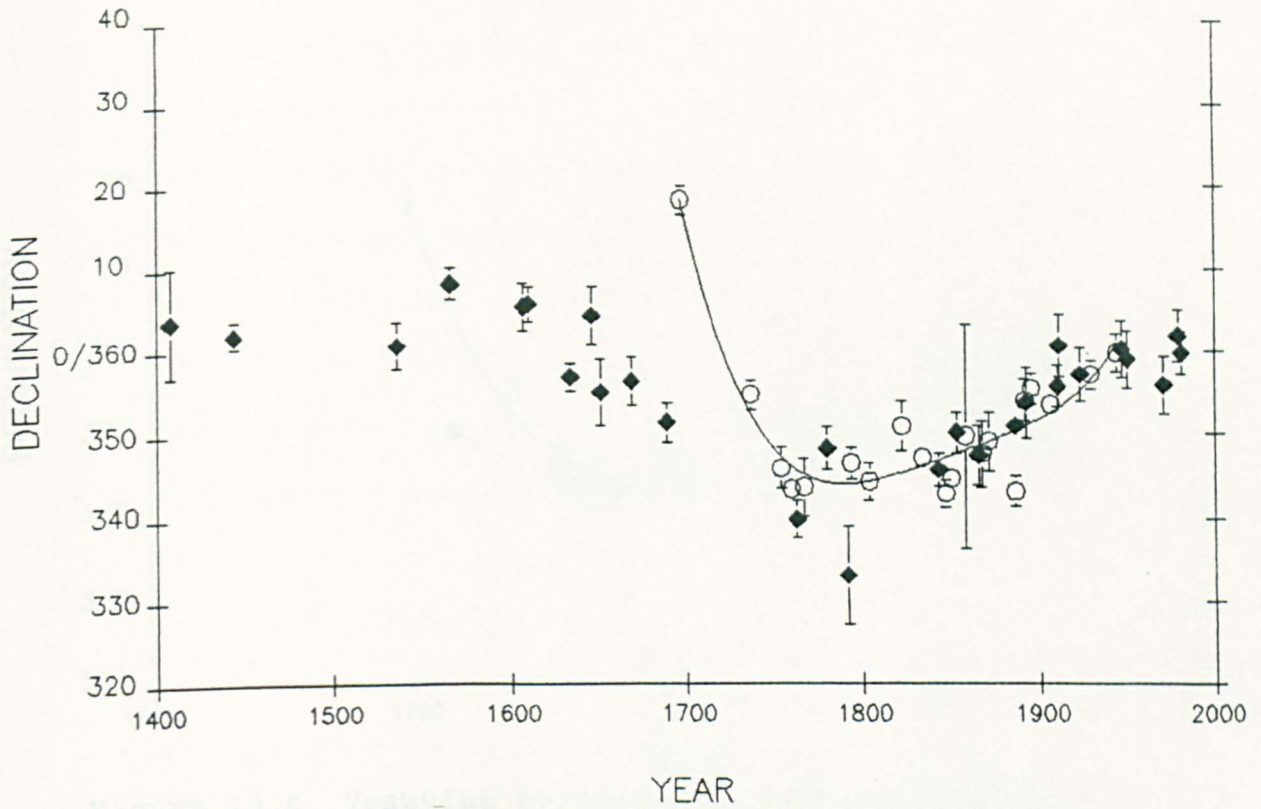
Figure 13.5 Vesuvian results comparison with those of Rolph & Shaw (1986) for Mount Etna. (Results from this study are shown as circles those of Rolph & Shaw as diamonds.
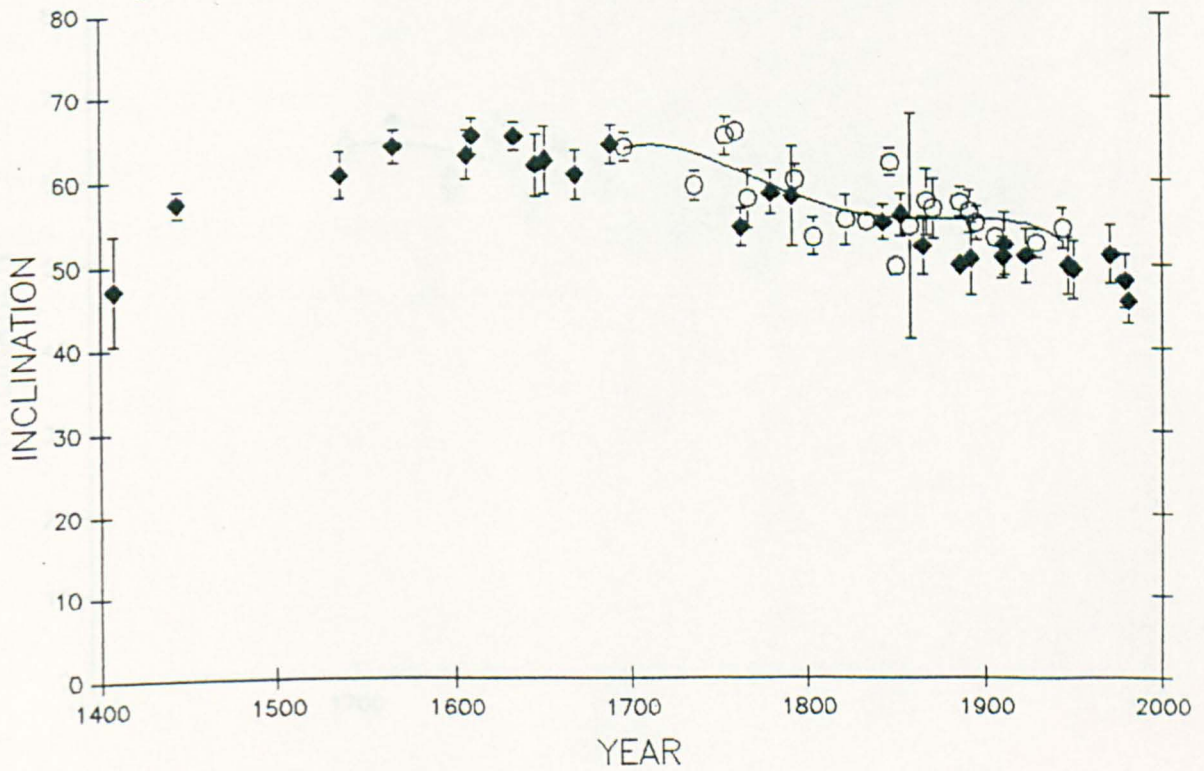
Figure 13.6 Vesuvian results comparison with those of
the Geomagnetic secular variation model. (Results from
this study are shown as circles those of the model as diamonds.)
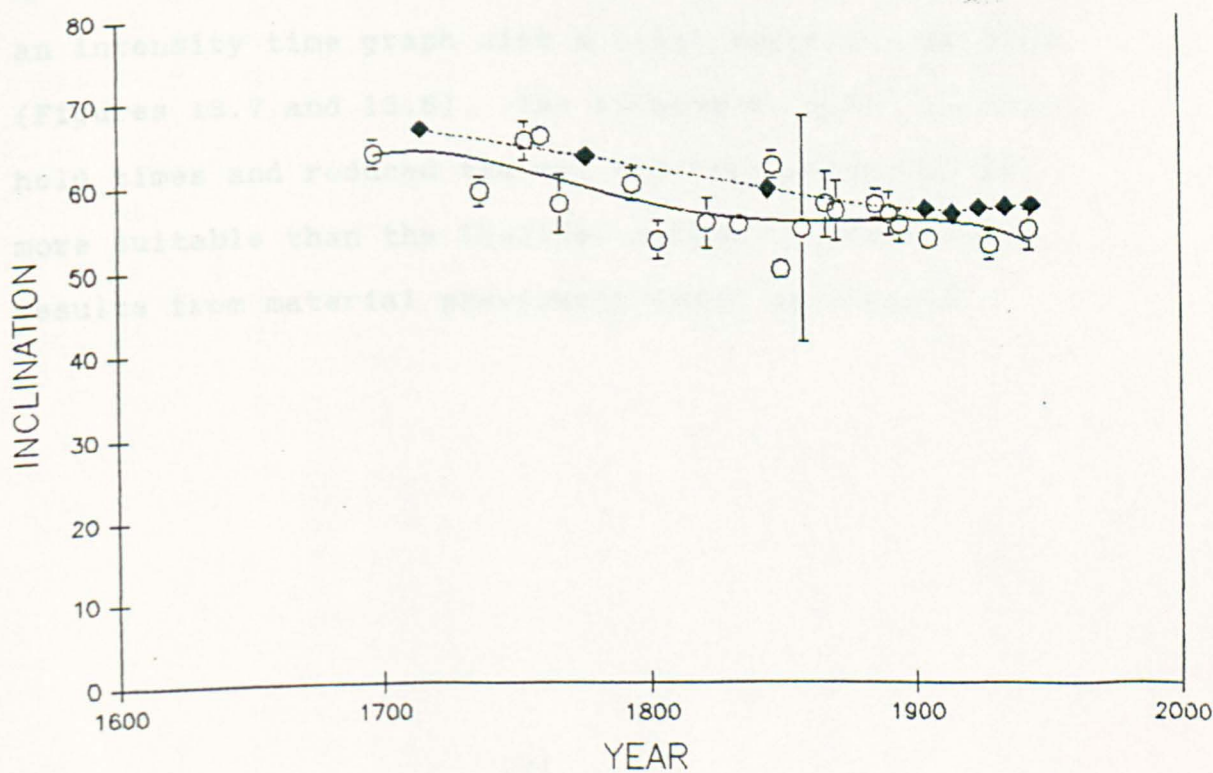
13.3 Secular variation of intensity.

Three techniques were applied, the Thellier, Boyd and Tanguy techniques. The Thellier technique proved to be inapplicable to the majority of samples yielding only small amounts of useful data. Full sets of data were, however, collected for both of the other techniques. The Tanguy technique in fact provided two full sets of data for each area since it was acquired from both the spinner and SQUID magnetometers.

13.3.1 The Boyd technique.

Results for the Boyd technique are given in Table 13.3, the gaps in the table indicating the unsuitability of some samples or unsuccessful runs due to excessive SQUID noise. Flow results were plotted on an intensity time graph with a least squares line-fits (Figures 13.7 and 13.8). The technique, with its short hold times and reduced thermal cycling, proved to be more suitable than the Thellier method by producing results from material previously found unsuitable.

Table 13.3 Boyd results for Canaries & Vesuvius.

Year	Sample values for Fa(μT)								Average	
	Fa	+/-	Fa	+/-	Fa	+/-	Fa	+/-	Fa	+/-
1470	36.0	4.0	25.5	1.0	51.0	2.0	47.5	2.0	40.9	9.2
	44.5	4.5	----	---	----	---	----	---		
1585	40.0	4.0	57.0	4.0	60.5	1.0	70.0	15	54.1	11.1
	43.0	3.0	----	---	----	---	----	---		
1646	51.5	6.0	32.5	3.5	41.0	5.0	40.0	2.5	41.2	6.8
1677	25.0	5.0	86.0	6.0	33.5	1.0	33.0	1.5	44.3	24.2
1704	22.0	4.0	47.0	4.5	37.5	1.0	----	---	35.5	10.3
1705	32.5	2.0	65.0	3.0	41.0	1.0	----	---	46.1	13.7
1706	28.5	3.0	30.0	2.5	----	---	----	---	29.3	0.8
1712	47.0	2.5	65.0	5.5	43.5	1.5	39.5	4.0	46.8	9.6
	39.0	2.5	----	---	----	---	----	---		
1730	58.0	6.0	72.5	7.0	67.0	5.0	----	---	65.8	6.0
1798	41.5	7.0	51.0	3.0	49.0	8.0	47.5	5.0	47.3	3.6
1824	42.5	5.0	45.5	5.0	26.0	3.0	42.5	5.0	39.1	7.7
1909	49.0	1.5	40.0	3.0	36.0	3.0	43.5	1.0	43.5	5.1
	49.0	1.0	----	---	----	---	----	---		
1949	30.0	1.5	65.0	3.0	----	---	----	---	47.5	17.5
1971	37.5	35	63.0	2.5	48.5	10	46.0	5.0	47.0	11.6
	51.5	1.5	41.0	5.0	26.0	3.0	62.5	2.5		

b) Mount Vesuvius.

Year	Fa	+/-	Fa	+/-	Fa	+/-	Fa	+/-	Fa	+/-
1697	61.5	20	43.0	4.5	40.5	4.5	36.0	5.5	42.9	8.0
	41.0	4.5	42.0	1.5	36.0	3.0	----	---		
1737	65.0	12	43.0	1.5	----	---	----	---	54.0	11.0
1754	48.5	1.5	----	---	----	---	----	---	48.5	1.5
1760	45.0	1.0	46.0	1.0	53.5	5.0	63.0	20	51.9	7.2
1767	40.5	2.0	27.5	1.5	30.5	2.0	41.1	2.5	36.9	5.2
	40.5	1.5	38.0	2.0	40.5	2.0	----	---		
1794	70.0	5.0	39.0	1.5	29.5	3.0	31.7	2.5	42.6	16.2
1804	37.5	1.5	23.0	1.0	26.7	3.0	29.5	3.0	29.1	5.3
1822	49.0	1.5	42.5	5.0	40.5	3.0	42.3	1.5	42.6	3.4
	39.0	4.0	----	---	----	---	----	---		
1834	32.0	5.0	32.0	5.5	46.5	7.0	37.0	6.5	37.7	5.6
	41.0	4.5	----	---	----	---	----	---		
1847	38.5	3.0	25.0	5.0	31.0	1.5	28.3	1.5	32.0	5.2
	37.5	4.0	----	---	----	---	----	---		
1850	44.5	5.0	42.0	3.0	44.5	9.0	----	---	43.6	1.2
1858	60.0	2.0	----	---	----	---	----	---	60.0	20.0
1867	76.5	4.0	51.0	1.5	48.5	0.5	33.8	2.0	51.9	13.7
	50.0	2.5	----	---	----	---	----	---		
1871	40.3	3.0	37.0	4.0	53.0	5.0	39.0	2.0	42.3	6.3
1872	30.0	5.0	23.8	6.0	36.0	2.0	----	---	29.9	4.9
1886	46.5	1.5	32.2	3.0	45.0	12	----	---	41.2	6.4
1891	47.0	1.0	36.5	5.0	----	---	----	---	41.8	5.3
1895	29.5	2.0	47.9	2.5	48.5	5.0	54.0	16	45.7	8.4
	41.0	4.5	53.5	1.5	----	---	----	---		
1906	46.5	1.5	53.0	5.3	55.0	6.0	37.5	7.0	45.0	6.7
	39.5	5.0	39.0	4.0	38.9	3.5	51.0	2.0		
1929	48.5	2.5	43.0	5.5	39.0	4.0	46.5	6.0	41.6	6.2
	31.0	1.5	----	---	----	----	----	----		
1944	51.5	1.5	53.0	8.0	35.0	2.00	51.0	1.00	47.6	7.3

Figure 13.7 Intensity variation for the Canary Islands found using the Boyd technique.
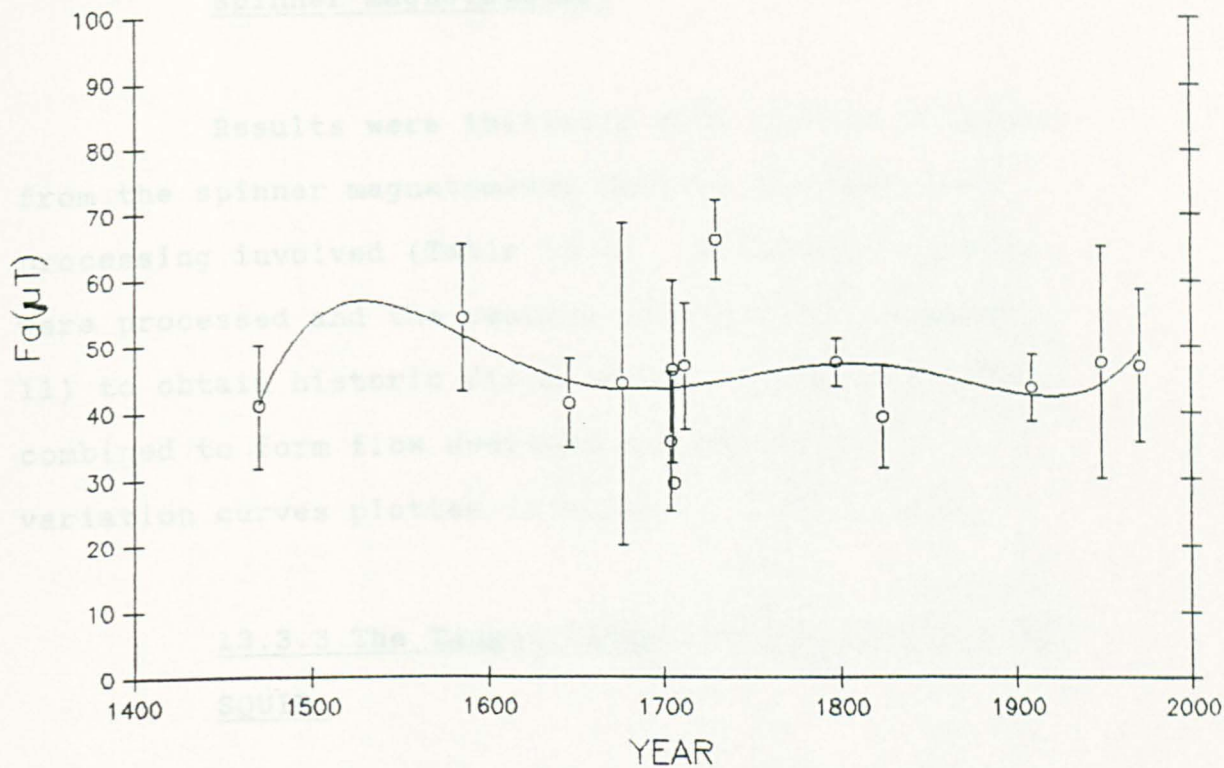
Figure 13.8 Intensity variation for Mount Vesuvius found using the Boyd technique.
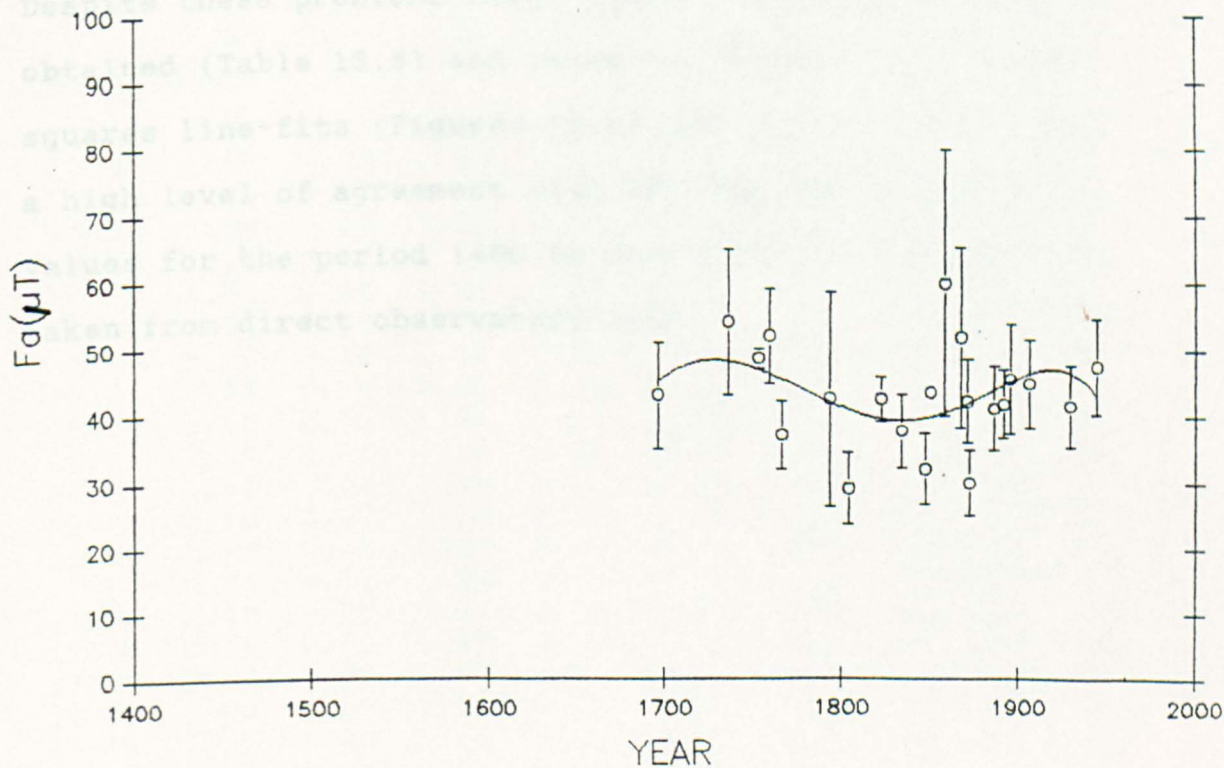
13.3.2 The Tanguy technique results from the spinner magnetometer.

Results were initially more readily obtained from the spinner magnetometer despite the laborious processing involved (Table 13.4). Batches of samples were processed and the results extrapolated (Chapter 11) to obtain historic field values. These were then combined to form flow averages and the secular variation curves plotted (Figures 13.9 and 13.10).

13.3.3 The Tanguy technique results from the SQUID.

Results from the SQUID were subject to error due to the problems of that system (Chapter 8). Despite these problems large numbers of results were obtained (Table 13.5) and these are plotted with least squares line-fits (Figures 13.11 and 13.12). They show a high level of agreement with the expected range of values for the period 1400 to 2000 A.D. (40 - 50μT) taken from direct observatory data.

Table 13.4 Spinner Tanguy results.

Year	TRM/NRM	+/-	TRM/NRM	+/-	TRM/NRM	+/-	Fa (µT)	+/-
1971/1	1.36	0.07	1.68	0.08	1.22	0.17	37.87	6.50
	1.61	0.15	1.03	0.06	----	----	-----	----
1971/2	0.98	0.09	1.33	0.10	----	----	43.29	7.80
1949	0.86	0.14	0.79	0.03	1.18	0.23	46.90	12.6
	1.34	0.14	1.21	0.03	----	----	-----	----
1909	1.35	0.21	0.95	0.02	1.21	0.24	42.73	7.05
1824	1.15	0.14	0.79	0.03	0.96	0.01	51.72	9.28
1798	0.78	0.02	0.61	0.28	0.64	0.42	75.87	9.17
	0.60	0.51	----	----	----	----	-----	----
1730	1.40	0.13	1.33	0.01	----	----	36.63	1.00
1712	0.85	0.62	1.29	0.17	1.09	0.07	37.00	11.5
	1.42	0.34	1.78	0.13	----	----	-----	----
1706	1.19	0.62	1.05	0.24	1.19	0.27	43.73	2.68
1705	1.67	0.17	0.78	0.07	1.78	0.27	35.21	22.27
	2.11	0.23	0.76	0.06	----	----	-----	----
1704	1.68	0.52	1.15	0.30	0.93	0.25	41.19	12.4
	1.09	0.13	----	----	----	----	-----	----
1677	1.41	0.08	1.25	0.10	1.40	0.06	39.40	4.10
	1.15	0.04	1.13	0.04	----	----	-----	----
1646	1.16	0.18	1.91	0.08	1.42	0.18	33.40	7.05
	1.65	0.02	1.34	0.03	----	----	-----	----
1585/1	1.15	0.27	1.29	0.27	1.70	0.14	40.50	11.6
	1.86	0.22	1.16	0.30	----	----	-----	----
1585/2	1.42	0.04	1.35	0.10	1.34	0.09	36.33	0.90
	1.39	0.07	----	----	----	----	-----	----
1470TN	0.62	0.15	0.68	0.16	0.66	0.05	77.6	3.27
	0.65	0.04	0.61	0.05	----	----	-----	----
1470LP	0.99	0.16	1.67	0.17	0.87	0.04	40.00	15.67
	1.69	0.14	1.04	0.27	----	----	-----	----

b) Vesuvius

Year	TRM/NRM	+/-	TRM/NRM	+/-	TRM/NRM	+/-	Fa (µT)	+/-
1944	1.31	0.01	1.23	0.04	1.41	0.06	37.97	2.25
1929	1.10	0.02	1.04	0.04	1.43	0.01	42.00	7.00
1906	1.29	0.08	1.37	0.05	1.26	0.06	38.00	1.43
1895	1.28	0.25	1.08	0.08	1.10	0.10	43.25	3.50
1891	1.15	0.02	1.16	0.06	----	----	43.29	0.00
1886	1.72	0.44	1.39	0.27	1.20	0.21	34.80	6.12
1871	1.39	0.04	1.24	0.02	1.25	0.01	38.65	2.17
1867	1.70	0.14	1.16	0.14	0.96	0.21	39.30	12.7
1858	0.97	0.14	2.02	0.04	----	----	31.50	20.0
1850	1.16	0.13	1.32	0.14	1.15	0.01	41.32	2.84
1847	1.05	0.03	1.15	0.03	1.07	0.06	45.87	1.90
1834	0.91	0.06	1.09	0.15	0.96	0.07	50.64	4.27
1822	1.14	0.22	1.00	0.03	1.27	0.02	43.82	4.63
1804	1.19	0.05	0.95	0.02	----	----	46.72	5.90
1794	0.88	0.02	1.34	0.05	1.04	0.02	46.05	9.80
1767	1.36	0.04	1.17	0.06	1.35	0.03	38.70	2.75
1760	0.95	0.08	1.54	0.02	1.21	0.04	50.00	9.10
1754	0.85	0.06	0.89	0.01	1.69	0.02	43.74	22.65
1737	1.00	0.00	1.47	0.02	----	----	40.40	10.0
1697	0.91	0.06	1.41	0.14	1.00	0.03	45.47	9.40
	1.12	0.03	----	----	----	----	-----	----

Figure 13.9 Intensity variation for the Canary Islands using the Tanguy technique on the spinner.
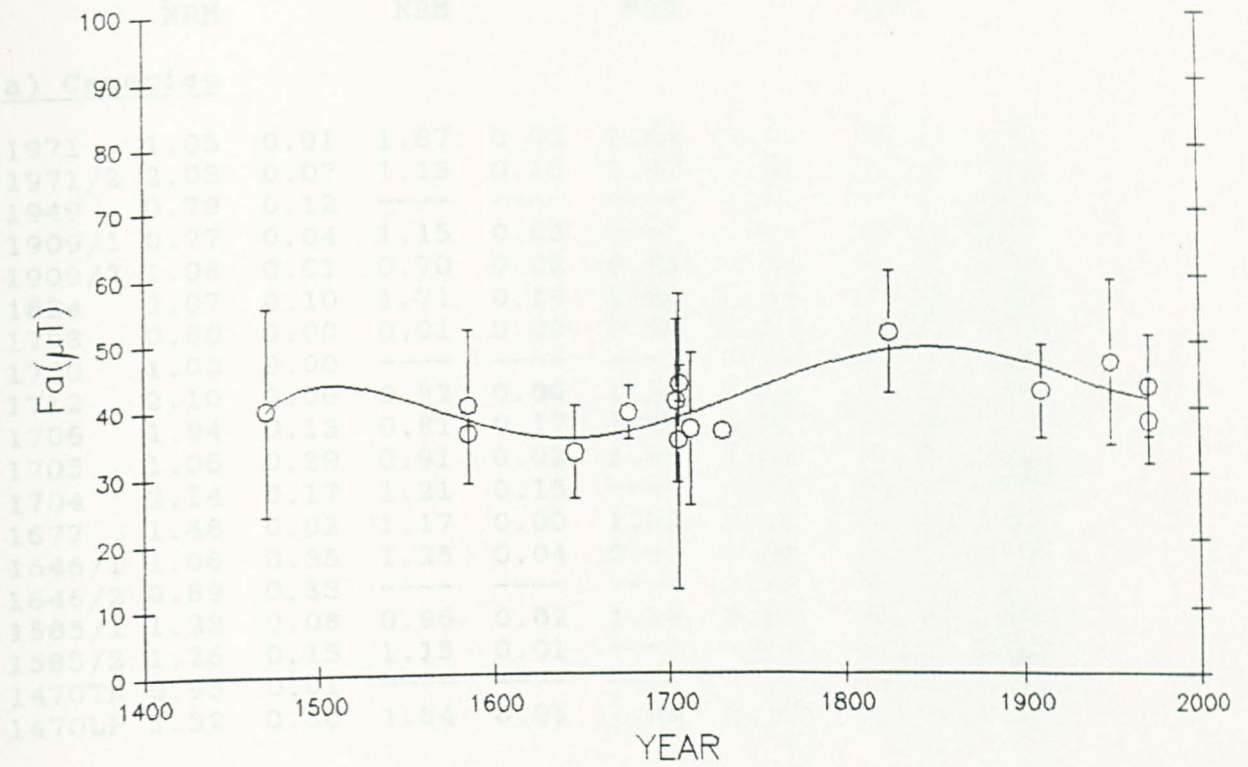

Figure 13.10 Intensity variation for Mount Vesuvius using the Tanguy technique on the spinner.
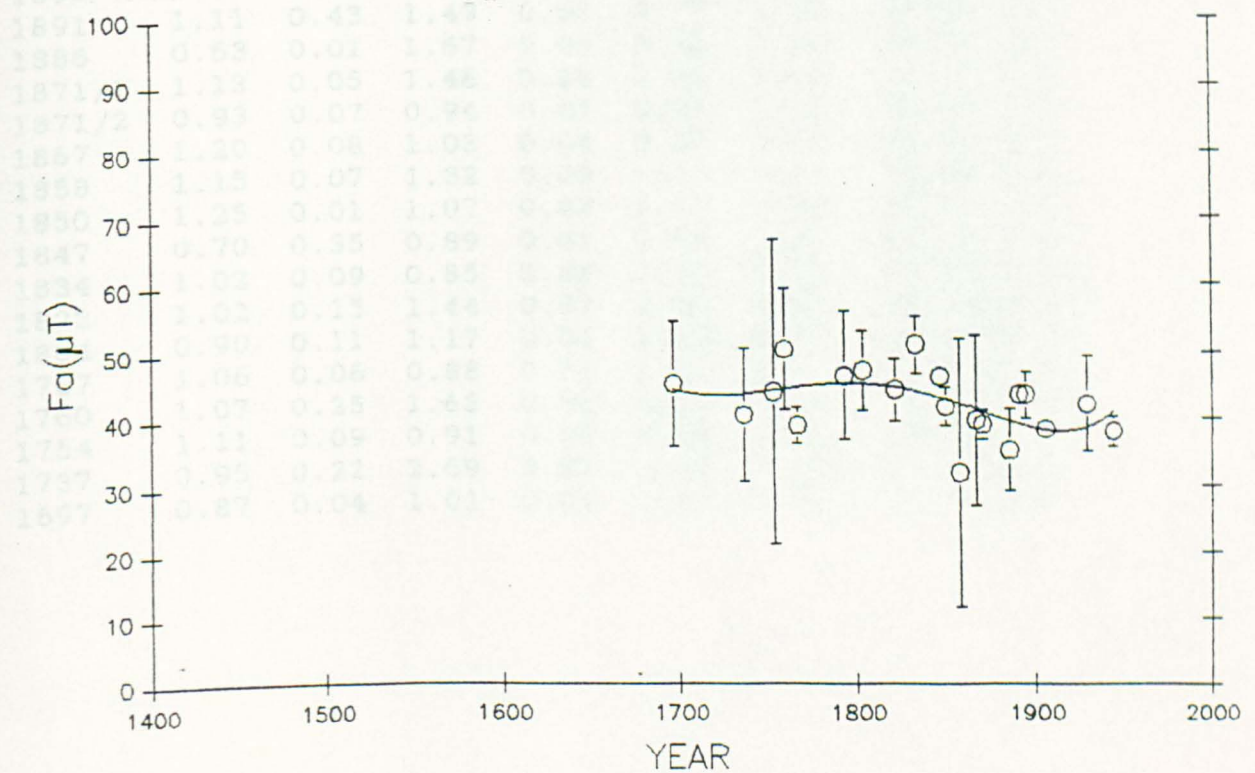
Table 13.5 SQUID Tanguy results.

Year	TRM/NRM	+/-	TRM/NRM	+/-	TRM/NRM	+/-	Fa (μT)	+/-

a) Canaries

Year	TRM/NRM	+/-	TRM/NRM	+/-	TRM/NRM	+/-	Fa (μT)	+/-
1971	1.05	0.01	1.87	0.03	1.64	0.00	32.90	7.35
1971/2	2.03	0.07	1.13	0.15	1.43	0.00	32.60	7.50
1949	0.79	0.12	----	----	----	----	63.30	10.0
1909/1	0.77	0.04	1.15	0.03	----	----	52.00	10.0
1909/2	1.08	0.01	0.70	0.02	0.89	0.01	56.10	9.50
1824	2.07	0.10	1.71	0.14	1.90	0.19	26.50	2.00
1798	0.80	0.00	0.91	0.00	0.62	0.01	64.90	9.50
1730	1.00	0.00	----	----	----	----	50.00	1.00
1712	2.10	0.06	0.82	0.00	1.16	0.02	36.80	14.5
1706	1.94	0.13	0.81	0.17	1.00	0.00	40.00	16.0
1705	1.06	0.29	0.91	0.02	1.61	0.26	41.60	10.0
1704	2.14	0.17	1.21	0.15	----	----	29.70	8.20
1677	1.48	0.02	1.17	0.00	1.53	0.04	36.20	4.00
1646/1	1.06	0.35	1.25	0.04	0.97	0.03	45.50	5.00
1646/2	0.89	0.33	----	----	----	----	56.00	20.7
1585/1	1.23	0.08	0.96	0.02	1.13	0.01	45.50	5.00
1585/2	1.26	0.15	1.15	0.01	----	----	41.60	2.00
1470TN	0.95	0.01	----	----	----	----	52.60	1.00
1470LP	1.32	0.30	1.84	0.01	1.34	0.01	33.30	6.00

b) Vesuvius.

Year	TRM/NRM	+/-	TRM/NRM	+/-	TRM/NRM	+/-	Fa (μT)	+/-
1944	0.93	0.02	0.86	0.01	1.04	0.05	53.20	4.0
1929	1.18	0.03	1.07	0.10	0.90	0.07	47.60	5.0
1906	0.88	0.04	1.02	0.13	0.91	0.00	53.70	4.0
1895	0.89	0.04	0.98	0.03	0.96	0.17	53.10	3.0
1891	1.11	0.43	1.49	0.05	0.77	0.02	44.60	13
1886	0.63	0.01	1.67	0.05	0.92	0.04	46.70	18
1871/1	1.13	0.05	1.46	0.24	1.25	0.01	39.00	4.0
1871/2	0.93	0.07	0.94	0.02	0.94	0.13	53.20	1.0
1867	1.20	0.08	1.03	0.04	0.83	0.04	49.00	8.0
1858	1.15	0.07	1.32	0.09	----	----	40.40	4.0
1850	1.25	0.01	1.07	0.03	1.17	1.31	43.00	4.0
1847	0.70	0.35	0.89	0.01	0.78	0.01	63.00	7.0
1834	1.02	0.09	0.85	0.03	1.01	0.05	52.00	5.0
1822	1.02	0.15	1.44	0.07	1.12	0.05	42.00	5.0
1804	0.90	0.11	1.17	0.08	1.29	0.10	44.60	5.0
1767	1.06	0.06	0.88	0.01	1.01	0.07	51.00	5.0
1760	1.07	0.25	1.63	0.30	0.80	0.04	43.10	12.5
1754	1.11	0.09	0.91	0.06	0.86	0.02	52.00	6.0
1737	0.95	0.22	2.69	0.87	1.00	0.02	51.30	2.0
1697	0.87	0.04	1.01	0.01	0.87	0.06	54.30	4.0

Figure 13.11 Intensity variation for the Canary
Islands using the Tanguy technique on the SQUID.
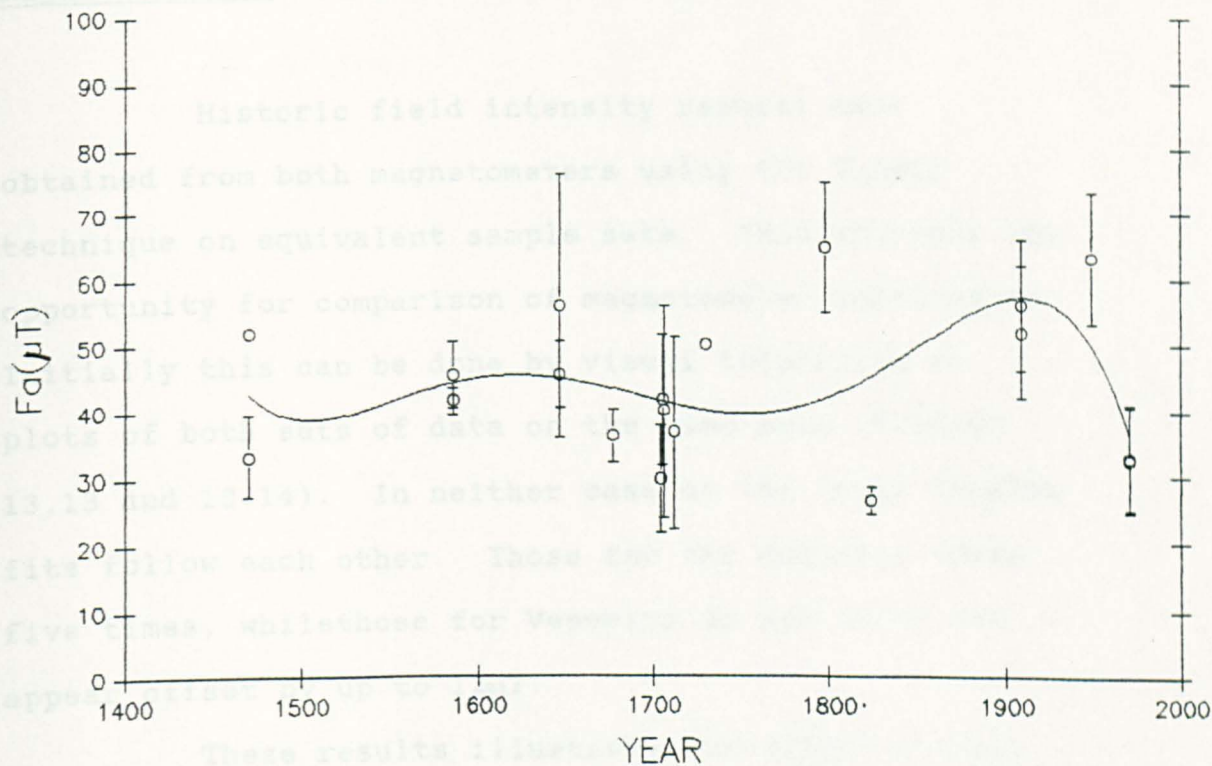
Figure 13.12 Intensity variation for Mount Vesuvius
using the Tanguy technique on the SQUID.
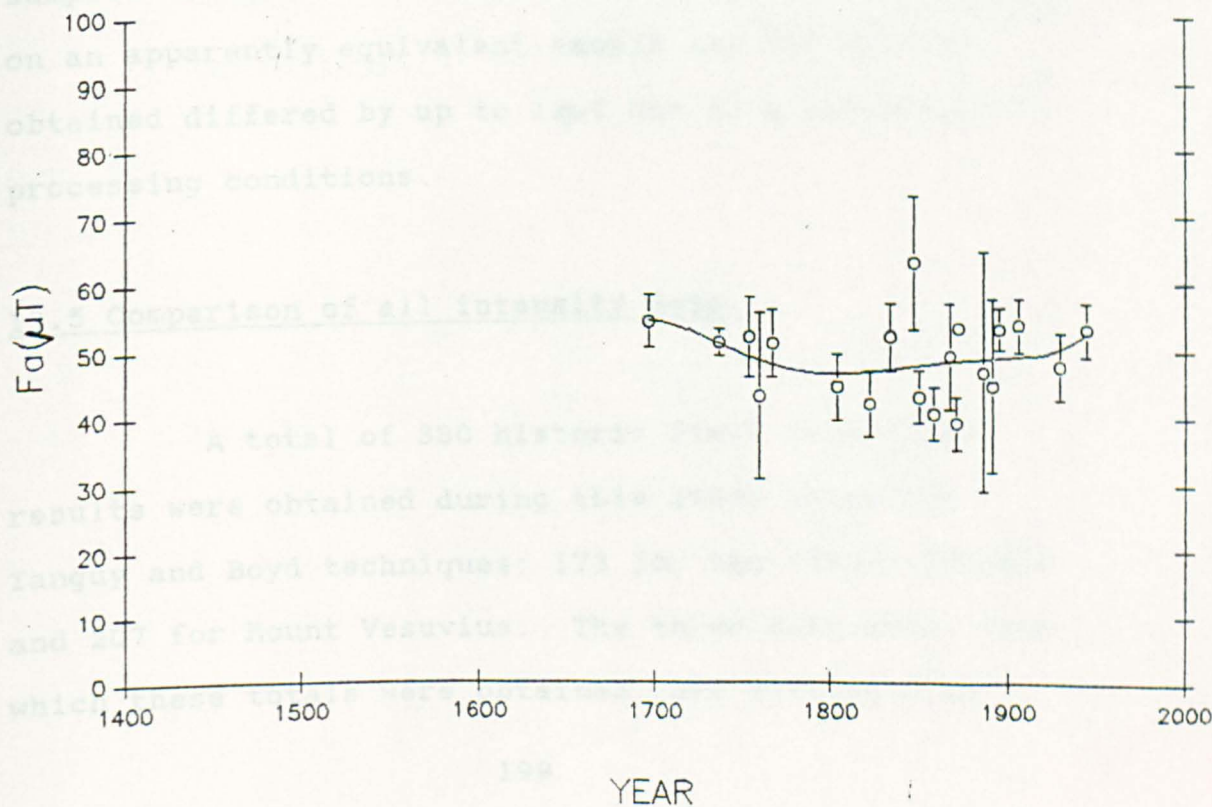
13.4 Comparison of results from SQUID and spinner magnetometers.

Historic field intensity results were obtained from both magnetometers using the Tanguy technique on equivalent sample sets. This provides the opportunity for comparison of magnetometer performance. Initially this can be done by visual inspection of plots of both sets of data on the same axes (Figures 13.13 and 13.14). In neither case do the least squares fits follow each other. Those for the Canaries cross five times, whilethose for Vesuvius do not cross but appear offset by up to 12μT.

These results illustrate the effect of the conditions, cooling rate for example, present during the stages of a technique and on the reaction of samples to them. Thus despite using the same technique on an apparently equivalent sample set the results obtained differed by up to 12μT due to a variation in processing conditions.

13.5 Comparison of all intensity data.

A total of 380 historic field intensity results were obtained during this study using the Tanguy and Boyd techniques; 173 for the Canary Islands and 207 for Mount Vesuvius. The three data sets, from which these totals were obtained, are plotted with

Figure 13.13   Comparison of Tanguy results for the
Canaries, obtained from the spinner (squares with
dashed line) and SQUID magnetometers (circles with
solid line).
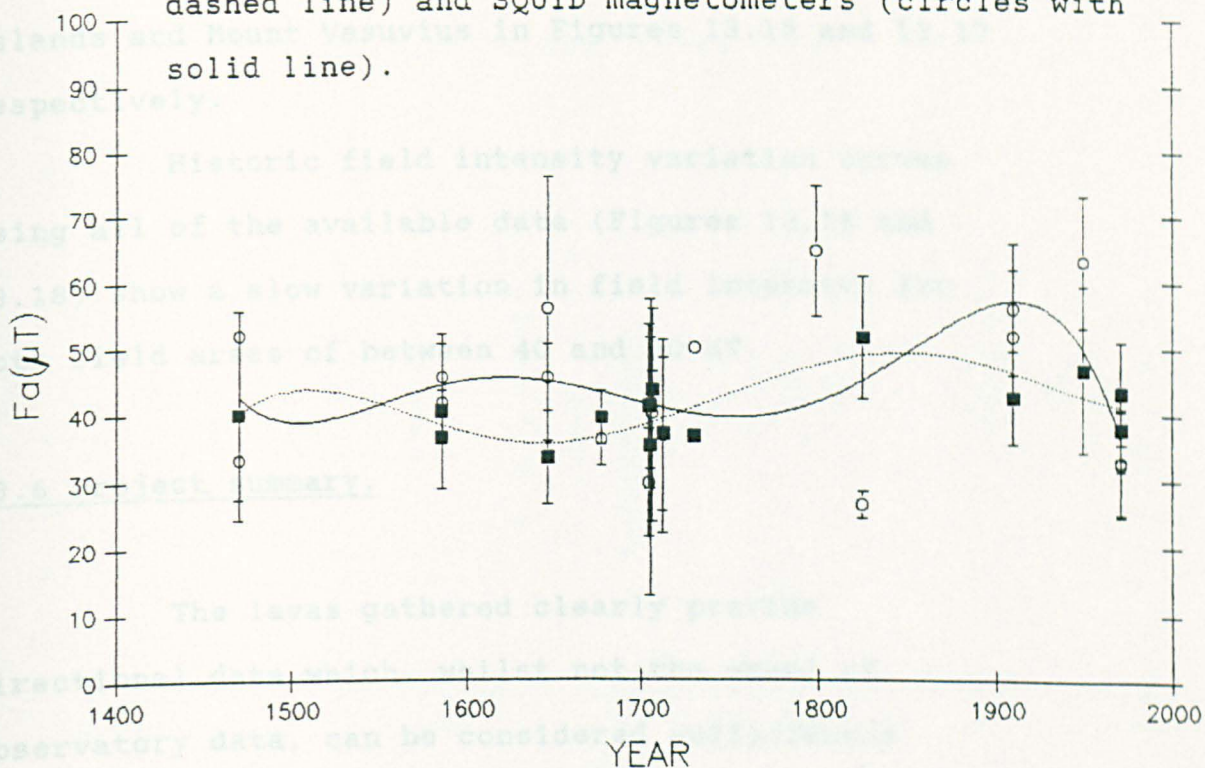
Figure 13.14   Comparison of Tanguy results for
Vesuvius, obtained from the spinner (squares with
dashed line) and SQUID magnetometers (circles with
solid line).
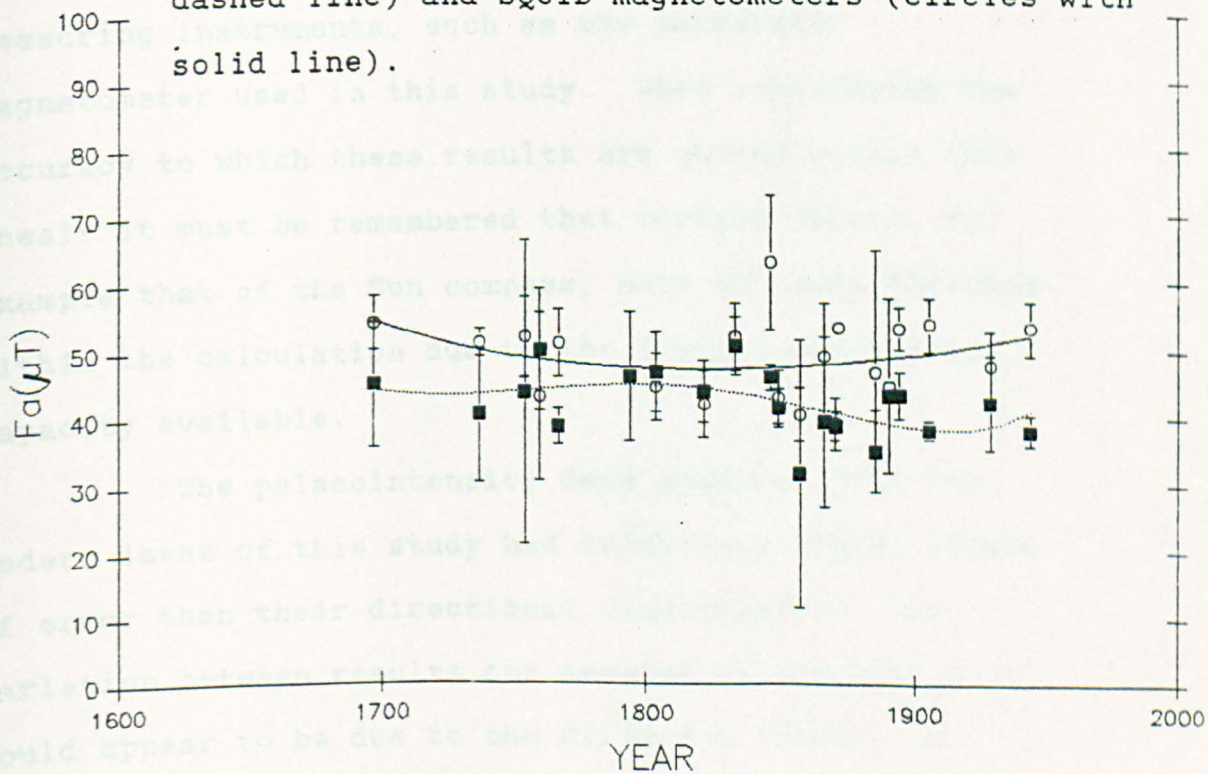
their respective least squares fits for the Canary
Islands and Mount Vesuvius in Figures 13.15 and 13.17
respectively.

Historic field intensity variation curves
using all of the available data (Figures 13.16 and
13.18) show a slow variation in field intensity for
both field areas of between 40 and 50 uT.

13.6 Project summary.

The lavas gathered clearly provide
directional data which, whilst not the equal of
observatory data, can be considered sufficiently
accurate to warrant its use in the extension of palaeo-
direction studies prior to direct measurement. Such
data can be acquired using inexpensive and simple
measuring instruments, such as the parastatic
magnetometer used in this study. When considering the
accuracy to which these results are quoted within this
thesis it must be remembered that certain errors, for
example that of the Sun compass, have not been included
within the calculation due to the limited processing
capacity available.

The palaeointensity data acquired from the
modern lavas of this study had relatively higher levels
of error than their directional counterparts. The
variation between results for samples of the same flow
would appear to be due to the different conditions

Figure 13.15 Comparison of all intensity results for the Canaries, Tanguy on the spinner squares with dashed line, Tanguy on the SQUID circles with solid line and Boyd shown by diamond and dotted line.

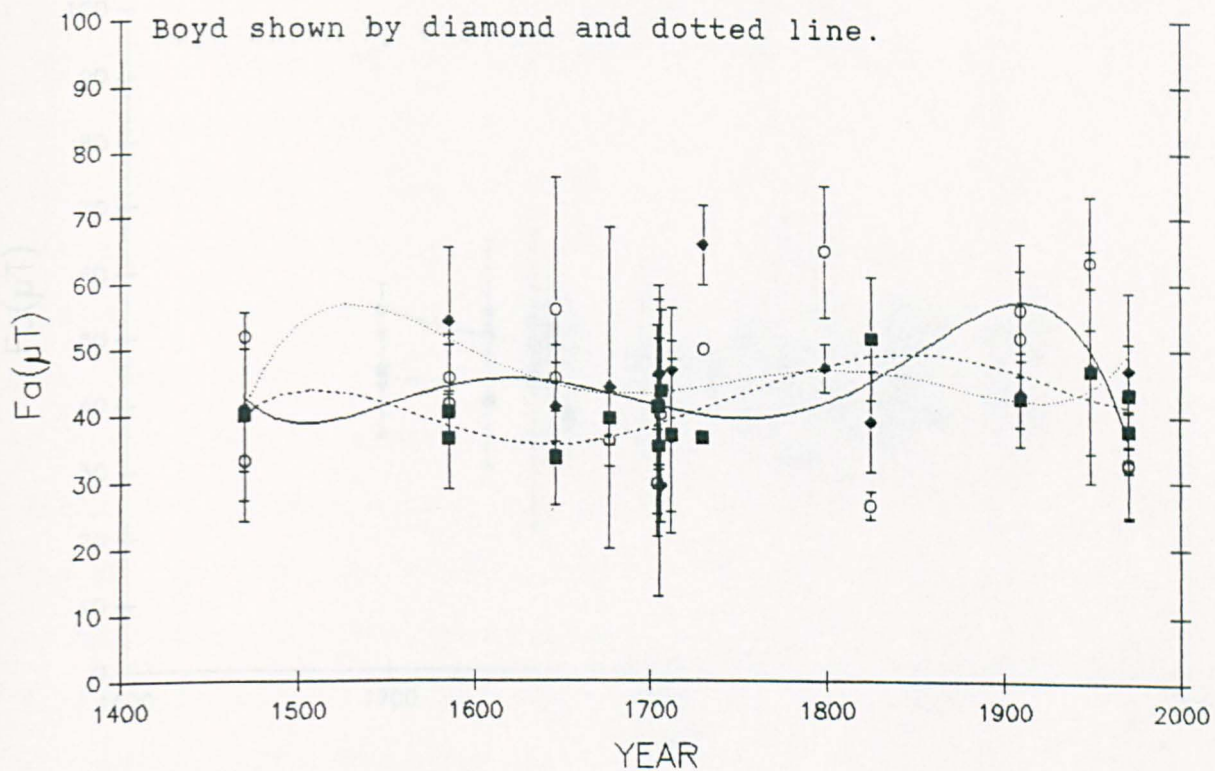Figure 13.16 Least squares fit for all Canary Island intensity data.

202
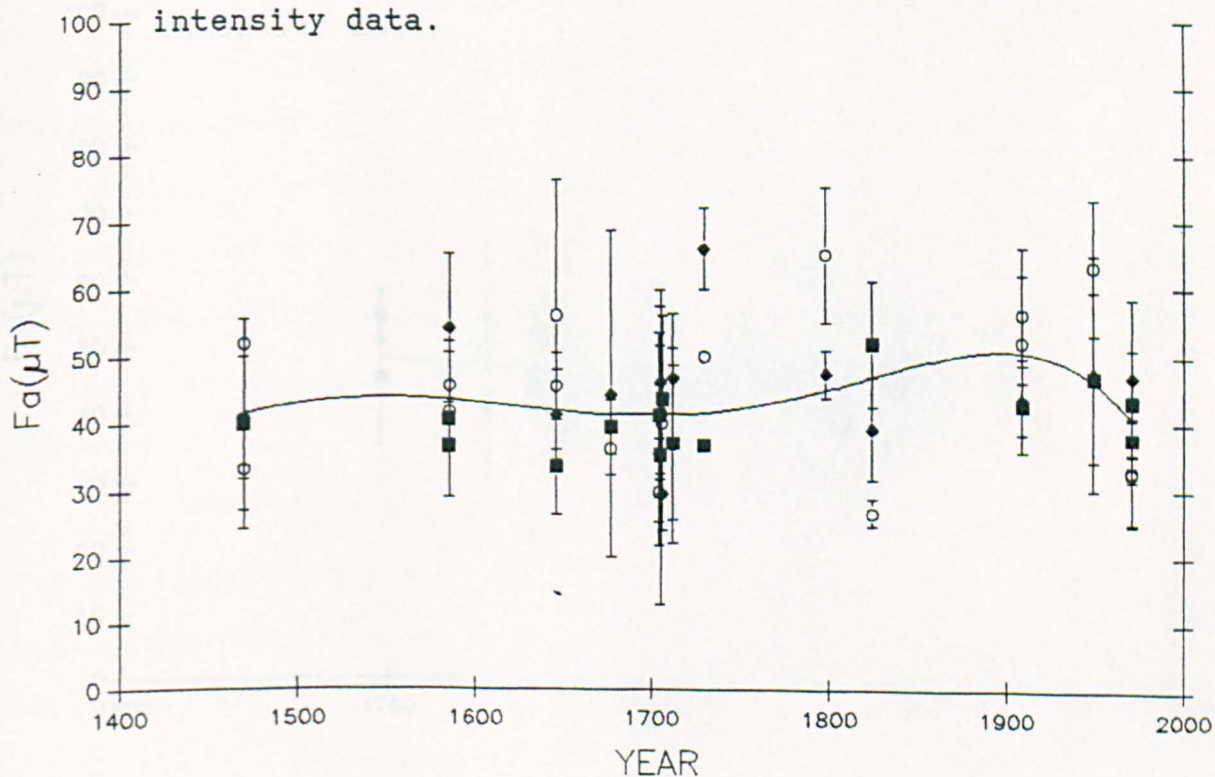
Figure 13.17 Comparison of all intensity results for Vesuvius, Tanguy on the spinner squares with dashed line, Tanguy on the SQUID circles with solid line and Boyd shown by diamond and dotted line.
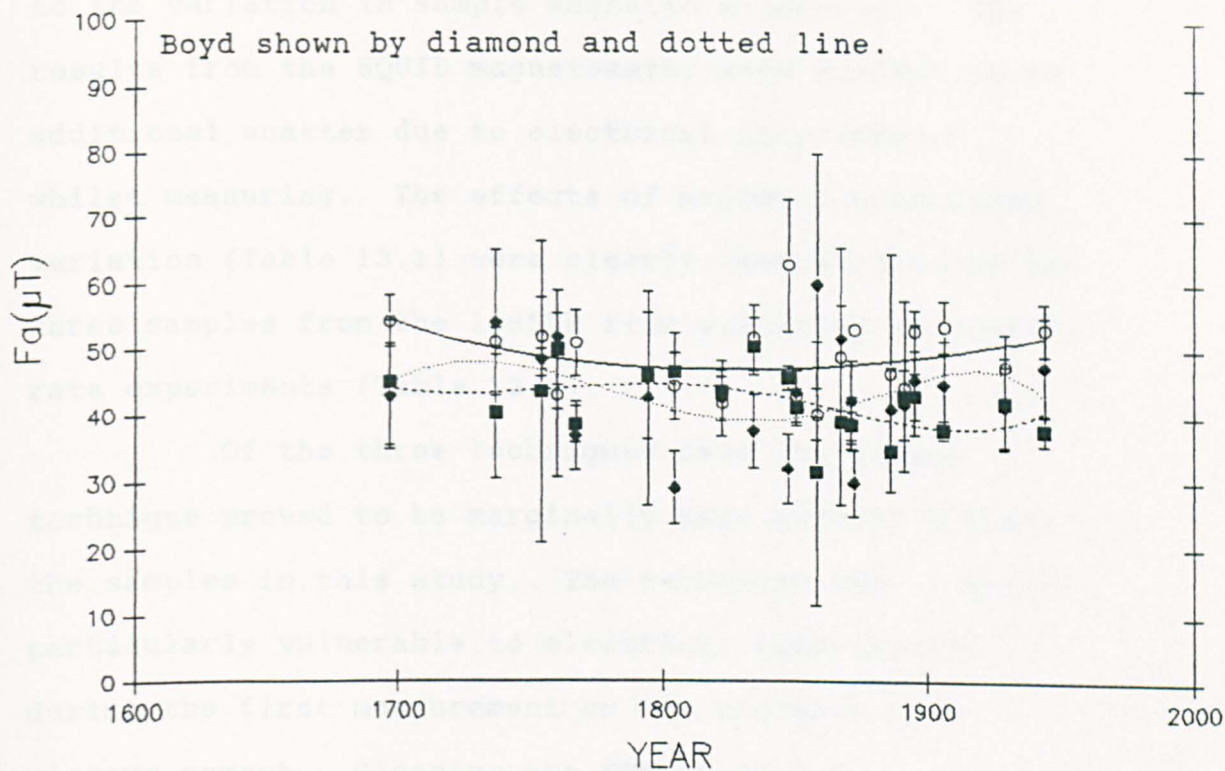
Figure 13.18 Least squares fit for all Vesuvian intensity data.
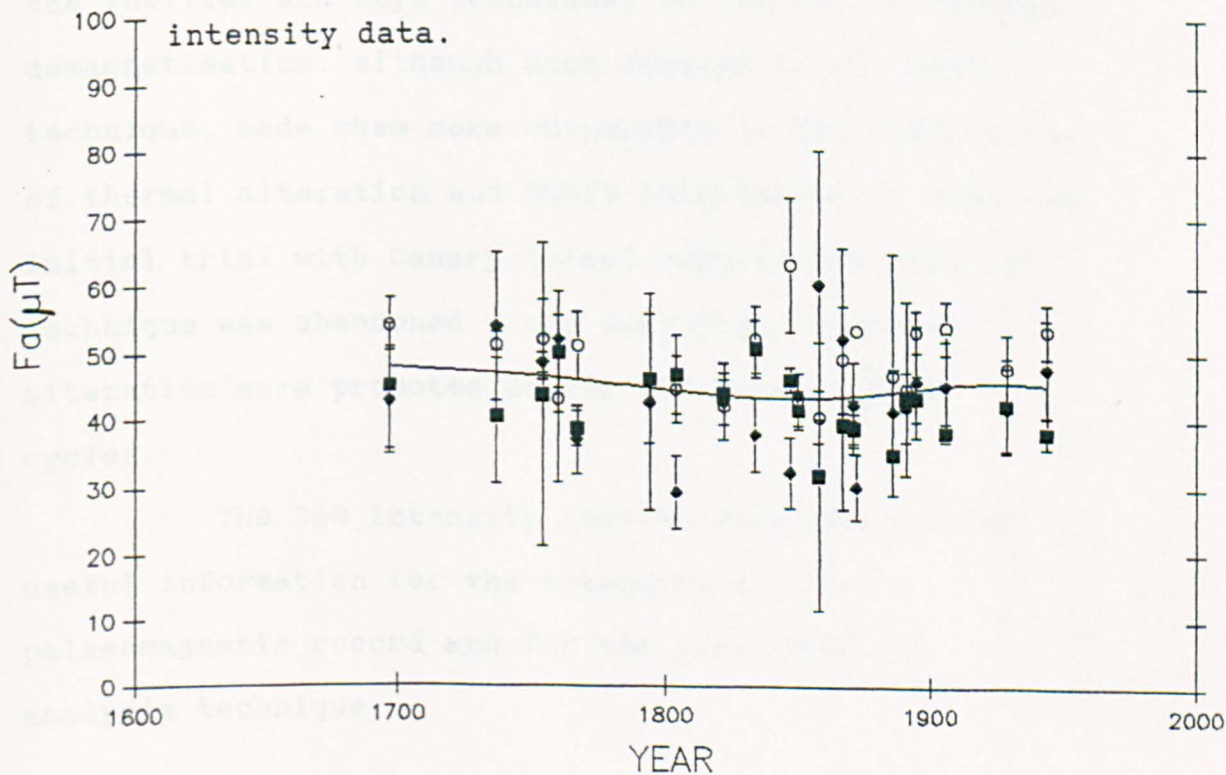
prevalent during processing for that technique and due to the variation in sample magnetic mineralogy. The results from the SQUID magnetometer were subject to an additional scatter due to electrical interference whilst measuring. The effects of magnetic mineralogy variation (Table 13.1) were clearly demonstrated by the three samples from the 1585LP flow subjected to cooling rate experiments (Table 12.1).

Of the three techniques used the Tanguy technique proved to be marginally more appropriate for the samples in this study. The technique was, however, particularly vulnerable to electrical interference during the first measurement or the presence of a viscous moment. Cleaning the NRM using A.F. demagnetisation proved to be of no value since few viscous moments were present. The dependence of both the Thellier and Boyd techniques on controlled thermal demagnetisation, although much reduced in the Boyd technique, made them more vulnerable to the combination of thermal alteration and SQUID interference. After an initial trial with Canary Island samples the Thellier technique was abandoned since very high levels of alteration were promoted during its long heating cycles.

The 380 intensity results obtained provide useful information for the extension of the palaeomagnetic record and for the assessment of analysis technique.

13.7 Suggestions for further work.

The variation within palaeo-intensity results would appear to be due to the differences in sample magnetic mineralogy and NRM acquisition. The different palaeointensity techniques applied may exacerbate these differences leading to an increased sample result diversity. To quantify the relationship between sample mineralogy and reaction to a measurement regime would require considerable work on factors such as cooling rate correction. This would lead to fewer but more valuable results and may justify the introduction of sample pre-selection based on mineralogy studies.

APPENDIX

Acknowledgments.

Programme Details.

Three programmes were written for the SQUID
magnetometer, two to determine the historic field
intensity using the Boyd (BOYD222) and Tanguy (TAN103)
techniques, the third to determine the importance of
the cooling rate to sample magnetisation (FOX223).
These programmes were based on the "Base" programme
(Share, 1987) and written in Basic with alphanumeric
control sequences for dedicated SQUID control unit.

A full programme listing is only included
for the FOX223 programme since the base programme is
common to all three. Although based on Share (1987)
changes, both major and minor, have been made to the
original programme in addition to the operational
package.

Precise programme details depended on the
particular requirements of the experiment, however, the
majority of the programming involved the rearrangement
of the operational segments known as procedures or
PROC's. Brief descriptions of these procedures are
given below.

PROCexchange - sends commands to the dedicated
                 controller.
PROCoper   - contains the experiment specific
               operations sequence.

PROCINPUT   — in conjunction with PROCheaders acquires
                and writes the sample data to the disc.

PROCzero   — before measurement commences values are
                acquired from the SQUID to compensate
                for electric motor interference.

PROCsquid   — SQUID interface values are read and
                converted to give a magnetic flux
                reading for the SQUID.

PROCmeloop   — when included allows for multiple
                measurement loops.

PROCmeasure — arranges the squid readings to obtain
                the four directional measurements of
                flux and the background reading.

PROCCALC   — determines the true values of
                declination, inclination and intensity
                using the input values.

PROCWRITE   — writes information back to disc.

PROCfieldinst— used with PROCfieldset to calculate the
                relative values of the current required
                to apply a magnetic field to the sample
                in the same direction as that measured.

PROCtempset — sets the temperature.

PROCdelay   — a delay sequence, used with PROCfdelay
                to provide a delay when a magnetic field
                is applied to the samples.

PROClastmeas — resets the SQUID for the next sample.

```
20 *FX8,3
30 *FX7,3
40 *FX5,1
50 DIM A$(11), A(8), V(10), E(7), M(6), Z(6), M1(10),
M2(10), M3(10), M4(10), C(50), D(50), P(4), F(3),
TB(10), VG(6), EG(6)
60 A$(1)_="X1": A$(2)="X ": A$(3)="Y1": A$(4)="Y ":
A$(5)="Z1": A$(6)="Z ": A$(7)="C1": A$(8)="C ":
A$(9)="NS": A$(10)="EW": A$(11)="VE"
70 RESET $=STRING$(8, "TRY AGAIN")
80 PROCINPUT
90 NUMBER=1:N9%=NUMBER
100 PROCoper
110 END
120 DEF PROCINPUT
130 CLS:INPUT "FILENAME",F$
140 CLS:VDU28,1,30,39,18
150 CODE1$="QIT2"
160 DEMAG$="TH"
170 CODE2$=F$
180 DIFF=7-LEN(CODE2$):IF DIFF<1 THEN 220
190 FOR I=1 TO DIFF
200 CODE2$=CODE2$+CHR$(9)
210 NEXT I
220 CODE2$=LEFT$(CODE2$,7)
230 OP$="AMT"240 D$="00/00/90"
250 DIFF=8-LEN(D$):IF DIFF<1 THEN290
260 FOTR I=1 TO DIFF
270 D$=D$+CHR$(9)
280 NEXT I
290 D$=LEFT$(D$,8)
300 A1=0
310 A2=0
320 A3=0:A4=0
330 A5=1
340 FI%=OPENOUT(F$)
350 HE$="*****SQIDO2"+CODE1$+DEMAG$+D$+OP$
360 PROCWRITE(HE$)
370 HE$=CODE1$+CODE2$+","+STR$(A1)+","+STR$(A2)+","+STR
(A3) +","+STR$(A4)+","+STR$(A5)
380 PROCWRITE(HE$)
390 DS1=A1:DS2=A2:DS3=A3:DS4=A4:DS5=A5
400 A1=RAD(A1):S1=SIN(A1):C1=COS(A1):A2=RAD(A2):
S2=SIN(A2): C2=COS(A2)
410 ENDPROC
420 DEF PROCCALC
430 X9=INT((V(1)-V(3))/2):V9=(INT((V(2)-
V(4))/2)):V=V(1)
=V(2)+V(3)+V(4):Z9=INT(V/4)::J=INT(SQR(X9^2+Y9^2+Z9^2))
: :V(6)=X9:V(7)=Y9:V(8)=Z9
440 A1=-X9
450 A2=-Y9
460 A3=-Z9
470 DEC=FNAT2(A2,A1):IFDEC<OTHENDEC=DEC+360
```

```
480 J=INT(J*565/RANGE)
490 INC=FNAT2(A3,SQR(A1*A1+A2*A2))
500 INC=(INT(INC*10))/10:DEC=(DEC*10))/10
510 *FX3,10
520 PRINTTAB (6);AT;TAB(20);J;TAB(35);DEC;TAB(50);INC
530 RES$=STR$(AT):PROCWRITE(RES$)
540 RES$ = STR$(J)+","+STR$(DEC)+",."+STR$(INC);
PROCWRITE(RES$)
550 RES$=STR$(V(0)): FORI%=1 TO 8: RES$=RES$+","+ STR$
(V(I%)):NEXT
560 *FX3,0
570 REM PROCWRITE(RES$)
580 *FX3,0
590 ENDPROC
600 DEF FNAT2(Y,X)
610 IF X=0 THEN X=0.0000001
620 LOCAL Z
630 Z=DEG(ATN(Y/X))
640 IF X<0THEN Z=180+Z
650 =Z
660 DEF PROCDISP(CH%)
670 Y=2*ADVAL(CH%)/65520
680 CH%=CH%+8:VDU
31,15,0:PRINTA$(CH%);:VDU31,18,0:PRINTY
690 ENDPROC
700 DEF PROCEND (E%)
710 IF E%=0 THEN 750
720 FOR I = 1 TO 9:ED$="1001":PROCWRITE(ED$): NEXT I
730 ED$="0,0,0,0"
740 PROCWRITE(ED$)
750 CLOSE.FI%
760 VDU28,0,30,39,3
800 ENDPROC
810 DEF PROCWRITE (A$)
820 LOCAL L,I
830 L=LEN(A$)
840 FOR I = 1 TO L
850 BPUT .FI%,ASC(MID$(A$,I,1))
860 VDU2:*FX3,10
870 VDU:*FX3,0
880 NEXT I
890 BPUT .FI%,13
900 ENDPROC
910 DEF PROC exchange
920 *FX5,2
930 VDU3
940 PRINT A$
950 VDU3
960 *FX2,2
970 INPUT reply
980 *FX2,2
990 *FX5,1
1000 ENDPROC
1010 DEF PROCsquid
1020 FOR VG=1 TO 1
1030 finish=TIME +50:REPEAT:UNTIL TIME>finish
1040 *FX5,2
```

```
1050 VDU3
1060PRINT"RX"
1070 VDU3
1080 *FX2,1
1090 INPUT C:INPUT D
1100 *FX2,2
1110 *FX5,1
1120 IF C>0 THEN PRINT "SPIKE"
1130 IF C>0 THEN LH=1000
1140 V(Y)=(32768*C)+D:E(Y)=TIME
1150 VG(Y)=VG(Y)+V(Y):EG(Y)=EG(Y)+E(Y)
1160 PRINT VG
1170 NEXT VG
1180 V(Y)=(VG(Y)/1):E(Y)/1);VG(Y)=0:EG(Y)=0
1190 ENDPROC
1200 DEF PROCtempset
1210 *FX5,2
1220 VDU2
1230 IFtemp<99 THEN A$="TS "ELSE A$="TS"
1240 PRINT A$;temp
1250 VDU3
1260 *FX2,2
1280 *FX5,1
1300 ENDPROC
1310 DEF PROCfieldset
1320 B$=LEFT$(A$,3):C=VAL(MID$(A$,4)):K$=RIGHT$(B$,2):
D$="+": IF SGN (C)<>1 THEND$="-"
1330 IF B$="OFN" THEN CAL=2
1340 IF B$="OFV" THEN CAL=1.33
1360 A$="FO":PROCexchange
1370 C=ABS(C):D=INT(C*CAL*10):G$="0.000"
1380 IF D>9 THEN G$="0.00"
1390 IF D>99 THEN G$="0.0"
1400 IF D>999 THEN G$="0."
1410 A$=K$+D$+G$+STR$(D):PROCexchange
1420 ENDPROC
1430 DEF PROCmeasure
1435 A$="SO":PROCexchange:A$="SZ":PROCexchange:LH=0:Y=0
:PROCsquid
1440 A$="SM":PROCexchange:LH=0
1460 Y=1:PROCsquid:V(Y)=V(Y)-M(Y)
1470 A$="RN":PROCexchange
1480 Y=2:PROCsquid:V(Y)=V(Y)-M(Y)
1490 A$="RN":PROCexchange:A$="TR"PROCexchange:AT=reply
1500 Y=3:PROCsquid:V(Y)=V(Y)-M(Y)
1510 A$="RN":PROCexchange
1520 Y=4:PROCsquid:V(Y)=V(Y)-M(Y)
1530 A$="RN":PROCexchange:A$="SO":PROCexchange
1540 Y=5:PROCsquid
1550 IF LH>100 THEN GOTO 1435
1560 IF ABS(V(0)-V(5))>32768 THEN GOTO 1435
1610 time=E(5)-E(0):drift=V(5)-V(0):rate=drift/time
1620 V(1)=INT(V(1)+(E(0)-E(1))*rate)-V(0):V(2)=INT(V(2)
+(E(0)-E(2))*rate)-V(0):V(3)=INT(V(3)+(E(3)-
E(0))*rate)-V(0):V(4)=INT(V(4)+(E(4)-E(0))*rate)-
V(0):V(5)=INT(V(5) +(time*rate))-V(0):V(0)=0
1630 ENDPROC
```

```
1640 DEF PROCzero
1650 VDU2
1660 VDU1,27,1,69
1670 VDU2
1680 PRINT"ZERO TEST"
1690 PRINT"V1";TAB(20);"V2";TAB(40);"V3";TAB(60);"V4"
1700 VDU1,27,1,70
1710 VDU3
1720 A$="SO":PROCexchange
1730 FOR zero=1 TO 5
1740 M(1)=0:M(2)=0:M(3)=0:M(4)=0
1750 PROCmeasure
1760 @%=&20309
1770 VDU2
1780 PRINT;V(1);TAB(20);V(2);TAB(40);V(3);TAB(60);V(4)
1790 VDU3
1800 @%=&90A
1810 Z(1)=Z(1)+V(1):Z(2)=Z(2)=V(2):Z(3)=Z(3)+V(3):
Z(4)=Z(4)+V(4)
1820 NEXTzero
1830 M(1)=INT(Z(1)/5):M(2)=INT(Z(2)/5):M(3)=INT(Z(3)/5)
: M(4)=INT(Z(4)/5)
1840 @%=&20309:VDU2
1850 VDU1,27,1,69
1860 PRINT:PRINT;
M(1);TAB(20);M(2);TAB(40);M(3);TAB(60); M(4):PRINT
1870 VDU1,27,1,69
1880 VDU3:@%=&90A
1890 ENDPROC
1900 DEF PROCoper
1910 A$="IR":PROCexchange:A$="IN":PROCexchange:A$="IL"
1920 PROCexchange
1930 A$="IG":PROCexchange:RANGE=reply
1940 IF V%=RANGE THEN 1990
1960 GOTO 1990
1970 ZE=0:A$="SO":PROCexchange:PROCzero;V%=RANGE:
W%=M(1):X%=M(2):Y%=M(3):Z%=M(4)
1980 A$="SL":PROCexchange
1990 M(1)=W%:M(2)=X%:M(3)=Y%:M(4)=Z%
2000 ZE=1
2010 Z$="Y":IF Z$<>"Y" THEN T8=4 ELSE T8=1
2020 INPUT "SAMPLE MOUNTED",Z$
2030 A$="TN":PROCexchange
2040 A$="SM":PROCexchange
2050 INPUT"SAMPLE POSITION ADJUST",Z$
2055 INPUT"TIME IN HOURS TO COOL",TS
2060 TS=TS*360000:FK=1
2070 T1=100:T2=600:T3=100
2071 TS=TS/(T2-T1):FK=1
2080 temp=T1:PRINT"SENT TO T1"T1
2090 Q=1:TA=TIME:TB=0
2100 PROCdelay:PROCmeloop
2101 FK=1
2110 temp=T2:PRINT"SENT TO T2"T2:SA=2:PRINT"TIME TS"TS
2120 Q=1:TA=TIME:TB=0
2130 PROCfdelay:A$="FCVNE":PROCexchange
2150 Q=0:TA=TIME:TC=0:IF FK=2 THEN 2290
```

```
2152 TG=TIME:PAUSE=TG+TS:REPEAT
2156 UNTIL TIME>PAUSE
2260 PROCdelay
2280 PROCmeloop:PRINT"TIME ELAPSED"((TC-TA)/6000):
FK=2:GOTO2110
2290 temp=T1:A$="AC":PROCexchange:A$="AN":PROCexchange
2295 PROCdelay:PROCmeloop:PRINT"TIME ELAPSED"((TC-
TA)/6000):TS=TS*3.5:IF TS*(T2-T1)>6E6 THEN 2300 ELSE
2101
2300 PROClastmeas
2340 PROCEND(1)
2350 A$="TF":PROCexchange:A$="SL":PROCexchange:ENDPROC
2360 DEFPROCheaders
2370 *FX3,10
2380 A1=DS1:A2=DS2:A3=DS3:A4=DS4:A5=DS5
2390 PRINT"SAMPLE    ";CODE1$+CODE2$
2400 GOTO 2440
2410 PRINT" SAMPLE       ";CODE$
2420 OP$=MID$(OP$,18,20):PRINT:PRINT"OPERATOR/DATE=
";OP$
2440 PRINT "FIELD/TEMP";TAB(20);"MOMENT";TAB(31);
"DECLINATION" ; TAB(46);"INCLINATION"
2450 *FX3,0
2460 ENDPROC
2470 DEFPROCdelay
2480 TE=150:IF temp>450 THEN TE=175:IF temp>550 THEN
TE=200: IF SA=1 THEN TE=300
2490 IF Q=0 THEN 2530
2500 A$="SO":PROCexchange
2510 PROCtempset:A$="TR":REPEAT:PROCexchange:PAUSE=TIME
+ 5 :REPEAT:UNTIL TIME>=PAUSE:UNTIL REPLY>=temp
2520 IF Q=1 THEN 2570
2530 A$="TF";PROCexchange;PRINT"TH OPS OFF":A$="SM":
PROCexchange
2540 A$="TR":REPEAT:PROCexchange:PAUSE=TIME+5 :
REPEAT:UNTIL TIME>=PAUSE:UNTIL REPLY<=temp
2550 A$="TN";PROCexchange;PRINT"TH OPS ON":A$="AP":
PROCexchange:A$="AO":PROCexchange:A$="FD":PROCexchange:
PROCtempset
2570 TC=TIME:A$="SO":PROCexchange:equilib=TIME+(90*TE):
REPEAT:PRINT "PAUSE"(equilib-time):UNTIL TIME >=equilib
2580 ENDPROC
2590 DEFPROCmeloop
2600 PROCmeasure:PROCCALC
2610 ENDPROC
2620 DEFPROCfieldinst
2630 Q1=0.71*((X9+Z9))
2640 Q2=0.71*(X9-Z9)
2650 Q3=-Y9
2660 P1=(SQR(Q1^2+Q2^2+Q3^2))
2670 P2=((Q1/P1)*(50))
2680 P3=((Q2/P1)*(50))
2690 P4=((Q3/P1)*(50))
2700 P1=(INT(P1*100)/100):P2(INT(P2*100)/100):
P3=(INT(P3*100)/100):P4=(INT(P4*100)/100)
2710 VDU2:*FX3,10
2720 PRINT"*****************************************"
```

```
2740 VDU3:*FX3,0
2750 IF P2<0 THEN 2770
2760 A$="OFV+"+STR$(P2):PROCfieldset:GOTO 2780
2770 A$="OFV"+STR$(P2):PROCfieldset
2780 IF P3<0 THEN 2800
2790 A$="OFN+"+STR$(P3):PROCfieldset
2800 A$="OFN"+STR$(P3):PROCfieldset
2810 IF P4<0 THEN 2830
2820 A$="OFE+"+STR$(P4):PROCfieldset
2830 A$="OFE+"+STR$(P4):PROCfieldset
2840 A$="FCVNE":PROCexchange
2850 ENDPROC
2860 DEFPROClastmeas
2870 PROCfieldinst
2880 temp=50:TA=TIME:TB=0:Q=0
2890 A$="AC":PROCexchange
2900 A$="TF":PROCexchange:A$="TR":REPEAT:PROCexchange:
pause=TIME+5:REPEAT:UNTIL TIME>=pause:UNTIL reply<=temp
2910 A$="AP":PROCexchange
2920 A$="FD":PROCexchange
2925 PROCmeloop
2927 A$="SL":PROCexchange
2930 ENDPROC
2940 DEFPROCfdelay
2950 A$="SO":PROCexchange:temp=temp+2
2960 PROCtempset:A$="TR":REPEAT:UNTIL TIME>=pause:UNTIL
reply>= temp
2970 TE=150 :IF temp>450 THEN TE 175:IF temp>550 THEN
TE=200
2979 A$="SM":PROCexchange:PROCfieldinst
2980 equilib=TIME+(40*TE):REPEAT:PRINT
"PAUSE(equilib - TIME):UNTIL TIME>=equilib
3010 ENDPROC
```

```
1900 DEFPROCoper
1910 A$="IR":PROCexchange:A$="IN":PROCexchange:A$="IL"
1920 PROCexchange
1930 A$="IG":PROCexchange:RANGE=reply
1940 IF V%=RANGE THEN 1990
1960 GOTO 1990
1970
ZE=0:A$="SO":PROCexchange:PROCzero:V%=RANGE:W%=M(1):
X%=M(2):Y%=M(3):Z%=M(4)
1980 A$="SL":PROCexchange
1990 M(1)=W%:M(2)=X%:M(3)=Y%:M(4)=Z%
2000 ZE=1
2010 Z$="Y":IF Z$<>"Y" THEN T8=4 ELSE T8=1
2020 INPUT "SAMPLE MOUNTED",Z$
2030 A$="TN":PROCexchange
2040 A$="SM":PROCexchange
2050 INPUT"SAMPLE POSN ADJUST",Z$
2060 PROCheaders
2070 T1=100:T2=650
2080 temp=T1:PRINT"SENT TO T1"T1
2090 Q=1:TA=TIME:TB=0
2100 PROCdelay:PROCmeloop
2105 FOR  GU=1 TO 5
2110 temp=T2:SA=2
2120 Q=1:TA=TIME:TB=0
2130 PROCfdelay:A$="FCVNE":PROCexchange
2140 temp=T1:PRINT"SENT TO T1"T1
2150 Q=0:TA=TIME:TB=0
2230 A$="AC":PROCexchange:A$="AN":PROCexchange
2260 PROCdelay
2280 PROCmeloop
2290 NEXT GU
2300 PROClastmeas
2340 PROCEND(1)
2350 A$="TF":PROCexchange:A$="SL":PROCexchange:ENDPROC
2360 DEF PROCheaders
2370 *FX3,10
2380 A1=DS1:A2=DS2:A3=DS3:A4=DS4:A5=DS5
2390 PRINT"SAMPLE   ";CODE1$+CODE2$
2400 GOTO 2430
2410 PRINT" SAMPLE   ":CODE$
2420 OP$=MID$(OP$,18,20):PRINT:PRINT"OPERATOR/DATE=
":OP$
2340 PRINT:PRINT"DIP= ";A1;TAB(20);"DEC= ";A2
2440 PRINT"  FIELD/TEMP";TAB(20);"MOMENT;TAB(31);
"DECLINATION" ;TAB(46);"INCLINATION"
2450 *FX3,0
2460 ENDPROC
2470 DEFPROCdelay
2480 TE=150:IF temp>450 THEN TE=175:IF temp>550 THEN
TE=200:IF SA=1 THEN TE=300
2490 IF Q=0 THEN 2530
2500 A$="SO":PROCexchange
2510 PROCtempset:A$="TR":REPEAT:PROCexchange:pause=TIME
+5 :REPEAT :UNTIL TIME>pause : UNTIL reply>=temp
```

```
2520 IF Q=1 THEN 2570
2530 A$="TF":PROCexchange:PRINT"TH OPS OFF":
A$="SM":PROCexchange
2540 A$="TR":REPEAT:PROCexchange:pause=TIME+5: REPEAT:
UNTIL TIME>=pause:UNTIL reply<=temp
2550 A$="TN":PROCexchange:PRINT"TH OPS ON":
A$="AP":PROCexchange:A$="AO":PROCexchange:A$="FD":
PROCexchange:PROCtempset
2570 A$="SO":PROCexchange:equilib=TIME+(50*TE):REPEAT:
PRINT "PAUSE"(equilib-TIME):UNTIL TIME>=equilib
2580 ENDPROC

PLEASE REFER TO FOX23 FOR LINES 2590 TO 2860

2860 DEF PROClastmeas
2870 A$="SL":PROCexchange
2880 temp=200
2890 A$="AC":PROCexchange
2900 A$="TF":PROCexchange:A$="TR":REPEAT:PROCexchange:
pause=TIME+5:REPEAT:UNTIL TIME>=pause:UNTIL reply<=temp
2910 A$="AP":PROCexchange
2920 A$="FD":PROCexchange
2930 ENDPROC
2940 DEFPROCfdelay
2950 A$="SO":PROCexchange
2960 PROCtempset:A$="TR":REPEAT:PROCexchange:
pause=TIME+5: REPEAT:UNTIL TIME>=pause:UNTIL
reply>=temp
2970 TE=150:IF temp>450 THEN TE=175: IF temp>550 THEN
TE=200
2979 A$="SM":PROCexchange:PROCfieldinst
2980 equilib=TIME+(40*TE):REPEAT:PRINT"PAUSE"(equilib-
TIME):UNTIL TIME>=equilib
3010 ENDPROC
```

```
1900 DEF PROCoper
1910 A$="IR":PROCexchange:A$="IN":PROCexchange:A$="IL"
1920 PROCexchange
1930 A$="IG":PROCexchange:RANGE=reply
1940 IF V%=RANGE THENINPUT"NEW ZERO TEST",Z$:IF Z$<>"Y"
THEN 1990
1960 PRINT"THERE IS NOT AT PRESENT A ZERO
TEST":INPUT"DO YOU WANT A ZERO TEST,Y OR N",Z$:IF
Z$<>"Y" THEN 1990
1970
ZE=0:A$="SO":PROCexchange:PROCzero:V%=RANGE:W%=M(1):
X%=M(2):Y%=M(3):Z%=M(4)
1980 A$="SL":PROCexchange
1990 M(1)=W%:M(2)=X%:M(3)=Y%:M(4)=Z%
2000 ZE=1
2010 PRINT"AC":INPUT"Y ORN",Z$:IF Z$<>"Y" THEN T8=4
ELSE T8=1
2020 INPUT"SAMPLE MOUNTED",Z$
2030 A$="TN":PROCexchange
2040 A$="SM":PROCexchange
2050 INPUT"SAMPLE POSN ADJUST",Z$
2060 PROCheaders
2070 TX=30:T1=135:T2=170:SA=1
2080 temp=t1:PRINT"SENT TO T1"T1
2090 Q=1:TA=TIME:TB=0
2100 PROCdelay:PROCmeloop:J(1)=J
2110 temp=T2:PRINT"SENT TO T2"T2:SA=2
2120 Q=1:TA=TIME:TB=0
2130 PROCdelay:PROCdelay:PROCdelay:PROCPLOOP:PROCmeloop
2140 temp=t1:PRINT"SENT TO T1"T1
2150 Q=0:TA=TIME:TB=0
2160 IF T8=1 THEN 2170 ELSE 2180
2170 A$="AC":PROCexchange
2180 PROCdelay:PROCmeloop
2190 QQ=1
2200 temp=T2:PRINT"SENT TO T2"T2
2210 Q=1:TA=TIME:TB=0
2220 PROCfdelay:A$="FCVNE":PROCexchange
2230 TA=TIME:Q=0:TB=0:temp=T1
2240 PRINT"SENT TO T1":IF T8=1 THEN 2250 ELSE 2260
2250 A$="AC":PROCexchange
2260 PROCdelay
2270 A$="FD":PROCexchange
2280 PROCmeloop
2290 REM NEXT QQ
2300 IF T2>400 THEN PROClastmeas
2310 IF T2>400 THEN2340
2320 T3=T1+40:T1=T1+40:T2=T2+40
2330 GOTO 2080
2340 PROCEND(1)
2350 A$="TF":PROCexchange:A$="SL":PROCexchange:ENDPROC
2360 DEF PROCheaders
2370 *FX3,10
2380 A1=DS1:A2=DS2:A3=DS3:A4=DS4:A5=DS5
2390 PRINT"SAMPLE   ";CODE1$+CODE2$
```

```
2400 GOTO 2430
2410 PRINT" SAMPLE  ":CODE$
2420 OP$=MID$(OP$,18,20):PRINT:PRINT"OPERATOR/DATE=
":OP$
2340 PRINT:PRINT"DIP= ";A1;TAB(20);"DEC= ";A2
2440 PRINT" FIELD/TEMP";TAB(20);"MOMENT;TAB(31);
"DECLINATION" ;TAB(46);"INCLINATION"
2450 *FX3,0
2460 ENDPROC
2470 DEFPROCdelay
2480 TE=150:IF temp>450 THEN TE=175:IF temp>550 THEN
TE=200:IF SA=1 THEN TE=300
2490 IF Q=0 THEN 2530
2500 A$="SO":PROCexchange
2510 PROCtempset:A$="TR":REPEAT:PROCexchange:pause=TIME
+5 :REPEAT :UNTIL TIME>pause : UNTIL reply>=temp
2520 IF Q=1 THEN 2570
2530 A$="TF":PROCexchange:PRINT"TH OPS OFF":
A$="SM":PROCexchange
2540 A$="TR":REPEAT:PROCexchange:
pause=TIME+5:REPEAT:UNTIL TIME>=pause:UNTIL reply<=temp
2550 A$="TN":PROCexchange:PRINT"TH OPS ON":
A$="AP":PROCexchange:PROCtempset
2560 equilib=TIME+(40*TE):REPEAT:PRINT"PAUSE"(equilib-
TIME):UNTIL TIME>=equilib
2570 A$="SO":PROCexchange:equilib=TIME+(90*TE):REPEAT:
PRINT "PAUSE"(equilib-TIME):UNTIL TIME>=equilib
2580 ENDPROC

PLEASE REFER TO *** FOR LINES 2590 TO 2850

2860 DEF PROClastmeas
2870 A$="SL":PROCexchange
2880 temp=150
2890 A$="AC":PROCexchange
2900 A$="TF":PROCexchange:A$="TR":REPEAT:PROCexchange:
pause=TIME+5:REPEAT:UNTIL TIME>=pause:UNTIL reply<=temp
2910 A$"AP":PROCexchange
2920 A$="FD":PROCexchange
2930 ENDPROC
2940 DEFPROCfdelay
2950 A$="SO":PROCexchange:temp=temp+2
2960 PROCtempset:A$="TR":REPEAT:PROCexchange:
pause=TIME+5: REPEAT:UNTIL TIME>=pause:UNTILreply>=temp
2970 TE=150 : IF temp>450 THEN TE=175:IF temp>550 THEN
TE=200
2980 equilib=TIME+(80*TE):REPEAT:PRINT"PAUSE"(equilib -
TIME):UNTIL TIME>=equilib
2990 A$="SM":PROCexchange:PROCfeildinst
3000 equilib=TIME+(80*TE):REPEAT:PRINT"PAUSE"(equilib-
TIME):UNTIL TIME>=equilib
3010 ENDPROC
3020 DEFPROCPLOOP
3030 VDU2:*FX3,10
3040 PRINT".....ALT CHK................."
3050 VDU3:*FX3,0
3060 ENDPROC
```

References.

Abrahamsen N., (1986), Refraction Error and Possible Refraction Correction in Palaeomagnetism, GeoSkrifter, No 24, 300 Aarhus University.

Aitken M.J. and Hawley H.N., (1971), Archaeomagnetism: Evidence for Magnetic Refraction in Kiln Structures, Archaeometry, 13, 1.

Barbetti M. & McElhinny M.W., (1972), Evidence for the Geomagnetic Excursion 30,000 yr B.C., Nature, Vol 239.

Barbetti M. & McElhinny M.W., (1976), The Lake Mungo Geomagnetic Excursion, Phil. Trans. Roy. Soc. London., A281, 515.

Barraclough D.R., (1974), Spherical Harmonic Analysis of the Geomagnetic Field for Eight Epochs Between 1600 & 1910, Geophys. J. R. Astr. Soc., 36, 497.

Bloxham J. and Gubbins D., (1985), The Secular Variation of the Earth's Magnetic Field, Nature, Vol 317.

Boyd M., (1986), Unpublished Ph.D Thesis, University of Cambridge.

Boyd M., (1986), A New Method for Measuring Palaeomagnetic Intensities, Nature, Vol 319.

Bullard E.C., Freedman C., Gellman H. and Nixon J., (1950), The Westward Drift of the Earth's Magnetic Field, Phil. Trans. Roy. Soc., A243, 67-92.

Collinson D.W., (1983), Methods in Rock Magnetism and Palaeomagnetism, Chapman and Hall.

Creer K.M., The Lac Du Bouchet Palaeomagnetic Record, in F J Lowes et al (Eds.), (1989), Geomagnetism and Palaeomagnetism, Kluwer Academic Publishers.

Dodson M.H. and McClelland-Brown E., (1980), Magnetic Blocking Temperatures of Single Domain Grains during Slow Cooling, J. Geophy. Res., 85, 2625-2637.

Dunlop D.J., (1981), The Rock Magnetism of Fine Particles, Physics of Earth and Planetary Interiors, 26, 1-26.

Fisher R.A., (1953), Dispersion on a Sphere, Proc. R. Soc. London, A217, 295-305.

Fox J.M.W., (1979), Unpublished M. Sc. Thesis, University of Oxford.

Fox J.M.W. and Aitken M.J., (1980), Cooling-rate
Dependence of Thermoremnant Magnetisation, <u>Nature</u>, Vol
283.

Gauss C.F., (1839), <u>Algermaine Theorie des</u>
<u>Erdmagnetismus.</u>

Gilbert W., (1600), <u>De Magnete.</u>

Gromme C.S., Wright T.L. and Peck D.L., (1969),
Magnetic properties and oxidation of iron-titanium
oxide minerals in Alae and Makaoputi lava lakes,
Hawaii, <u>J. Geophys. Res.</u>, 74, 5277-5293.

Gubbins D., <u>Historic Secular Variation and Geomagnetic</u>
<u>Theory</u>, in F.J. Lowes et al (Eds.), (1989),
Geomagnetism and Palaeomagnetism, Kluwer Academic
Press.

Haggerty S.E., (1976), Opaque mineral oxidesin
terrestrial igneous rocks, in D. Rummble, (Editor),
Oxide minerals. <u>Mineral Soc. Am.</u>, 3, 101-300

Halgedahl S.L., Day R. and Fuller M., (1980), The
Effect of Cooling Rate on the Intensity of Weak Field
TRM in Single Domain Magnetite, <u>J. Geophys. Res.</u>, 85,
3690.

Hoffman K.A., Constantine V.L. and Morse D.L., (1989), Determination of absolute palaeointensity using a mulit-specimen proceedure, _Nature_, Vol 339, 295-297.

Hopkinson J., (1889), Magnetic and other physical properties of iron at a high temperature, _Phil. Trans. R. S. (London)_, A180, 443.

Hoye G.S., (1981), Archaeomagnetic Secular Variation Record of Mount Vesuvius, _Nature_, Vol 291.

Kischvink J.L., (1980), The Least-squares Line and Plane and the Analysis of Palaeomagnetic Data, _Geophys. J. R. Soc._, 62, 699-718.

Mankinen E.A., Prevot M and Gromme C.S., (1985), The Steens mountain (Oregon) geomagnetic polarity transition 1, directional history,duration of episodes and rock magnetism, _J. Geophys. Res._, 90, 10393-10416.

McClelland-Brown E., (1984), Experiments on TRM Intensity Dependence on Cooling Rate, _Geophy. Res. Letters_, Vol 11, No 3, 205-208.

McElhinny M.W. and Senanayake W.E., (1982), Variations in the Geomagnetic Dipole 1: The Past 50,000 Years, _J. Geomag. Geoelectr._, 34, 39-51.

Merril R.T. and McElhinny M.W., (1983), The Earth's Magnetic Field - It's History, Origin and Planetary Perspective, Academic Press.

Neel L., (1955), Some Theoretical Aspects of Rock Magnetism, P. M. Suppl.

Nagata T., (1943), The Natural Remnant Magnetism of Volcanic Rocks and its Relation to Geomagnetic Phenomena, Bull. Earthquake Res. Inst., 21, 1-196.

O'Reilly W., (1984), Rock and Mineral Magnetism, Blackie.

Radhakrishnamurty C. and Likhite S.D., (1970), Hopkinson Effect, Blocking Temperatures and Curie Point in Basalts, Earth and Planetary Science Letters, 7, 389-396.

Radhakrishnamurty C., Raja P.S.K., Likhite S.D. and Sahasrabudhe P.W., (1972), Problems concerning the magnetic behaviour and determination of Curie points of certain basalts, Pure Appl. Geophysics, 93, 129-140

Radhakrishnamurty C., Likhite S.D. and Sahasrabudhe P.W., (1977), Nature of Magnetic Grains and Their Effect on the Remnant Magnetization of Basalts, Physics of Earth and Planetary Interiors, 13, 289-300.

Radhakrishnamurty C., Likhite S.D., Deutsch E.R., and
Murthy G.S, (1978), Nature of Magnetic Grains in
Basalts and implications for Palaeomagnetism, Proc.
Indian Acad. Sci. Sect. A, 87, 235-243.

Radhakrishnamurty C., Deutsch E.R. and Murthy G.S,
(1979), On the presence of Titanomagnetites in Basalts,
J. Geophys., 45, 443-446.

Radhakrishnamurty C., (1985), Identification of
Titanomagnetites by Simple Magnetic Techniques and
Application to Basalt Studies, J. Geological Soc.
of India, Vol 26, 640-651.

Rolph T.C., (1984), Unpublished Ph.D Thesis, University
of Wales.

Rolph T.C. and Shaw J., (1985), A New Method of
Palaeofield Magnitude Correction for Thermally Altered
Lavas and its Application to Lower Carboniferous Lavas,
Geophys. J. R. Astr. Soc., 80, 773-781.

Rolph T.C. and Shaw J., (1986), Variations of the
Geomagnetic Field in Sicily, J. Geomag. Geoelectr., 38,
1269-1277.

Share J.A., (1987), Unpublished Ph.D Thesis, University
of Wales.

Share J.A., (1989), An active low pass filter for a 16 bit ADC, Electronic technology, 23, 176-177.

Sharma (1966)

Shaw J., (1974) A New Method of Determining the Magnitude of the Palaeomagnetic Field, Geophys. J. R. Astr. Soc., 40, 345-350.

Shaw J. and Share J., (1986), A Microcomputer Controlled System for Low Temperature Magnetic Susceptibility Measurements, Physics of Earth and Planetary Interiors, 42, 1-4.

Senanayake W.E. and McElhinny M.W., (1981), Hysteresis and Susceptibility Characteristics of Magnetite and Titanomagnetites, Physics of Earth and Planetary Interiors, 26, 47-55.

Senanayake W.E. and McElhinny M.W., (1982), The Effects of Heating on Low-temperature Susceptibility and Hysteresis Properties of Basalts, Physics of Earth and Planetary Interiors, 30, 317-321.

Sherwood G.J., (1986), Unpublished Ph.D Thesis, University of Wales.

Sherwood G.J., (1988), Rock magnetic studies of Miocene volcanics in eastern Otago and Banks peninsular, New Zealand: comparison between Curie temperature and low temperature susceptibility behaviour, New Zealand J. of Geol. and Geophys., 31, 225-235.

Soler V., Carracedo J.C. and Heller F., (1984), Geomagnetic Secular Variation in Historical Lavas from the Canary Islands, Geophys J. R. Astr. Soc., 1984.

Tarling D.H., Geomagnetic Secular Variation in Britain during the last 2000 years, in F J Lowes et al (Eds.), (1989), Geomagnetism and Palaeomagnetism, Kluwer Academic Publishers.

Tarling D.H., (1983), Palaeomagnetism, Chapman and Hall.

Tanguy J.C., (1975), Intensity of the Geomagnetic Field from Recent Italian Lavas using a New Palaeointensity Method, Earth and Planetary Science Letters, 27, 314-320.

Tanguy J.C., (1985), Geomagnetic Secular Variation in Sicily and Revised Ages of Historic Lavas from Mount Etna, Nature, Vol 318.

Thellier E. and Thellier O., (1959), Sur L'intensite du
Champ Magnetique Terrestre dans le Passe Historique et
Geologique, Ann. Geophys., 15, 285-376.

Thompson R. and Oldfield F., (1986), Environmental
magnetism, Allen and Unwin.

Vestine E.H., Laporte L., Lange I., Cooper C. and
Hendrix W.C., (1947), Description of the Earth's Main
Magnetic Field, 1905-1945, Carnegie Institution of
Washington Pub., 578.

Walton D., (1977), Archaeomagnetic Intensity
Measurements using a SQUID Magnetometer, Archaeometry,
19, 192-200.

Williams W., (1986), Unpublished Ph.D Thesis,
University of Cambridge.
Wilson R.L., (1961), Palaeomagnetism in Northern
Island. Part 2. On the Reality of a Reversal of the
Earth's Magnetic field, Royal Astro. Soc. Geophy. J.,
Vol. 5, 59-69.

Yukutake T. and Tachinaka H., (1969), Separation of the
Earth's Magnetic Field into Drifting and Standing
Parts, Bull. Earthquake Res. Inst., Tokyo, 47, 65-97.

Yukutake T., (1979), Fluctuation in the Earth's rate of rotation related to changes in the geomagnetic field. J. Geomagn. Geoelect., 25, 195-212.

Zijderveld J.D.A., (1967), A.C. Demagnetisation of Rocks: Analysis of Results, 254-286, in Collinson D.W., Creer K.M., and Runcorn S.K. (Editors), Methods in Palaeomagnetism, Elsevier.